

**Application of Sliding Mode Methods  
to the Design of Reconfigurable Flight Control Systems**

by

Scott R. Wells

B.S. Aeronautical Engineering (Embry-Riddle Aeronautical University) 1987  
M.S. Aeronautical Engineering (Air Force Institute of Technology) 1991

DISSERTATION

Submitted in partial satisfaction of the requirements for the degree of

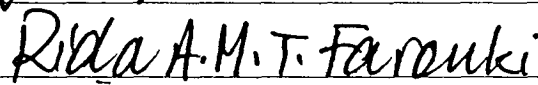
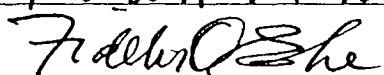
DOCTOR OF PHILOSOPHY

in

Mechanical and Aeronautical Engineering

in the  
OFFICE OF GRADUATE STUDIES  
of the  
UNIVERSITY OF CALIFORNIA  
DAVIS

Approved:

  
\_\_\_\_\_  
  
\_\_\_\_\_  
  
\_\_\_\_\_

Committee in Charge

2002



DEPARTMENT OF MECHANICAL AND  
AERONAUTICAL ENGINEERING  
TELEPHONE (530) 752-0580  
FAX (530) 752-4158  
<http://mae.engr.ucdavis.edu>

ONE SHIELDS AVENUE  
DAVIS, CALIFORNIA 95616-5294

**DELINQUENT FINAL REPORT**  
**Summary of Research**

September 28, 2002

ATTN: Carol Dancy, Document Processing Section  
NASA Center for AeroSpace Information (CASI)  
7121 Standard Drive  
Hanover MD 21076-1320

Dear Ms Dancy

This concerns NASA Cooperative Agreement NCC-1-01010. Enclosed are copies of two graduate theses completed under the identified agreement. Also enclosed are copies of three manuscripts that have also been completed under the agreement. These latter manuscripts are under review by, or will be submitted to, technical journals for publications. All these documents are intended to serve as the Summary of Research for the agreement identified above.

Sincerely,

A handwritten signature in black ink, appearing to read "Ron Hess".

Ronald A. Hess  
Professor and Vice Chairman

cc: René H. Domino

## Disclaimer

The views expressed in this work are those of the author and do not reflect the official policy or position of the United States Air Force, Department of Defense, or the U. S. Government.

## Acknowledgements

“I do not know what I seem to the world, but to myself I appear to have been like a boy playing upon the seashore and diverting myself by now and then finding a smoother pebble or prettier shell than ordinary, while the great ocean of truth lay before me all undiscovered.” These immortal words of Sir Isaac Newton very eloquently capture my feelings as I complete this work. It is an immensely complex and awesome world in which we live, and I cannot help but be overcome with wonder at God’s creation and the physical laws by which it is governed. I am thankful that He has left it to us to discover and understand these laws, for this quest drives us to reach beyond ourselves—stretching our intellects and creativity. However, when I look at the pebble I found on the shore—which is not even particularly smooth or pretty—its significance seems almost laughable in light of the great expanse of precious stones yet uncovered. I am left echoing the psalmist, “When I consider Thy heavens, the work of Thy fingers, the moon and the stars, which Thou hast ordained; what is man, that Thou art mindful of him? And the son of man that Thou visiteth him?” I can only say that I am thankful that I had some time to play on the shore.

My wife, Sherry, has endured yet another three years of being a grad student widow. This is her third time through it, and again she has been my strength and joy. It may sound trite, but it is a true statement that I would not be where I am today without her. I am also thankful to my children, Ben, Lacey, and Eli, for their patience and understanding during my hours of absence. I love you all and am looking forward to having more time with you.

I came to UC Davis because of Prof Baughn. During the snowy carpool days in Colorado, he was always carrying on about how the “roses are probably blooming in Davis by now.” He paved the way for me to get here and has been a wonderful mentor during my time here. He was right about the roses, and he was also right in his recommendation that Prof Hess be my research advisor. It is true that a grad student’s experience is largely determined by his relationship with his advisor. My experience has been an excellent one. I am very thankful for Prof Hess’ expertise, time, direction, and understanding of my compressed timeline. I look forward to many cooperative research efforts in the future. Thanks, too, to my cellmate Travis. We spent a lot of time bouncing ideas off each other and wrestling with concepts we didn’t understand. The ideas weren’t always good, but the bouncing exercises were always valuable.

Finally, I’d like to thank the Air Force. There are not many grad students who get to go to school full time, pay no tuition, and receive a substantial salary. I recognize the wonderful, unique opportunity I have been given, and I am unspeakably grateful.

# Table of Contents

<i>Disclaimer</i> .....	<i>ii</i>
<i>Acknowledgements</i> .....	<i>iii</i>
<i>Table of Contents</i> .....	<i>iv</i>
<i>List of Figures</i> .....	<i>vi</i>
<i>Abstract</i> .....	<i>xiv</i>

## **Chapter 1: Overview**

1.1 Introduction .....	1
1.2 Thesis Overview .....	4
1.3 Overview of Reconfigurable Flight Control .....	5
1.3.1 Failure Detection .....	5
1.3.2 Parameter Estimation .....	7
1.3.3 Reconfiguration Control Algorithms .....	20
1.3.4 Control Allocation .....	25
1.4 Literature Summary .....	39

## **Chapter 2: Sliding Mode Control**

2.1 Introduction to Sliding Mode Control .....	40
2.1.1 Sliding Mode Control History .....	41
2.1.2 Concept of the Sliding Mode .....	42
2.1.3 Sliding Mode Control Problem Statement .....	47
2.1.4 Equivalent Control Concept .....	48
2.1.5 Properties of the Sliding Mode .....	50
2.1.6 The Reachability Problem .....	52
2.1.7 Design Approaches .....	54
2.1.8 Implementation Issues .....	59
2.2 Application Example: Inverted Pendulum on a Translating Cart .....	64

## **Chapter 3: Parasitic Dynamics and SMC**

3.1 Introduction .....	83
3.2 Postfilter Design with Dynamic Boundary Layer .....	90
3.2.1 Application Example: Pitch Rate Tracking for an F-16 .....	91
3.2.2 Application Example: Bank Angle Tracking for a DC-8 .....	104
3.3 Observer-Based SMC .....	111
3.3.1 Observer-Based Design, SISO Case .....	113
3.3.2 Observer-Based Design, MIMO Case .....	118
3.3.3 Observers with Failed Plants .....	121

3.4	Model Reference Hedging .....	123
3.4.1	Creating the Hedge Model.....	135
3.4.2	Selecting Hedge Gain.....	137
3.4.3	Hedging in MIMO Systems.....	139
3.4.4	Observer Gains and Hedging with Failed Plants .....	141
3.4.5	A Hedge By Any Other Name.....	147
3.5	Robustness Issues.....	148
3.5.1	Difficulties with SMC Robustness Proofs.....	148
3.5.2	Difficulties with Hybrid Nature of the Observer-based SMC .....	157
3.6	Robustness Summary .....	157

**Chapter 4: Design Procedure**

4.1	Interpretation of Linear SMC Design in the Frequency Domain .....	158
4.2	Instantaneous Adaptation .....	159
4.3	Design Procedure Summary .....	165
4.4	Task-Dependent Analytical Handling Qualities Assessment.....	169
4.5	Application Example: F-18/HARV Longitudinal SISO Model.....	171
4.6	Application Example: F-18/HARV Lat-Dir MIMO Model .....	200
4.7	Application Example: ICE MIMO 6-DOF Model.....	238

**Chapter 5: Conclusions and Recommendations**

5.1	Summary.....	270
5.2	Potential Future Research.....	271
5.2.1	Robustness Proofs.....	271
5.2.2	Full Flight Envelope Issues .....	271
5.2.3	Adaptive Hedging.....	272
5.2.4	Dynamic Hedged Observer .....	273
5.2.5	Dynamic Control Allocation.....	276
5.2.6	Actuator Position Limiting Issues.....	276

<b>Bibliography.....</b>	<b>277</b>
--------------------------	------------

<b>Subject Index.....</b>	<b>291</b>
---------------------------	------------

## List of Figures

Figure 1-1: Reduced Model Order, ad hoc Approach .....	17
Figure 1-2: Indirect Adaptive Controller .....	21
Figure 1-3: Model Reference Adaptive Control System .....	22
Figure 1-4: Boeing Tailless Advanced Fighter Aircraft .....	25
Figure 2-1: Time History of Oscillator .....	42
Figure 2-2: Phase Plane Plot of Oscillator .....	42
Figure 2-3: Time History of VSC System .....	43
Figure 2-4: Phase Plane Plot of VSC System .....	43
Figure 2-5: Time History for SMC System .....	44
Figure 2-6: Phase Plane Plot for SMC System .....	44
Figure 2-7: Phases of Sliding Mode Control .....	45
Figure 2-8: Time History of Sliding Surface .....	45
Figure 2-9: SMC Phase Plane Plot for System with Non-linear Term .....	46
Figure 2-10: Phase Plane Plot of Domain of Attraction .....	53
Figure 2-11: State Trajectories for Ideal Sliding Mode and Sliding Mode with Boundary Layer .....	61
Figure 2-12: Pendulum/Cart Nonlinear System Block Diagram .....	65
Figure 2-13: Pendulum/Cart SMC Controller Block Diagram .....	67
Figure 2-14: LQR Regulator (Linear Model) .....	69
Figure 2-15: SMC Regulator (Linear Model) with $u = U_{eq}$ .....	70
Figure 2-16: SMC Regulator (Linear Model) with $u = 20 \text{ sat}(\sigma/0.005)$ .....	71
Figure 2-17: SMC Regulator (Linear Model) with $u = U_{eq} + 5 \text{ sat}(\sigma/0.0001)$ .....	72
Figure 2-18: SMC Regulator (Linear Model) with $u = U_{eq} + 5 \text{ sat}(\sigma/0.1)$ .....	73
Figure 2-19: LQR Regulator (Non-linear System) with Control Input Disturbances .....	75
Figure 2-20: SMC Regulator (Non-linear System) with Control Input Disturbances .....	76
Figure 2-21: Decoupled SMC Tracking, Baseline Case .....	78
Figure 2-22: LQR Tracking with System Failure .....	79
Figure 2-23: SMC Tracking with System Failure .....	80
Figure 2-24: SMC Tracking with System Failure (Insufficient $\rho_x$ & $\rho_\theta$ ) .....	81
Figure 2-25: SMC Tracking with System Failure (Insufficient $\rho_\theta$ ) .....	82
Figure 3-1: SMC Control, No actuator .....	84
Figure 3-2: SMC Control, With Actuator: $\frac{\delta}{u_c}(s) = \frac{20}{s+20}$ .....	85
Figure 3-3: SMC Control, With Actuator: $\frac{\delta}{u_c}(s) = \frac{13}{s+13}$ .....	86
Figure 3-4: Simple Plant with Actuator .....	87
Figure 3-5: F-16 SISO Longitudinal System Block Diagram .....	93
Figure 3-6: F-16 SISO SMC Controller Block Diagram .....	93
Figure 3-7: F-16 SISO Pitch Rate Tracking, SMC, No Failure, No Limits .....	94
Figure 3-8: F-16 SISO Pitch Rate Tracking, SMC, With Failure, No Limits .....	95
Figure 3-9: F-16 SMC, $u_p = 0.1 \text{ rad/s}$ , With Failure, With Limits, Static BL .....	97
Figure 3-10: F-16 SMC, $u_p = 0.2 \text{ rad/s}$ , With Failure, With Limits, Static BL .....	98

Figure 3-11: F-16 SMC, $u_p = 0.2$ rad/s, With Failure, With Limits, Dynamic BL	100
Figure 3-12: F-16 SMC, $u_p = 0.2$ rad/s, With Failure, With Limits, Dynamic BL, Known Slow Actuator	101
Figure 3-13: F-16 SMC, $u_p = 0.2$ rad/s, With Failure, With Limits, Dynamic BL, Unknown Slow Actuator	103
Figure 3-14: Schematic of DC-8 Lat/Dir Control System	106
Figure 3-15: Inner Loop Sliding Mode Controller	106
Figure 3-16: Actuator Loop Sliding Mode Controllers	107
Figure 3-17: DC-8 Roll Angle Tracking Results, No Failure	109
Figure 3-18: DC-8 Roll Angle Tracking Results, With Failure	110
Figure 3-19: Observer-Based SMC Block Diagram	111
Figure 3-20: Equivalent Plant with Observer	112
Figure 3-21: F-16 Bode Plots, $\frac{y}{y_c}$ Nominal System and Actuator	114
Figure 3-22: F-16 Bode Plots, $\frac{\hat{y}}{y_c}$ Observer System Output	114
Figure 3-23: F-16 Bode Plots, $\frac{\hat{y}}{y_c}$ Various Observer Speeds	116
Figure 3-24: F-16 Bode Plots, $\frac{\hat{y}}{y_c}$ Choosing Observer Speed	117
Figure 3-25: F-16 Pitch Rate Step Responses, Various Observer Speeds	118
Figure 3-26: Multiple Observer-Based SMC Block Diagram	119
Figure 3-27: F-16 Bode Plots, Nominal Plant $\frac{y}{y_c}$ , Failed Plant $\frac{y_{fail}}{y_c}$ , Fast Observer $\frac{\hat{y}}{y_c}$	122
Figure 3-28: F-16 Bode Plots, Nominal Plant $\frac{y}{y_c}$ , Failed Plant $\frac{y_{fail}}{y_c}$ , Slow Observer $\frac{\hat{y}}{y_c}$	123
Figure 3-29: 2 <sup>nd</sup> Order Hedged Reference Model	125
Figure 3-30: 3 <sup>rd</sup> Order Hedged Reference Model	125
Figure 3-31: Hedged System Architecture	126
Figure 3-32: Equivalent Hedged System Architecture	127
Figure 3-33: Equivalent Plant with Observer and Hedge	128
Figure 3-34: System with Hedging, Bode Plots $\frac{\hat{y}_h}{y_c}$ , $K_h=0.01$	131
Figure 3-35: System with Hedging, Bode Plots $\frac{\hat{y}_h}{y_c}$ , $K_h=0.8$	132
Figure 3-36: Simplified Hedge System, $\frac{y_f}{u_a}$	134
Figure 3-37: System with Simplified Hedging, Bode Plots $\frac{\hat{y}_h}{y_c}$ , $K_h=8.0$	135

Figure 3-38: Creating the Hedge Model, $\frac{\hat{y}_h}{y_c}$ .....	136
Figure 3-39: System with Simplified Hedging, Bode Plots $\frac{\hat{y}_h}{y_c}$ , $K_h=20.0$ .....	138
Figure 3-40: System with Simplified Hedging, Step Responses .....	139
Figure 3-41: Hedge Model Example with Cross-Coupled Terms .....	140
Figure 3-42: F-18/HARV Step Response, Nominal System, Nominal Actuators, No Time Delay .....	142
Figure 3-43: F-18/HARV Step Response, FAILED System, Nominal Actuators, No Time Delay .....	143
Figure 3-44: F-18/HARV Step Response, Nominal System, FAILED Actuators, No Time Delay .....	144
Figure 3-45: F-18/HARV Step Response, Nominal System, Nominal Actuators, 50 mS Time Delay .....	145
Figure 3-46: F-18/HARV Step Response, FAILED System, FAILED Actuators, 50 mS Time Delay .....	146
Figure 4-1: Bode Plots, F-16 Pitch Rate $\frac{q}{q_c}$ , Nominal and Failed Plants .....	161
Figure 4-2: Bode Plots, F-16 Equivalent Unity Feedback Loop Transmission .....	162
Figure 4-3: Bode Plots, F-16 Equivalent Serial Compensator, $G_{c_c}$ and $G_{c_c \text{ adapted}}$ .....	164
Figure 4-4: Bode Plots, Nominal Equiv Serial Compensator with Failed Plant .....	165
Figure 4-5: F-18/HARV Longitudinal System Block Diagram .....	173
Figure 4-6: Pilot Model for F-18/HARV Pitch Angle Tracking Task .....	174
Figure 4-7: q Loop Transmission of Compensator*Plant, F-18/HARV .....	175
Figure 4-8: SMC Pitch Rate Controller for F-18/HARV .....	176
Figure 4-9: F-18/HARV Inner Loop SMC Pitch Rate Tracking .....	177
Figure 4-10: F-18/HARV Inner Loop SMC Pitch Rate Tracking with Boundary Layer .....	178
Figure 4-11: F-18/HARV Inner Loop SMC Pitch Rate Tracking, Actuators Included .....	180
Figure 4-12: Bode Plots, F-18/HARV Pitch Rate $\frac{\hat{q}}{u_c}$ , Various Observer Speeds .....	181
Figure 4-13: Unit Step Response, F-18/HARV Pitch Rate, Various Observer Speeds .....	182
Figure 4-14: Outer Loop Tracking, Nominal F-18/HARV, with Actuators, Observer, and Noise .....	183
Figure 4-15: Inner Loop Tracking, Nominal F-18/HARV, with Actuators, Observer, and Noise .....	183
Figure 4-16: Actuator Deflections, Nominal F-18/HARV, with Observer and Noise .....	184
Figure 4-17: Actuator Rates, Nominal F-18/HARV, with Observer and Noise .....	184
Figure 4-18: Nominal F-18/HARV Handling Qualities Assessment, $\theta$ Tracking Task .....	185
Figure 4-19: Nominal F-18/HARV PIO Assessment, $\theta$ Tracking Task .....	185
Figure 4-20: Outer Loop Tracking ( $\theta$ ), F-18/HARV, with SMC, Actuators, Observer, and Noise, Failure at $t = 10$ sec .....	187

Figure 4-21: Inner Loop Tracking ( $q$ ), F-18/HARV, with SMC, Actuators, Observer, and Noise, Failure at $t = 10$ sec .....	187
Figure 4-22: Actuator Deflections, F-18/HARV, with SMC, Observer, and Noise, Failure at $t = 10$ sec.....	188
Figure 4-23: Actuator Rates, F-18/HARV, with SMC, Actuators, Observer, and Noise, Failure at $t = 10$ sec.....	188
Figure 4-24: Failed F-18/HARV, Handling Qualities Assessment, $\theta$ Tracking Task ..	189
Figure 4-25: Failed F-18/HARV, PIO Assessment, $\theta$ Tracking Task .....	189
Figure 4-26: Bode Plots $\frac{\hat{q}_h}{u_c}$ , F-18/HARV Pitch Rate Observer & Hedge Design ..	190
Figure 4-27: Outer Loop Tracking, F-18/HARV, with SMC, Actuators, Observer, Hedging, and Noise, Failure at $t = 10$ sec.....	191
Figure 4-28 Inner Loop Tracking, F-18/HARV, with SMC, Actuators, Observer, Hedging, and Noise, Failure at $t = 10$ sec.....	191
Figure 4-29: Failed F-18/HARV, Handling Qualities Assessment, $\theta$ Tracking Task, With Hedging .....	192
Figure 4-30: Failed F-18/HARV, PIO Assessment, $\theta$ Tracking Task, With Hedging..	192
Figure 4-31 Bode Plots $\frac{\hat{q}_h}{u_c}$ , F-18/HARV Modified Observer & Hedge Design.....	194
Figure 4-32: Outer Loop Tracking, Failed F-18/HARV, with SMC, Actuators, Observer, Hedging, and Noise, (Failure #2) .....	195
Figure 4-33: Inner Loop Tracking, Failed F-18/HARV, with SMC, Actuators, Observer, Hedging, and Noise, (Failure #2) .....	195
Figure 4-34: Actuator Deflections, Failed F-18/HARV, with SMC, Observer, Hedging, and Noise, (Failure #2) .....	196
Figure 4-35 Actuator Rates, Failed F-18/HARV, with SMC, Observer, Hedging, and Noise, (Failure #2).....	196
Figure 4-36: Failed F-18/HARV Handling Qualities Assessment, $\theta$ Tracking Task, With Hedging (Failure #2).....	197
Figure 4-37: Failed F-18/HARV PIO Assessment, $\theta$ Tracking Task, With Hedging (Failure #2).....	197
Figure 4-38: Bode Plots, F-18/HARV Pitch Rate Loop Transmission for Loop Shaped Design .....	198
Figure 4-39. Outer Loop Tracking ( $\theta$ ) for Loop-Shaped Controller, Failed F-18/HARV, with Actuators and Noise, (Failure #2) .....	199
Figure 4-40: F-18/HARV Lateral-Directional System Block Diagram .....	202
Figure 4-41: Pilot Model for F-18/HARV Roll Angle Tracking Task .....	203
Figure 4-42: p-Loop Transmission of Compensator*Plant, F-18/HARV, $\beta$ -Loop Open .....	205
Figure 4-43: $\beta$ -Loop Transmission of Compensator*Effective Plant, F-18/HARV, p-Loop Closed .....	205
Figure 4-44: SMC Roll Rate and Sideslip Angle Controller for F-18/HARV .....	206
Figure 4-45: F-18/HARV Inner Loop SMC Roll Rate Tracking .....	207

Figure 4-46: F-18/HARV Inner Loop SMC $\beta$ Tracking .....	207
Figure 4-47: F-18/HARV Inner Loop SMC Roll Rate Tracking with Boundary Layer..	208
Figure 4-48: F-18/HARV Inner Loop SMC $\beta$ Tracking with Boundary Layer .....	209
Figure 4-49: Inner Loop p-Tracking, Nominal F-18/HARV, SMC with Actuators .....	210
Figure 4-50: Inner Loop $\beta$ -Tracking, Nominal F-18/HARV, SMC with Actuators .....	210
Figure 4-51: Bode Plots, $\frac{\hat{p}}{u_{cp}}$ , F-18/HARV, Various Observer Speeds.. .....	211
Figure 4-52: Bode Plots, $\frac{\hat{\beta}}{u_{c\beta}}$ , F-18/HARV, Various Observer Speeds... .....	212
Figure 4-53: Bode Plots, $\frac{p}{u_{cp}}$ and $\frac{p}{u_{c\beta}}$ , F-18/HARV Nominal Vehicle .....	213
Figure 4-54: Bode Plots, $\frac{\beta}{u_{c\beta}}$ and $\frac{\beta}{u_{cp}}$ , F-18/HARV Nominal Vehicle.....	213
Figure 4-55: Bode Plots, $\frac{\hat{p}_h}{u_{cp}}$ , F-18/HARV Hedge Design .....	215
Figure 4-56: Bode Plots, $\frac{\hat{\beta}_h}{u_{c\beta}}$ , F-18/HARV Hedge Design.....	215
Figure 4-57: Bode Plots, $\frac{\hat{p}_h}{u_{c\beta}}$ (cross term), F-18/HARV Hedge Design....	216
Figure 4-58: Bode Plots, $\frac{\hat{\beta}_h}{u_{cp}}$ (cross term), F-18/HARV Hedge Design. ....	217
Figure 4-59: Step Response for p and $\beta$ , F-18/HARV, no Cross-Coupled Hedging ....	218
Figure 4-60: Step Response for p and $\beta$ , F-18/HARV, with Cross-Coupled Hedging .	218
Figure 4-61: Outer Loop Tracking ( $\phi$ ), Nominal F-18/HARV, with SMC, Actuators, Observers, Hedging, and Noise.....	220
Figure 4-62: Inner Loop Tracking ( $p_s$ and $\beta$ ), Nominal F-18/HARV, with SMC, Actuators, Observers, Hedging, and Noise.....	220
Figure 4-63: Actuator Deflections, Nominal F-18/HARV, with SMC, Observers, Hedging and Noise .....	221
Figure 4-64: Actuator Rates, Nominal F-18/HARV, with SMC, Observers, Hedging and Noise .....	222
Figure 4-65: Nominal F-18/HARV Handling Qualities Assessment, $\phi$ Tracking Task..	223
Figure 4-66: Nominal F-18/HARV PIO Assessment, $\phi$ Tracking Task .. .....	223
Figure 4-67: Outer Loop Tracking ( $\phi$ ), F-18/HARV, with SMC, Actuators, Observer, Hedging, and Noise, Failure #1 at t = 25 sec .....	225
Figure 4-68: Inner Loop Tracking ( $p_s$ and $\beta$ ), F-18/HARV, with SMC, Actuators, Observer, Hedging, and Noise, Failure #1 at t = 25 sec .. .....	225
Figure 4-69: Actuator Deflections, F-18/HARV, with SMC, Observer, Hedging, and Noise, Failure #1 at t = 25 sec.....	226

Figure 4-70: Actuator Rates, F-18/HARV, with SMC, Actuators, Observer, Hedging, and Noise, Failure #1 at t = 25 sec .....	227
Figure 4-71: F-18/HARV, Failure #1, Handling Qualities Assessment, $\phi$ Tracking Task .....	228
Figure 4-72: F-18/HARV, Failure #1, PIO Assessment, $\phi$ Tracking Task .....	228
Figure 4-73: Bode Plots, F-18/HARV Roll Rate Loop Transmission for Loop Shaped Design, $\beta$ -Loop Open .....	229
Figure 4-74: Bode Plots, F-18/HARV $\beta$ Loop Transmission for Loop Shaped Design, p-Loop Closed .....	230
Figure 4-75: Outer Loop Tracking ( $\phi$ ), F-18/HARV, with Loop Shaped Controller, Actuators, and Noise, Failure #1 at t = 25 sec .....	231
Figure 4-76: Inner Loop Tracking ( $p_s$ and $\beta$ ), F-18/HARV, with Loop Shaped Controller, Actuators, and Noise, Failure #1 at t = 25 sec .....	231
Figure 4-77: Actuator Deflections, F-18/HARV, with Loop Shaped Controller and Noise, Failure #1 at t = 25 sec .....	232
Figure 4-78: Actuator Rates, F-18/HARV, with Loop Shaped Controller and Noise, Failure #1 at t = 25 sec .....	233
Figure 4-79: Outer Loop Tracking ( $\phi$ ), SMC with and without Cross-Coupled Hedging .....	234
Figure 4-80: Inner Loop Tracking ( $\beta$ ), SMC with and without Cross-Coupled Hedging .....	235
Figure 4-81: Outer Loop Tracking ( $\phi$ ), F-18/HARV, SMC vs Reconfigured QFT, Failure #2 at t = 0 sec .....	236
Figure 4-82: $\beta$ Tracking, F-18/HARV, SMC, Failure #2 at t = 0 sec .....	237
Figure 4-83: Innovative Control Effectors (ICE) Aircraft .....	238
Figure 4-84: ICE Control Deflection Definitions .....	241
Figure 4-85: ICE System Block Diagram .....	243
Figure 4-86: Pilot Models for ICE Angle of Attack and Roll Angle Tracking Tasks ..	245
Figure 4-87: ICE $\alpha$ -Loop Transmission of Compensator*Plant, p-Loop Open, $\beta$ -Loop Open .....	246
Figure 4-88: ICE p-Loop Transmission of Compensator*Effective Plant, $\alpha$ -Loop Closed, $\beta$ -Loop Open .....	247
Figure 4-89: ICE $\beta$ -Loop Transmission of Compensator*Effective Plant, $\alpha$ -Loop Closed, p-Loop Closed .....	247
Figure 4-90: SMC Controller for ICE .....	248
Figure 4-91: ICE Inner Loop SMC Tracking .....	249
Figure 4-92: ICE Inner Loop SMC Control Outputs .....	249
Figure 4-93: ICE Inner Loop SMC Tracking with Boundary Layer .....	250
Figure 4-94: ICE SMC Control Outputs with Boundary Layer .....	251
Figure 4-95: Inner Loop Tracking, Nominal ICE, SMC with Actuators .....	252
Figure 4-96: Bode Plots, $\frac{\hat{\alpha}}{u_{ca}}$ , ICE, Various Observer Speeds .....	253

Figure 4-97: Bode Plots, $\frac{\hat{p}}{u_{cp}}$ , ICE, Various Observer Speeds.....	253
Figure 4-98: Bode Plots, $\frac{\hat{\beta}}{u_{c\beta}}$ , ICE, Various Observer Speeds. ....	254
Figure 4-99: Inner Loop Step Responses, ICE, SMC with Observers .....	255
Figure 4-100: Bode Plots, $\frac{\alpha}{u_{c\alpha}}$ , $\frac{\alpha}{u_{cp}}$ and $\frac{\alpha}{u_{c\beta}}$ , ICE Nominal Vehicle ...	256
Figure 4-101: Bode Plots, $\frac{p}{u_{c\alpha}}$ , $\frac{p}{u_{cp}}$ and $\frac{p}{u_{c\beta}}$ , ICE Nominal Vehicle .	256
Figure 4-102: Bode Plots, $\frac{\beta}{u_{c\alpha}}$ , $\frac{\beta}{u_{cp}}$ and $\frac{\beta}{u_{c\beta}}$ , ICE Nominal Vehicle ...	257
Figure 4-103: Bode Plots, $\frac{\hat{\alpha}_h}{u_{c\alpha}}$ , ICE Hedge Design.....	259
Figure 4-104: Bode Plots, $\frac{\hat{p}_h}{u_{cp}}$ , ICE Hedge Design .....	259
Figure 4-105: Bode Plots, $\frac{\hat{\beta}_h}{u_{c\beta}}$ , ICE Hedge Design .....	260
Figure 4-106: Bode Plots, $\frac{\hat{\alpha}_h}{u_{c\beta}}$ (cross term), ICE Hedge Design.....	260
Figure 4-107: Bode Plots, $\frac{\hat{p}_h}{u_{c\beta}}$ (cross term), ICE Hedge Design.....	261
Figure 4-108: Bode Plots, $\frac{\hat{\beta}_h}{u_{cp}}$ (cross term), ICE Hedge Design .....	261
Figure 4-109: Inner Loop Step Responses, ICE, SMC with Observers and Hedging .	262
Figure 4-110: Outer Loop Tracking ( $\alpha$ , $\phi$ , and $\beta$ ), ICE, with SMC, Actuators, Observers, Hedging, and Noise, Failure at t = 20 sec .....	264
Figure 4-111: Inner Loop Tracking ( $\alpha$ , and $p_s$ ), ICE, with SMC, Actuators, Observers, Hedging, and Noise, Failure at t = 20 sec.....	264
Figure 4-112: $\alpha$ -Tracking Task HQ and PIO Predictions, ICE Nominal System .....	265
Figure 4-113: $\phi$ -Tracking Task HQ and PIO Predictions, ICE Nominal System....	265
Figure 4-114: $\alpha$ -Tracking Task HQ and PIO Predictions, ICE Failed System .....	266
Figure 4-115: $\phi$ -Tracking Task HQ and PIO Predictions, ICE Failed System .....	266
Figure 4-116: ICE Loop Shaped Controller, $\alpha$ -Loop Transmission of Compensator*Plant, p-Loop Open, $\beta$ -Loop Open .....	267
Figure 4-117: ICE Loop Shaped Controller, p-Loop Transmission of Compensator*Effective Plant, $\alpha$ -Loop Closed, $\beta$ -Loop Open .....	268

Figure 4-118: ICE Loop Shaped Controller, $\beta$ -Loop Transmission of Compensator*Effective Plant, $\alpha$ -Loop Closed, p-Loop Closed .....	268
Figure 4-119: Outer Loop Tracking ( $\alpha$ , $\phi$ , and $\beta$ ), ICE, with Loop-Shaped Controller, Actuators, and Noise, Failure at $t = 20$ sec .....	269
Figure 5-1: Hedged Observer.....	273
Figure 5-2: Inner Loop Pitch Rate Tracking, F-18/HARV, Dynamic Observer Hedging, Failure #2 at $t = 10$ sec.....	275

## Abstract

Observer-based sliding mode control is investigated for application to aircraft reconfigurable flight control. A comprehensive overview of reconfigurable flight control is given, including a review of the current state-of-the-art within the subdisciplines of fault detection, parameter identification, adaptive control schemes, and dynamic control allocation. Of the adaptive control methods reviewed, sliding mode control (SMC) appears very promising due its property of invariance to matched uncertainty. An overview of sliding mode control is given and its remarkable properties are demonstrated by example. Sliding mode methods, however, are difficult to implement because unmodeled parasitic dynamics cause immediate and severe instability. This presents a challenge for all practical applications with limited bandwidth actuators. One method to deal with parasitic dynamics is the use of an asymptotic observer in the feedback path. Observer-based SMC is investigated, and a method for selecting observer gains is offered. An additional method for shaping the feedback loop using a filter is also developed. It is shown that this SMC prefilter is equivalent to a form of model reference hedging. A complete design procedure is given which takes advantage of the sliding mode boundary layer to recast the SMC as a linear control law. Frequency domain loop shaping is then used to design the sliding manifold. Finally, three aircraft applications are demonstrated. An F-18/HARV is used to demonstrate a SISO pitch rate tracking controller. It is also used to demonstrate a MIMO lateral-directional roll rate tracking controller. The last application is a full linear six degree-of-freedom advanced tailless fighter model. The observer-based SMC is seen to provide excellent tracking with superior robustness to parameter changes and actuator failures.

# Chapter 1

---

## Overview

### 1.1 Introduction

Reconfigurable flight control is an area of research that has seen exponential growth within the control community in the last two decades. The early works in reconfigurable flight control-- just a few research papers--began to appear in the 1960's and 1970's. The 1980's saw a growing interest with a few dozen papers, and the 1990's saw an explosion of effort in reconfigurable flight control. There are hundreds of reconfigurable-related papers from the 1990's, many of them from the latter part of the decade. Considerable progress has been made, but the problem is a difficult one and continues to see increasing interest on the part of researchers worldwide.

It is difficult to find a precise definition in the literature of *reconfigurable* flight control. There is an entire body of work in the area of *adaptive* control in which the term *reconfigurable* never appears. The basic purpose of an adaptive control law is to control a system with unknown and/or time-varying parameters. However, this is exactly what a *reconfigurable* control law is intended to do. In fact, all the reconfigurable control approaches use some type of adaptive control scheme or adaptive control redistribution. Strictly speaking, a reconfigurable control law *is* adaptive. Likewise, an adaptive control law *is* one that reconfigures itself. On the surface, *reconfigurable* and *adaptive* seem to be synonymous terms. However, there does appear to be a difference between the terms when one considers what each one implies.

*Reconfiguration* in the literature always implies a response to some type of system failure or damage. This failure may be the loss of a control effector (i.e. a control surface locked in a hard-over or zero position, a broken linkage allowing the control surface to float, degraded controller effectiveness, or degraded actuator rate response). The failure may be damage to an aerodynamic surface resulting in large changes to the stability and control derivatives. The failure could also be related to the thrust or thrust vectoring or could be simply a failed sensor. Whatever the failure type, *reconfigurable flight control* implies that a sudden, large, unknown failure has occurred. *Adaptive control* does not always connote this kind of failure. Changes to system parameters are generally implied (or explicitly stated) to be smooth and non-catastrophic—usually due to mechanical wear, unmodeled dynamics, and structured uncertainty due to environmental variations throughout the operating envelope. With this in mind, an exact definition of reconfigurable flight control is offered. Reconfigurable control is an automatic control system which is able to compensate for sudden, potentially large, unknown failure events in real-time using on-line adaptive control laws and/or adaptive redistribution of control effort with the objective of guaranteeing system stability and achieving some level of required performance and handling qualities.

The motivation for developing reconfigurable flight controls is clear. Failures during flight are inevitable—especially in combat aircraft. If the flight control system is capable of stabilizing the aircraft and providing acceptable control, it may be possible to return the damaged aircraft to base, salvage the airframe, and save lives. “Lessons learned from the Vietnam Era show 20% of aircraft losses were due to flight control damage. Loss of hydraulics, actuator damage, and surface damage are responsible for

most of the flight control system losses.”<sup>1</sup> In addition, high performance fighter aircraft tend to be so inherently unstable that a pilot is incapable of controlling it without the stabilizing influence of the control system. This, combined with the increasingly complex workload on the pilot, dictates the need for a highly fault-tolerant control system. Commercial transport aircraft can also profit from the potential safety benefits of reconfigurable flight controls. “In the majority of cases surveyed, major flight control system failures . . . have resulted in crashes, with a total of over 1200 fatalities”<sup>2</sup>

The approach for designing a reconfigurable flight control system has undergone a fundamental shift in philosophy in the last five to eight years. Initially, the concept was to design a control law robust enough to guarantee system stability in the face of the full range of potential failures. Then, upon the event of a failure, the system would identify the fault, isolate the failure mode, estimate new system parameters, and select new control law gains and/or control input distribution to regain some level of performance. The schedule of gains for each condition was calculated off-line. Today, most reconfigurable control schemes being proposed are fully adaptive—continuously reconfiguring themselves using dynamic on-line algorithms which do not require any *a priori* schedule of gains. Some perform continuous estimation of system parameters. Others do not even require this, deriving adaptive laws based on performance-related measures only. In the words of one set of authors, the control system is “self-designing”<sup>3</sup> This shift in philosophy is leading to classes of controllers that are highly robust to both “normal” parameter variations as well as damage/failures. They are more flexible, cost efficient, and general in nature. It is almost certain that future advanced

aircraft flight control systems will incorporate some form of on-line reconfigurable control law.

## 1.2 Thesis Overview

The purpose of this research is to demonstrate a design strategy for a multi-input, multi-output (MIMO) flight control system which is:

- able to provide satisfactory performance for a coupled-axis, statically unstable, high performance aircraft with a highly redundant control effector suite
- robust to model uncertainty, smooth parameter variations, and sensor and process noise
- able to adapt to sudden, unknown, potentially large system parameter changes due to a failure event
- able to provide satisfactory handling qualities and present no tendencies for pilot-induced oscillation (PIO) before and after a failure event
- based on current approaches utilizing sliding modes.

First, an overall view of reconfigurable flight control is given. Chapter 1 contains a comprehensive look at the current state of all key aspects of reconfigurable control. Based on this review, the sliding mode control method is chosen as a key focus area. Chapter 2 provides a brief introduction to sliding mode control. Chapter 3 investigates potential solutions to key implementation issues associated with sliding mode controllers. Based on this work, a tutorial design procedure along with several application examples is given in Chapter 4. Conclusions and recommendations for future research are found in Chapter 5.

### 1.3 Overview of Reconfigurable Flight Control

There are four main aspects of flight control reconfiguration that must be addressed for a complete treatment of the subject.

- Failure detection
- System parameter estimation
- Flight control law reconfiguration
- Control allocation

These four subdisciplines have traditionally been treated as separate problems because each has fundamentally different objectives. However, recent works<sup>4,5</sup> are addressing the interaction between them and demonstrating the need to consider the system as a whole. For example, it is shown later that the control allocation process can create a condition in which system parameter identification becomes impossible without considerable preconditioning. In the sections that follow, each of these components of reconfigurable flight controls are introduced individually. In this respect, the following introduction follows the traditional approach. However, the problematic interactions between the components (where they are known to exist) are also introduced.

#### 1.3.1 Failure Detection

In the time-sequence of events that occur after a failure, detection is logically the task that must be accomplished first. This task has traditionally been the job of the pilot. It is up to the pilot to recognize that something is wrong and to initiate efforts to compensate for the failure. While this method may not be suitable for high performance applications, it still finds its place in practical applications. In a proof-of-concept flight test program,<sup>2</sup> an MD-11 is flown using a propulsion-only emergency control system.

To activate the system, the pilot essentially flips a switch. This requires the pilot to be the one to detect and isolate the failure. Although this approach works well in this application, automatic failure detection is often required.

While little emphasis is placed on fault detection in the current literature, the early efforts in reconfigurable controls include fault detection as a primary concern. A key component in the Self-Repairing Flight Control System (SRFCS)<sup>1</sup> study, conducted by the Air Force Wright Aeronautical Laboratory (AFWAL), McDonnell Douglas, General Electric, and Alphatech<sup>6</sup> in the early 1980's, is their so-called Failure Detection and Isolation (FDI) procedure. This includes a local FDI algorithm to detect actuator failures and a global FDI algorithm to detect surface failures. The global FDI compares the outputs of a nominal system model and the actual aircraft. This error signal is passed through a set of hypothesis-testing filters. The output of each filter represents the statistical likelihood that the failure hypothesized by the filter has occurred. This approach was flight tested on a NASA F-15 and was shown to have "high potential for the concepts evaluated."<sup>7</sup> In the same time period, the Control Reconfigurable Combat Aircraft (CRCA) program, conducted by Grumman, Lear Astronautics, Charles River Analytics, and AFWAL, was using a similar approach.<sup>8</sup> Again banks of Kalman filters operate in parallel and test a predetermined set of failure hypotheses. The CRCA program concluded with piloted simulations and flight tests in which the method performed well, but extensive adjustments were needed throughout the testing. This multiple model approach has the advantage of being able to provide very fast and efficient detection of failures among a set of preplanned conditions. Unfortunately, as the number of hypothesized failures grows, it becomes increasingly difficult to classify

all the possible combinations of failure conditions. This leads to either an unreasonably large set of classifications or an unacceptably large number of gaps in potential failure modes. Also, since failure detection relies on models of the nominal, unfailed system, any differences between the actual system and the nominal system model can result in a false detection of a failure. False alarms are a major difficulty with this method. Despite these difficulties, the basic idea of this method is further developed in recent works and is termed the Multiple Model Adaptive Estimation (MMAE) method<sup>9-12</sup>. MMAE, which encompasses an entire control scheme, has been successfully flight tested on the VISTA/F-16.

Another approach appearing in the current literature for failure detection involves the use of the sliding mode control technique. In particular, a sliding mode observer is designed with either an additive perturbation parameter<sup>13,14</sup> or a multiplicative parameter.<sup>15</sup> This parameter is then adaptively estimated. Using thresholds on this parameter, actuator failures are determined.

Probably the largest reason for the lack of extensive work in fault detection is the fact that many of the adaptive algorithms being proposed do not need it. The algorithms either continually estimate system parameters (and thus automatically “see” a failure) or do not require the parameters explicitly at all. Most current works do not even make mention of fault detection. Those that do require knowledge of a failure event typically assume that this knowledge is provided to them “somehow.”

### **1.3.2 Parameter Estimation**

System parameters are those elements of a dynamic system model which define its dynamic response. In linear state space where  $x \equiv$  state variables,  $u \equiv$  input vector,

and  $y \equiv$  output variables, the system parameters are the components of the  $\mathbf{A}$ ,  $\mathbf{B}$ ,  $\mathbf{C}$ , and  $\mathbf{D}$  matrices, as shown in equation ( 1.1 )

$$\begin{aligned}\dot{x}(t) &= \mathbf{A} x(t) + \mathbf{B} u(t) \\ \dot{y}(t) &= \mathbf{C} x(t) + \mathbf{D} u(t)\end{aligned}\quad ( 1.1 )$$

For aircraft, these components are the stability and control derivatives. System parameters might also be variables in transfer functions (e.g., time constants, damping ratios, natural undamped frequencies, etc.) as in equation ( 1.2 ).

$$\frac{\theta}{-\delta_e}(s) = K_{\theta\delta_e} \frac{(s+1/T_{\theta_1})(s+1/T_{\theta_2})}{(s^2 + 2\zeta_{sp}\omega_{sp}s + \omega_{sp}^2)(s^2 + 2\zeta_{ph}\omega_{ph}s + \omega_{ph}^2)} \quad ( 1.2 )$$

Of course, the actual plant parameters are never known exactly, even with careful modeling. Unmodeled high order dynamics, linearization approximations, rigid body approximations, operating envelope effects, axis coupling, control effector limits, hysteresis effects, and stochastic randomness may all be present in the actual plant. However, the model used for designing the control system can not encompass all these effects perfectly. This is a common problem for all control designers and is addressed by careful attention to modeling the dominant plant dynamics and concerted efforts to ensure controller robustness. A key point in a traditional design problem is that the work of identifying the system parameters is all done off-line. The control algorithm may be required to switch through a schedule of gains, but all these gains are calculated *a priori* based on off-line estimates of the plant parameters.

In a reconfigurable control design, the controller must be able to handle large, sudden, unknown changes to system parameters. These changes greatly exacerbate the design problem. Some adaptive design methods require knowledge of the plant; but

after a system “failure,” the new effective plant is unknown. This leads to the requirement for on-line system parameter identification. There are many parameter estimation techniques in use; however, in reconfigurable control applications, the requirement of the algorithm to run in real time narrows the choices of algorithms to only the most computationally efficient. Some on-line parameter estimation techniques include: Lyapunov design approach, gradient methods (with instantaneous cost functions and integral cost functions), pure least squares, pure least squares with covariance resetting, modified least squares with forgetting factor, gradient methods with projection, least squares with projection, and hybrids.<sup>16</sup> The most common ways of performing on-line system parameter estimation in the current literature include: time domain least squares parameter estimation, frequency domain parameter estimation, reduced-order transfer function estimation, and neural nets. Each of these methods are introduced in the following sections.

All parameter estimation techniques are faced with two difficult problems: noise and data information content.<sup>17</sup> Noise poses a large obstacle in accurate parameter estimation because it is difficult to distinguish between noise and a sudden change in a system parameter. In the time domain, large data records are required and special techniques, like “forgetting factors,” are used. Data information content is an especially prevalent problem in aircraft applications. Aircraft frequently spend large amounts of time in a steady state condition with relatively constant state and control variables. This lack of persistent excitation leads to a lack of information content in the signals used by the parameter estimation algorithm and can cause the calculations to become ill-conditioned. In the most extreme case, if the input signal  $u = 0 \forall t \geq 0$ , it is clear that no

useful information will be available for the identification algorithm. In fact, it is well known that it is *impossible* to establish parameter error convergence to zero without imposing some kind of conditions on the input to the system.<sup>16</sup> Another effect that leads to a lack of information content is data colinearity due to the control system or control allocation routine.<sup>18-21</sup> Unfortunately, when the states and controls are nearly proportional to one another, or if the control deflections are linearly correlated, it is impossible to identify individual stability and control derivatives from the measured data alone.<sup>17,18</sup> These two data content problems--persistent excitation and data colinearity--are major issues in parameter identification.

### 1.3.2.1 Time Domain Least Squares Parameter Estimation

Clearly the most commonly used method for system identification is some variation of a least squares approach in the time domain. There are many references which utilize this approach.<sup>6,19,22-36</sup> The basics are as follows:<sup>37</sup>

Consider  $k = 1 \dots n$  discrete measurements of a scalar signal  $y(k)$ , and a regressor vector  $w(k)$ , where

$$y(k) = w^T(k) \theta \quad (1.3)$$

and  $\theta$  is the vector of unknown parameters to be determined. For a linear system in state space,  $w$  consists of stacked state variables. At time instant  $n$ , a least squares criterion is defined:

$$J[\theta(n)] = \sum_{k=1}^n \left( y(k) - w^T(k) \theta(n) \right)^2 \lambda^{n-k} + \alpha (\theta(n) - \theta(n-1))^2 \quad (1.4)$$

When  $\alpha = 0$  and  $\lambda = 1$ , this is the standard least-squares parameter identification scheme.

The constant  $\lambda$  is the so-called exponential forgetting factor and is often included to

minimize the cumulative effects of noise. When the constant  $\alpha \neq 0$ , variations of the parameter vector  $\theta$  from one time step to the next are penalized. This is an example of one of several common modifications which can be made to the least squares approach. This optimization problem has a well known standard solution which can be given in “batch” form or in regressive form. This formulation is able to follow time-varying parameters and is a popular starting point for most reconfigurable control efforts. The main problem that plagues this approach is the need for persistently exciting input signals. One solution to this is active noise injection, called dithering. This, however, can have undesirable effects upon handling qualities.

### 1.3.2.2 Frequency Domain Parameter Estimation

Another approach is to frame the problem as a least squares error minimization in the frequency domain.<sup>17</sup> This algorithm is typically able to converge to the correct parameter values in less than one period of the dominant dynamic mode. The basics of the technique are as follows.

Take the Fourier transform of the linear, time invariant state space equations to obtain

$$\begin{aligned} j\omega \tilde{\mathbf{x}}(\omega) &= \mathbf{A} \tilde{\mathbf{x}}(\omega) + \mathbf{B} \tilde{\mathbf{u}}(\omega) \\ \tilde{\mathbf{y}}(\omega) &= \mathbf{C} \tilde{\mathbf{x}}(\omega) + \mathbf{D} \tilde{\mathbf{u}}(\omega) \end{aligned} \quad (1.5)$$

where  $\mathbf{A} \in \mathcal{R}^{n \times n}$ ,  $\mathbf{B} \in \mathcal{R}^{n \times m}$ . Next, form the cost function for the  $r^{\text{th}}$  state equation of the vector equation (1.5). This is given in (1.6).

$$J_r = \frac{1}{2} \sum_{k=1}^f \left| j\omega_k \tilde{x}_r(k) - \mathbf{A}_r \tilde{\mathbf{x}}(k) - \mathbf{B} \tilde{\mathbf{u}}(k) \right|^2 \quad (1.6)$$

where  $\mathbf{A}_r$  and  $\mathbf{B}_r$  are the  $r^{\text{th}}$  rows of matrices  $\mathbf{A}$  and  $\mathbf{B}$ ;  $\tilde{x}_r(k)$  is the  $r^{\text{th}}$  element of the vector  $\tilde{\mathbf{x}}$  for frequency  $\omega_k$ ; and  $\tilde{\mathbf{x}}(k)$  and  $\tilde{\mathbf{u}}(k)$  are the Fourier transforms of the state

and control vectors for frequency  $\omega_k$ . These transforms are calculated recursively using the discrete Fourier transform in the following manner,

$$\begin{aligned} X_i(\omega) &= X_{i-1}(\omega) + x_i e^{-j\omega i\Delta t} \\ \tilde{x}_i(\omega) &= X_i \Delta t \end{aligned} \quad (1.7)$$

where  $\Delta t$  is the sampling interval, and  $i\Delta t$  represents the current time at sample  $i$ .

Define the vector of unknown model parameters in the  $r^{\text{th}}$  row as

$$\hat{\theta}_r \equiv [A_{r,1} \quad A_{r,2} \quad \dots \quad A_{r,n} \quad B_{r,1} \quad B_{r,2} \quad \dots \quad B_{r,m}]^T \quad (1.8)$$

Also, define

$$\mathbf{Y} \equiv \begin{bmatrix} j\omega_1 \tilde{x}_r(1) \\ j\omega_2 \tilde{x}_r(2) \\ \vdots \\ j\omega_r \tilde{x}_r(f) \end{bmatrix} \quad \mathbf{X} \equiv \begin{bmatrix} \tilde{x}^T(1) & \tilde{u}^T(1) \\ \tilde{x}^T(2) & \tilde{u}^T(2) \\ \vdots & \vdots \\ \tilde{x}^T(f) & \tilde{u}^T(f) \end{bmatrix} \quad (1.9)$$

Then, the problem can be cast as a standard least squares regression problem with complex data,

$$\mathbf{Y} = \mathbf{X}\theta + \varepsilon \quad (1.10)$$

where  $\varepsilon$  is the complex equation error in the frequency domain. The least squares cost function in equation (1.6) now takes the form

$$J_r = \frac{1}{2} (\mathbf{Y} - \mathbf{X}\hat{\theta})^* (\mathbf{Y} - \mathbf{X}\hat{\theta}) \quad (1.11)$$

Finally, the parameter vector estimate which minimizes this cost function is given by

$$\hat{\theta}_r = [\text{Re}(\mathbf{X}^* \mathbf{X})]^{-1} \text{Re}(\mathbf{X}^* \mathbf{Y}) \quad (1.12)$$

Note that  $\hat{\theta}_r \in \mathfrak{R}^{(n+m) \times f}$ , and equation ( 1.12 ) must be solved for each row of the state vector each time the routine is called. Fortunately, the matrix  $\mathbf{X}^* \mathbf{X}$  is the same for each row, so the inverse  $[\text{Re}(\mathbf{X}^* \mathbf{X})]^{-1} \in \mathfrak{R}^{(n+m) \times (n+m)}$  only needs to be calculated once per pass. The existence of this inverse is not guaranteed, and in fact,  $\text{Re}(\mathbf{X}^* \mathbf{X})$  is nearly singular for the first few time steps due to a lack of information content in the data during the initial seconds.

There are several advantages which make this method attractive:

- Using a carefully chosen limited frequency band for the Fourier transforms restricts the analysis to the band of frequencies where the system dynamics occur. This automatically filters out all unwanted high frequency data due to noise and higher order system dynamics. Also, excluding zero frequency eliminates trim values and measurement biases, so it is not necessary to estimate bias parameters. For aircraft (where the rigid body dynamics typically lie in the band of approximately 0.01-1.5 Hz), the frequency band which seems to work well is 0.1-1.5 Hz.
- The algorithm requires no initial values for the parameters and does not need to be regularized with a priori values or constraints.
- The algorithm is robust to noisy state measurements and data dropouts
- The algorithm does not require persistent input excitation; and it is not upset by intermittent input excitation.
- The algorithm has fixed memory requirements regardless of data record length.

- The method has low computational requirements due to the recursive Fourier transforms and the simplicity of the algorithm.

After trying to duplicate this work,<sup>17</sup> some additional comments about this method are in order. Some of these findings present obstacles which must be overcome if this method is to be used in a reconfigurable control setting

- As with any parameter estimation algorithm, the stability of convergence of the parameter values is highly dependent on the control input excitation signal. This signal must be frequency-rich in order to achieve acceptable results.<sup>38</sup> Inputs such as a step, a sinusoidal doublet, or a series of sine waves with several distinct frequencies, produce reasonable results as long as they excite the dominant system modes. However, more frequency-rich inputs produce better results. Also, the excitation must be of sufficient duration to achieve convergence. Experiments with short, periodic pulses yield very poor results.
- The convergence of the parameter values are also dependent on the range of frequencies chosen for the Fourier transforms. Both the range of frequencies and the fineness of the frequency spacing affect the solution convergence. Since both of these are arbitrary, it is not clear how to select the optimal frequency band and spacing. Experiments show that the frequency range used for an F-16 needs to be completely different than the range used for a DC-8. Unfortunately, simply choosing a wider frequency band is not necessarily the best answer. A wider frequency range increases the computational and memory requirements (for a given bin spacing) and

reduces the accuracy of the algorithm. Low frequency bins tend to “pick up” bias signals. High frequency bins tend to pick up noise and high frequency modes. Ideally, the frequency range chosen should be just large enough to capture the dominant system dynamics being modeled. This could be an interesting task in a reconfigurable control setting where the system dynamics could potentially have modes considerably different than that of the healthy vehicle.

- The algorithm assumes constant system parameters. If a parameter changes suddenly (or gradually) during the estimation process, the algorithm converges to incorrect values. This is because the algorithm has “infinite memory,” by nature of the recursive Fourier transform being used. This problem could be overcome by restarting the recursive Fourier series at given time intervals and assuming the parameters remain constant throughout this time interval. If the Fourier transforms are not reset, the parameter estimates will be some average of the changed and unchanged dynamics, weighted by the information content in the data.
- The algorithm assumes zero initial conditions for the states. Nonzero initial states cause the solution to converge to completely incorrect values. When using relatively low frequency bins (as in the case of aircraft parameter estimation), any constant bias (zero frequency component) in the signal “spills over” into the adjacent frequency bins, thus polluting the frequency domain data used for the parameter estimation. Non-zero initial states appear in the signal as just such a bias. One way to overcome this

difficulty is to subtract a low-pass filtered version of the original signal, leaving only the frequency components to be used for the parameter estimation. The low pass filter introduces a small time lag, but that is not an issue because the value being computed is low frequency in nature.

Overall, this method appears attractive—especially for initial flight test work<sup>39</sup> It is interesting that the infinite memory of the Fourier transforms is both a key strength and a key downfall of the method. For constant parameters, the infinite memory means persistent excitation is not required. Unfortunately, it also means it can not track time-varying parameters in its current form. The initial efforts to modify this method to accommodate varying parameters are somewhat promising; however, there are unresolved implementation issues

### 1.3.2.3 Reduced-Order Transfer Function Estimation

A method which is attractive in a reconfigurable control setting is reduced-order transfer function estimation. Rather than trying to estimate all the parameters for the full system model, a lower order model is assumed and its parameters are estimated. This concept can be incorporated in both the time domain and frequency domain least-squares approaches.<sup>25</sup> Also, a more simplistic ad hoc approach can be applied. For example refer to Figure 1-1. If the system is pulsed with a step input, by measuring outputs like rise time, period, maximum amplitude, response slope, and delay time, it is possible to estimate the parameters in a standard second order transfer function with delay, as in (1.13).

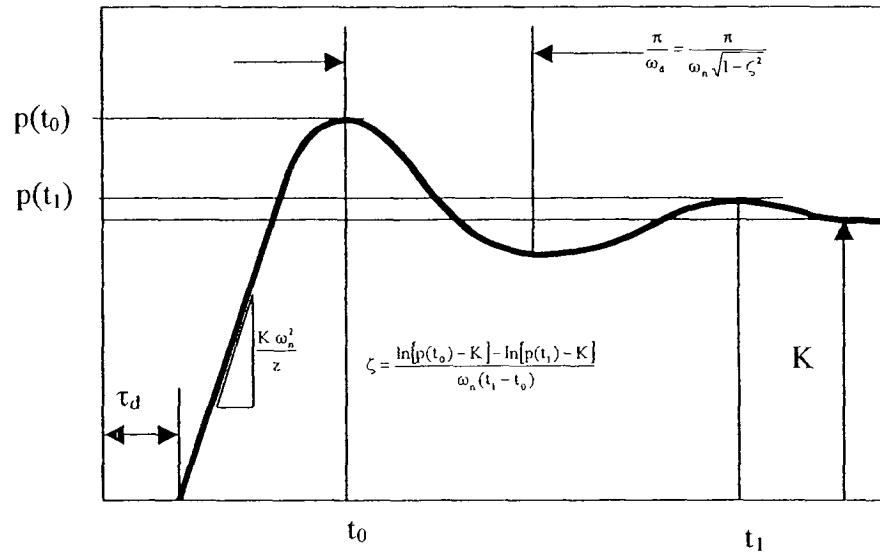


Figure 1-1: Reduced Model Order, ad hoc Approach

$$P(s) = \frac{K \omega_n^2}{z} \cdot \frac{(s+z) e^{-\tau_d s}}{s^2 + 2\zeta \omega_n s + \omega_n^2} \quad (113)$$

This approach is used successfully in several references.<sup>40-43</sup>

#### 1.3.2.4 Neural Nets

Neural nets are receiving a great deal of attention in the current literature and are being used in a hugely diverse range of application types. Even though neural nets are finding their way into a multitude of applications, there seems to be some resistance to their use in systems employing a human operator. This is probably due to at least two factors. First, due to their highly nonlinear structure, stability convergence is often difficult to prove for certain kinds of networks. It is also sometimes difficult to extract the “knowledge base” contained in the net after training and to predict results for cases outside the training set. Second, even though many networks can be proven to model a linear system to any arbitrary degree of accuracy,<sup>44</sup> there is little incentive to favor a neural net over traditional linear control methods for which there is a wealth of theory

and experience. However, in cases where the system is complex and nonlinear, neural nets are finding their place. They appear in the literature dealing with reconfigurable controls due to the inherent nonlinear nature of the problem. Functional link neural nets combined with an adaptive critic algorithm are utilized by Cox *et al.*<sup>45,46</sup> in a system identification/adaptive algorithm scheme. Although not exactly a system parameter identification application, neural nets are also being used successfully to remove the inversion error in dynamic inversion algorithms.<sup>24,34,35,47,48</sup>

### 1.3.2.5 System Identification for Correlated Effectors

Whether a time domain approach or a frequency domain approach is used, correlation of the control effectors is a problem. All approaches utilize some type of regressor matrix which must be inverted. When the control effectors are correlated, there will be collinear columns in the regressor matrix—thus making accurate parameter identification impossible.<sup>18</sup> There are at least two ways the effectors can become correlated

First is feedback control. Feedback control correlates the effectors' displacement with the aerodynamic angles. One way to deal with this problem is to break the parameter identification into two steps. First perform a singular value decomposition on the regressor matrix, remove all small singular values, and estimate the reduced set of parameters. Next, reconstruct the full parameter estimate with some *a priori* knowledge.<sup>18,21,34,49</sup>

A second way control effectors can become correlated is the use of control allocation. Redundant control suites require some means of distributing control demands to the multiple effectors. Unfortunately, almost all common control allocation

schemes result in highly correlated effectors. There are several ways to deal with this problem. First, use the extra degrees of freedom to add decorrelating excitation. For example, when using a pseudo-inverse allocation approach, randomly vary the weighting matrix in the optimization cost function<sup>18,19</sup> (see Eqn ( 1.22 ), pg 34). Another approach is to use *a priori* models in the control allocation and create a reduced set of pseudo-effectors.<sup>19</sup> The control effectiveness matrix for these pseudo-effectors is then identified rather than for the full effector suite. Another alternative is to provide the control allocation algorithm with enough information to compensate for the modeling errors rather than trying to provide the control law with correctly identified parameters.<sup>19</sup>

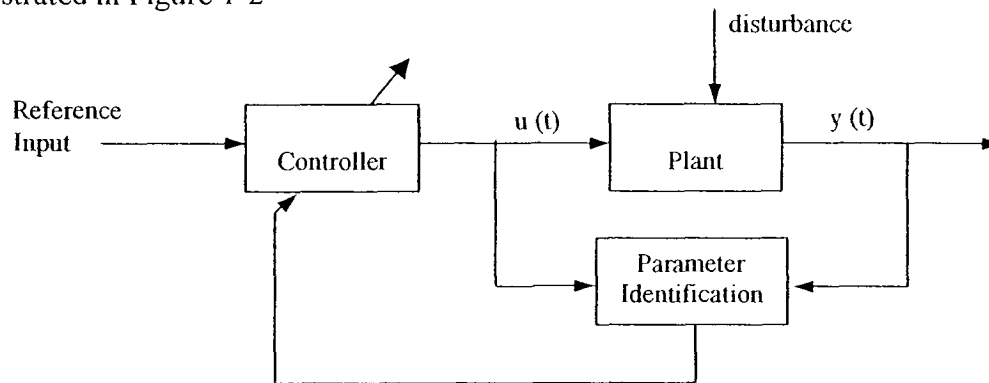
Accurate system identification is a complex problem. Even under the best conditions, identification is difficult and takes time. Then, with the addition of issues like persistent excitation and correlated control effectors, an already difficult problem becomes much worse. System identification, if required by the control law, is a key bottleneck in the reconfigurable control problem.

### 1.3.3 Reconfiguration Control Algorithms

Adaptive control strategies can be loosely grouped into two categories, *indirect* and *direct* adaptive control. In indirect adaptive control, the process/plant model is constructed (usually by means of an on-line observer/parameter estimator), and an appropriate control law is then calculated based on this model. This is also called *explicit* adaptive control<sup>16</sup> because the design depends on an explicit plant model. Direct adaptive control, on the other hand, synthesizes the controller utilizing performance criteria only without the explicit construction of the plant model<sup>44</sup>. This is sometimes called *implicit* adaptive control<sup>16</sup> because the design is based on an estimation of an implicit plant model. These definitions sound straight-forward; however, the distinction between direct and indirect methods can become easily confused. In fact, a direct adaptive scheme can be made to appear identical to an indirect adaptive scheme “by including a block for calculations with an identity transformation between updated parameters and control parameters. In general, for a given plant model, the distinction between the direct and indirect approach [only] becomes clear if we go into the details of design and analysis.”<sup>16</sup> There are several works which compare different adaptive schemes. Bodson *et al.*<sup>22,50</sup> compare three model reference adaptive schemes: 1) Indirect method, 2) Direct method based on output error; and 3) Direct method based on input error. They provide a nice comparison, but draw no strong conclusions. In a later paper, Bodson *et al.*<sup>23</sup> compare four adaptive schemes in light of actuator saturation. Steinberg<sup>31</sup> compares seven different non-linear adaptive control laws. Again this work provides a good top level overview of the methods, but makes no strong conclusions.

### 1.3.3.1 Indirect Adaptive

While the indirect controller may appear to be more complex, it does allow some separation between the system parameter estimation and the controller synthesis (the certainty-equivalence principle).<sup>44</sup> The overall concept of an indirect control scheme is illustrated in Figure 1-2



**Figure 1-2: Indirect Adaptive Controller**

Two indirect methods which receive the most attention in the literature are receding horizon optimal control (RHO) and multiple model estimation. Eberhardt *et al.* use a RHO controller on the Innovative Control Effector (ICE) aircraft combined with a least squares parameter ID algorithm utilizing a lower order equivalent system flying qualities model.<sup>19,25</sup> Pachter *et al.* use a RHO controller with a one-step-ahead actuator rate constraint enforcement.<sup>29</sup> RHO control with a modified least squares parameter ID is also demonstrated on an F-16/MATV.<sup>3</sup> In Ward *et al.*<sup>33</sup>, a RHO controller with least squares parameter ID is used in an inner loop, and a polynomial neural net is used for an outer loop shipboard landing task of an unmanned airvehicle. Maybeck *et al.* use the method of Multiple Model Adaptive Estimation (MMAE).<sup>10,12</sup> Adaptation occurs via a control redistribution, and the parameter estimates are provided by the MMAE algorithms. Napolitano *et al.*<sup>51</sup> also use multiple Kalman filters to estimate the model of

the damaged aircraft and use these results in an adaptive control law. Boškovic *et al.*<sup>52</sup> recast the aircraft model in terms of a damage parameter. They then use multiple observers to estimate this damage parameter. The control law involves multiple reference models and output feedback. Other examples of indirect control methods are model reference adaptive controllers,<sup>53,54</sup> and a simple adaptive PID controller with modified least square parameter ID.<sup>37</sup> Another interesting approach is to form a multiple objective cost function which includes optimal control and parameter identification in a single cost function.<sup>55</sup> Since parameter identification and control performance are competing objectives, this approach allows a direct tradeoff between the two. Rather than performing continuous parameter identification, one method proposes taking the pilot out of the control loop, inputting control steps/doublets, and estimating lower order plant models.<sup>41,42</sup> This model is then used in an adaptive multi-loop scheme with inner loop linear dynamic inversion and outer loop quantitative feedback control.

### 1.3.3.2 Direct Adaptive

Direct adaptive methods almost always include some form of model reference following as illustrated in Figure 1-3.

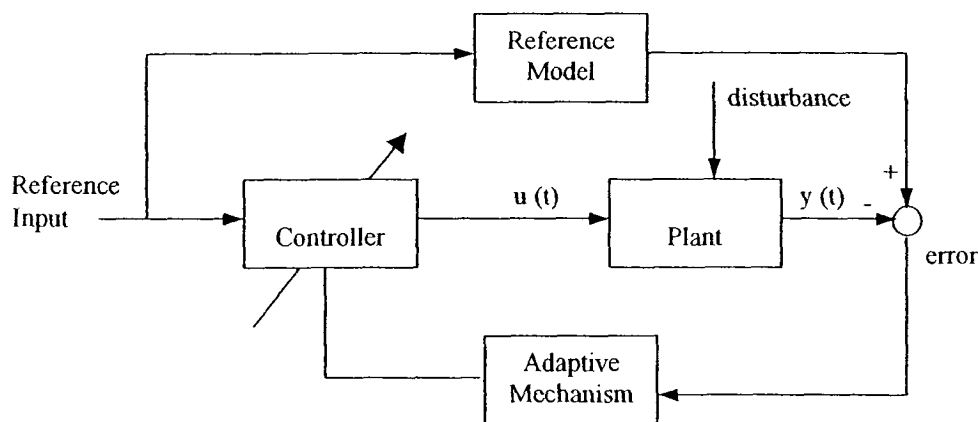


Figure 1-3: Model Reference Adaptive Control System

There are, in general, four elements in the MRAC system.<sup>44</sup>

- The plant, which may be nonlinear, time-varying, with unknown parameters.
- The reference model, which is usually a lower order linear dynamic model which generates a desired closed-loop system output response
- A controller with time-varying components.
- Some type of adaptive algorithm which adjusts the controller based on the error between the model reference outputs and the actual plant outputs.

One of the direct methods that has dominated the literature is the method of dynamic inversion (DI). As the name implies, the controller attempts to invert the plant in order to cancel its dynamics and then replace these dynamics with those of a reference model. There are several successful examples of this approach. Dynamic inversion with a neural net to regulate the inversion error is demonstrated on the Tailless Advanced Fighter Aircraft (TAFA) for the RESTORE program.<sup>24</sup> This approach was successfully tested with full piloted simulations.<sup>35</sup> Others have also demonstrated DI with neural nets to remove the inversion error.<sup>34,47,48</sup> Bacon *et al.*<sup>56</sup> employ non-linear dynamic inversion using acceleration and position feedback. Another example of a direct adaptive method is an approach called backstepping. Several works utilize this method.<sup>57,58</sup> Ferrara *et al.*<sup>59</sup> use a classical backstepping approach for the first (n-1) steps, and then use a second order sliding mode controller to find the control for the n<sup>th</sup> step. Other approaches include decentralized adaptive neuro-fuzzy design,<sup>60</sup> an adaptive proportional plus integral control for the AFTI/F-16 with gain adjustment based on errors between the model reference and actual output,<sup>61</sup> and a structured model reference adaptive technique in which the kinematic differential equations are assumed to be

known exactly--which reduces the amount of uncertainty for which adaptation is required.<sup>62</sup> Finally, a method which is receiving notable attention is the method of sliding mode control (SMC). Shtessel *et al.* demonstrate a multi-loop application of SMC on an F-16<sup>63-65</sup> and the ICE aircraft.<sup>66</sup> This method provides some of the best tracking results of any of the other works, and it does so without any parameter identification. Actuator limits are handled by adaptively varying the sliding surface boundary layer. Sliding mode control is well known for being very robust (in fact, invariant) to certain kinds of uncertainty. This makes it a very attractive choice for a reconfigurable control problem.

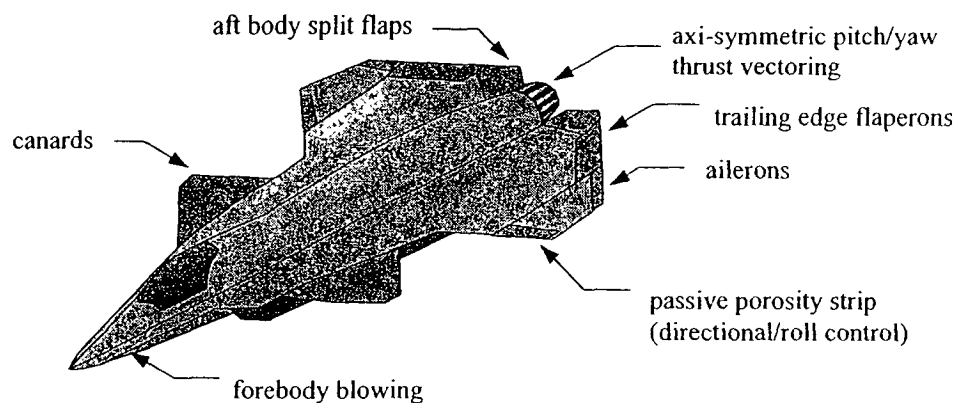
### 1.3.3.3 Others

There are other schemes which address adaptation to large system failures but do not fit well in either a direct or indirect adaptive category. For example, Burken<sup>2</sup> proposes an emergency augmentation system for an MD-11 transport. A control law which utilizes asymmetric thrust capability is designed off-line. If the aircraft experiences control actuator failure, the pilot turns on the emergency control augmentation system. In another work<sup>67</sup>, Burken *et al.* examine two methods as applied to the X-33. In the first method, system failures are modeled as disturbances, and an LQR controller is designed to handle these disturbances. No reconfiguration takes place—it is simply a robust design. In the second method, reconfiguration is accomplished by a quadratic programming control reallocation and a nominal control law based on the healthy system. Lyshevski<sup>68</sup> presents a robust control law based on dynamic programming and Lyapunov to handle system failures. Again no active reconfiguration takes place.

### 1.3.4 Control Allocation

A conventional aircraft creates moments about its three axes via three control effectors: elevator, ailerons, and rudder. While the ailerons and rudder do not create strictly decoupled moments, the three conventional control effectors can sometimes be loosely considered decoupled for design purposes. Control allocation for this kind of configuration is not an issue. A pitch moment is created exclusively by the elevator; a roll moment by the ailerons; and a yaw moment by the rudder. If the coupling of the ailerons and rudder is not negligible, the control allocation problem becomes one of scheduling the ailerons and rudder such that a decoupled moment is generated (e.i. roll moment without yaw). This is traditionally accomplished mechanically by the use of aileron-rudder interconnects.<sup>69</sup>

With the advent of sophisticated, highly unconventional aircraft with a large suite of coupled control effectors, the problem of control allocation has become a significant design issue. The aircraft shown in Figure 1-4 is a conceptual design for which considerable work is currently being done in the literature.<sup>24,30,34,35,47,52,70</sup> Note the multiple, coupled control effectors available to generate moments.



**Figure 1-4: Boeing Tailless Advanced Fighter Aircraft**

In order to create a desired moment about a given axis with an unconventional design, the moment demand must be divided up among several control effectors according to some control allocation scheme. Of course, issues like relative control power, preferred-positions, and rate and position saturation must all be considered. Control allocation often becomes an issue in reconfigurable control applications because it is often a control effector which is assumed to be failed or degraded. This, then, can necessitate an on-line re-allocation of the controls. Also, highly redundant control effector suites are typically assumed in reconfigurable applications because some level of control redundancy is required in order control the aircraft after a failure

In general, the problem to be solved in control allocation is the following:

$$\mathbf{B} u = m_d \quad (1.14)$$

where  $\mathbf{B}$  is the  $\mathcal{R}^{n \times m}$  control power derivative matrix,  $m_d$  is the desired moment vector, and  $u$  is the control vector for which a solution is sought<sup>4</sup>. Since control allocation is used for systems with multiple control effectors, it is assumed that the dimension of  $u$  is greater than the dimension of  $m_d$ . Note, the “moments” in the moment vector need not all be actual moments in this context. It is understood, without loss of generality, that “moments” are taken to mean “the desired control effect.” In the unconstrained case, Equation (1.14) has, in general, an infinite number of solutions. However, when control constraints (position and rate limits) are considered, there may exist a unique solution, no solution, or an infinite number of solutions. The determination of the control vector  $u$ , given the desired moment, is the linear control allocation problem

Control allocation is, by itself, a large and challenging field of interest and is receiving considerable attention in the literature. Several of the most common

---

*Chapter 1: Overview* *1.3 Overview of Reconfigurable Flight Control*

approaches are: ganging, direct allocation, linear and quadratic programming, pseudo-inverse, cascaded generalized inverse, and daisy chaining. Each of these, as well as some of their variants, are introduced below.

#### 1.3.4.1 Ganging

The simplest control allocation is a static scheme. The controls are “ganged” together by some predetermined static distribution matrix. Due to its simplicity, this scheme is often used when the main focus of the research is the demonstration of some control law. The weights in the allocation can be somewhat arbitrary, although certain actuators can be favored for some given reason. This method does not optimize any dynamic cost function and can not span the entire attainable moment space. However, its simplicity makes it an attractive approach in many instances. There are a number of examples of recent works which use ganged controls.<sup>27,28,40,41,47,48,61,71,72</sup>

#### 1.3.4.2 Direct Allocation (Attainable Moment Subset)

The Direct Allocation method is based on the Attainable Moment Subset (AMS)--the set of all “moments” which can be produced by a set of control effectors constrained to move within their given limits,  $u_{i_{\min}} \leq u_i \leq u_{i_{\max}}$ .<sup>69</sup> Note that this is a position limit and does not account for rate limits. The AMS is found by mapping the  $m$ -dimensional control space into the desired moment space. For the 3-moment problem, Durham<sup>69,73</sup> gives a geometric interpretation of this subspace as a 3-dimensional closed surface polytope with vertices, edges, faces, and facets. There are  $2^{m-2}m![2!(m-2)!]$  facets in the control space. Since most of these facets map to the interior of the AMS, only  $m(m-1)$  facets lie on the exterior boundary. Each facet is a parallelogram with four corners called vertices and four sides called edges. There are  $m(m-1)+2$  vertices in the AMS.<sup>74</sup>

First, the AMS must be calculated for the given system. Then, the solution on the boundary of the AMS is found in the direction of the desired moment. This represents the maximum attainable moment in the given direction, and the associated control vector is given the designation  $u_d^*$ . If the desired moment lies within the AMS, the desired moment is *attainable*, and the control vector  $u_d$  is found by scaling the boundary solution down while preserving the desired direction, according to

$$u_d = u_d^* \frac{|m_d|}{a} \quad (1.15)$$

where “a” is found by solving equation (1.16).<sup>73</sup> If the desired moment lies outside the AMS, the desired moment is *unattainable*. Note that since this method defines the entire attainable moment space, if the moment lies outside the AMS, it is unattainable by *any* allocation method within the given control effector constraints. Solutions that do not violate effector constraints are called *admissible*; solutions that do violate effector constraints are called *inadmissible*. If the solution turns out to be inadmissible, the solution is taken on the boundary of the AMS in the desired direction. This method turns out to be computationally intensive due to the difficulty of finding the AMS boundary solution. Because of this, there are a few different approaches to the actual application of this method. Three are introduced here.

#### 1.3.4.2.1 Sequential Facet Search

The most difficult part of the Direct Allocation method is identifying the point of intersection of a line in the direction of the desired moment with the bounding surface of the AMS. The brute force way to find this intersection is the sequential facet search. A

facet is defined by three vectors,  $m_i^*$ ,  $m_{i-j}^*$ , and  $m_{i-k}^*$ . At the intersection of a facet with a line in the direction of the desired moment,  $m_d$ , the simple vector equation is:

$$a m_d = m_i^* + b m_{i-j}^* + c m_{i-k}^*$$

or

$$m_d = \begin{bmatrix} m_i^* & m_{i-j}^* & m_{i-k}^* \end{bmatrix} \begin{bmatrix} \frac{1}{a} \\ \frac{b}{a} \\ \frac{c}{a} \end{bmatrix} \quad (1.16)$$

During the process of identifying all the facets on the AMS, the solutions of  $\begin{bmatrix} m_i^* & m_{i-j}^* & m_{i-k}^* \end{bmatrix}^{-1}$  are calculated and stored for each facet. Then, the values of  $a$ ,  $b$ , and  $c$  can be evaluated for a given  $m_d$ . A candidate facet is then selected and tested to see if it intersects the line in the desired direction. If it does, it will satisfy the conditions<sup>73</sup>

$$a > 0, \quad 0 \leq b \leq 1, \quad 0 \leq c \leq 1 \quad (1.17)$$

If the candidate facet is not the correct one, the next one is checked, and so on. Unfortunately, this search can be unreasonably large. For example, with 20 controls, there are almost 50 million facets in the subset of constrained controls.<sup>75</sup> Of course, the search for the correct facet is narrowed considerably if done in a selective manner. Durham offers a more efficient algorithm<sup>75</sup> to perform the facet search. It is considerably better than sequential searching from a random location, but it is still computationally cost prohibitive for real time on-line implementation.

#### 1.3.4.2.2 Edge-Bisecting Facet Search

Recently, Durham presented another more efficient method for locating the desired facet.<sup>76</sup> In this method, the AMS subset is first transformed such that the direction of the desired moment is aligned with the x-axis. The edge of the 2-dimensional figure that crosses the x-axis is identified and its z-component is calculated. The polytope is then rotated about the x-axis and another edge is identified. This is repeated until the z-component of the identified edge changes sign. The last two edges identified (one “behind” the x-axis and one “in front” of it) are candidates for defining the desired facet. The facet is tested according to the conditions in ( 1.16 ) and ( 1.17 ). If the facet is the correct one, the problem is solved. If not, the direction of rotation is reversed and a smaller rotation angle is used. This process is repeated until the correct facet is identified.<sup>76</sup> This method of bisecting edge searching results in computational requirements on par with other control allocation methods currently in use. The number of computations increase roughly linearly with the number of controls (as in other methods), whereas the sequential facet search computations increase roughly quadratically.<sup>76</sup>

#### 1.3.4.2.3 Spherical Coordinate Transformations

Peterson and Bodson present two options for finding the correct facet based on a spherical coordinate transformation.<sup>74</sup> The first option requires more on-line calculations but requires less memory. The second option eliminates virtually all on-line computations but requires a significant amount of memory. The spherical coordinate transformation effectively turns the AMS into a 2-dimensional system, where special techniques can be used to accelerate the search. Each option is comprised of off-line and

on-line computations. In Option 1, ranges are computed for the coordinates of the facets (in spherical coordinates) off-line. These ranges define search boxes in which the facets are located. These boxes are used on-line to quickly assess whether the desired moment is likely to lie within a given facet. If the test is successful, the facet is found quickly and the solution is obtained. Option 2 makes use of a lookup table. The azimuth and elevation angles are quantized and facet numbers are associated with a given pair of spherical coordinates. The creation of the table is performed off-line. The size of the table can easily reach  $1 \times 10^6$  elements, depending on the fineness of the quantization. The on-line computations to find the correct facet then consist of converting the desired moment into spherical coordinates followed by a simple table lookup. This guarantees a known fixed amount of time to locate the desired facet.<sup>74</sup> Both methods offer considerable computational improvements over the sequential search of facets based on Durham's 3D tests. An interesting note, however, is that although the spherical coordinate table lookup method provides very fast on-line performance, it is completely unsuitable for a reconfigurable control setting. If a control effector fails or is degraded, the entire lookup table would need to be recalculated. Since this is a large off-line task, it is not a reasonable candidate for used in an adaptive environment.

#### **1.3.4.3 Linear Programming**

Page and Steinberg<sup>4</sup> provide an excellent summary of the Linear Programming approach. This summary is duplicated below. The Linear Programming method has two steps. First, the following linear program is solved,

$$\begin{aligned} \min_{\mathbf{u}} J &= \mathbf{W}_d^T \mathbf{u}_s \\ \text{subject to} \quad & \begin{bmatrix} \mathbf{u}_s \\ -\mathbf{u} \\ \mathbf{u} \\ -\mathbf{B}\mathbf{u} + \mathbf{u}_s \\ \mathbf{B}\mathbf{u} + \mathbf{u}_s \end{bmatrix} \geq \begin{bmatrix} 0 \\ -u_{\max} \\ u_{\min} \\ -m_d \\ m_d \end{bmatrix} \end{aligned} \quad (1.18)$$

where  $\mathbf{u}_s$  is a vector of slack variables, and  $\mathbf{W}_d$  is a positive weighting vector. If  $J > 0$ , the desired moment is unattainable and the solution (denoted  $\mathbf{u}^*$ ) is that which minimizes the weighted 1-norm distance between  $\mathbf{B}\mathbf{u}^*$  and  $m_d$ . If the solution to equation (1.18) yields  $J = 0$ , then the desired moment is attainable and a second linear program is solved:

$$\begin{aligned} \min_{\mathbf{u}} J &= \mathbf{W}_u^T \mathbf{u}_s \\ \text{subject to} \quad & \begin{bmatrix} \mathbf{u}_s \\ -\mathbf{u} \\ \mathbf{u} \\ -\mathbf{u} + \mathbf{u}_s \\ \mathbf{u} + \mathbf{u}_s \end{bmatrix} \geq \begin{bmatrix} 0 \\ -u_{\max} \\ u_{\min} \\ -u_{\text{pref}} \\ u_{\text{pref}} \end{bmatrix} \\ & \mathbf{B}\mathbf{u} = m_d \end{aligned} \quad (1.19)$$

where  $\mathbf{u}_s$  is again a vector of slack variables,  $\mathbf{W}_u$  is a positive weighting vector, and  $\mathbf{u}_{\text{pref}}$  is a vector of control preferences. In this case, the weighted 1-norm distance between the control vector solution ( $\mathbf{u}^*$ ) and the control preference vector ( $\mathbf{u}_{\text{pref}}$ ) is minimized. There are a number of examples of works which use this method.<sup>4,18,77-79</sup>

#### 1.3.4.4 Quadratic Programming

The Quadratic Programming method is similar to the Linear Programming method, except it has a quadratic cost function. Again, it is a two step process.<sup>4</sup> First, the equation

$$\min_u J = \frac{1}{2} (\mathbf{B}u - m_d)^T \mathbf{W}_d (\mathbf{B}u - m_d) \quad (1.20)$$

$$\text{subject to } u_{\min} \leq u \leq u_{\max}$$

is solved, where  $\mathbf{W}_d$  is a positive definite symmetric weighting matrix. If  $J > 0$ , the desired moment is unattainable and the solution (denoted  $u^*$ ) is that which minimizes the weighted 2-norm distance between  $\mathbf{B}u^*$  and  $m_d$ . If the solution of equation (1.20) yields  $J = 0$ , the desired moment is attainable and a second quadratic program is solved:

$$\min_u J = \frac{1}{2} (u - u_{\text{pref}})^T \mathbf{W}_u (u - u_{\text{pref}}) \quad (1.21)$$

$$\text{subject to } u_{\min} \leq u \leq u_{\max}$$

$$\mathbf{B}u = m_d$$

where  $\mathbf{W}_u$  is a positive definite symmetric weighting matrix. In this case, the weighted 2-norm distance between the control vector solution ( $u^*$ ) and the control preference vector ( $u_{\text{pref}}$ ) is minimized. There are a number of works which use this method.<sup>4,34,66,67,70</sup>

#### 1.3.4.5 Pseudo-Inverse

There are several variants of the Pseudo-Inverse. In each, the basic idea is to minimize the same quadratic cost function that the Quadratic Programming solved.<sup>4</sup>

$$\min_u J = \frac{1}{2} (u - u_{\text{pref}})^T \mathbf{W}_u (u - u_{\text{pref}}) \quad (1.22)$$

$$\text{subject to } \mathbf{B}u = m_d$$

Note that this is posed with no limits on  $u$ . With  $-\infty \leq u \leq \infty$ , the solution to (1.22) is

$$u = u_{\text{pref}} + \mathbf{W}_u^{-1} \mathbf{B}^T (\mathbf{B} \mathbf{W}_u^{-1} \mathbf{B}^T)^{-1} (m_d - \mathbf{B} u_{\text{pref}}) \quad (1.23)$$

This solution is a biased weighted pseudo-inverse, for which it gets its name. For the special case of identity weighting ( $\mathbf{W}_u = \mathbf{I}$ ), this is referred to as the *Pseudo-Inverse* method. With constraints on the control effectors, equation (1.23) may produce an inadmissible solution. There are two common ways of dealing with the saturated actuators. First, only the individual commands that have violated the given constraints are scaled down so each is at its corresponding limit. Note that this individual clipping does not preserve the direction of desired moment. The second method works to preserve the direction of the resulting moment by scaling all commands by a single factor until no constraints are violated by any effector. This method is called the *Direction Preserving Weighted Pseudo-Inverse* method. There are a number of works which use some variant of the pseudo-inverse allocation.<sup>4,5,19,21,24,25,35,76,80-83</sup>

#### 1.3.4.6 Cascaded Generalized Inverse

This approach is similar to the Weighted Pseudo-Inverse except in the way it handles violations of effector constraints. If an actuator command reaches its limit, it is set to its limit, its effect is subtracted from the desired moment, and it is removed from the problem--which is then solved again.<sup>4</sup> This cascading process is repeated until 1) no new controls saturate (the desired moment is attainable); 2) all remaining controls

saturate (the desired moment is unattainable); or 3) fewer controls remain than the number of desired moments. When (3) occurs, the left pseudo-inverse solution is used

$$u = (\mathbf{B}^T \mathbf{B})^{-1} \mathbf{B}^T m_d \quad (1.24)$$

There are several examples of works which use this method.<sup>4,76,84</sup>

#### 1.3.4.7 Daisy Chaining

In the Daisy Chaining method, the available controls are separated into two or more groups. In order to meet the demand of the desired moment, one group is activated while the others remain constant. If any elements of the operating group reach their limits, that group of controls are held at their last position and the next group of controls are activated.<sup>69</sup> At first glance, this approach sounds similar to the Cascaded General Inverse, but it is different in that entire groups of controls may remain completely unused when daisy chained. As an example, consider two groups of controls: three aerodynamic controls,  $u_1$ ; and three thrust vectoring controls,  $u_2$ . The control effectiveness matrix is then partitioned into two 3x3 matrices,  $\mathbf{B}_1$  and  $\mathbf{B}_2$ .

$$\mathbf{B}u = [\mathbf{B}_1 \quad \mathbf{B}_2] \begin{bmatrix} u_1 \\ u_2 \end{bmatrix} = \mathbf{B}_1 u_1 + \mathbf{B}_2 u_2 \quad (1.25)$$

Since in this application,  $\mathbf{B}_1$  and  $\mathbf{B}_2$  are square and assumed to be invertible by design, their inverses are unique. For a given desired moment, the aerodynamic controls will be used first until the point of saturation. That is, while  $u_{1_{\min}} \leq u_1 \leq u_{1_{\max}}$ ,

$$u_1 = \mathbf{B}_1^{-1} m_d \quad u_2 = 0 \quad (1.26)$$

If any of the aerodynamic controls reach their limit, the group of aerodynamic controls are held at that position ( $u_{1(\text{sat})}$ ), and the thrust vectoring controls are brought on-line.

$$u_1 = u_{1(\text{sat})} \quad u_2 = \mathbf{B}_2^{-1} (m_d - \mathbf{B}_1 u_{1(\text{sat})}) \quad (127)$$

A notable problem arises in the Daisy Chaining method when control deflection rates are considered. “Cooperative control efforts are those in which all available controls are simultaneously varied to meet a time-varying demand. The total rate of change of the moment produced is a linear combination of the individual control rates. For a given rate of change of the required moment, in magnitude and/or direction, a cooperative effort among all available controls will require lower individual control rates than will a noncooperative effort. Daisy chaining is a noncooperative allocation scheme and potentially will command unattainable deflection rates that would not be commanded by cooperative control allocation methods.”<sup>69</sup> There are several examples of works which use this method.<sup>69,85-87</sup>

#### 1.3.4.8 Discrete Time Methods

As introduced above, all the methods account for position limit constraints on the control effectors. They do not, however, account for rate limits. Rate limits are typically incorporated within a discrete time framework by considering how far an effector can travel within a single time step.<sup>4</sup> Therefore, the control effectors are constrained by:

$$\Delta u_{\min} \leq \Delta u \leq \Delta u_{\max}$$

where

$$\begin{aligned}\Delta u_{\min} &= \max\left[\dot{u}_{\max}^- \Delta t, (u_{\min} - u_k)\right] \\ \Delta u_{\max} &= \min\left[\dot{u}_{\max}^+ \Delta t, (u_{\max} - u_k)\right]\end{aligned}\quad (1.28)$$

and  $\Delta t = t_{k+1} - t_k$ ;  $\Delta u = u_{k+1} - u_k$ ;  $u_{\min}$  and  $u_{\max}$  are effector position limits; and  $\dot{u}_{\max}^-$  and  $\dot{u}_{\max}^+$  are the negative and positive effector rate limits. Each of the control allocation methods discussed above can be modified to include these discrete time effector rate constraints.

#### 1.3.4.9 Control Allocation Performance Measures

Much of the early comparisons between the different control allocation methods involve an evaluation of the ability of the allocation method to reach 100% of the volume of the Attainable Moment Subset. Bordignon and Durham<sup>87</sup> offer methods to compute the volume of the AMS reachable by different allocation schemes. They show that, while the Direct Allocation method can access 100% of the AMS, the pseudo-inverse methods can only access 13-42% of the AMS, and daisy chaining only reaches about 22%. They conclude that the Direct Allocation method must be superior since it can achieve moments the other methods can not. This seems to be a reasonable conclusion; however, recent studies show otherwise. Page and Steinberg<sup>5</sup> ran several different control law designs with four different control allocation schemes in order to investigate potential adverse interactions between the control laws and the control allocation algorithms. They conclude that “the choice of control allocation technique can have a dramatic impact on system performance.” They show by example that unexpected interactions with the Direct Allocation method (which produces admissible solutions for 100% of the AMS) occur in some cases which drive the effectors to

saturation and greatly degrade the system performance. For these same cases, the Weighted Pseudo-Inverse technique (which produces admissible solutions for only 10% of the attainable moment subset), did not cause saturation, and performed very well. One conclusion of their work is that it is important to integrate the control allocation effort with the adaptive control laws because unexpected interactions can occur. A follow-on study compares the open-loop and closed-loop performance of sixteen different control allocation methods using a single dynamic inversion control law<sup>4</sup>. It shows that because the allocation approach is generally designed to meet an instantaneous moment demand and not to optimize any closed-loop properties over time, the open-loop measures of control allocation performance do not necessarily translate to closed-loop performance. The Direct Allocation method again did not perform as well as might be expected and the Discrete Time Weighted Pseudo-Inverse method provided the best closed-loop tracking performance for the application investigated.

## 1.4 Literature Summary

Section 1.3 has attempted to summarize the varied approaches to reconfigurable control system design that are described in the literature. It is obvious that the requirements of failure detection, failure isolation, system identification, and control law reconfiguration present significant challenges to the control engineer and to the practical implementation of a reconfigurable flight control system. It is particularly evident that most, if not all, of the approaches reviewed require varying amounts of time to reach a “reconfigured” state. With the advent of modern combat aircraft with highly unstable unaugmented dynamics, this reconfiguration time can become a critical issue in the viability of the design approach. Of all the works reviewed, those which utilize sliding mode control appear to have the most promising results. In these works, the tracking performance after failure is impressive; there is no reconfiguration time at all, and no parameter identification is required. For these reasons, sliding mode methods are selected for investigation for their applicability to the design and implementation of a practical reconfigurable control system.

# Chapter 2

---

## Sliding Mode Control

### 2.1 Introduction to Sliding Mode Control

Of all the reconfigurable control schemes appearing in the current literature, those based on the concept of sliding modes appear to be the most promising. While results from many of the other reconfigurable control methods are very good (the aircraft remains stable, and tracking performance, while degraded, ranges from acceptable to very good), the recent works utilizing sliding mode control (SMC) show no performance degradation at all<sup>63,64,66</sup>. This is because these controllers are invariant to matched uncertainty/disturbances. If the controller is invariant to certain system parameter changes, there is no need to perform system failure detection or parameter identification. Since parameter identification is the main bottleneck in control reconfiguration, employing a controller that does not require it provides a large advantage. Not only this, but its variable structure allows SMC to adapt to parameter disturbances “instantaneously.” An ideal sliding mode controller with no parasitic dynamics or actuator limits easily handles noise, parameter changes, and unmodeled nonlinearities with absolutely no degradation in tracking performance. However, since real systems always have parasitic dynamics and actuator limits, the actual implementation of an SMC design becomes challenging. The general concepts of sliding mode control, including basic theory, properties, design techniques, implementation difficulties, and several examples are offered this chapter.

### 2.1.1 Sliding Mode Control History

The basic concepts of sliding mode control first appeared in the Russian literature in the early 1930's. Kulebakin (1932) used essentially a sliding mode controller in the context of voltage control for a DC generator on an aircraft. He called it "vibration control" of the voltage signal. Nikolski (1934) proposed sliding mode relays for controlling the course of a ship. He actually used many of the terms currently in use today, including phase plane, switching line, and sliding mode.<sup>88</sup> Emelyanov and Barbashin continued the pioneering work in Russia in the early 1960's. It wasn't until the mid 1970's that the ideas of sliding modes appeared outside Russia when a text by Itkis<sup>89</sup> and a survey paper by Utkin<sup>90</sup> were published in English.<sup>91</sup> Vladimir Utkin is one of the key figures who championed the concepts of sliding modes through the 1970's and 1980's, and continues to publish numerous works in the area. The 1980's saw a large increase in interest in SMC including several often-cited survey works<sup>92-94</sup> Several newer survey works<sup>95-97</sup> are also regularly cited. Utkin has several texts on the subject.<sup>88,98</sup> Slotine includes a chapter in his text on non-linear control,<sup>99</sup> and Edwards & Spurgeon have a recent text<sup>91</sup> devoted entirely to SMC. Applications of SMC in the literature are too numerous to list. By 1993, general application areas included: robotic control, motor control, aircraft and spacecraft control, flexible structure control, load frequency control of power systems, servomechanisms, pulse-width modulation control, guidance, process control, phase-locked loop control, power converters, and remote vehicle control.<sup>95</sup> Sliding mode controllers are even being used for controlling the convergence rates for neural net learning algorithms.<sup>100</sup> Other interesting applications which have appeared in very recent works include: direct robust exact differentiation,<sup>101</sup>

large-scale, time-delay systems;<sup>102</sup> missile autopilot;<sup>103</sup> multiple unmanned air vehicles in close-formation flight,<sup>104,105</sup> and of course, reconfigurable flight control.<sup>31,63-66,106</sup>

### 2.1.2 Concept of the Sliding Mode

Sliding mode controllers are a subset of a class of controllers known as Variable Structure Controls (VSC)--although the terms are often used interchangeably. VSC systems are characterized by a control structure that changes according to some predefined rule which is a function of the states of the system. In order to illustrate this concept, consider the double integrator in equation ( 2.1 ) with a feedback control law in equation ( 2.2 ). See Edwards & Spurgeon<sup>91</sup> for much of the following development

$$\ddot{y}(t) = u(t) \quad (2.1)$$

$$u(t) = -k y(t) \quad (2.2)$$

This results in a pure undamped harmonic motion as shown in Figure 2-1 with  $\dot{y}(0) = 0$ ,  $y(0) = 1$ , and  $k = 4$ . The phase plane portrait of this system is shown in Figure 2-2. Obviously, this control law would not be appropriate for this system since the state variables do not move toward the origin for any value of gain chosen. The gain only changes the orientation and eccentricity of the ellipse in the phase plane.

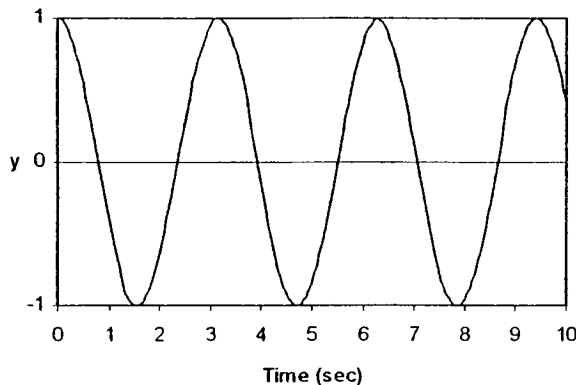


Figure 2-1: Time History of Oscillator

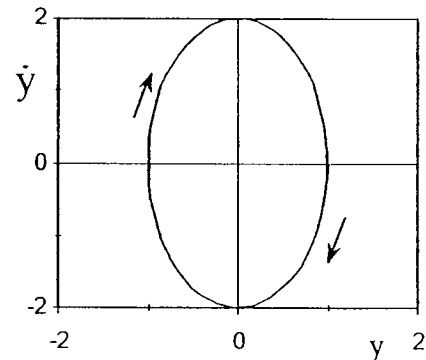
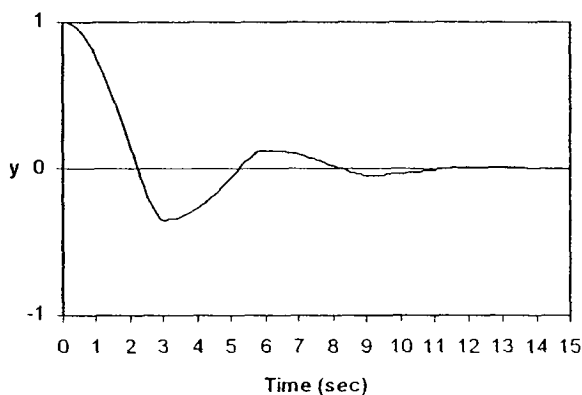


Figure 2-2: Phase Plane Plot of Oscillator

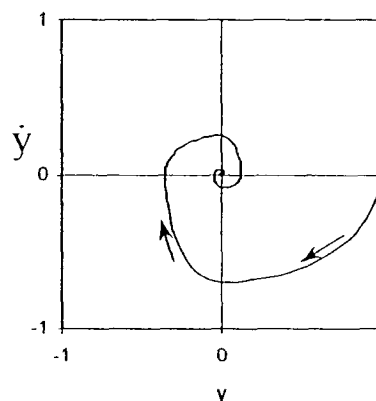
Consider, instead, a Variable Structure Control law as shown in ( 2.3 ).

$$u(t) = \begin{cases} -k_1 y(t) & \text{if } y\dot{y} < 0 \\ -k_2 y(t) & \text{otherwise} \end{cases} \quad (2.3)$$

This causes the control law to change depending on the quadrant of the phase plane in which the state variables are moving. When in quadrants 1 & 3, the gain is  $k_1$ ; when in quadrants 2 & 4, the gain is  $k_2$ . The resulting motion, for  $\dot{y}(0) = 0$ ,  $y(0) = 1$ ,  $k_1 = 0.5$ ,  $k_2 = 4$ , is shown in Figure 2-3 and Figure 2-4.



**Figure 2-3: Time History of VSC System**



**Figure 2-4: Phase Plane Plot of VSC System**

This simple example shows that by introducing a rule for switching between two control structures, a stable closed-loop system can be obtained. This occurs even though neither of the two control structures individually are able to provide convergence of the state variables to zero.

Next, instead of using the phase plane quadrants for the switching rule, consider using a switching function:

$$\sigma(y, \dot{y}) = m y + \dot{y} \quad (2.4)$$

Where  $m$  is a positive scalar.

Then, the control law is defined in terms of the switching function as follows:

$$u(t) = \begin{cases} -1 & \text{if } \sigma(y, \dot{y}) > 0 \\ 1 & \text{if } \sigma(y, \dot{y}) < 0 \end{cases} \quad (2.5)$$

The resulting motion (with  $m = 1$ ) for this system is shown in Figure 2-5 and Figure 2-6

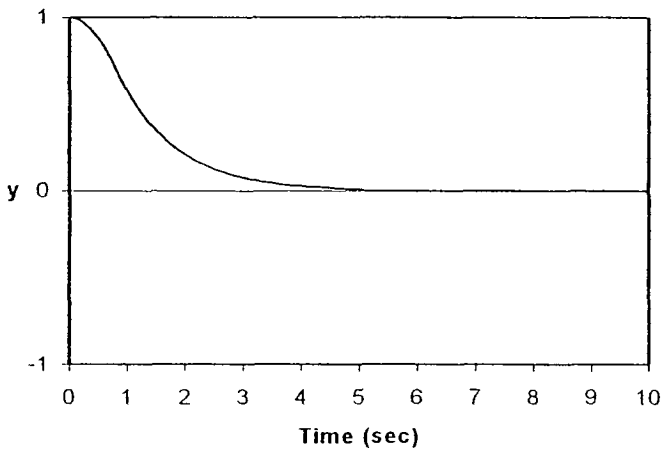


Figure 2-5: Time History for SMC System

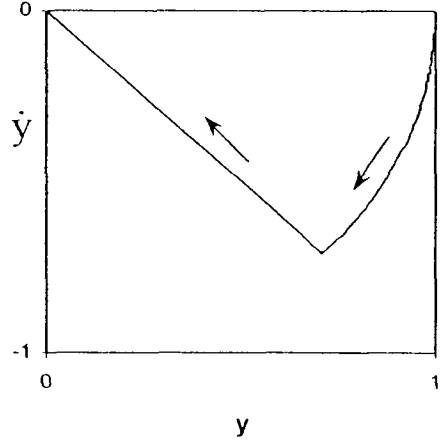
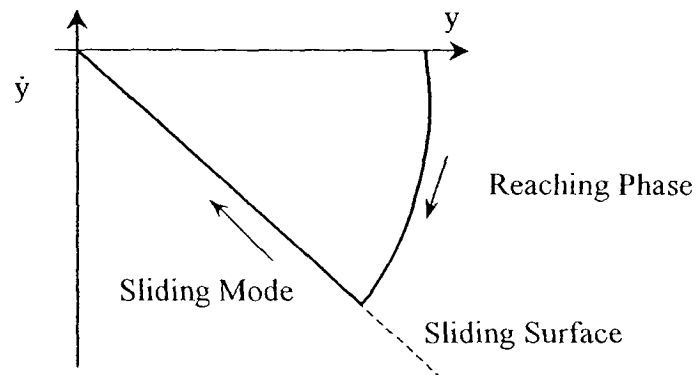


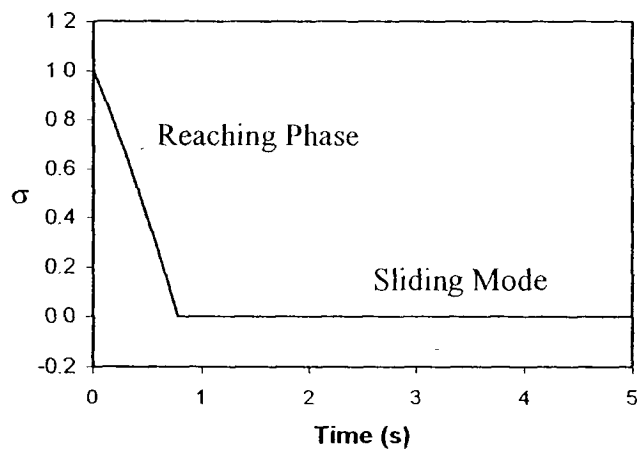
Figure 2-6: Phase Plane Plot for SMC System

This is called a Sliding Mode controller because, after reaching the switching function, the state trajectory follows (or “slides along”) the switching line to the equilibrium point. This is the goal of any sliding mode controller: drive the states to the switching surface in a finite time and constrain the states to remain on the surface  $\sigma = 0$  for all subsequent time. As illustrated in Figure 2-7, the time period where the states are moving toward the sliding surface is known as the *reaching phase*, and the phase where the states follow the surface  $\sigma = 0$  is called the *ideal sliding mode*



**Figure 2-7: Phases of Sliding Mode Control**

This is also clearly illustrated in the time history of the switching function from the previous example. In this case, the system reaches the sliding mode in about  $t = 0.8$  sec.



**Figure 2-8: Time History of Sliding Surface**

In order to maintain the motion on the sliding mode, the control effort requires infinite frequency switching because the control law is undefined on the surface  $\sigma = 0$ . If this infinite frequency switching were possible, the motion would be constrained to the sliding mode, and the dynamics of the closed-loop system would be that of the

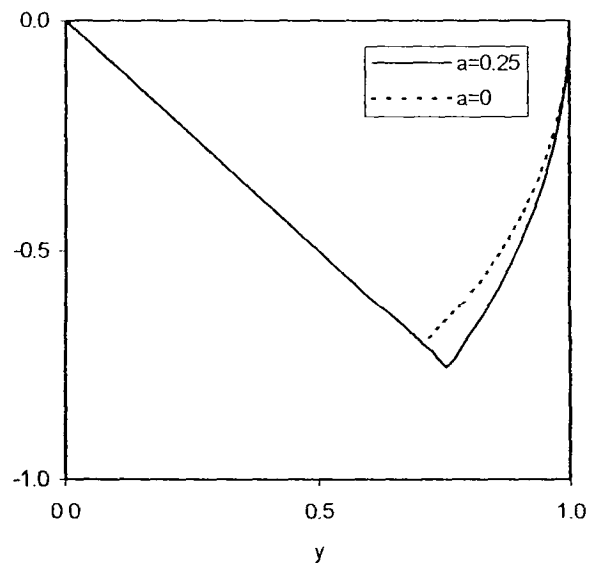
switching surface  $\sigma = 0$ . For this example, setting  $\sigma = 0$  and rearranging gives the motion for the closed-loop system after reaching the sliding mode:

$$\dot{y}(t) = -m y(t) \quad (2.6)$$

This is a first-order decay which depends only on the design parameter  $m$ . To further illustrate the fact that the dynamics depend only on  $m$ , consider adding a non-linear term to the double integrator system:

$$\ddot{y}(t) = -a \sin(y) + u(t) \quad (2.7)$$

This new system looks like a normalized frictionless pendulum. Using the exact same sliding mode controller as before and including the non-linear plant term, the resulting phase plane plot looks like.



**Figure 2-9: SMC Phase Plane Plot for System with Non-linear Term**

The previous solution of the double integrator ( $a=0$ ) is shown for comparison purposes. Note that there is a difference between the two cases during the reaching phase;

however, once on the sliding mode, both systems exhibit identical closed-loop response. The non-linear term ( $a \sin(y)$ ), which can be interpreted as a structured modeling error or disturbance, has been completely rejected. Although not proven here, there are four basic notions about SMC that can be observed:<sup>95</sup>

- The line (or hypersurface) that describes  $\sigma = 0$  defines the transient response of the system during the sliding mode.
- During the sliding mode, the trajectory dynamics are of a lower order than the original model.
- While on the sliding mode, the system dynamics are solely governed by the parameters that describe the line  $\sigma = 0$ .
- The trajectory of the sliding mode is one that is not inherent in either of the two control structures alone

A formal statement of the sliding mode control problem is now developed.

### 2.1.3 Sliding Mode Control Problem Statement

Consider the uncertain system with  $m$  inputs and  $n$  states given by:

$$\dot{x}(t) = \mathbf{A}(x, t) + \mathbf{B}(x, t)u(t) + f(t, x, u) \quad (28)$$

where  $\mathbf{A} \in \mathfrak{R}^{n \times n}$  and  $\mathbf{B} \in \mathfrak{R}^{n \times m}$ ;  $\mathbf{B}$  is full rank, and  $1 \leq m < n$ . The function  $f: \mathfrak{R} \times \mathfrak{R}^n \times \mathfrak{R}^m \mapsto \mathfrak{R}^n$  represents the parameter uncertainty or nonlinearities present in the system and is assumed to be unknown but bounded by some known functions of the state.

The objective is to define:

- $m$  switching functions, represented in vector form as  $\sigma(x)$  with the desired state trajectories
- a variable structure control

$$u(x, t) = \rho \operatorname{sgn}(\sigma) \quad (2.9)$$

such that any state outside the switching surface is driven to the surface in finite time and remains on this surface for all subsequent time

#### 2.1.4 Equivalent Control Concept

Since the control action in the ideal sliding mode is discontinuous, the resulting differential equation can not be analyzed with traditional methods. The approach which is almost always cited in the literature is the classic method proposed by Filippov<sup>107</sup> for differential equations with discontinuous right hand sides. While Filippov's construction provides a theoretical basis for solving the discontinuous problem, a more useful approach is Utkin's concept of the *equivalent control*<sup>90</sup>. Loosely speaking, the equivalent control is the *continuous* control action needed to maintain the ideal sliding motion. One of its key strengths is that it allows a continuous analysis and provides a means to prove certain properties of the sliding mode.

Assume the switching surface is reached at some time  $t_s$  and an ideal sliding motion is established. By definition, this means  $\sigma(t) = 0$  for all  $t > t_s$ , which implies that  $\dot{\sigma}(t) = 0$  for all  $t \geq t_s$ . Since, as will be shown later, the order of the switching surface is designed to be exactly one degree less than the relative order of the plant, the input  $u$  will appear in the derivative of the switching function. Setting this equal to zero and

solving for  $u$  results in the so-called equivalent control. As a simple example, recall the problem of the normalized pendulum:

$$\ddot{y}(t) = -a \sin(y) + u(t) \quad (2.10)$$

The switching line is defined as:

$$\sigma(t) = m y(t) + \dot{y}(t) \quad (2.11)$$

Taking its derivative and substituting equation (2.10) gives:

$$\begin{aligned} \dot{\sigma}(t) &= m \dot{y}(t) + \ddot{y}(t) \\ &= m \dot{y}(t) - a \sin(y) + u(t) \end{aligned} \quad (2.12)$$

Finally, setting  $\dot{\sigma} = 0$  and solving for  $u$  gives  $u_{eq}$ :

$$u_{eq}(t) = a \sin(y) - m \dot{y}(t) \quad (t \geq t_s) \quad (2.13)$$

In general, assuming a linear, time invariant state space model and a switching surface

$$\sigma(x) = S x \quad (2.14)$$

where  $S \in \mathcal{R}^{m \times n}$  is full rank and chosen by design to meet dynamic closed-loop requirements, it is easy to show that the equivalent control is uniquely defined by:<sup>91</sup>

$$u_{eq}(t) = -(SB)^{-1} S A x(t) \quad (2.15)$$

If the control action is purely discontinuous as in equation (2.9),  $u_{eq}$  can be thought of as the averaged control signal applied. It can also be shown to be equivalent to the low frequency component of the discontinuous signal by passing that signal through a low pass filter<sup>91</sup>. The equivalent control, however, is not actually applied in practice—at least, not alone. If the plant model is exactly correct (i.e. there are no unmodeled dynamics or disturbances),  $u_{eq}$  will maintain the sliding mode assuming the switching manifold has been reached (by definition). This will be demonstrated in an example

later. However, the discontinuous control function is required to maintain the sliding mode in the presence of model uncertainties and disturbances. It is common to see the equivalent control included in the control law, as in ( 2.16 ).

$$u(x,t) = u_{eq} + \rho \operatorname{sgn}(\sigma) \quad (2.16)$$

This has the advantage of reducing the activity of the discontinuous portion of the control. Even so, it is not usually implemented because it adds complexity to the controller. It is common to see it included in initial problem developments and then set equal to zero for the implementation. One of its main strengths is its use in proofs concerning sliding mode properties and stability.

### 2.1.5 Properties of the Sliding Mode

Unfortunately, very little can be found in the literature about the properties of transient response while in the reaching phase. Hung *et al.*<sup>95</sup> make only a brief comment about it in their survey paper. Utkin<sup>98</sup> and Edwards & Spurgeon<sup>91</sup> also discuss it briefly but do not offer a full treatment. Choi, *et al.*<sup>108</sup> offer some of the best treatment of the reaching phase, but is too involved to include here. Since the reaching phase is typically very short, and since the states are moving toward a stable manifold, the reaching phase is usually neglected and its properties are of little interest.

For the following analysis, assume a linear, time invariant state space plant and assume the switching surface is defined by equation ( 2.14 ) with the square matrix  $\mathbf{SB}$  nonsingular. The ideal sliding motion is found by substituting the equivalent control, equation ( 2.15 ), into the state space equation, which yields a free motion independent of the control action:

$$\dot{x}(t) = \left( \mathbf{I}_n - \mathbf{B}(\mathbf{SB})^{-1} \mathbf{S} \right) \mathbf{A} x(t) \quad \forall t \geq t_s \text{ and } \mathbf{S}x(t_s) = 0 \quad (2.17)$$

**SMC Property 1:** The sliding motion given in equation ( 2.17 ) is of reduced order and the eigenvectors associated with any nonzero eigenvalues of the system matrix

$$\mathbf{A}_{\text{eq}} = \left( \mathbf{I}_n - \mathbf{B}(\mathbf{S}\mathbf{B})^{-1} \mathbf{S} \right) \mathbf{A} \quad (2.18)$$

belong to the null space of the matrix  $\mathbf{S}$ .

**Proof:** See Edwards & Spurgeon.<sup>91</sup>

It follows that  $\mathbf{A}_{\text{eq}}$  can have, at most,  $n-m$  nonzero eigenvalues.

Next, the invariance property is developed. Let the disturbance function  $f$  (from equation ( 2.8 )) be  $f(t,x,u) = \mathbf{D} \xi(t,x)$  where the matrix  $\mathbf{D} \in \mathcal{R}^{n \times l}$  is known and the function  $\xi : \mathcal{R}_+ \times \mathcal{R}^n \rightarrow \mathcal{R}^l$  is unknown. This function can be interpreted as an exogenous disturbance acting on the system or uncertainty in the system matrices  $\mathbf{A}$  and  $\mathbf{B}$ . The uncertain linear system can then be expressed as.

$$\dot{x}(t) = \mathbf{A} x(t) + \mathbf{B} u(t) + \mathbf{D} \xi(t, x) \quad (2.19)$$

Any uncertainty in form given above with  $R(\mathbf{D}) \subset R(\mathbf{B})$  is called *matched uncertainty*.

Any uncertainty which does not lie with the range space of  $\mathbf{B}$  is called *unmatched uncertainty*<sup>91</sup>

Using the term in equation ( 2.17 ), define for convenience:

$$\mathbf{P}_s \equiv \left( \mathbf{I}_n - \mathbf{B}(\mathbf{S}\mathbf{B})^{-1} \mathbf{S} \right) \quad (2.20)$$

Edwards & Spurgeon<sup>91</sup> call this a projection operator and show that it satisfies two important properties:

$$\mathbf{S}\mathbf{P}_s = 0 \quad \text{and} \quad \mathbf{P}_s\mathbf{B} = 0 \quad (2.21)$$

With these definitions in place, the invariance property can be stated:

**SMC Property 2:** The ideal sliding motion is completely insensitive to the uncertain function  $\xi(t,x)$  in equation ( 2.19 ) if  $R(\mathbf{D}) \subset R(\mathbf{B})$ .

**Proof (from<sup>91</sup>):** The equivalent control for ( 2.19 ) assuming ( 2.14 ) is found as before and is given by

$$u_{\text{eq}}(t) = -(\mathbf{S}\mathbf{B})^{-1}(\mathbf{S}\mathbf{A}x(t) + \mathbf{S}\mathbf{D}\xi(t)) \quad \text{for } t \geq t_s \quad (2.22)$$

Substituting this into ( 2.19 ) gives

$$\dot{x}(t) = \mathbf{P}_s \mathbf{A} x(t) + \mathbf{P}_s \mathbf{D} \xi(t, x) \quad \forall t \geq t_s \quad \text{and} \quad \mathbf{S}x(t_s) = 0 \quad (2.23)$$

Now, if  $R(\mathbf{D}) \subset R(\mathbf{B})$ , then  $\mathbf{D}$  can be decomposed into  $\mathbf{D} = \mathbf{B}\mathbf{R}$ , where  $\mathbf{R} \in \mathfrak{R}^{m \times l}$  is a matrix of elementary operations. As a result, it follows that  $\mathbf{P}_s \mathbf{D} = \mathbf{P}_s (\mathbf{B}\mathbf{R}) = (\mathbf{P}_s \mathbf{B})\mathbf{R} = 0$  by the property given in equation ( 2.21 ). The sliding motion equation then reduces to

$$\dot{x}(t) = \mathbf{P}_s \mathbf{A} x(t) \quad \forall t \geq t_s \quad \text{and} \quad \mathbf{S}x(t_s) = 0 \quad (2.24)$$

which is independent of the exogenous signal.

This is a very important result and is the primary reason sliding mode control is attractive for a reconfigurable control setting. Note, it says nothing about invariance to unmatched uncertainty. In fact, SMC is *not* invariant to unmatched uncertainty; however, measures can be taken to ensure a certain level of robustness.

### 2.1.6 The Reachability Problem

So far, nothing has been said about guaranteeing that the system will reach the sliding mode or that it will remain on the sliding mode once it gets there. In fact, this is actually the primary concern and is the area that receives the most attention when developing the control law. Existence of the sliding mode requires stability of the state trajectory to the sliding surface  $\sigma(x) = 0$ , at least in some neighborhood surrounding the

surface. This neighborhood is known as the *region of attraction*.<sup>93</sup> If the sliding mode is globally reachable, the domain of attraction is the entire state space. The most common approach for proving stability, at least in the SISO case, is a Lyapunov analysis.

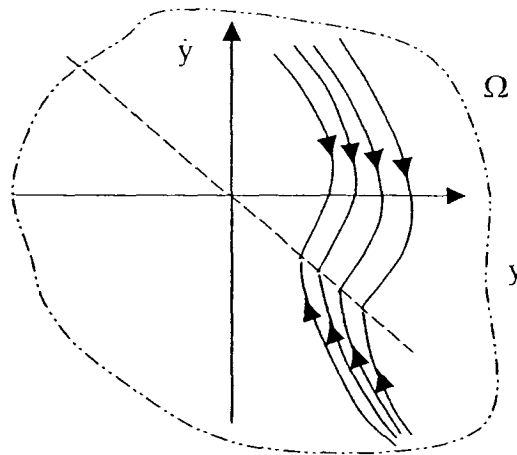
Geometrically, in order for the sliding surface to be attractive, the trajectories of  $\sigma(t)$  must always be directed toward it. Stated more formally,

$$\lim_{\sigma \rightarrow 0^+} \dot{\sigma} < 0 \quad \text{and} \quad \lim_{\sigma \rightarrow 0^-} \dot{\sigma} > 0 \quad \text{in some domain } \Omega \subset \mathfrak{R}^n \quad (2.25)$$

This can be stated in a more succinct manner as

$$\dot{\sigma} \sigma < 0 \quad (2.26)$$

This is called the *reachability condition*.<sup>91</sup> As illustrated in Figure 2-10, if state variables are within the domain  $\Omega$ , they will be attracted to the switching surface and remain on the surface if the reachability condition is met



**Figure 2-10: Phase Plane Plot of Domain of Attraction**

Noting that (in the SISO case)  $\frac{1}{2} \frac{d}{dt} \sigma^2 = \dot{\sigma} \sigma$ , it follows that the positive definite

function

$$V(\sigma) = \frac{1}{2} \sigma^2 \quad (2.27)$$

is a good candidate Lyapunov function. If it can be shown that  $\dot{V}(\sigma) < 0$ , the system is guaranteed to reach the sliding surface asymptotically.<sup>91</sup>

A stronger condition which guarantees an ideal sliding motion in a finite time is the so-called  $\eta$ -reachability condition given by

$$\dot{\sigma} \leq -\eta |\sigma| \quad (2.28)$$

where  $\eta$  is a small positive constant<sup>91</sup>. Noting that  $\frac{1}{2} \frac{d}{dt} \sigma^2 = \dot{\sigma} \sigma$ , and integrating equation (2.28) from 0 to  $t_s$ , it follows that

$$|\sigma(t_s)| - |\sigma(0)| \leq -\eta t_s \quad (2.29)$$

This, then can be solved for the time ( $t_s$ ) required to reach the sliding surface ( $\sigma = 0$ ):

$$t_x \leq \frac{|\sigma(0)|}{\eta} \quad (2.30)$$

Typically, what is done in a design analysis is the candidate Lyapunov function  $V(\sigma) = \frac{1}{2} \sigma^2$  is assumed. The control law has parameters (for example,  $\rho$  in equation (2.9)) which need to be determined. System uncertainties are parameterized and replaced into the state equation, which then appear in the Lyapunov function. Then the control parameter(s) are found in terms of the given uncertainty bounds such that the sliding mode is globally attractive.

### 2.1.7 Design Approaches

There are many design approaches in the literature—too many, in fact, to present here. In theory, there are an infinite variety of control strategies to achieve the sliding

mode. There are diagonalization methods, hierarchical methods, relays with constant gains, relays with state dependent gains, linear feedback with switched gains, linear continuous feedback, and univector non-linearity with scale factor.<sup>93</sup> All approaches consist of two basic steps: 1) design of the sliding surface(s), and 2) design of the control law to achieve the sliding mode. Two common approaches which are the most intuitive and which will be employed in this work are given below

One of the most commonly cited approaches is some variation of the so-called regular form approach. Edwards & Spurgeon<sup>91</sup> present this most succinctly, so their development is essentially duplicated here:

Consider the nominal linear model of an uncertain system, given by

$$\dot{x}(t) = \mathbf{A}x(t) + \mathbf{B}u(t) \quad (2.31)$$

where  $\text{rank}(\mathbf{B}) = m$  and  $(\mathbf{A}, \mathbf{B})$  is a controllable pair. Define an associated switching function

$$\sigma(t) = \mathbf{S}x(t) \quad (2.32)$$

This system can be transformed into *regular form* via a change of coordinates defined by an orthogonal matrix  $\mathbf{T}_r$  such that:

$$z(t) = \mathbf{T}_r x(t) \quad (2.33)$$

where  $\mathbf{T}_r$  is found by a QR decomposition of the input distribution matrix, that is,

$$\mathbf{T}_r \mathbf{B} = \begin{bmatrix} 0 \\ \mathbf{B}_2 \end{bmatrix} \quad (2.34)$$

Then, defining

$$\mathbf{T}_r \mathbf{A} \mathbf{T}_r^T = \begin{bmatrix} \mathbf{A}_{11} & \mathbf{A}_{12} \\ \mathbf{A}_{21} & \mathbf{A}_{22} \end{bmatrix} \quad (2.35)$$

and

$$\mathbf{S} \mathbf{T}_r^T = [\mathbf{S}_1 \quad \mathbf{S}_2] \quad (2.36)$$

The system can be expressed in the well-known regular form:

$$\begin{aligned} z_1(t) &= \mathbf{A}_{11} z_1(t) + \mathbf{A}_{12} z_2(t) \\ z_2(t) &= \mathbf{A}_{21} z_1(t) + \mathbf{A}_{22} z_2(t) + \mathbf{B}_2 u(t) \end{aligned} \quad (2.37)$$

and

$$\sigma(t) = \mathbf{S}_1 z_1(t) + \mathbf{S}_2 z_2(t) \quad (2.38)$$

Note that in this form, it is easy to identify matched and unmatched uncertainty. Anything appearing in the input line is “matched.” Therefore, the closed-loop response is insensitive to variations in  $\mathbf{A}_{21}$ ,  $\mathbf{A}_{22}$ , and  $\mathbf{B}_2$ .

During the sliding motion, the switching function must be identically zero, so

$$\mathbf{S}_1 z_1(t) + \mathbf{S}_2 z_2(t) = 0 \quad (2.39)$$

It can be shown that  $\mathbf{S}_2$  is nonsingular, so  $z_2$  can be solved for on the sliding mode.

$$\begin{aligned} z_2(t) &= -\mathbf{S}_2^{-1} \mathbf{S}_1 z_1(t) \\ &= -\mathbf{M} z_1(t) \end{aligned} \quad (2.40)$$

where  $\mathbf{M} \in \mathcal{R}^{m \times (n-m)}$  is defined as

$$\mathbf{M} \equiv \mathbf{S}_2^{-1} \mathbf{S}_1 \quad (2.41)$$

The sliding mode is then governed by equations (2.42) and (2.43)

$$\dot{z}_1(t) = \mathbf{A}_{11} z_1(t) + \mathbf{A}_{12} z_2(t) \quad (2.42)$$

$$z_2(t) = -\mathbf{M} z_1(t) \quad (2.43)$$

This is an  $(n - m)^{\text{th}}$  order system in which  $z_2$  acts in the role of a linear full-state feedback control signal. Closing this loop gives the free motion of the system:

$$\dot{z}_1(t) = (\mathbf{A}_{11} + \mathbf{A}_{12} \mathbf{M}) z_1(t) \quad (2.44)$$

Notice, once again, that the terms which contain the matched uncertainty do not appear—thus demonstrating again SMC’s invariance to matched uncertainty. Notice, too, that the problem of selecting the sliding surface has turned into a standard linear full-state feedback problem. In order to ensure the reaching condition, it must be ensured that  $z_1$  is asymptotically stable. Further, since all the unmatched uncertainty appears here, it is desired that this system be made as robust as possible. Edwards & Spurgeon detail two standard methods: robust eigenstructure assignment and quadratic minimization (the standard LQR problem).

Another method for SMC design is based on the ideas of feedback linearization. Fernández & Hedrick<sup>94</sup> and Slotine<sup>99</sup> approach the problem this way, as does Yuri Shtessel, a very prolific SMC proponent in the recent literature.<sup>63-66,106,109-120</sup> A major assumption with this approach is that the system must be square—equal number of inputs and outputs, and it must be feedback linearizable. If the system is square and feedback linearizable, it is possible to decouple the outputs with the given inputs. This turns the design into  $m$  simple SISO-like designs.

Consider a non-linear square MIMO system

$$\begin{aligned}\dot{x} &= f(x) + \mathbf{G}(x) u \\ y &= h(x)\end{aligned}\tag{2.45}$$

where  $x \in \mathfrak{R}^n$ ,  $y \in \mathfrak{R}^m$ ,  $u \in \mathfrak{R}^m$ . Assume the functions  $f(x)$ ,  $h(x)$  and columns  $g_i(x)$   $\forall i = \overline{1, m}$  of the matrix  $\mathbf{G}(x) \in \mathfrak{R}^{n \times m}$  are smooth vector fields. Further, assume the system is completely linearizable in a reasonable domain  $x \in \Gamma$ . The control system will be designed to track a real-time reference profile,  $y_r(t)$ .

This system can be transformed to a normal form<sup>99</sup>

$$\begin{aligned} \begin{bmatrix} y_1^{(r_1)} \\ y_2^{(r_2)} \\ \dots \\ y_m^{(r_m)} \end{bmatrix} &= \begin{bmatrix} L_f^{r_1} h_1(x) \\ L_f^{r_2} h_2(x) \\ \dots \\ L_f^{r_m} h_m(x) \end{bmatrix} + \mathbf{E}(x) u, \\ \mathbf{E}(x) &= \begin{bmatrix} L_{g_1}(L_f^{r_1-1}h_1) & L_{g_2}(L_f^{r_1-1}h_1) & \dots & L_{g_m}(L_f^{r_1-1}h_1) \\ L_{g_1}(L_f^{r_2-1}h_2) & L_{g_2}(L_f^{r_2-1}h_2) & \dots & L_{g_m}(L_f^{r_2-1}h_2) \\ \vdots & \vdots & \ddots & \vdots \\ L_{g_1}(L_f^{r_m-1}h_m) & L_{g_2}(L_f^{r_m-1}h_m) & \dots & L_{g_m}(L_f^{r_m-1}h_m) \end{bmatrix} \quad |\mathbf{E}(x)| \neq 0 \quad \forall x \in \Gamma \end{aligned} \quad (2.46)$$

Where  $L_f^i h_i$  and  $L_{g_i}(L_f^{i-1}h_i) \quad \forall i = \overline{1, m}$  are corresponding Lie derivatives<sup>120</sup>

Next design  $m$  independent sliding surfaces (note, these have orders exactly one less than the relative order for the corresponding state variable):

$$\sigma_i = e_i^{(r_i-1)} + c_{i,r_i-2} e_i^{(r_i-2)} + \dots + c_{i,1} e_i^{(1)} + c_{i,0} e_i \quad \forall i = \overline{1, m} \quad (2.47)$$

where  $e_i = y_{r_i}(t) - y_i(t)$ ,  $e_i^{(j)} = \frac{d^j e_i}{dt^j}$ . The coefficients  $c_{i,j}$ ,  $\forall i = \overline{1, m}$  and  $\forall j = \overline{0, r_i - 2}$ , are design parameters which are chosen to achieve the desired eigenvalue placement of the decoupled differential equations of the output variables. It is also common to include an integral term,  $c \int e_i d\tau$ , in the sliding equations to account for potential steady state error which can occur when utilizing a sliding mode boundary layer (to be discussed later)

The control law which can be used is

$$u_i = u_{eq_i} + \rho_i \operatorname{sgn}(\sigma_i) \quad (2.48)$$

In order to prove system stability, assume the candidate Lyapunov function  $V_i = \frac{1}{2} \sigma_i^2$ , take the derivative of the sliding functions,  $\sigma_i$ , and solve for  $\rho_i$  which provides global attractiveness to the sliding surface in finite time.

### 2.1.8 Implementation Issues

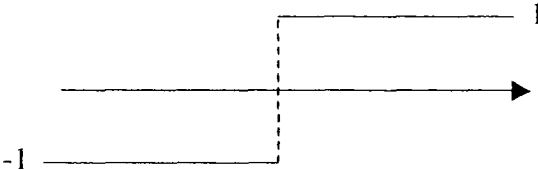
While sliding mode controllers are very attractive from a robustness standpoint, there are some implementation issues which must be addressed. In fact, much of what appears in the literature for sliding mode control is related to the issue of chatter<sup>59,109,112,113,116,119-128</sup>. Without a solution to the chatter problem, SMC would be relegated to only a very few applications where the control action can attain the high frequency switching required, such as control of electric motors and power converters.

#### 2.1.8.1 Chatter

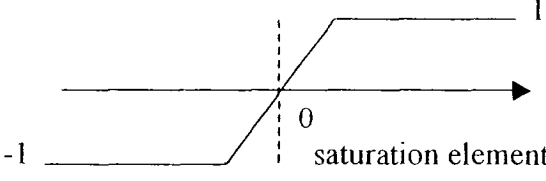
Chatter is defined by many authors as the high frequency action of the actuators. Young & Utkin<sup>97</sup> take a more purist stand on the definition of chatter. The high frequency action of the control—by their definition—is not chatter, but rather the expected result of the SMC control law (recall the control output is undefined on the surface  $\sigma = 0$ ). An infinite frequency switching is actually required while on the sliding mode. This results in a smooth ideal sliding along the sliding manifold with smooth state trajectories. However, due to parasitic dynamics in the real system, such as actuator dynamics and time delays, the switching can not take place at the required frequency, and the *state trajectories* chatter along the sliding manifold. After working with some example models, it is found that not only do actuator dynamics result in chatter, but they can drive the system unstable. At first, this may seem to contradict the invariance property (since the actuator dynamics are part of the control action). However, recall that the invariance property is only valid while on the sliding mode. Theoretically, this requires an infinite frequency switching. Actuator dynamics prevent the controller from maintaining the sliding mode. There are several methods proposed

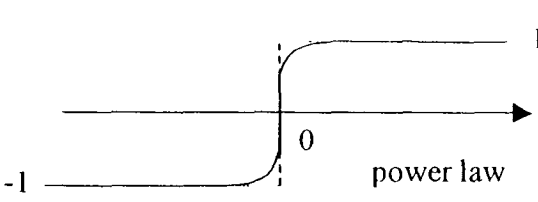
in the literature to deal with the chatter problem. Two of the most common approaches are briefly introduced.

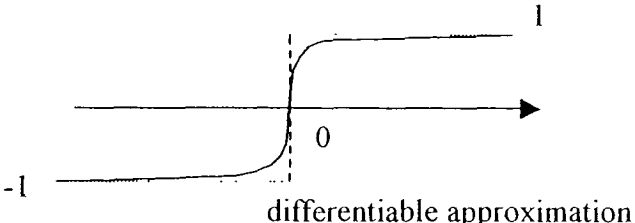
The simplest and clearly most popular approach is the so-called boundary layer. The basic idea is to replace the discontinuous signum function with an arbitrarily close approximation. The signum function looks like

$$v = \text{sgn}(\sigma) = \begin{cases} 1 & \text{if } \sigma > 0 \\ -1 & \text{if } \sigma < 0 \end{cases}$$


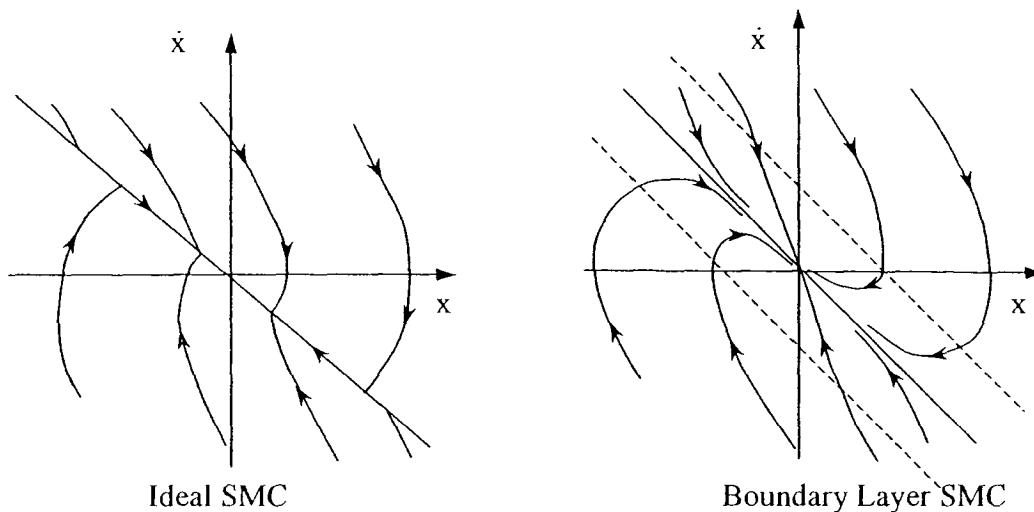
Several such approximations include.

$$v = \text{sat}\left(\frac{\sigma}{\varepsilon}\right) = \begin{cases} \frac{\sigma}{|\sigma|} & \text{if } \sigma \geq \varepsilon \\ \frac{\sigma}{\varepsilon} & \text{otherwise} \end{cases}$$


$$v = \begin{cases} \frac{\sigma}{|\sigma|} & \text{if } |\sigma| > \varepsilon \\ \frac{\delta^{q-1}\sigma}{|\sigma|^q} & \text{if } 0 < |\sigma| \leq \varepsilon \\ 0 & \sigma = 0 \end{cases}$$


$$v = \frac{\sigma}{|\sigma| + \varepsilon}$$


Some research has been done to determine the performance of these different approximations to the signum function. Results show that there are no significant differences between them in the application to SMC.<sup>91</sup> The result of using one of these continuous approximations is the states become attracted to a small boundary layer surrounding the switching surface, rather than to the switching surface itself. Convergence proofs show stability to the boundary layer and the states remain arbitrarily close to the switching surface. Figure 2-11 demonstrates the effect of a saturation element boundary layer on the state trajectories.



**Figure 2-11: State Trajectories for Ideal Sliding Mode and Sliding Mode with Boundary Layer**

Of course, the ideal sliding mode is lost and the resulting motion is often referred to in the literature as pseudo-sliding. While invariance is also lost, the system still retains much of its robustness. The boundary layer can be made arbitrarily small to approach ideal sliding. Typically in the design process, the boundary layer thickness is tuned to achieve an acceptable balance between maximum performance/robustness and reduced chatter. This approach has the advantage of being very simple to implement and is the

choice of many authors.<sup>31,63,66,103-105,121,129-131</sup> One disadvantage is the resulting control becomes essentially a high gain controller—something that is typically avoided in control design.

Another method to reduce chatter in SMC systems is an approach called second-order sliding modes, or 2-SMC.<sup>59,101,113,122,127,128</sup> The basic idea of this approach is to use the first derivative of the control as a pseudo-control during the design. Therefore all the high frequency switching will occur in  $\dot{u}$ , and when this signal is integrated, the actual control will be continuous. There are also higher order sliding mode controllers which have been proposed.<sup>128</sup> This technique works well, but a key disadvantage is that derivatives of the states appear in the switching function—which means these derivatives must be measured or calculated

### 2.1.8.2 Actuator Limits

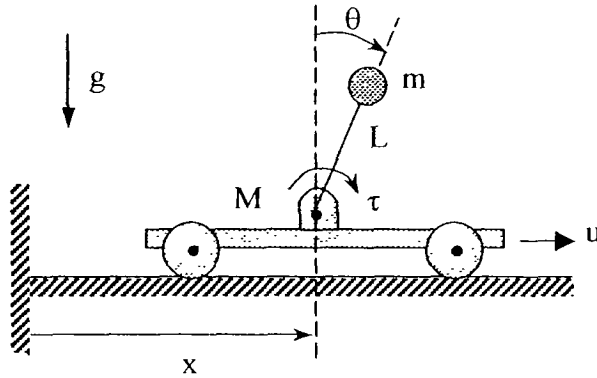
Little attention is given in the literature concerning the effects of actuator limits in SMC. Unfortunately, actuator limits can have large, undesirable effects on the system. The type of actuator limits that are typically associated with degraded control performance are rate and position saturation. If a rate limit is encountered, it appears as a degradation of actuator bandwidth. The result is added phase lag—a condition which almost always results in chattering or loss of the sliding mode. If a position limit is encountered, global stability can not be guaranteed. Probably one reason position limits are not discussed is the very nature of the SMC control law. Consider, again, equation (2.9) :  $u(x,t) = \rho \operatorname{sgn}(\sigma)$ . The maximum position this control will see is  $\pm\rho$ . If  $\rho$  is less than the maximum allowable control effort, there will not be any position saturation. Since  $\rho$  is a design parameter, it should be chosen to be less than the maximum

available. However, since  $\rho$  is typically a function of the maximum expected uncertainty or disturbance, it is possible to desire more control authority than what is available. This results in a reduced region of attraction, and if the states are outside of this region, stability can be lost. This is demonstrated in one of the examples in Chapter 3. Madani-Esfahani *et al.*<sup>132</sup> investigate the problem of estimating regions of asymptotic stability (RAS) in variable structure systems with hard bounds on the control action. The paper is highly theoretical and shows that, using their approach, the RAS cannot be found analytically using a single Lyapunov function.

The problem of finite bandwidth actuators with rate and position limits is a major implementation issue and comprises the major of the effort in this research. Chapter 3 is develops the problem further and outlines some potential solutions.

## 2.2 Application Example: Inverted Pendulum on a Translating Cart

In order to demonstrate the basic concepts of sliding mode control, the classic problem of an inverted pendulum on a translating cart is considered:



System parameters:

Cart mass	=	M
Pendulum mass	=	m
Pendulum length	=	L

State variables:

Cart position	=	x
Pendulum angle	=	$\theta$

Control inputs:

Horizontal Force	=	u
Pendulum Torque	=	$\tau$

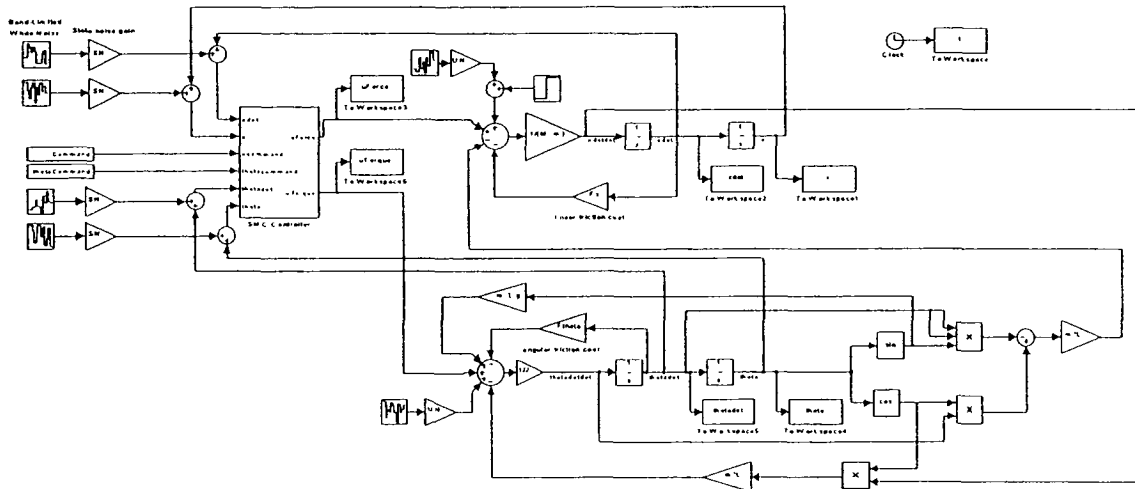
If the horizontal friction force and the frictional torque on the pendulum are included, the non-linear equations of motion are given by.<sup>111</sup>

$$\begin{aligned} (M+m)\ddot{x} + F_x \dot{x} + (mL \cos\theta)\ddot{\theta} - mL\dot{\theta}^2 \sin\theta &= u \\ J\ddot{\theta} + F_\theta \dot{\theta} - mLg \sin\theta + (mL \cos\theta)\ddot{x} &= \tau \end{aligned} \quad (2.49)$$

Linearizing about the equilibrium point,  $\theta=0$ , the linearized state space equations are:

$$\begin{aligned} \begin{bmatrix} \dot{z}_1 \\ \dot{z}_2 \\ \dot{z}_3 \\ \dot{z}_4 \end{bmatrix} &= \begin{bmatrix} 0 & 0 & 1 & 0 \\ 0 & 0 & 0 & 1 \\ 0 & \frac{-m^2L^2g}{J(M+m)-m^2L^2} & \frac{-JF_x}{J(M+m)-m^2L^2} & \frac{mLF_\theta}{J(M+m)-m^2L^2} \\ 0 & \frac{(M+m)mLg}{J(M+m)-m^2L^2} & \frac{mLF_x}{J(M+m)-m^2L^2} & \frac{-(M+m)F_\theta}{J(M+m)-m^2L^2} \end{bmatrix} \begin{bmatrix} z_1 \\ z_2 \\ z_3 \\ z_4 \end{bmatrix} \\ &+ \begin{bmatrix} 0 & 0 \\ 0 & 0 \\ J & -mL \\ \frac{J(M+m)-m^2L^2}{-mL} & \frac{J(M+m)-m^2L^2}{(M+m)} \\ \frac{J(M+m)-m^2L^2}{J(M+m)-m^2L^2} & \frac{J(M+m)-m^2L^2}{J(M+m)-m^2L^2} \end{bmatrix} \begin{bmatrix} u \\ \tau \end{bmatrix} \end{aligned} \quad (2.50)$$

The full non-linear simulation block diagram is given in Figure 2-12



**Figure 2-12: Pendulum/Cart Nonlinear System Block Diagram**

The numerical values for the parameters used in this example are:

Parameter	Nominal Value	Value after "Failure"
Cart Mass, M	3.0 kg	30.0 kg
Pendulum Mass, m	0.50 kg	5.0 kg
Rod Length, L	0.4 m	0.8 m
Linear Friction Coef, $F_x$	6.0 kg/s	25.0 kg/s
Angular Friction Coef, $F_\theta$	0.005 kg-m <sup>2</sup>	0.05 kg-m <sup>2</sup>

Initially, consider a SISO system with the force as the only input ( $\tau = 0$ ). Then, the state space representation of the linearized system is

$$\begin{bmatrix} \dot{z}_1 \\ \dot{z}_2 \\ \dot{z}_3 \\ \dot{z}_4 \end{bmatrix} = \begin{bmatrix} 0 & 0 & 1 & 0 \\ 0 & 0 & 0 & 1 \\ 0 & -1.6345 & -2 & 0.0042 \\ 0 & 28.6037 & 5 & -0.0729 \end{bmatrix} \begin{bmatrix} z_1 \\ z_2 \\ z_3 \\ z_4 \end{bmatrix} + \begin{bmatrix} 0 \\ 0 \\ 0.3333 \\ -0.8333 \end{bmatrix} [u]$$

A sliding mode controller is designed using the regular form approach.

- Design the sliding surface
- Change coordinates of given system to regular form (see Edwards & Spurgeon<sup>91</sup>, p.66 for m-file)
- Perform QR decomposition on input distribution matrix to get  $\mathbf{T}_r$
- Obtain  $\mathbf{A}_{reg}$  and  $\mathbf{B}_{reg}$  using  $\mathbf{T}_r$
- Obtain matrix sub-blocks in the regular form equations

$$\mathbf{T}_r = \begin{bmatrix} 0 & 1 & 0 & 0 \\ -0.3714 & 0 & 0.8621 & 0.3448 \\ 0.9285 & 0 & 0.3448 & 0.1379 \\ 0 & 0 & -0.3714 & 0.9285 \end{bmatrix}$$

$$\begin{bmatrix} \dot{\chi}_1 \\ \dot{\chi}_2 \\ \dot{\chi}_3 \\ \dot{\chi}_4 \end{bmatrix} = \begin{bmatrix} 0 & 0.3448 & 0.1379 & 0.9285 \\ 8.4543 & -0.3276 & -0.1310 & 0.1179 \\ 3.3817 & 0.7974 & 0.3190 & -0.3528 \\ 27.1650 & 4.6185 & 1.8474 & -2.0643 \end{bmatrix} \begin{bmatrix} \chi_1 \\ \chi_2 \\ \chi_3 \\ \chi_4 \end{bmatrix} + \begin{bmatrix} 0 \\ 0 \\ 0 \\ -0.8975 \end{bmatrix} \mathbf{u}$$

- Use linear quadratic cost function to design the switching function matrix coefficients (see Edwards & Spurgeon,<sup>91</sup> p.74 for m-file)
- Transform weighting matrix to regular form coordinates

The weighing matrices in the original coordinates are the standard weights in an LQG problem. For this example, the values chosen are:

$$\mathbf{Q} = \begin{bmatrix} 10 & 0 & 0 & 0 \\ 0 & 10 & 0 & 0 \\ 0 & 0 & 1 & 0 \\ 0 & 0 & 0 & 1 \end{bmatrix} \quad \mathbf{R} = 0.01$$

- Compatibly partition weighting matrix with regular form description

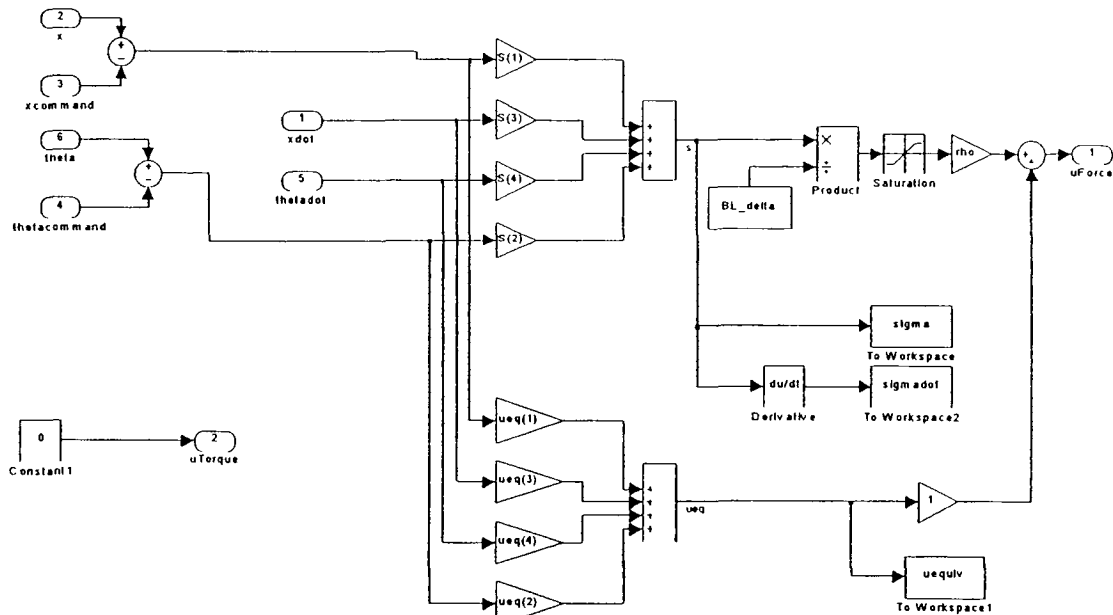
- Form reduced order system description and associated weighting matrix
- Solve the LQR problem
- Transform solution back into original coordinates

$$S = \begin{bmatrix} 3.1632 & 10.1219 & 2.7436 & 2.1745 \end{bmatrix} \quad (\text{in original coordinates})$$

Calculate  $U_{eq}$ :  $U_{eq} = -(\mathbf{SB})^{-1} \mathbf{SA} x$

$$U_{eq} = \begin{bmatrix} 0 & 64.3035 & 9.5233 & 11.1136 \end{bmatrix} x$$

- The final control parameter to design is the gain  $\rho$ . In the following examples, the value of  $\rho$  varies depending on the particular case being run. Its value will be called out in each example. The block diagram of the sliding mode controller just designed is given in Figure2-13.



**Figure2-13: Pendulum/Cart SMC Controller Block Diagram**

For the sake of comparison, an LQR controller is designed using the same weights as above. The resulting feedback control gains for the LQR controller are:

$$K_{LQR} = [-31.6 \quad -179.1 \quad -38.7 \quad -35.8]$$

The next series of figures are ones which demonstrate the basic operation of the SMC just designed. A simulation with the linear model and no noise is used. These demonstrate the effects of equivalent control and the boundary layer.

Figure 2-14. LQR Regulator (Linear Model)

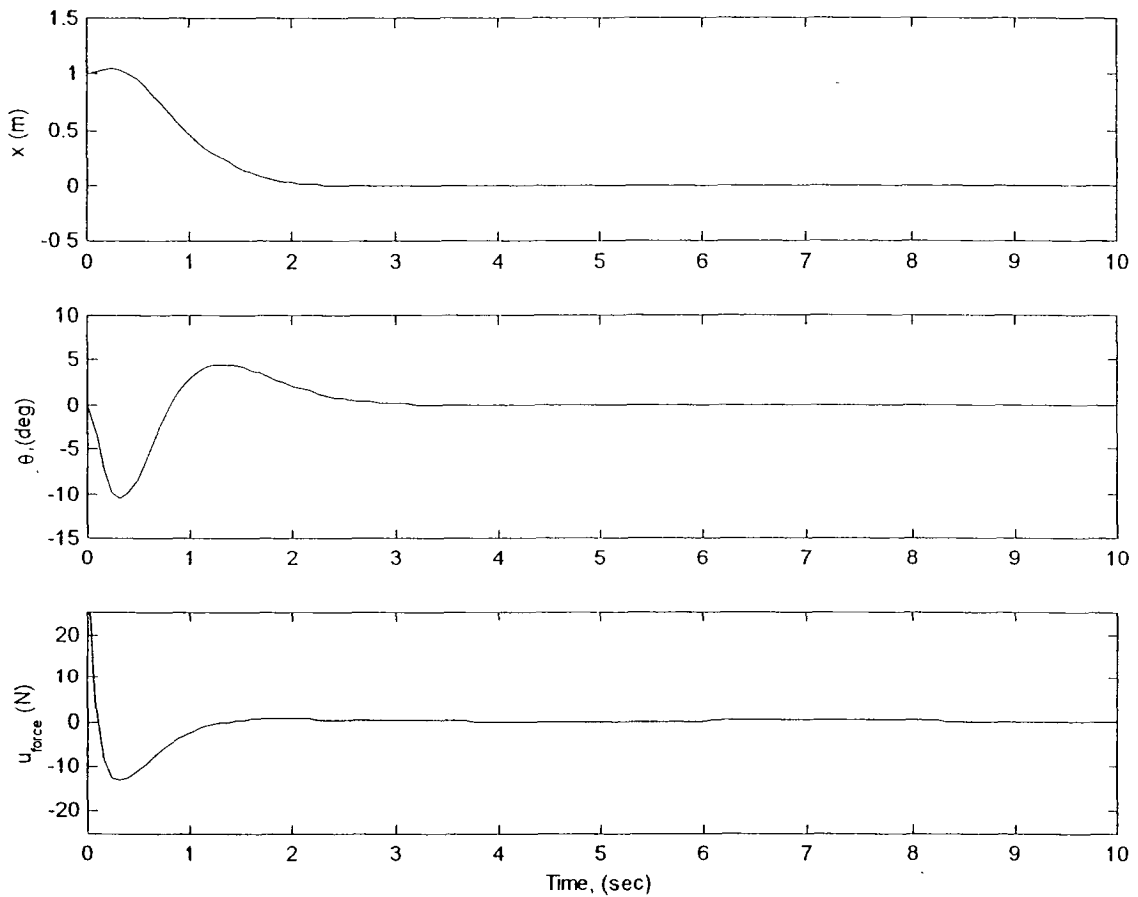
Figure 2-15: SMC Regulator (Linear Model) with  $u = U_{eq}$

Figure 2-16. SMC Regulator (Linear Model) with  $u = 20 \text{ sat}(\sigma/0.005)$

Figure 2-17. SMC Regulator (Linear Model) with  $u = U_{eq} + 5 \text{ sat}(\sigma/0.0001)$

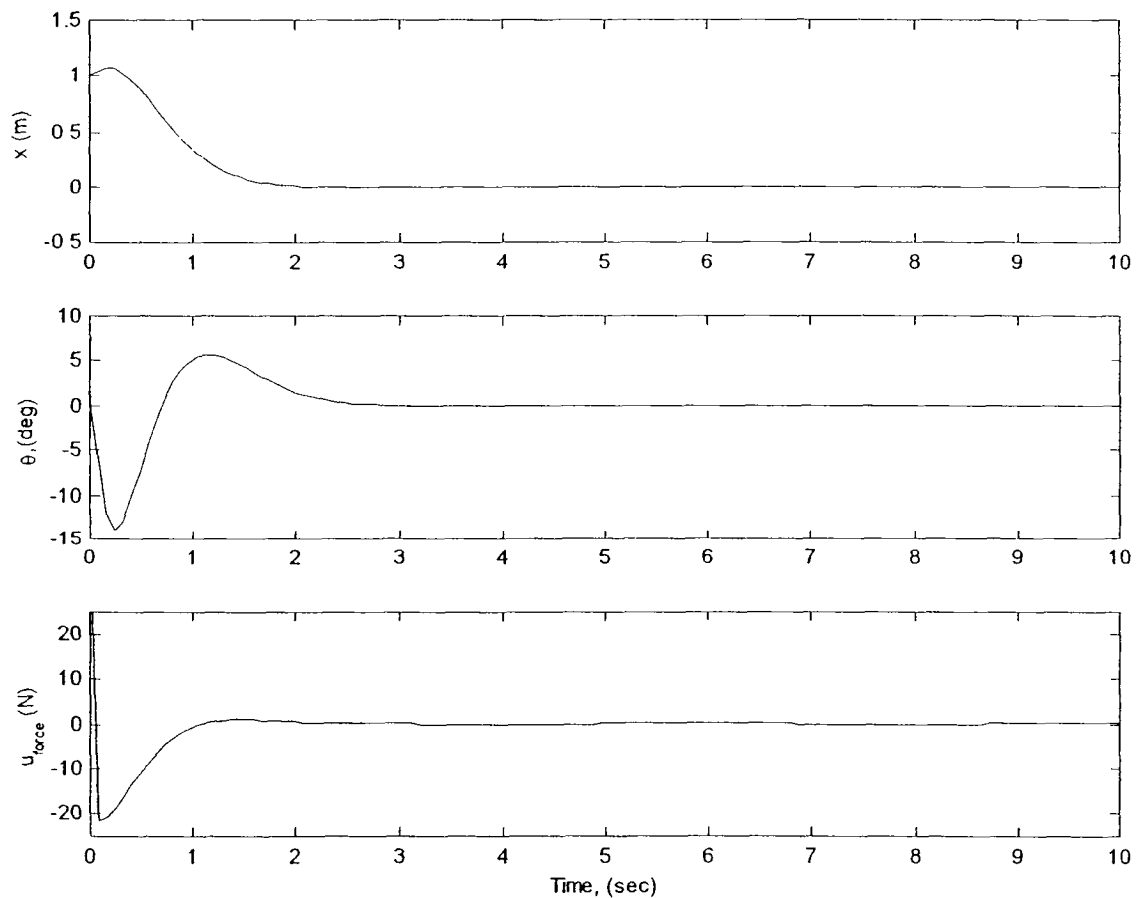
Figure 2-18: SMC Regulator (Linear Model) with  $u = U_{eq} + 5 \text{ sat}(\sigma/0.1)$

For the sake of comparison, this plot shows the results of a simulation using a standard LQR regulator using the same weights given above. As expected, an LQR controller does an acceptable job. This same controller is used on the full non-linear system simulation and achieves exactly the same results. That plot is not given because it looks essentially the same as this one



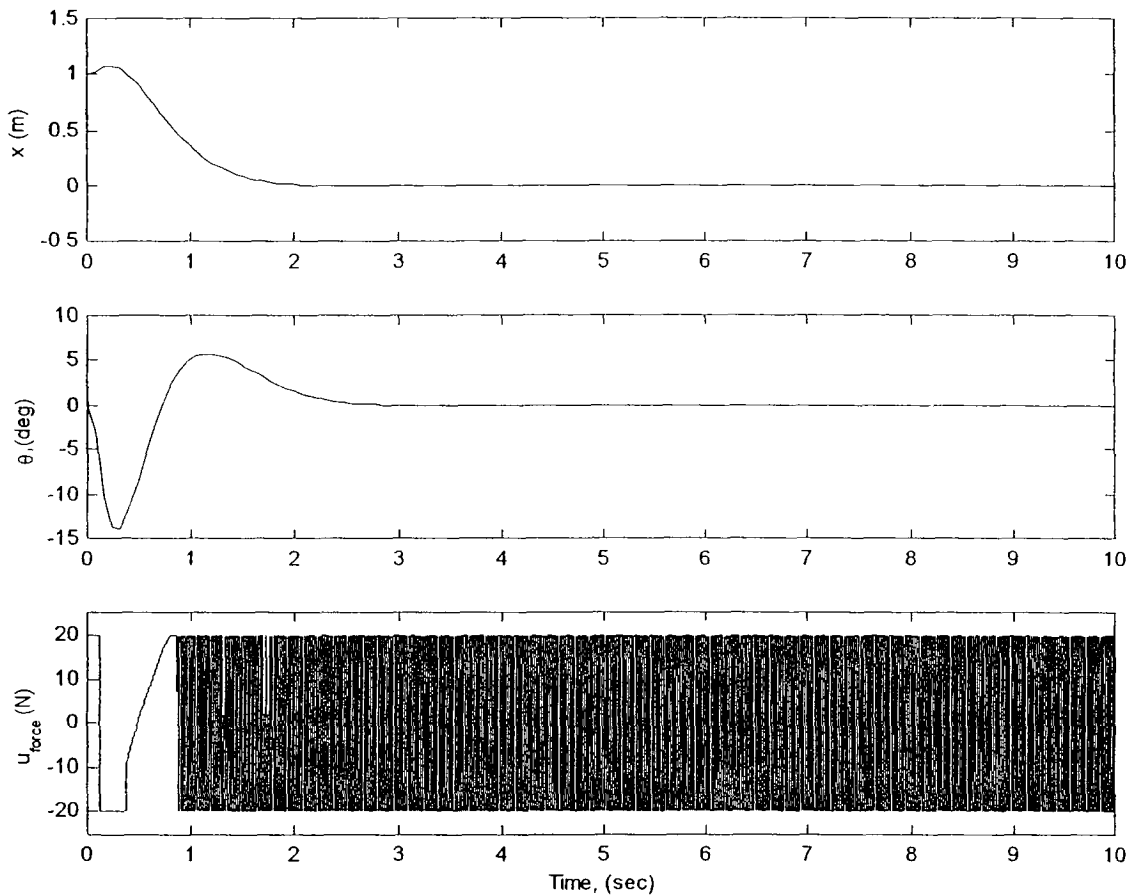
**Figure 2-14: LQR Regulator (Linear Model)**

This SMC controller uses only the equivalent control—it has no discontinuous control element. Note,  $U_{eq}$  will not reach the sliding mode by itself. A typical discontinuous element is used during the reaching phase ( $0 < t < 0.15$  sec) and turned off as soon as the sliding mode is reached. As expected,  $U_{eq}$  maintains the sliding mode for this case because the simulation model is exactly the same as the design model, and there is no noise. When this same control is applied to the non-linear simulation (or if noise is present), stable control is lost.



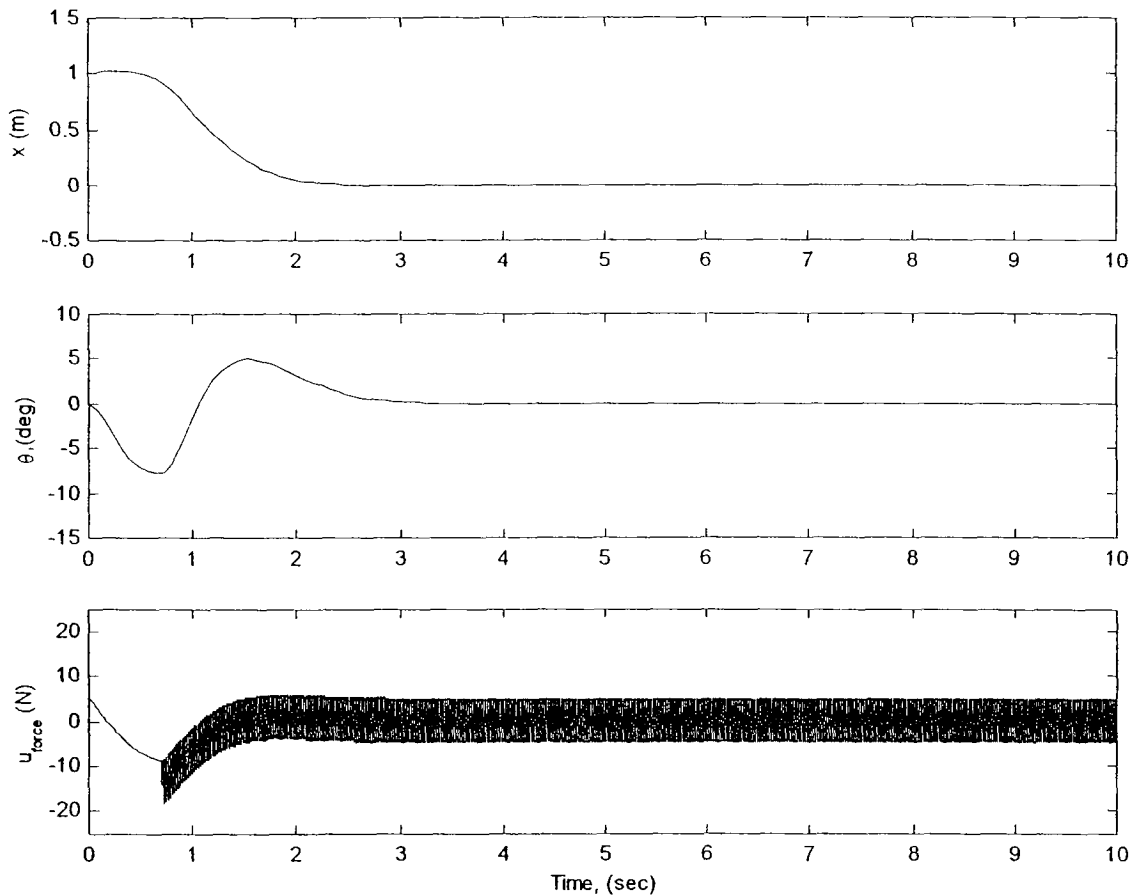
**Figure 2-15: SMC Regulator (Linear Model) with  $u = U_{eq}$**

This SMC controller uses no equivalent control. Notice the high activity of the control (near infinite frequency) This is because this case uses a fairly small boundary layer. As the boundary layer approaches zero (ideal sliding mode), the frequency of the control activity becomes infinite. This same controller is used on the full non-linear system simulation and achieves exactly the same results.



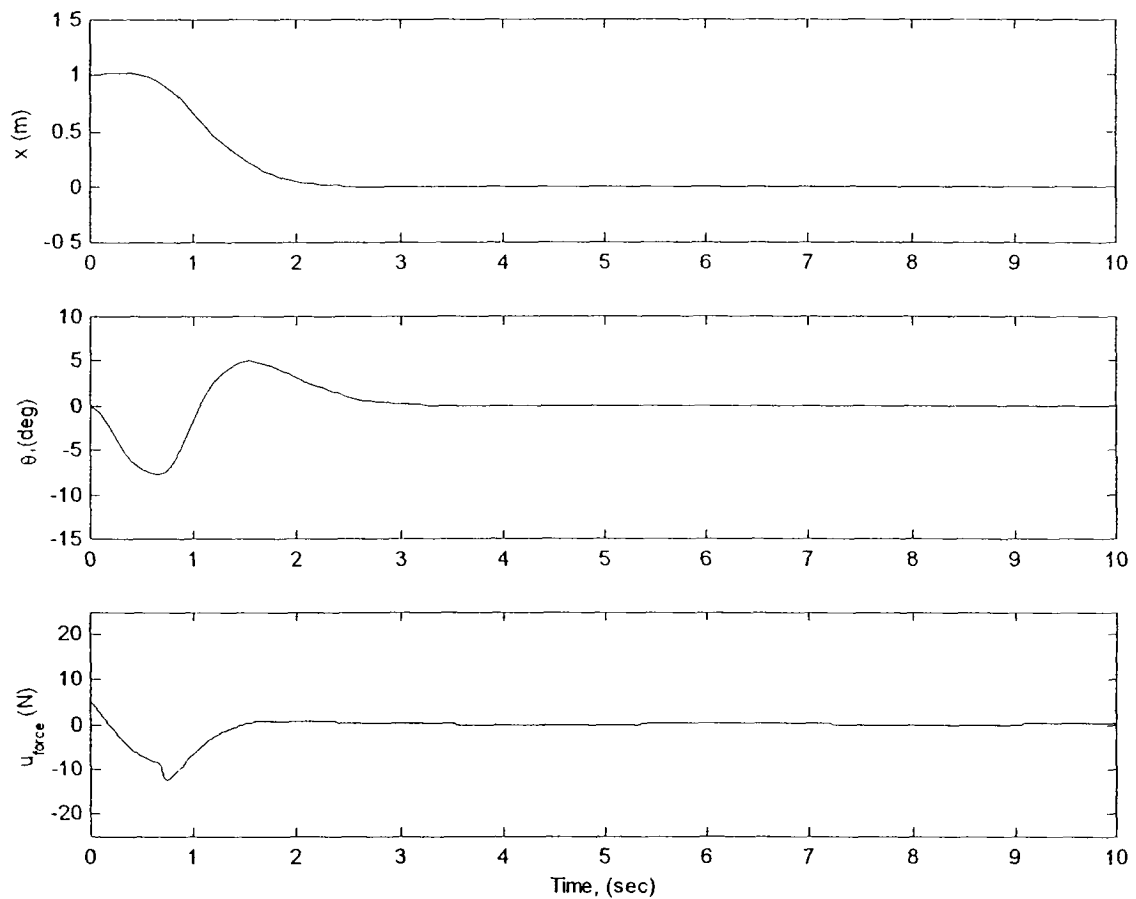
**Figure 2-16: SMC Regulator (Linear Model) with  $u = 20 \text{ sat}(\sigma/0.005)$**

This SMC controller uses both the equivalent control and the discontinuous element. Note that the magnitude of the discontinuous part is considerably less than that required for the previous example. That is because the continuous equivalent control is doing much of the work. The boundary layer is very small in this case to show the effect of approaching the ideal sliding mode. This same controller is used on the full non-linear system simulation and achieves exactly the same results.



**Figure 2-17: SMC Regulator (Linear Model) with  $u = U_{eq} + 5 \text{ sat}(\sigma/0.0001)$**

This SMC controller uses both the equivalent control and the discontinuous element. This case differs from the previous case in the size of the boundary layer. In this case the boundary layer is increased to the point that control appears completely continuous. If the boundary layer is increased too much, the performance becomes noticeably degraded. This same controller is used on the full non-linear system simulation and achieves exactly the same results.



**Figure 2-18: SMC Regulator (Linear Model) with  $u = U_{eq} + 5 \text{ sat}(\sigma/0.1)$**

Next the invariance property of the sliding mode controller is tested. If the physical properties of the system are varied, the controller proves to be remarkably robust. However, it is not much more robust than the LQR controller—which also performs very well. This result is to be expected. SMC systems are not invariant to unmatched uncertainty. If the system in regular form is examined, it is clear that the physical properties all appear in the unmatched terms of  $A_{eq}$ . This means, that while the SMC will be invariant to variations in the  $A_{21}$  and  $A_{22}$  terms, it will only be as robust to changes in  $A_{11}$  and  $A_{12}$  as the system in equation ( 2.44 ) can be made to be—which was designed using an LQR approach. The plots for these cases are not presented, but both the LQR controller and the SMC controller perform very well with state noise, a non-linear system simulation, large state initial conditions, and varying system parameters. In general, the SMC controller is more robust, but not by much

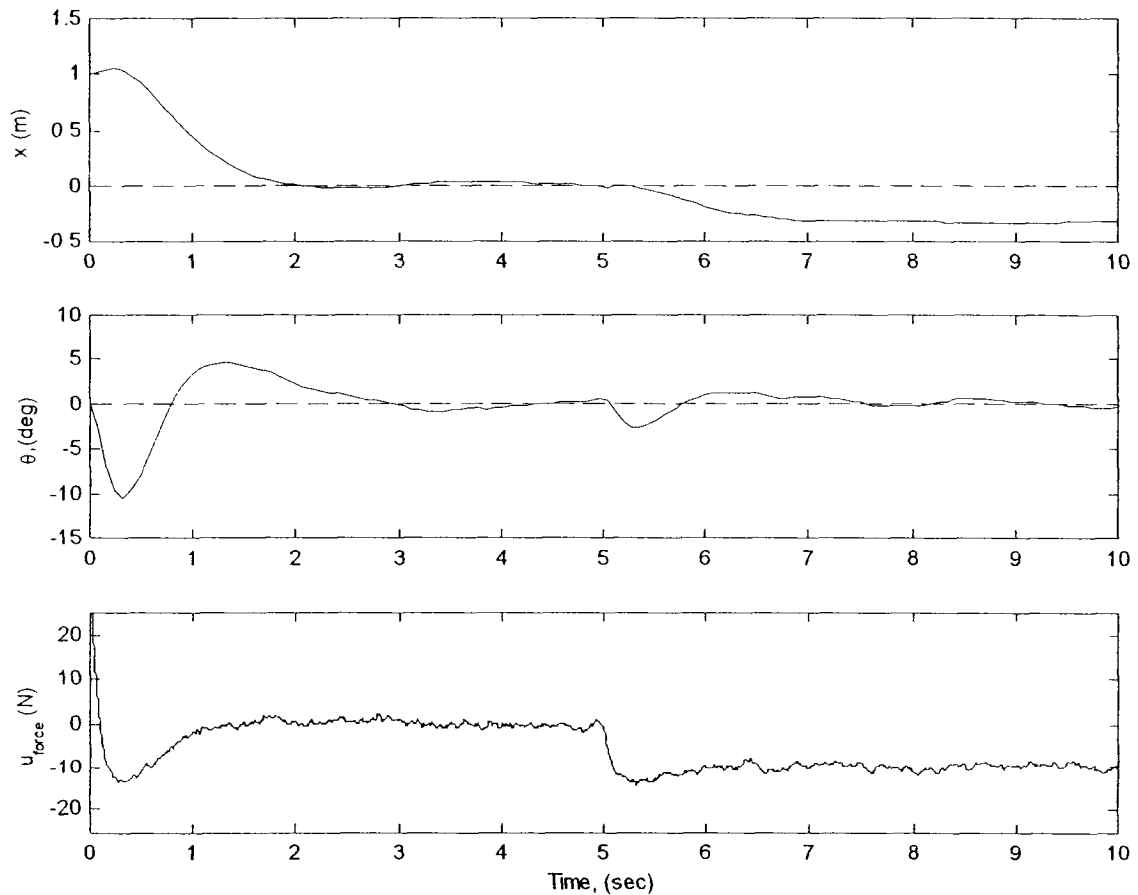
In order to properly test the invariance property, *matched* disturbances need to be input into the system. The simplest way to implement this is to inject disturbances directly at the control input. A white noise is added directly to the control input. Additionally, at  $t = 5$  sec, a single step bias with an amplitude of 10 is injected at the control input. This might simulate a control “hard over.”

The results of this simulation for the LQR system and the SMC system are given in the next two figures.

Figure 2-19 LQR Regulator (Non-linear System) with Control Input Disturbances

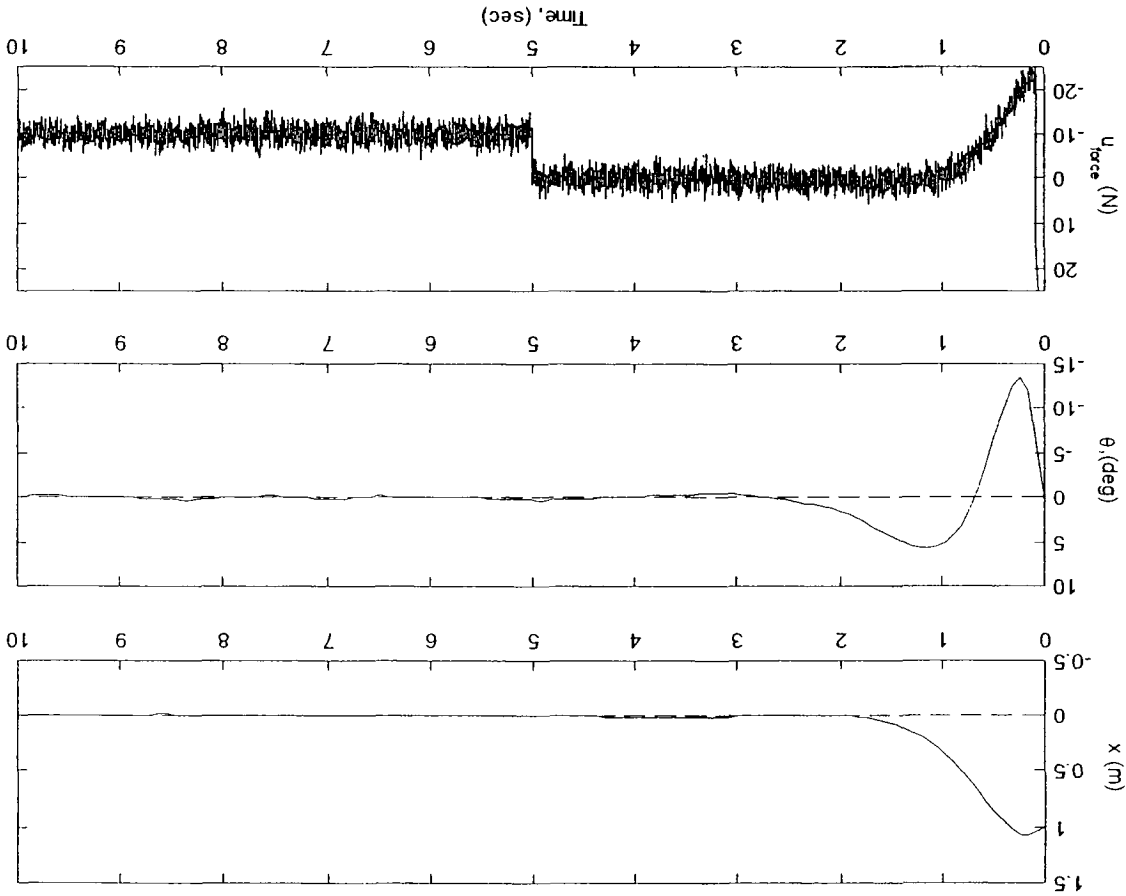
Figure 2-20: SMC Regulator (Non-linear System) with Control Input Disturbances

This is the LQR controller using the same weights as previously. White Gaussian noise is injected at the control input. A disturbance bias of 10 is added to the control input at  $t = 5$  sec. Pendulum angle tracking is noisy. Cart position has a noticeable bias after 5 sec



**Figure 2-19: LQR Regulator (Non-linear System) with Control Input Disturbances**

Figure 2-20: SMC Regulator (Non-linear System) with Control Input Disturbances



This is the SMC controller using the control law:  $u = U_{eq} + 50 \text{ sat}(\sigma/0.1)$ . White Gaussian noise is injected at the control input. A disturbance bias of 10 is added to the control input at  $t = 5$  sec. Pendulum angle and cart position regulation is very good. A fairly small boundary layer is used--the control effort can be smoothed some by using a larger boundary layer. This demonstrates SMC's ability to completely reject matched disturbances

Next, the control torque is included in the system to make the system square. Using the idea of feedback linearization outlined above, a sliding mode controller which decouples the outputs is designed. The resulting design is:

$$\sigma_x = (\dot{x}_c - \dot{x}) + 10(x_c - x) \quad \sigma_\theta = (\dot{\theta}_c - \dot{\theta}) + 10(\theta_c - \theta) \quad \text{Switching surfaces}$$

$$u = 50 \operatorname{sat}\left(\frac{\sigma_x}{0.4}\right) \quad \tau = 10 \operatorname{sat}\left(\frac{\sigma_\theta}{0.4}\right) \quad \text{Control laws}$$

As before, a LQR controller is also designed for comparison purposes.

For the following plots, the command signal for  $x$  is a sine wave and the initial state of  $x(0) = 0$ . The command signal for  $\theta$  is a cosine and the initial state of  $\theta(0) = 1$ . All cases are run with the non-linear system

The first plot is the SMC baseline case with a healthy plant. The next four plots show the results when the plant model experiences a “failure” as defined above.

Figure 2-21. Decoupled SMC Tracking, Baseline Case

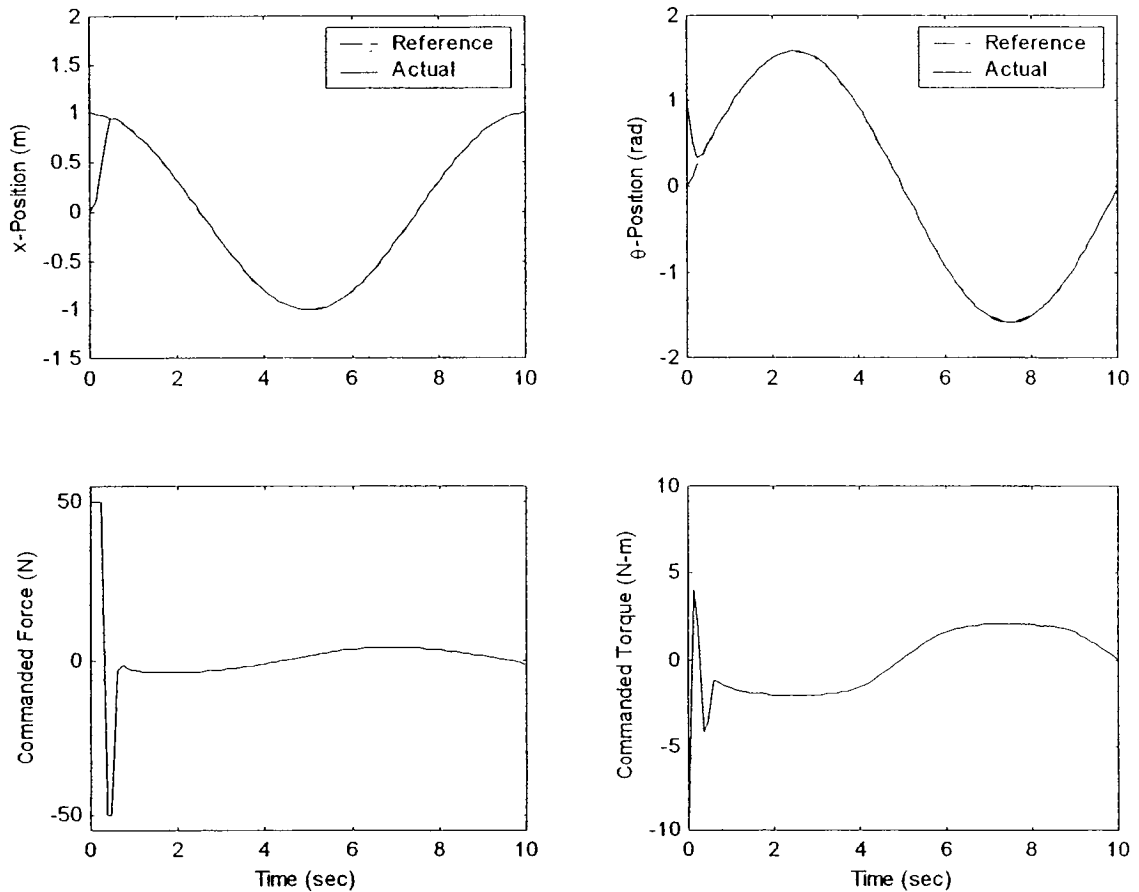
Figure 2-22: LQR Tracking with System Failure

Figure 2-23: SMC Tracking with System Failure

Figure 2-24: SMC Tracking with System Failure (Insufficient  $\rho_x$  &  $\rho_\theta$ )

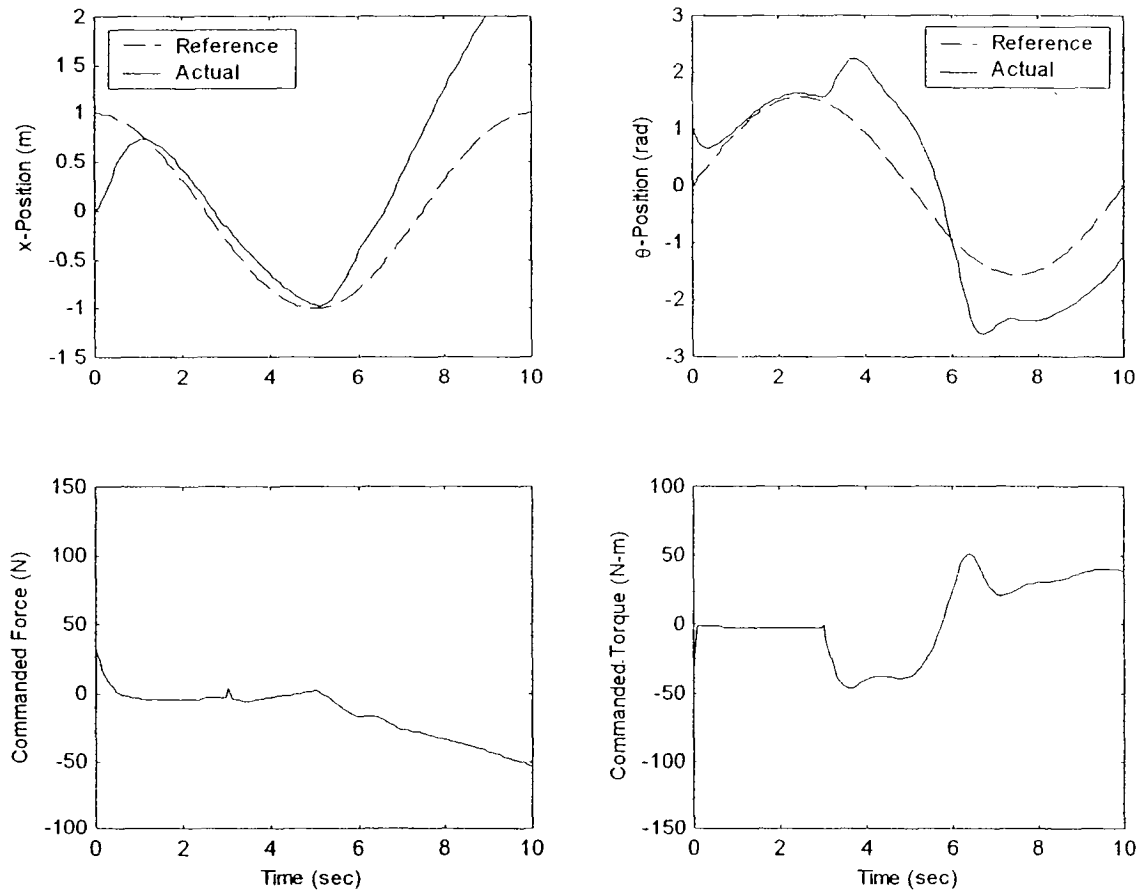
Figure 2-25: SMC Tracking with System Failure (Insufficient  $\rho_\theta$ )

This plot shows the SMC controller with:  $u = 50 \operatorname{sat}\left(\frac{\sigma_x}{0.4}\right)$  and  $\tau = 10 \operatorname{sat}\left(\frac{\sigma_\theta}{0.4}\right)$ . A non-linear system simulation is run with no system failure. Very nice decoupled tracking is demonstrated. The baseline LQR simulation performance looks the same



**Figure 2-21: Decoupled SMC Tracking, Baseline Case**

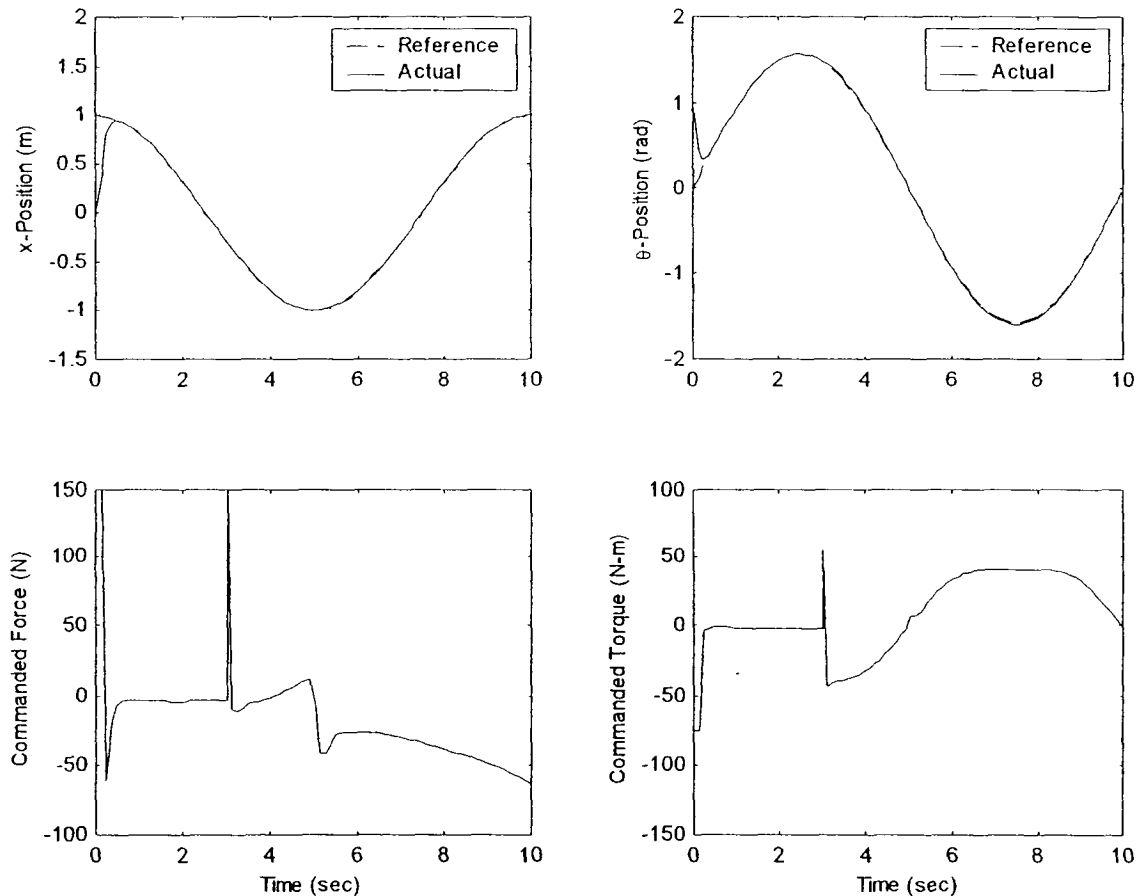
This plot shows the results of the LQR controller with failures. The disturbance bias at 5 sec has magnitude of 50. A non-linear system simulation is run with system failure at 3 sec. Tracking performance is severely degraded.



**Figure 2-22: LQR Tracking with System Failure**

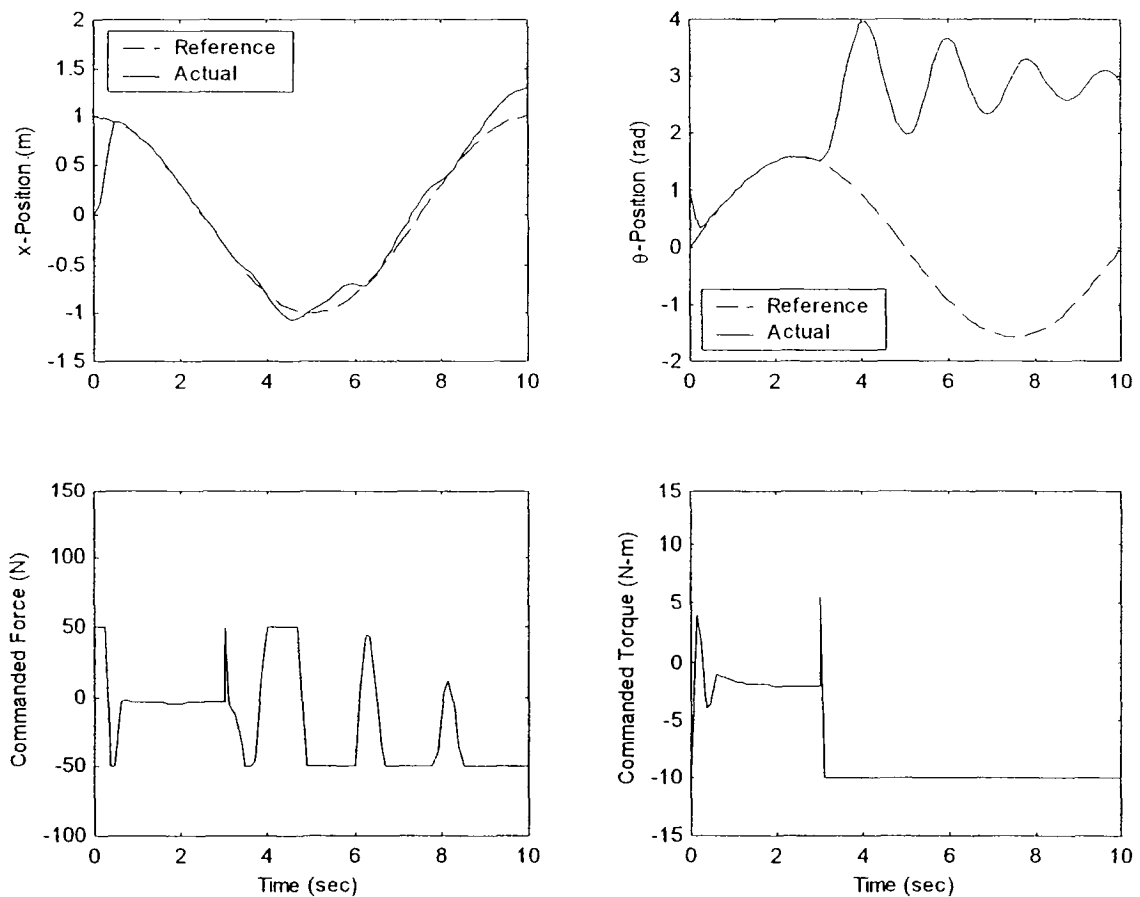
This plot shows the SMC controller with:  $u = 175 \operatorname{sat}\left(\frac{\sigma_x}{0.4}\right)$  and  $\tau = 75 \operatorname{sat}\left(\frac{\sigma_\theta}{0.4}\right)$

The disturbance bias at 5 sec has magnitude of 50. A non-linear system simulation is run with system failure at 3 sec. Very nice decoupled tracking is demonstrated. Notice the gains on the discontinuous control elements are higher than the baseline case. This is because a larger value is needed to provide the reaching condition in the face of the increased uncertainty.



**Figure 2-23: SMC Tracking with System Failure**

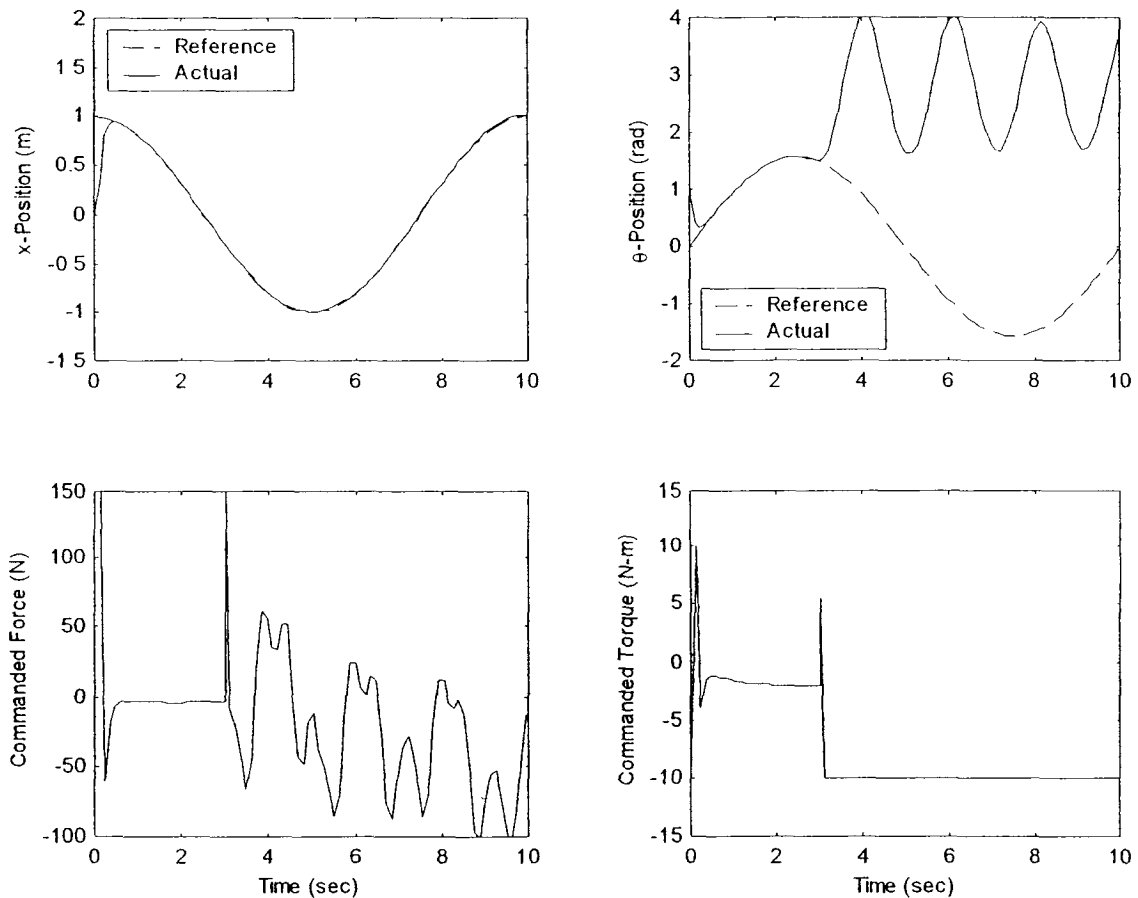
This plot shows the SMC controller with:  $u = 50 \operatorname{sat}\left(\frac{\sigma_x}{0.4}\right)$  and  $\tau = 10 \operatorname{sat}\left(\frac{\sigma_\theta}{0.4}\right)$ . The disturbance bias at 5 sec has magnitude of 50. A non-linear system simulation is run with system failure at 3 sec. Note the controller is still tracking  $x$  after the failure at 3 sec (although some degradation is apparent), but the disturbance bias at 5 sec causes  $x$  to diverge. The significance of this plot is that it demonstrates that if the disturbance level is higher than designed for, the SMC will not be able to stabilize the system—and, in fact, may drive a statically stable state unstable



**Figure 2-24: SMC Tracking with System Failure (Insufficient  $\rho_x$  &  $\rho_\theta$ )**

This plot shows the SMC controller with:  $u = 175 \text{ sat}\left(\frac{\sigma_x}{0.4}\right)$  and  $\tau = 10 \text{ sat}\left(\frac{\sigma_\theta}{0.4}\right)$ .

The disturbance bias at 5 sec has magnitude of 50. A non-linear system simulation is run with system failure at 3 sec. Note the controller is tracking  $x$  throughout, but  $\theta$  breaks tracking shortly after the system failure. The significance of this plot is that it demonstrates the ability of the controller to track one state even though another (coupled) state is not on its sliding mode.



**Figure 2-25: SMC Tracking with System Failure (Insufficient  $\rho_\theta$ )**

# Chapter 3

---

## Parasitic Dynamics and SMC

### 3.1 Introduction

As introduced in Chapter 2, unmodeled parasitic dynamics and physical limits are a significant implementation problem for sliding mode controllers. In order for the system to remain on the ideal sliding mode, an infinite frequency switching must occur. Real actuators and sensors prevent this infinite frequency switching, and the sliding mode is lost (along with all its desirable characteristics). In order to demonstrate the effects of actuator dynamics on a SMC system, the problem of the inverted pendulum on a translating cart is revisited. The single control input case with the regular form design is used. In all cases, the linear system model is used in the simulation. There is no noise and no bias disturbance. In each case, the initial state of the cart position is  $x(0) = -1.0$ , and the initial state of the pendulum angle is  $\theta(0) = -10$  deg. The control law is:

$u = 50 \operatorname{sat}\left(\frac{\sigma}{0.1}\right)$  with the same sliding surface as the first example in Section 2.2. Three

cases are presented. The only difference between them is the bandwidth of a simulated actuator: Figure 3-1: SMC Control, No actuator; Figure 3-2: SMC Control, With

Actuator:  $\frac{\delta}{u_c}(s) = \frac{20}{s+20}$ ; Figure 3-3: SMC Control, With Actuator:  $\frac{\delta}{u_c}(s) = \frac{13}{s+13}$ .

This is the baseline case with no actuator. Of course, excellent regulation of the states is evident.

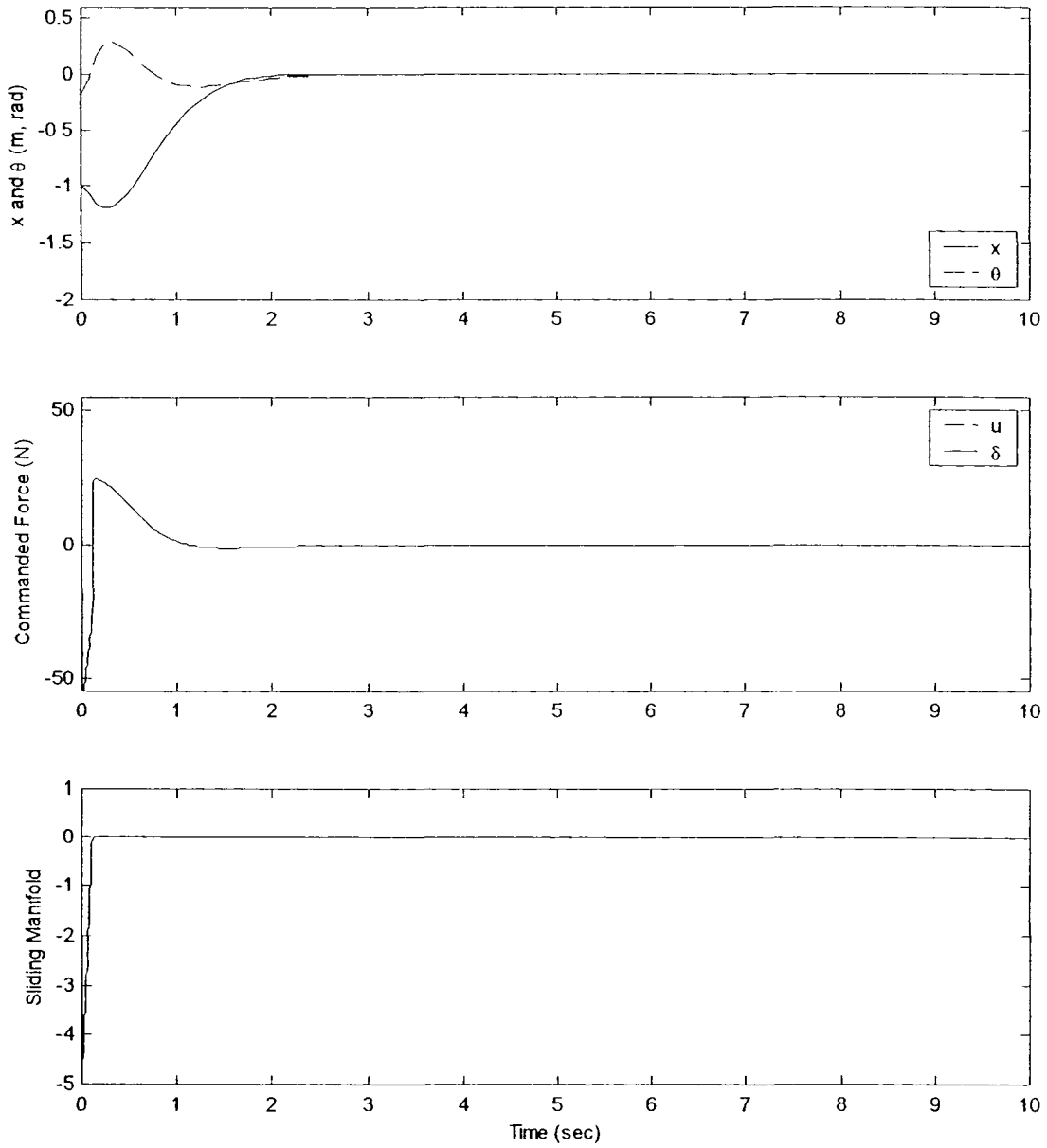
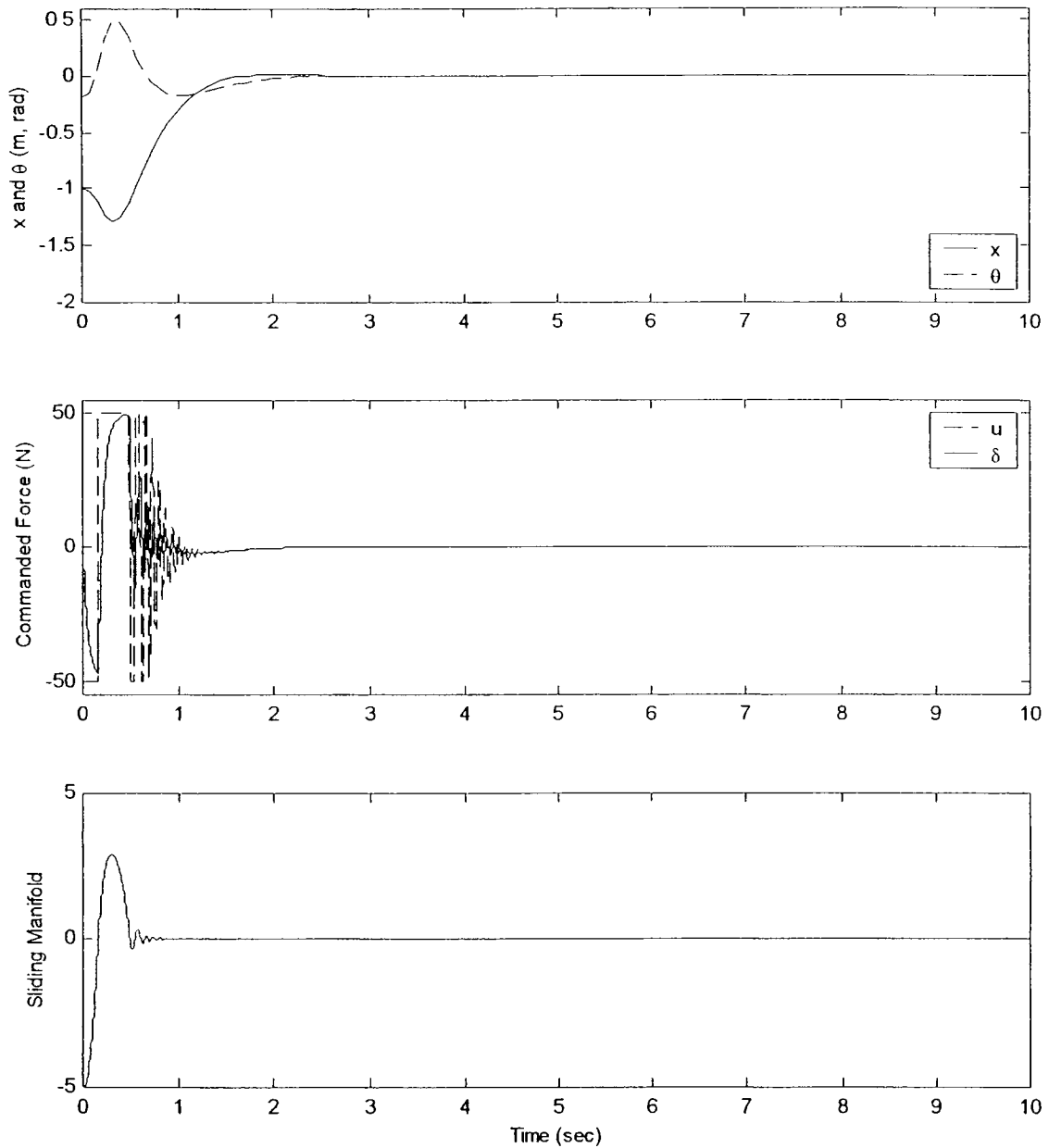


Figure 3-1: SMC Control, No actuator

This is the case with an actuator possessing a bandwidth well beyond the highest plant eigenvalue magnitude. Already, undesired oscillations appear.



**Figure 3-2: SMC Control, With Actuator:**  $\frac{\delta}{u_c}(s) = \frac{20}{s+20}$

By reducing the actuator bandwidth, the controller is unable to control the states. In fact, it drives both states unstable.

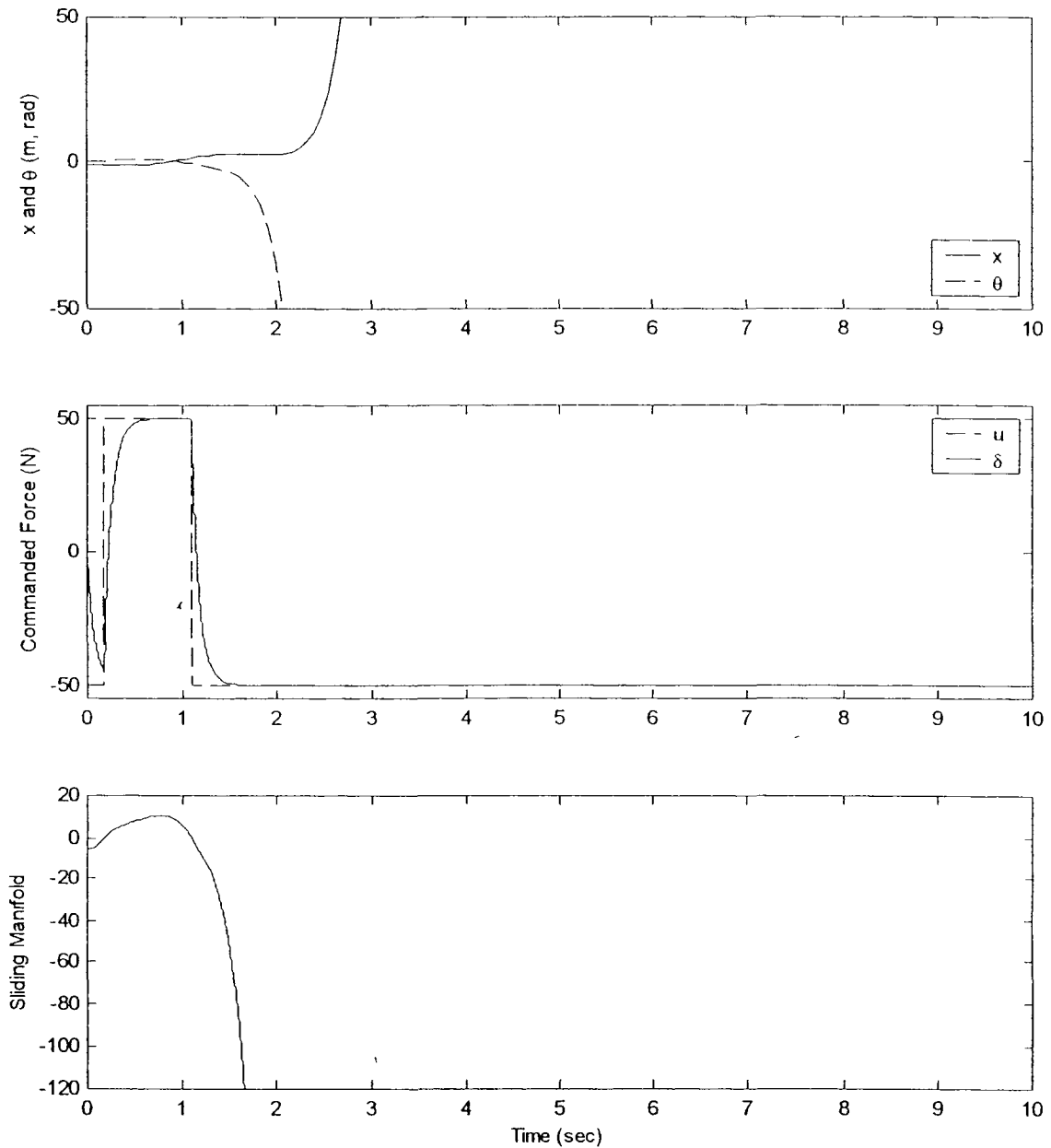
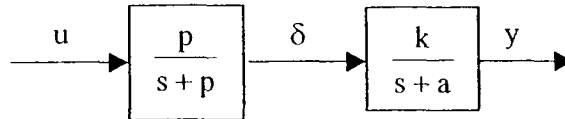


Figure 3-3: SMC Control, With Actuator:  $\frac{\delta}{u_c}(s) = \frac{13}{s+13}$

One approach to solve the actuator problem is to include the actuator in the initial design process. In this approach, the actuator is lumped together with the plant, and the sliding manifold is defined with the increased order associated with the addition of the actuator dynamics. For example, consider the following system.



**Figure 3-4: Simple Plant with Actuator**

Including the actuator dynamics, the input-output differential equation for the system is:

$$\ddot{y} + (p + a) \dot{y} + (pa) y = p k u \quad (3.1)$$

Define the sliding manifold as

$$\sigma = m \dot{y} + y \quad (3.2)$$

The order of this manifold is consistent with a traditional SMC—one degree less than the relative order of the state variable to be controlled. If the actuator had been neglected, the order of the manifold would have been zero instead of one. Next, find the equivalent continuous control,  $u_{eq}$ , needed to maintain ideal sliding motion by setting  $\dot{\sigma} = 0$  and solving for  $u$  (see Section 2.1.4)

$$u_{eq} = \left( \frac{m(p+a)-1}{m p k} \right) \dot{y} + \left( \frac{a}{k} \right) y \quad (3.3)$$

Substitute  $u_{eq}$  from (3.3) into the original differential equation (3.1) to obtain the closed loop, unforced system dynamics.

$$\ddot{y} = -\frac{1}{m} \dot{y} \quad (3.4)$$

Note that none of the parameters ( $p$ ,  $k$ , or  $a$ ) appear, implying that, when on the sliding surface, the system output is invariant to changes in both plant and actuator parameters. Indeed, simulations of this simple system confirm that this is the case. An interesting note is that, while the system output,  $y$ , is invariant to changes in both the actuator and plant parameters, the intermediate state,  $\delta$ , is only invariant to changes in the actuator parameters. This can become an issue if there are physical limits for  $\delta$  and can result in system instability if those limits are reached

The simple solution to the actuator problem would appear to be the inclusion of the actuator in the SMC design. The resulting system is robust to both actuator and plant variations. Unfortunately, this is difficult to implement in practice because of the increased order of the sliding manifold associated with the additional dynamics. In general, the order of the manifold will increase by the same order as the modeled actuator dynamics. This means, for a second order actuator, at least two derivatives of the output signal are required. For a real system with measurement noise, these additional derivatives make this approach very unattractive. While it is true that the SMC is very effective at rejecting the input noise, it does so by high frequency control commands. A noisy signal passed through two derivatives and an SMC would have highly undesired characteristics at the actuator input.

Young, Utkin, and Özgüner's classic survey paper, "A Control Engineer's Guide to Sliding Mode Control,"<sup>97</sup> briefly discusses the actuator bandwidth issue.

In plants where control actuators have limited bandwidth, e.g., hydraulic actuators, there are two possibilities: First, the actuator is outside the required closed-loop bandwidth. Thus the actuator dynamics become unmodeled dynamics.... While it is possible to ignore the actuator dynamics in linear control design, doing so in VSC requires extreme care. By ignoring actuator dynamics in a classical SMC design, chattering is likely to occur since the switching frequency is limited by the actuator dynamics even in the absence of other parasitic dynamics. Strictly speaking, sliding mode cannot occur, since the control input to the plant is continuous.

Second, the desired closed-loop bandwidth is beyond the actuator bandwidth. In this case, regardless of whether SMC or other control designs are to be used, the actuator dynamics are lumped together with the plant, and the control design model encompasses the actuator-plant in series. With the actuator dynamics no longer negligible, often the matching conditions for disturbance rejection and insensitivity to parameter variations in sliding mode which are satisfied in the nominal plant model are violated.

They then offer several approaches to deal with the problem of parasitic dynamics

- **Boundary Layer Control.** By increasing the boundary layer thickness, the effective linear gain is reduced, and the undesirable oscillations about the sliding manifold can be eliminated in some cases. While this method is often proposed, Young et al. are quick to point out that this is not a recommended approach. A worst case boundary layer control design is usually required, resulting in poor SMC disturbance rejection properties. For a tracking task, this means poor tracking. Further, boundary layer control can not always stabilize the chatter.
- **Observer-Based SMC.** An asymptotic observer is placed in the feedback path for the SMC. This observer acts as a high frequency bypass loop and

can eliminate chatter due to the unmodeled actuator dynamics. Section 3.3 investigates this approach further.

- **Disturbance Compensation.** An SMC disturbance estimator is used. The control law consists of a conventional linear feedback component and a discontinuous component based on the estimated disturbance.
- **SMC Design with Prefilter.** Actuator dynamics are incorporated as a prefilter to the SMC. A form of this approach is utilized by Shtessel and is demonstrated in Section 3.2. It is actually more of a postfilter, but the concept is similar. He does not refer to his method as this, but the approach falls into this general category.
- **Frequency Shaping.** The sliding manifolds are defined as linear operators and are “introduced to suppress frequency components of the sliding mode response in a designated frequency band.”

Of these different approaches, the two which appear most straightforward and applicable to the problem at hand are the observer-based and postfilter-based designs. A large body of work is available in the literature utilizing the postfilter approach, so this method is investigated first. It has some drawbacks which are discussed in the next section. The observer-based design is developed in Section 3.3. This approach is the one used in the final design methodology of this work.

### **3.2 Postfilter Design with Dynamic Boundary Layer**

Shtessel and his associates have a number of papers addressing the issue of finite bandwidth actuators with rate and position limits.<sup>63-66,106,110</sup> Actuator dynamics are handled by defining the sliding manifold in terms of the derivative of the output states,

creating a pseudo command which is the derivative of the desired actuator command. Note, this is similar to the approach of a 2-SMC. The actual actuator command is then obtained by integrating the pseudo command through a model of the actuator. It should be emphasized that this approach requires measurement of the actuator output. Again, although not referred as such, this method is essentially an SMC postfilter. As will be demonstrated in the examples to follow, this method works very well for a first order actuator with a known bandwidth. In order to handle rate and position limits, they use what they call “reconfigurable sliding modes.” Probably a more accurate description is “dynamic boundary layer.” The main idea is to dynamically adjust the boundary layer thickness to keep the controller operating in the linear region of a boundary layer saturation element. By increasing the boundary layer thickness, the tracking performance is degraded but the states remain within the boundary layer, stability is maintained, actuator limits are not violated, and integrator wind-up is avoided. For known limits, this method works very well, as will be shown in the following examples.

### 3.2.1 Application Example: Pitch Rate Tracking for an F-16

In order to exercise the ideas of Shtessel’s dynamic boundary layer and validate the operation of an example SMC, the exact same model from Shtessel’s work<sup>63</sup> is used.



Consider the linearized longitudinal short period mode approximation of an F-16 at Mach = 0.7, and h = 10,000 ft.

$$\begin{bmatrix} \dot{\alpha} \\ \dot{q} \end{bmatrix} = \tilde{\mathbf{A}} \begin{bmatrix} \alpha \\ q \end{bmatrix} + \tilde{\mathbf{B}} \delta_e \quad \dot{\delta}_e = -20 \delta_e + 20 u \quad (3.5)$$

where

$$\tilde{\mathbf{A}} = \mathbf{A}_n + \Delta\mathbf{A}, \quad \tilde{\mathbf{B}} = \mathbf{B}_n + \Delta\mathbf{B}$$

$$\mathbf{A}_n = \begin{bmatrix} -1.1500 & 0.9937 \\ 3.7240 & -1.2600 \end{bmatrix} \quad \Delta\mathbf{A} = \begin{bmatrix} 0.0400 & 0.0031 \\ 1.8560 & 0.4200 \end{bmatrix} \cdot \mathbf{1}(t-5)$$

$$\mathbf{B}_n = \begin{bmatrix} -0.1770 \\ -19.5000 \end{bmatrix} \quad \Delta\mathbf{B} = \begin{bmatrix} 0.0885 \\ 9.7500 \end{bmatrix} \cdot \mathbf{1}(t-5)$$

The “failure” simulated at  $t = 5$  sec represents a 50% loss of horizontal tail area

The pilot command,  $u_p$ , consists of 0.1 rad/s pitch rate pulses of 1.0 sec duration with polarities of -, +, -, and + at times of 0.0, 3.0, 6.0, and 9.0 seconds respectively. These commands are filtered by a reference model which is given in state space as:

$$\mathbf{A}_r = \begin{bmatrix} -1.2693 & 0.9531 \\ -9.4176 & -5.7307 \end{bmatrix} \quad \mathbf{B}_r = \begin{bmatrix} -0.1770 \\ -19.5000 \end{bmatrix}$$

The designed SMC control law is:

$$\sigma = (\dot{q}_r - \dot{q}) + 5(q_r - q) + 25 \int (q_r - q) d\tau$$

$$\delta_c = \delta + \left( \frac{1}{20} \right) \left( -10 \operatorname{sat} \left( \frac{\sigma}{0.1} \right) \right)$$

The block diagrams for the overall model and the SMC controller are given below.

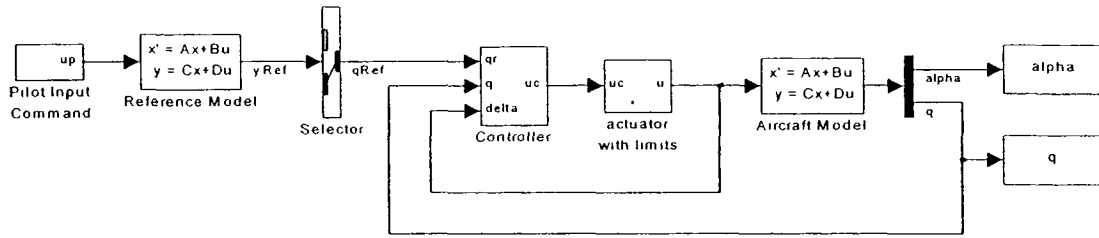


Figure 3-5: F-16 SISO Longitudinal System Block Diagram

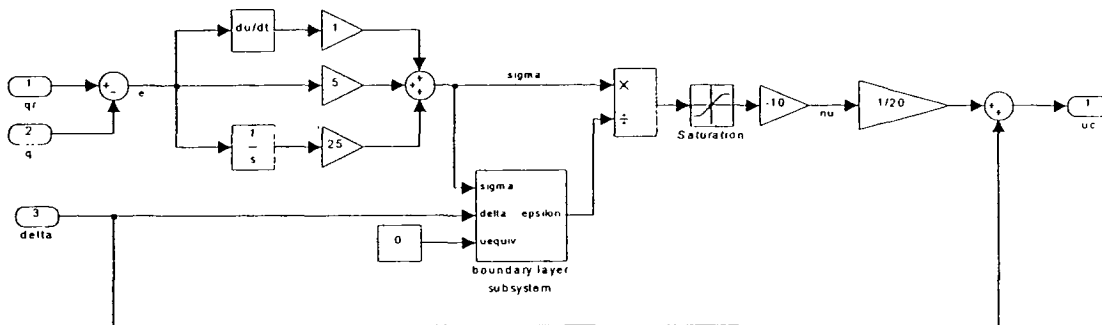
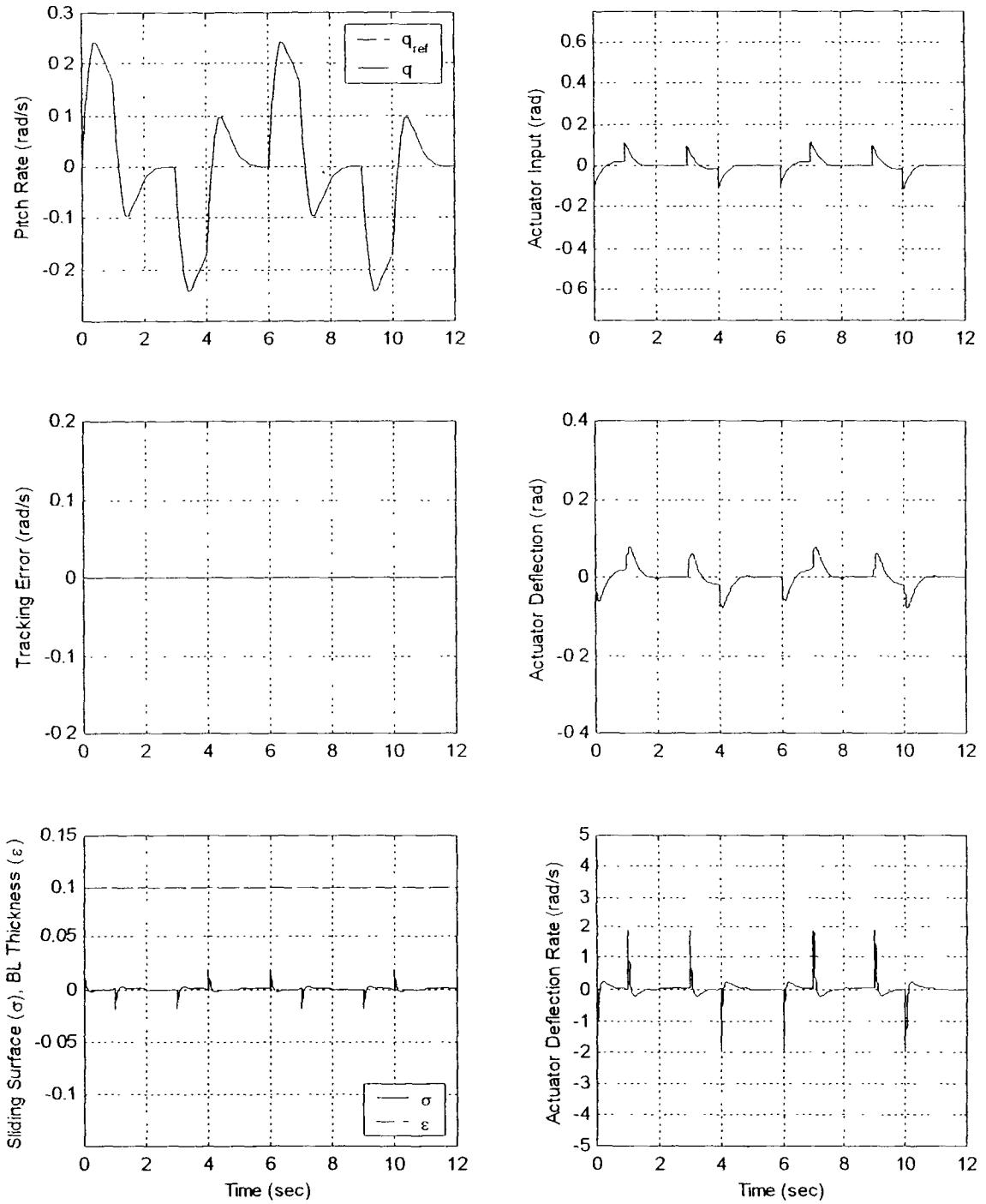
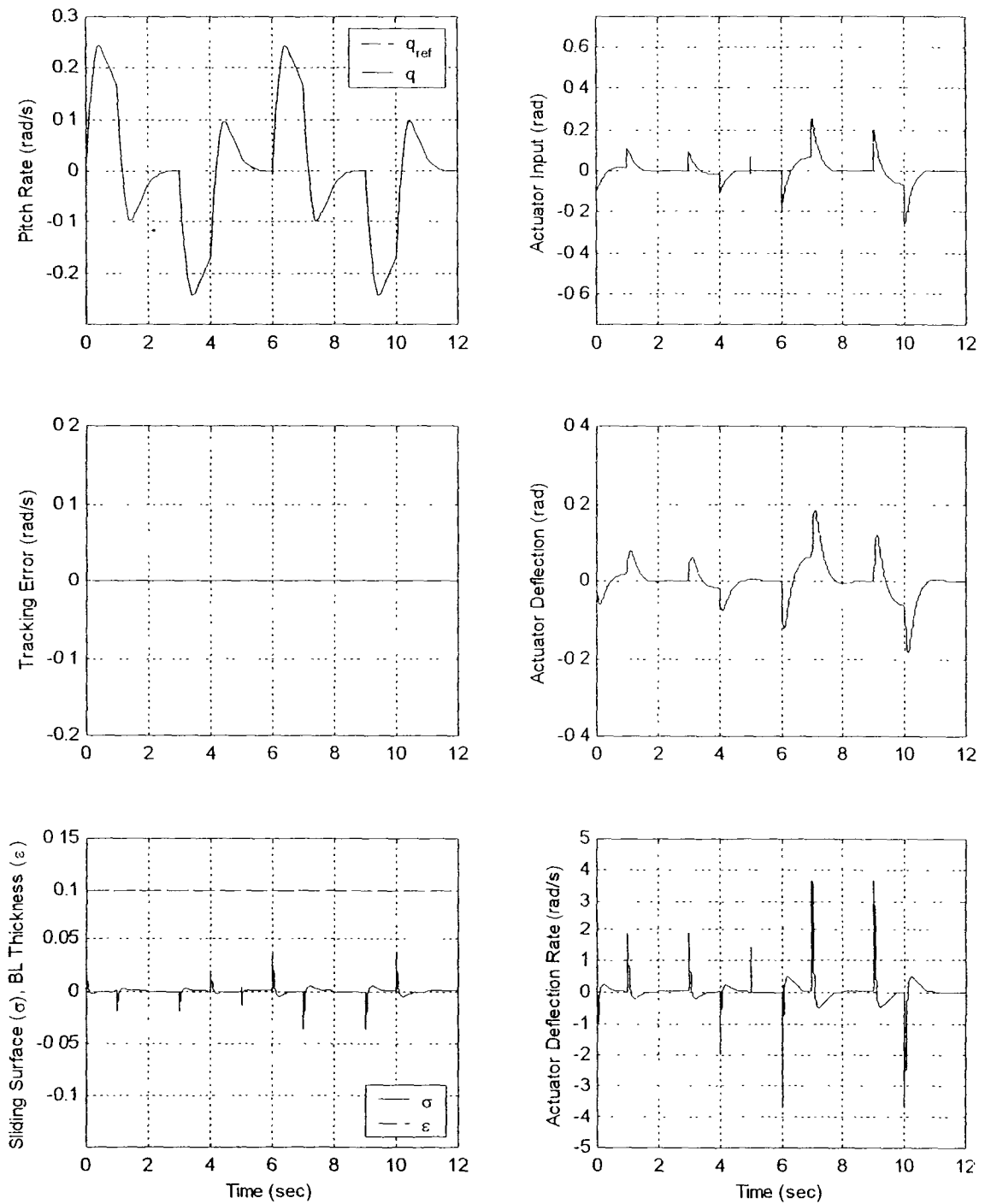


Figure 3-6: F-16 SISO SMC Controller Block Diagram

The simulation results for the healthy aircraft are shown in Figure 3-7. The results for the failed aircraft (failure at  $t = 5$  sec) are shown in Figure 3-8. In both cases, actuator dynamics are included, but actuator limits are not. The results are excellent tracking in both cases.



**Figure 3-7: F-16 SISO Pitch Rate Tracking, SMC, No Failure, No Limits**

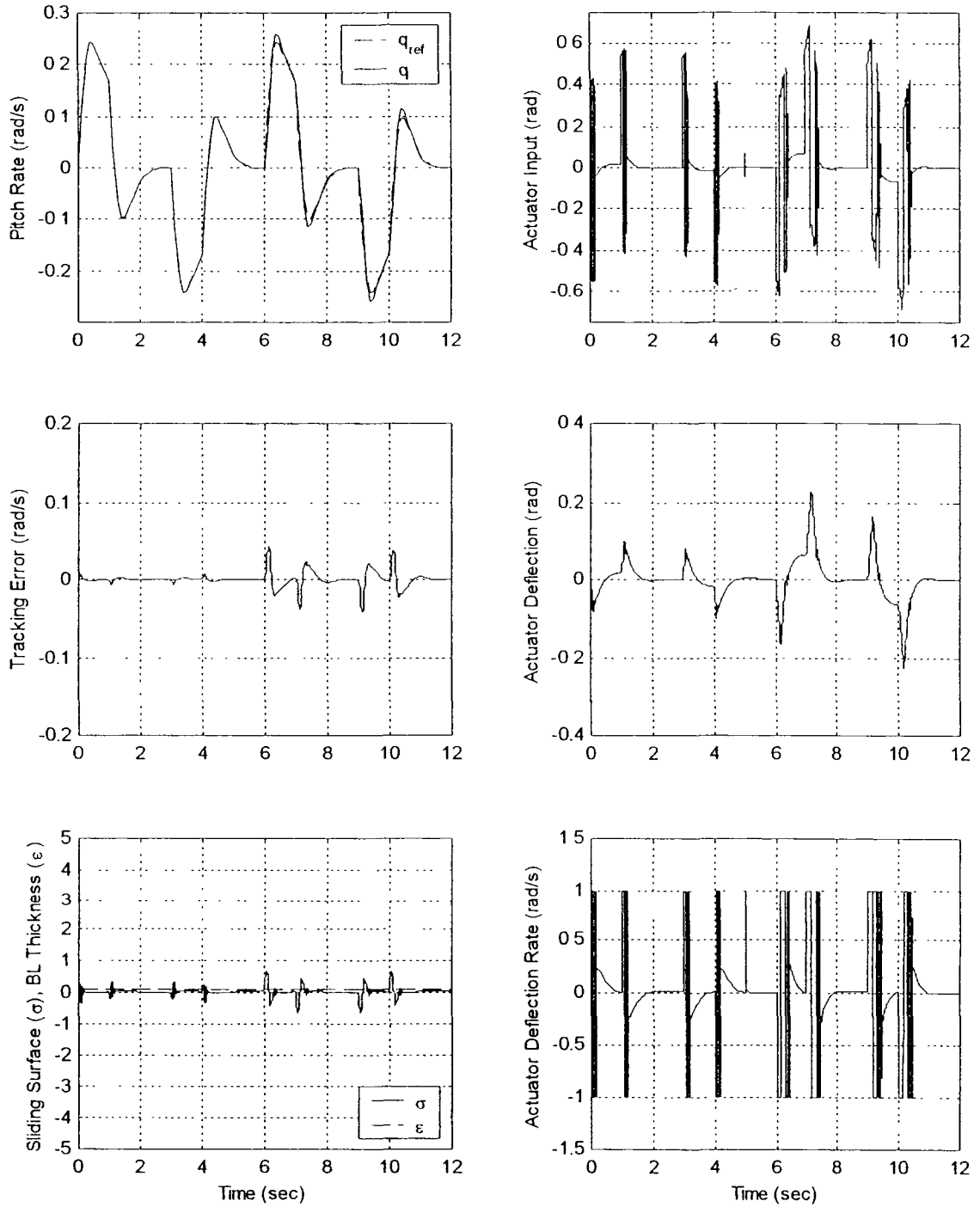


**Figure 3-8: F-16 SISO Pitch Rate Tracking, SMC, With Failure, No Limits**

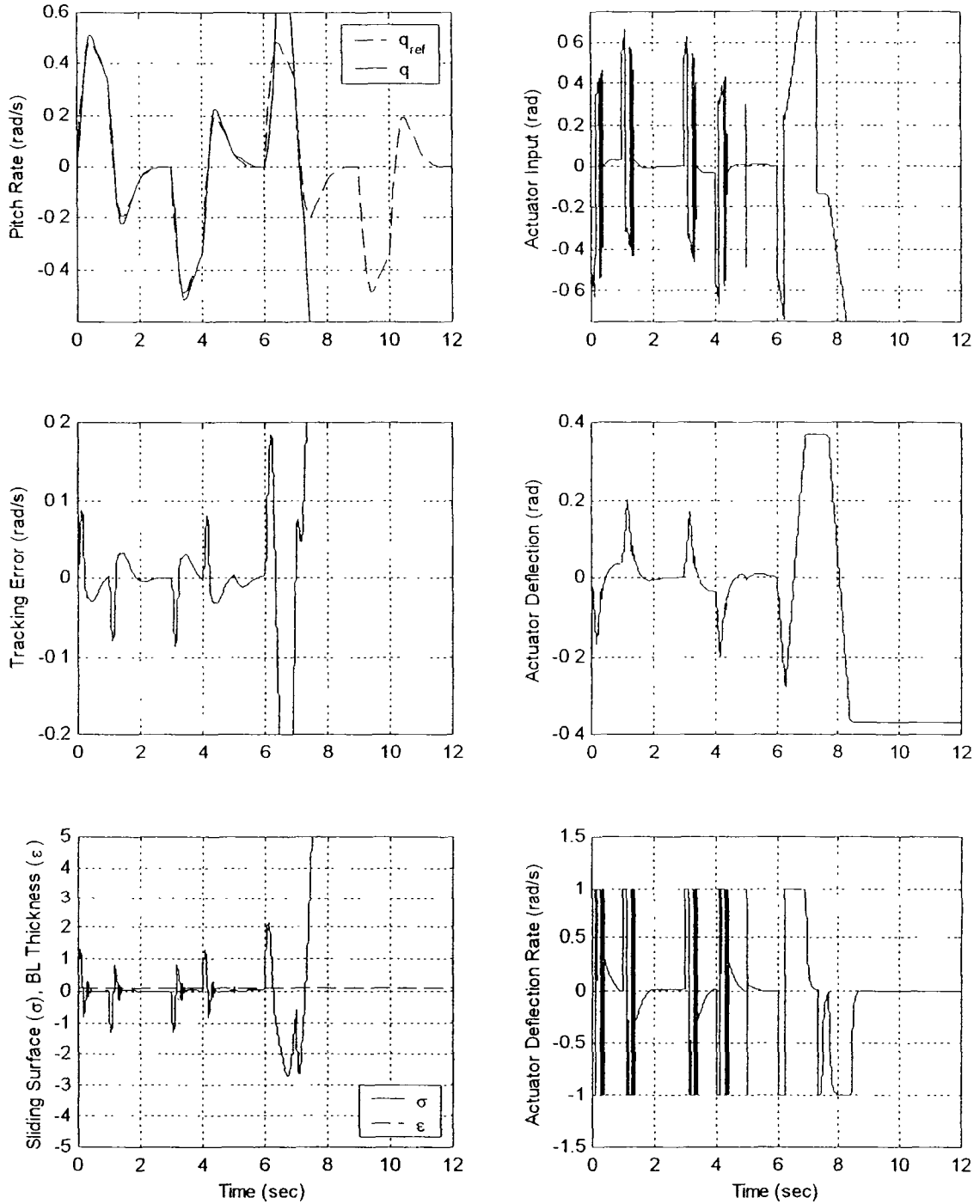
Next, actuator positions and rate limits  $\delta_{\max} = 0.37$  rad,  $\dot{\delta}_{\max} = 1.0$  rad/s are modeled. All the following plots use these limits. At this point, the boundary layer is static—Shtessel's dynamic boundary layer is not in use yet.

First, the case with same input profile as the baseline cases is given. The only difference between this case and the previous case is the inclusion of actuator limits in the simulation actuator models. The results are shown in Figure 3-9. Notice that some minor rate limiting occurs, but the position limit is never reached. The result is slightly degraded tracking performance. This tends to be typical—some rate limiting is usually tolerated.

Next, in order to cause the system to hard limit, the input profile is changed to 0.2 rad/s pitch rate pulses (instead of 0.1 rad/s). The results are shown in Figure 3-10. Once the actuator hits the position limits, the system no longer tracks the input and it becomes unstable. This also tends to be typical—with a static boundary layer and nonredundant control effectors, position limits are almost always fatal to SMC when encountered.



**Figure 3-9: F-16 SMC,  $u_p = 0.1$  rad/s, With Failure, With Limits, Static BL**



**Figure 3-10: F-16 SMC,  $u_p = 0.2$  rad/s, With Failure, With Limits, Static BL**

Shtessel *et al.*<sup>63-66,110</sup> propose a method to account for actuator limits in the SMC design. They use a dynamic boundary layer. The boundary layer thickness,  $\varepsilon$ , is calculated to satisfy the following inequalities which guarantees compliance with actuator displacement and rate limits and avoidance of integrator windup.<sup>63</sup>

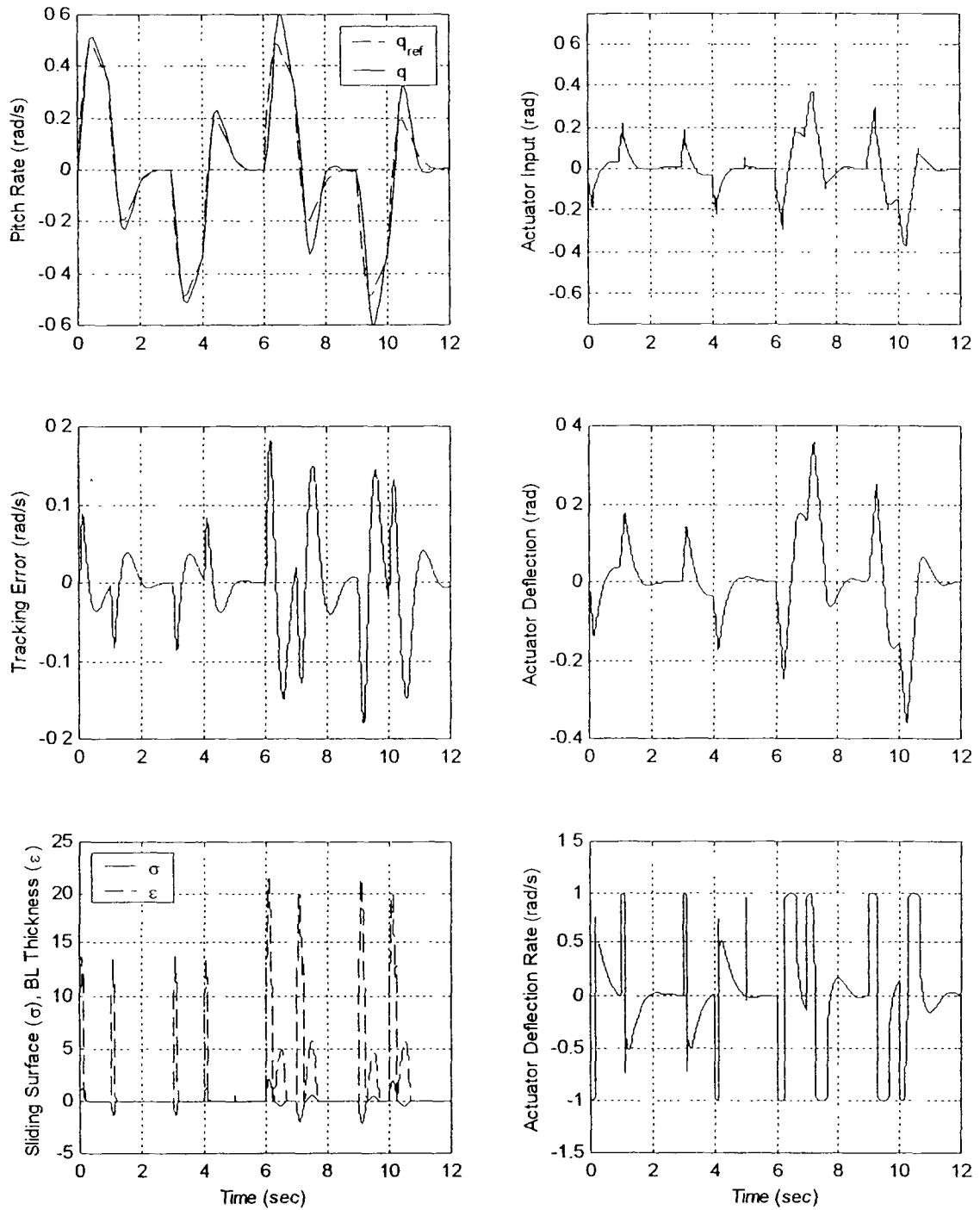
$$\text{Integrator Windup:} \quad |\sigma_i| \leq \varepsilon_i \quad \forall i = \overline{1, 3} \quad (3.6)$$

$$\text{Actuator Deflection Limit:} \quad \left| \delta_i + (1/a_\delta) \left[ \hat{v}_{eq_i} + \rho_i \left( \frac{\sigma_i}{\varepsilon_i} \right) \right] \right| \leq \delta_m \quad \forall i = \overline{1, 3} \quad (3.7)$$

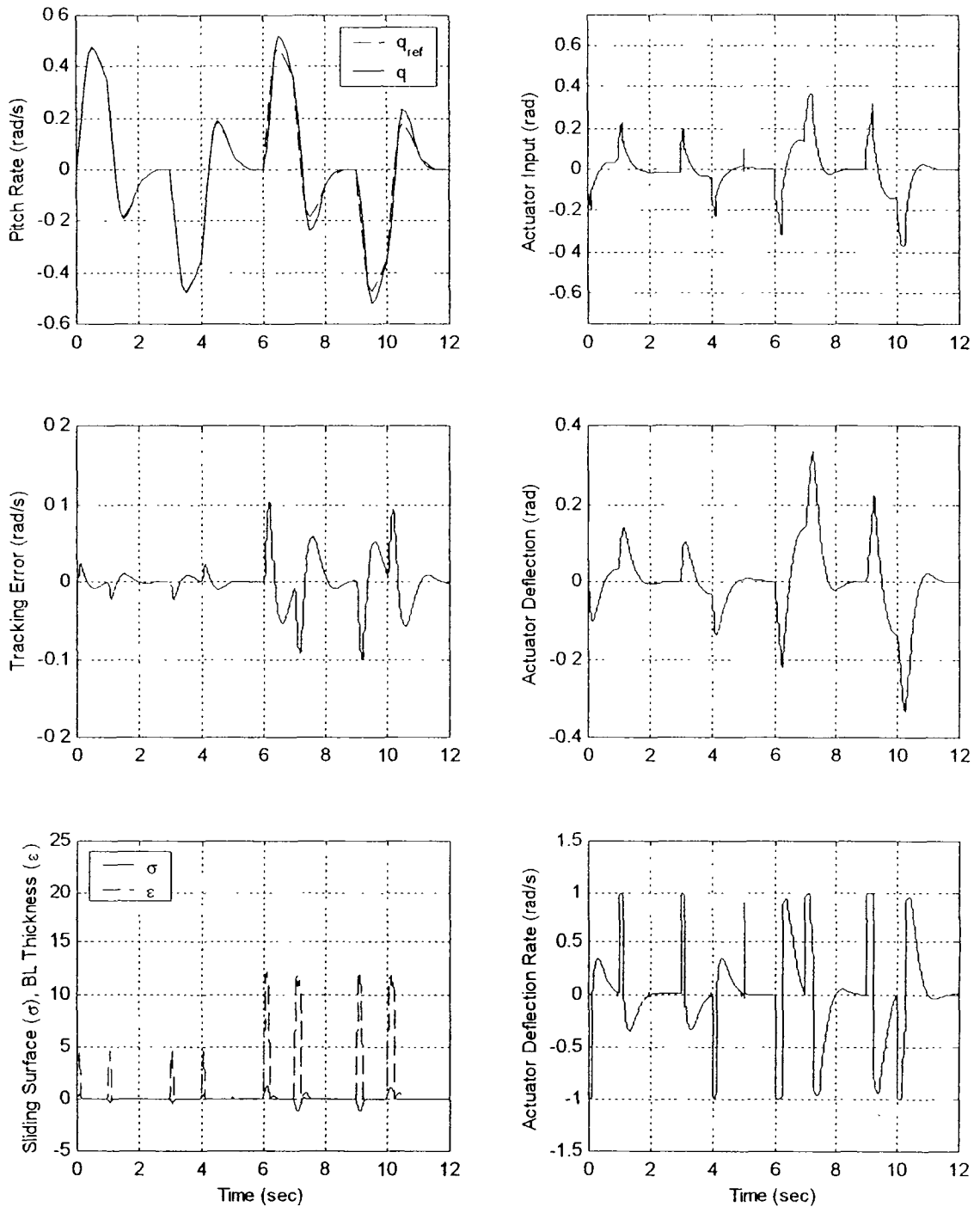
$$\text{Actuator Rate Limit:} \quad \left| \hat{v}_{eq_i} + \rho_i \left( \frac{\sigma_i}{\varepsilon_i} \right) \right| \leq \dot{\delta}_m \quad \forall i = \overline{1, 3} \quad (3.8)$$

The next case is the same as the previous case except it includes this dynamic boundary layer. The results are shown in Figure 3-11. The dynamic boundary layer keeps the system stable and achieves remarkably good tracking performance in the face of the actuator limiting. Tracking performance is degraded somewhat, but this is to be expected when limits are reached.

Next, the actuator bandwidth is decreased. Both the actual actuator model bandwidth and the design actuator model term in Eqn (3.7) are halved ( $a_\delta = 10$ ). Results are shown in Figure 3-12. Results are comparable to the last case.



**Figure 3-11: F-16 SMC,  $u_p = 0.2$  rad/s, With Failure, With Limits, Dynamic BL**



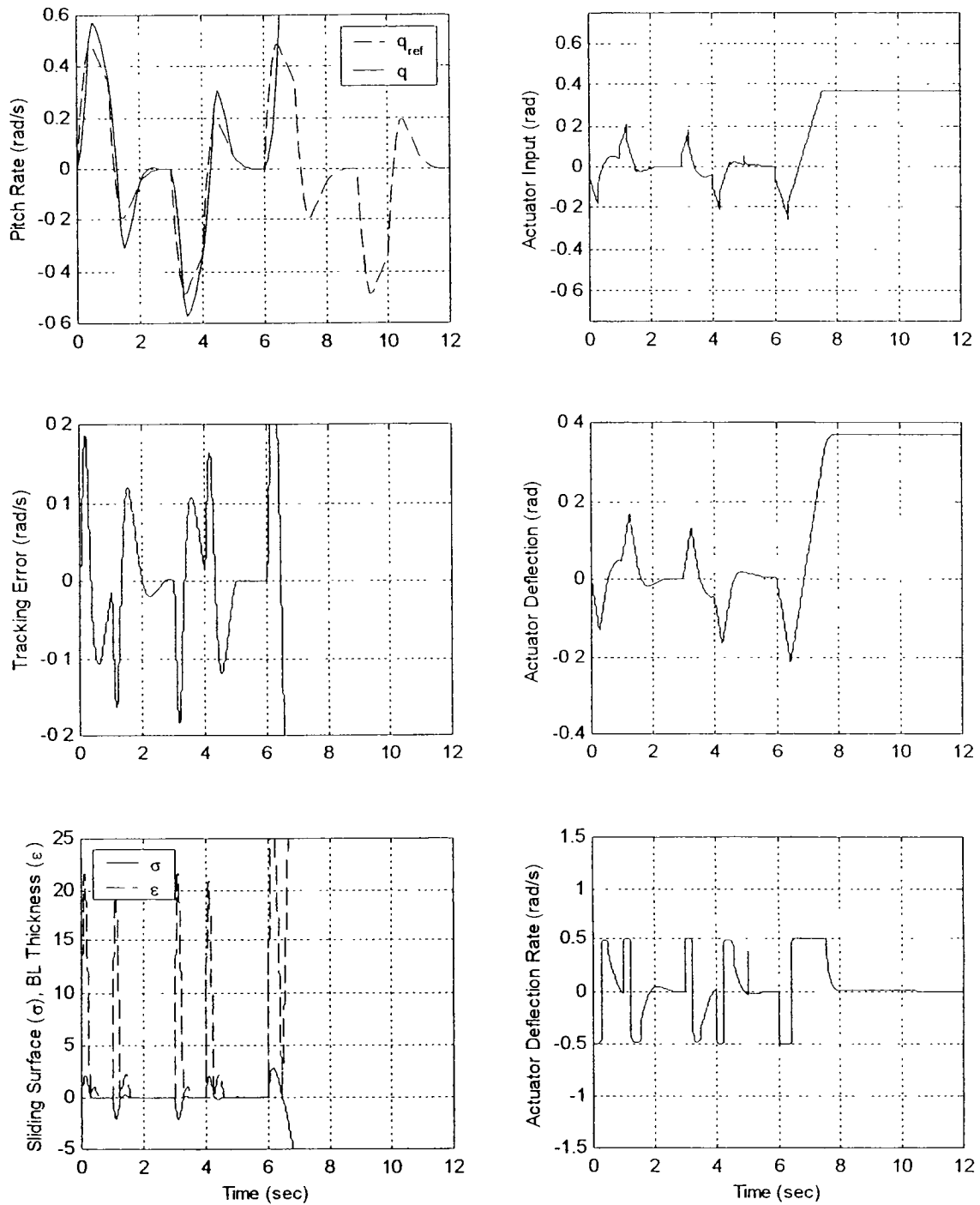
**Figure 3-12: F-16 SMC,  $u_p = 0.2$  rad/s, With Failure, With Limits, Dynamic BL, Known Slow Actuator**

Unfortunately, the actuator model term in Eqn ( 3.7 ) is a design parameter and has a static value. If the actual actuator dynamics do not match this, there could be problems. Figure 3-13 shows the results when the actuator model bandwidth is decreased but the design parameter in Eqn ( 3.7 ) remains the same. The system fails.

This presents a problem when considering an application for a reconfigurable design. After an actuator failure, the actuator dynamics are not known. Therefore, the very situation demonstrated here is likely to happen. Also, the rate and position limits are not known after a failure. Although not shown here, it turns out that off-design limits also result in an unstable SMC.

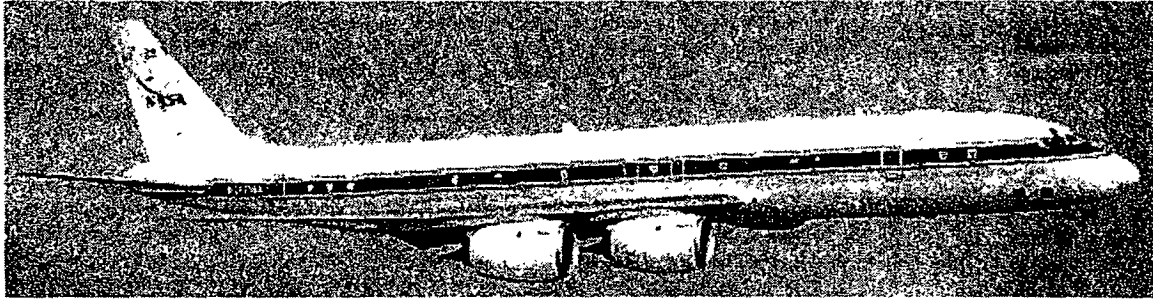
Another major drawback to this method is the assumption of a first order actuator in the control law. If a second order (or higher) actuator is used, the current control law fails. It seems plausible to re-derive the control law postfilter assuming a second order actuator. However, this would require the second derivative of the output states for the sliding manifold—which is unreasonable from a practical standpoint. Plus, this solution would only be valid for a second order actuator.

The conclusion is this: for actuators with known order, bandwidth, and limits, this method works exceptionally well. The results are the most impressive of any in the current literature. In fact, these results initially defined the direction of this research. However, the issues relating to changes in the true actuator dynamics have proven to be difficult to overcome.



**Figure 3-13: F-16 SMC,  $u_p = 0.2$  rad/s, With Failure, With Limits, Dynamic BL, Unknown Slow Actuator**

### 3.2.2 Application Example: Bank Angle Tracking for a DC-8



The problem of sensitivity to changes in actuator dynamics can be partially addressed using a multiple-loop scheme also proposed by Shtessel.<sup>66</sup> In this approach, an SMC is designed to track outer loop flight attitude angle commands. The output is a pseudo command for an inner loop SMC which tracks angular rates. In addition, a “very inner” loop is wrapped around the actuator and is controlled by another SMC.

For simplicity in an initial demonstration, a linear lateral-directional model of a DC-8 is taken from McRuer, Ashkenas and Graham.<sup>133</sup> The goal is to design a bank angle tracker. In this case, the longitudinal variables are not controlled, and the only actuators are the ailerons and rudder. This results in a square system, as required. Sideslip angle is also not controlled, but the yaw rate is regulated to zero.

Using the stability and control derivatives for flight condition 8003, the state space representation of the linear lateral-directional perturbation equations for the healthy DC-8 are:<sup>133</sup>

$$\begin{bmatrix} \dot{v} \\ \dot{p} \\ \dot{r} \\ \dot{\phi} \end{bmatrix} = \begin{bmatrix} -0.0868 & 0 & -824.2 & 32.174 \\ -0.0054 & -1.1810 & 0.3340 & 0 \\ 0.0026 & -0.0204 & -0.2280 & 0 \\ 0 & 1 & 0 & 0 \end{bmatrix} \begin{bmatrix} v \\ p \\ r \\ \phi \end{bmatrix} + \begin{bmatrix} -18.3300 & 0 \\ -0.5490 & 2.110 \\ 1.1640 & 0.0652 \\ 0 & 0 \end{bmatrix} \begin{bmatrix} \delta_a \\ \delta_r \end{bmatrix}$$

The healthy actuator dynamics are assumed be

$$\frac{\delta_a}{\delta_{ca}}(s) = \frac{\delta_r}{\delta_{cr}}(s) = \frac{20}{s+20}$$

**Outer Loop Design.** Although an SMC can be used for the outer loop, for simplicity a basic loop shaping technique is used here. It is assumed the inner loop SMC has provided decoupled control of the roll rate, so the effective system seen by the outer

loop is simply the roll rate model reference transfer function:  $\frac{p}{p_c}(s) = \frac{4}{s^2 + 2(0.8)2 + 2^2}$

The result of the loop shaping design gives the outer loop compensator:

$$G_c(s) = 1778 \frac{(s+2)^2}{(s+20)^3}$$

**Inner Loop Design:** The sliding mode control is designed using the derivative of the actuator position, and then the actual actuator command is calculated using the model of the actuator dynamics:  $\dot{\bar{\delta}} = -\mathbf{A}_\delta (\bar{\delta} - \bar{\delta}_c)$ . This means the system being controlled has relative order  $\bar{r} = \{2, 2\}^T$  and the sliding surfaces are given by

$$\sigma = \dot{\eta} + \mathbf{C}_2\eta + \mathbf{C}_3 \int \eta \, d\tau, \quad \sigma, \eta \in \mathbb{R}^2 \quad (3.9)$$

where  $\eta = \{(p_r - p), (r_r - r)\}^T$ .

The control law is

$$\delta_{ci} = \delta_i + \frac{1}{a_\delta} \left[ \rho_i \operatorname{sat} \frac{\sigma_i}{\varepsilon} \right] \quad \forall i = \overline{1,2} \quad (3.10)$$

Notice, again, this is a postfilter approach assuming a first order actuator. The chosen design parameters are:

$$C_2 = \text{diag}\{5\}, \quad C_3 = \text{diag}\{25\}, \quad \varepsilon = 1, \quad \rho_{\delta_a} = -50, \quad \rho_{\delta_r} = 25$$

**Actuator Loop Design:** The sliding surfaces are given by:

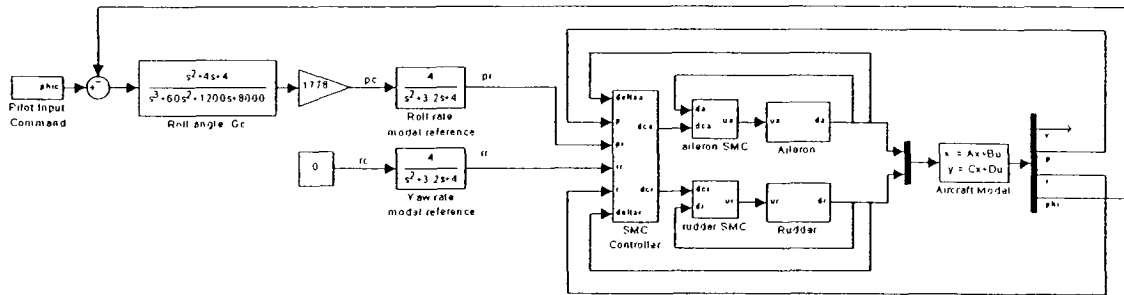
$$\sigma_{\delta_a} = (\delta_{ca} - \delta_a) + 10 \int (\delta_{ca} - \delta_a) d\tau$$

$$\sigma_{\delta_r} = (\delta_{cr} - \delta_r) + 10 \int (\delta_{cr} - \delta_r) d\tau$$

and the SMC control law is

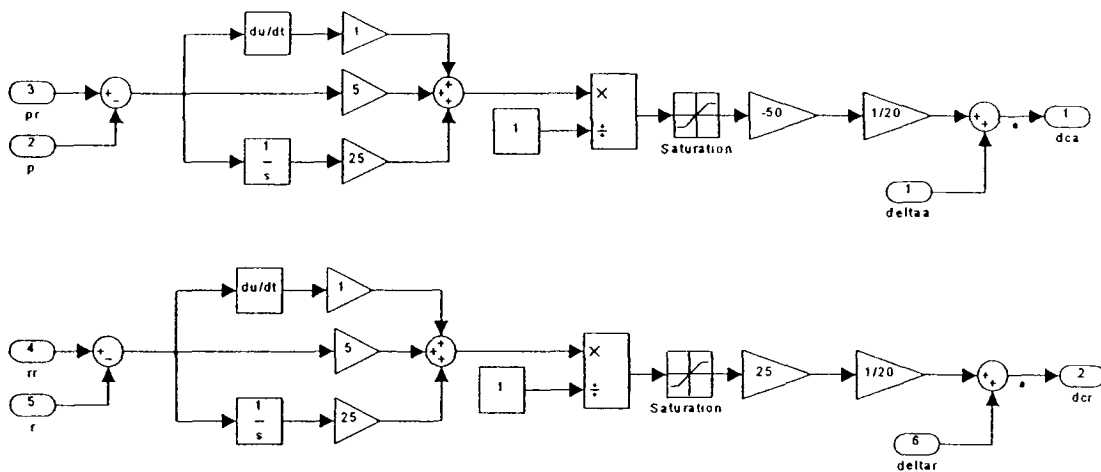
$$u_{\delta_a} = 10 \text{ sat}\left(\frac{\sigma_{\delta_a}}{1}\right) \quad u_{\delta_r} = 10 \text{ sat}\left(\frac{\sigma_{\delta_r}}{1}\right)$$

A schematic of the overall system is shown in Figure 3-14.



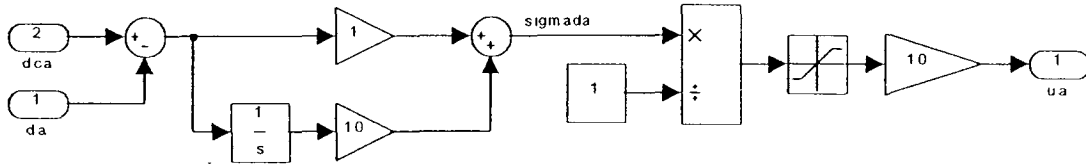
**Figure 3-14: Schematic of DC-8 Lat/Dir Control System**

A schematic of the inner loop SMC is shown in Figure 3-15.



**Figure 3-15: Inner Loop Sliding Mode Controller**

A schematic of the actuator loop SMC is shown in Figure 3-16 (note both actuator controllers are the same; only one is shown).



**Figure 3-16: Actuator Loop Sliding Mode Controllers**

Results for a case with no failure and no noise is given in Figure 3-17. The controller achieves excellent tracking.

Next, a failure is simulated to test the system's ability to handle a failure. The "failure" is defined as

System A-matrix

$$A_{\text{FAIL}} = \begin{bmatrix} 0.5 a_{11} & 0.5 a_{12} & 0.5 a_{13} & 0.5 a_{14} \\ 0.5 a_{21} & 0.5 a_{22} & 0.5 a_{23} & 0.5 a_{24} \\ 0.5 a_{31} & 0.5 a_{32} & 0.5 a_{33} & 0.5 a_{34} \\ a_{41} & a_{42} & a_{43} & a_{44} \end{bmatrix}$$

Aileron Control Power Derivatives

$$Y_{\delta_a(\text{FAIL})} = 0.2 Y_{\delta_a} \quad L_{\delta_a(\text{FAIL})} = 0.2 L_{\delta_a} \quad N_{\delta_a(\text{FAIL})} = 0.2 N_{\delta_a}$$

Aileron Actuator Bandwidth

$$\frac{\delta_a}{\delta_{ca}}(s)_{\text{FAIL}} = \frac{(0.2) 20}{s + (0.2) 20}$$

Results for a case with a simulated failure at  $t = 4.0$  sec and no noise is given in Figure 3-18. Again, the controller achieves excellent tracking. In fact, there is no difference in the tracking performance between this case and the un-failed case. The multi-loop system is invariant to the changes in the A-matrix, the B-matrix, and even to the reduced bandwidth of the actuator.

Unfortunately, the required control action is completely unrealistic. If actuator rate and position limits are considered, this system fails. Of course, if Shtessel's dynamic boundary layer is employed in the inner loop, stability can be maintained in the face of actuator limits (with the expected degradation in performance). However, in order for the dynamic boundary layer to work, the limits must be known. While this approach handles changes to actuator dynamics nicely, it still does not solve the problem of unknown limits. It also does not solve the problem of unknown actuator order. Again, a first order actuator is assumed. If a higher order actuator is present, the control law fails. Another drawback to this approach is the assumption that the states of the actuator (position and rate) are available. This could present actual implementation issues—especially in a reconfigurable setting.

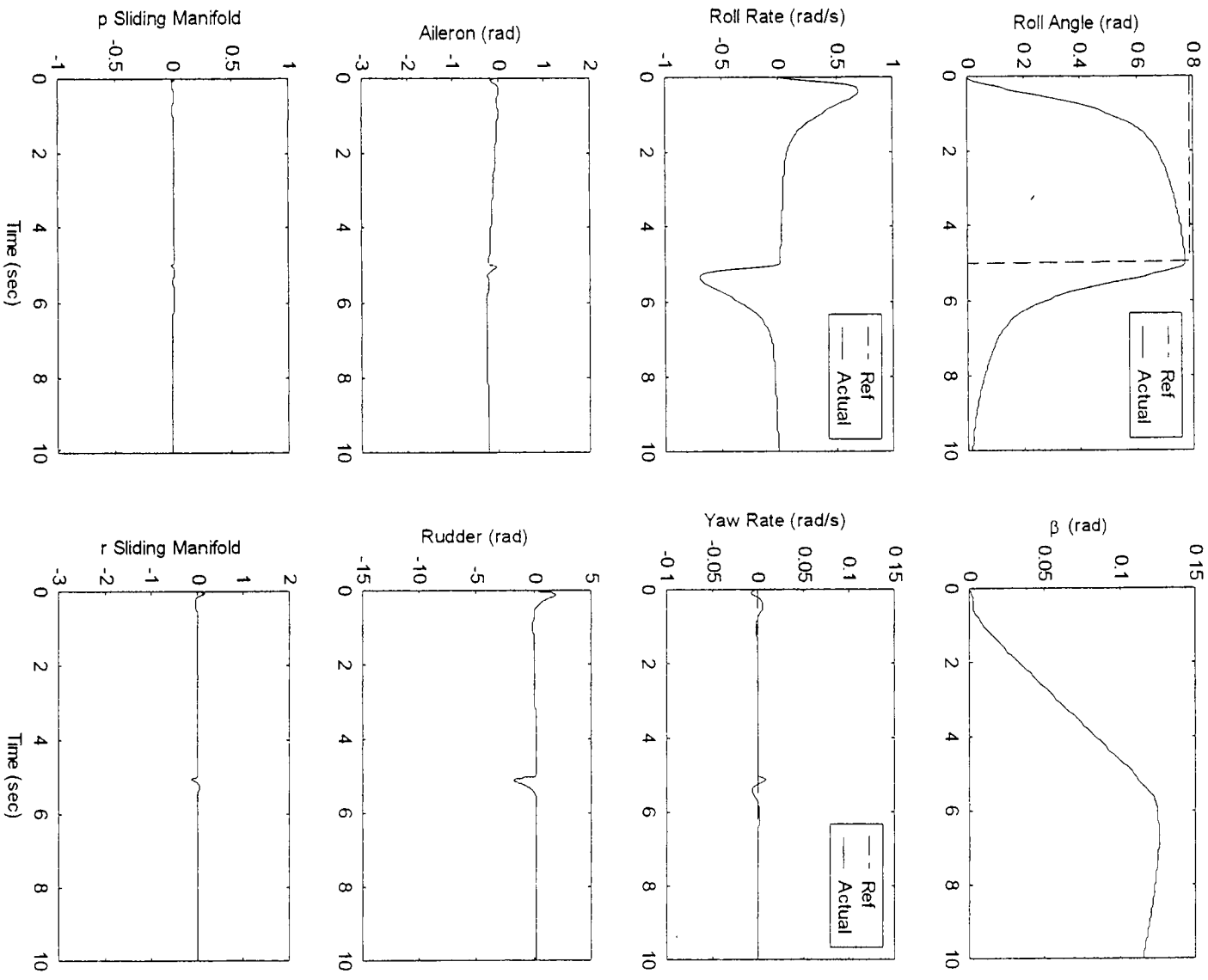
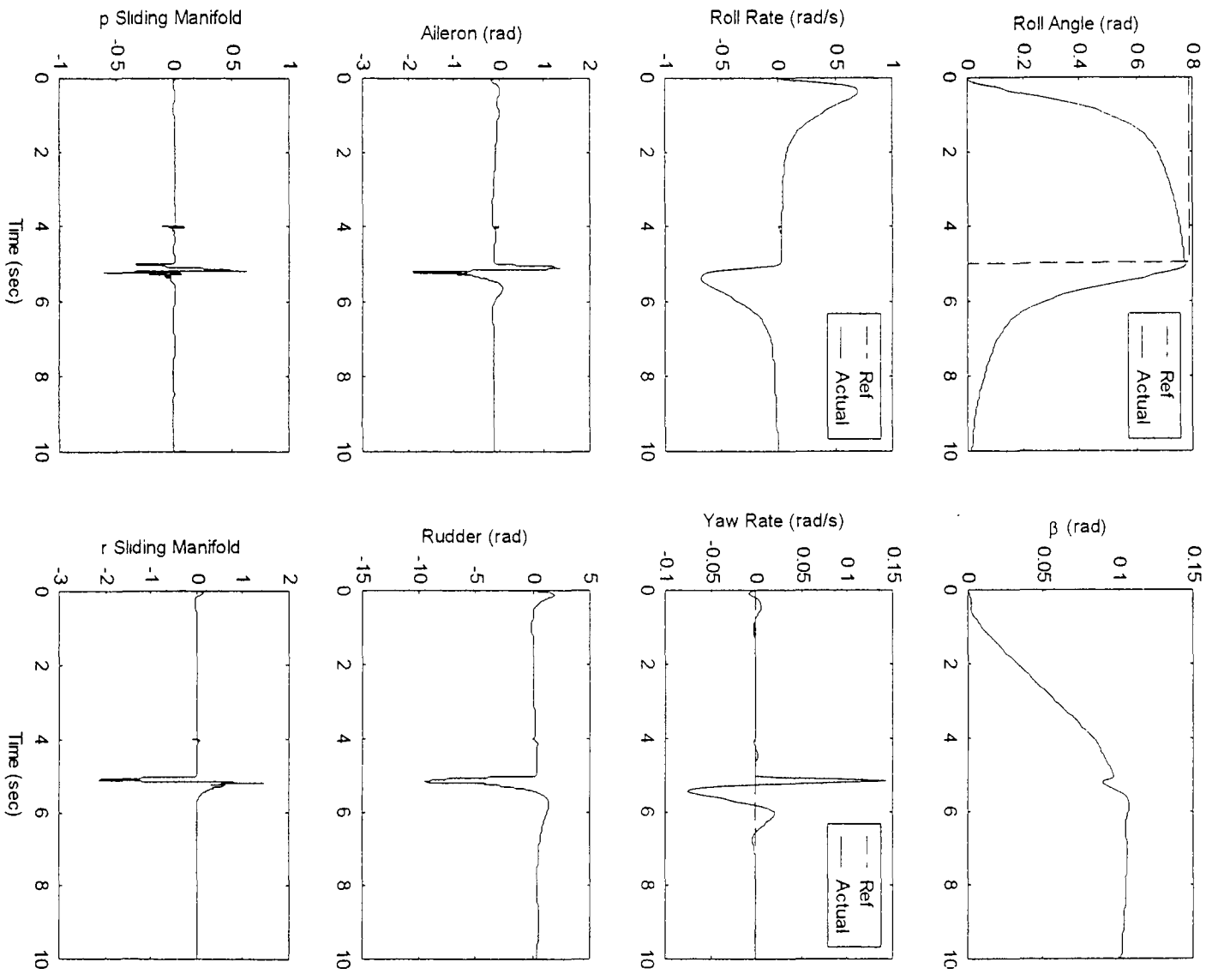


Figure 3-17: DC-8 Roll Angle Tracking Results, No Failure



**Figure 3-18: DC-8 Roll Angle Tracking Results, With Failure**

### 3.3 Observer-Based SMC

Recognizing the essential triggering mechanism for chattering is due to the interactions of the switching action with the parasitic dynamics, an approach which utilizes asymptotic observers to construct a high-frequency pass loop has been proposed. This design exploits a localization of the high-frequency phenomenon in the feedback loop by introducing a discontinuous feedback control loop which is closed through an asymptotic observer of the plant. Since the model imperfections of the observer are supposedly smaller than those in the plant, and the control is discontinuous only with respect to the observer variables, chattering is localized inside a high-frequency loop which bypasses the plant. However, this approach assumes that an asymptotic observer can indeed be designed such that the observation error converges to zero asymptotically.<sup>97</sup>

This is a good qualitative description of how an observer-based SMC works. However, what is not clear is exactly why the observer helps and how to choose the appropriate observer gains. Initial simulation runs confirmed the utility of the observer-based design. The observer does, indeed, enable an SMC to run in the presence of unmodeled finite bandwidth actuators. However, the performance is highly dependent upon the speed of the observer (the observer gains). In general, if the observer gains are too high, chatter and instability result. Sensor noise also becomes a problem. If the observer gains are too low, robustness to system parameter variations is lost.

In order to investigate this further, consider the following system.

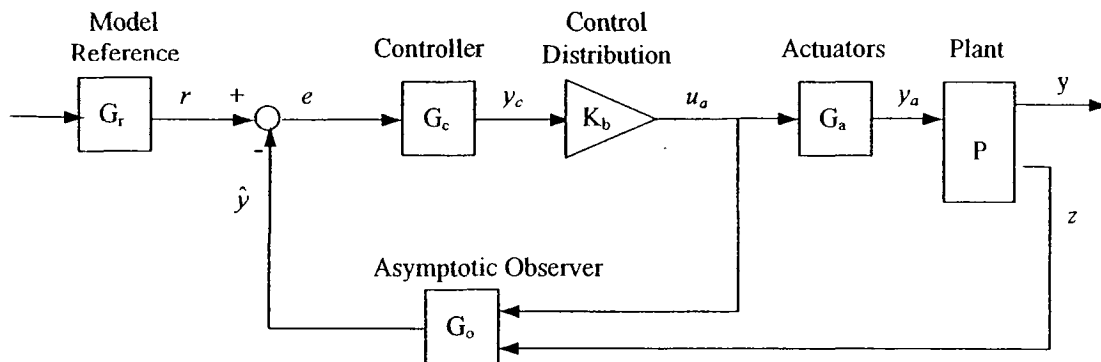


Figure 3-19: Observer-Based SMC Block Diagram

Define the following state space representations for the given system:

$$\begin{aligned} x \in \mathfrak{R}^n, \quad x_a \in \mathfrak{R}^{n_a}, \quad x_c \in \mathfrak{R}^{n_c}, \quad x_r \in \mathfrak{R}^{n_r}, \quad \hat{x}_o \in \mathfrak{R}^{n_o} \\ y \in \mathfrak{R}^{m_y}, \quad y_a \in \mathfrak{R}^m, \quad y_c \in \mathfrak{R}^{m_y}, \quad y_r \in \mathfrak{R}^{m_y}, \quad \hat{y} \in \mathfrak{R}^{m_y}, \quad z \in \mathfrak{R}^{m_z} \end{aligned} \quad (3.11)$$

Linear Plant

$$\dot{x} = \mathbf{A} x + \mathbf{B} y_a$$

$$y = \mathbf{C}_y x + \mathbf{D}_y y_a$$

$$z = \mathbf{C}_z x + \mathbf{D}_z y_a$$

Actuators

$$\dot{x}_a = \mathbf{A}_a x_a + \mathbf{B}_a \mathbf{K}_b y_c$$

$$y_a = \mathbf{C}_a x_a + \mathbf{D}_a \mathbf{K}_b y_c$$

Reference Model

$$\dot{x}_r = \mathbf{A}_r x_r + \mathbf{B}_r r_p$$

$$y_r = \mathbf{C}_r x_r + \mathbf{D}_r r_p$$

Observer

$$\dot{\hat{x}} = (\mathbf{A}_o - \mathbf{G} \mathbf{C}_z) \hat{x} + \mathbf{B}_o \mathbf{K}_b y_c + \mathbf{G} z$$

$$\hat{y} = \mathbf{C}_o \hat{x}$$

For the sake of analysis, consider an equivalent plant in which the control distribution, actuators, nominal plant, and observer are lumped together as shown below.

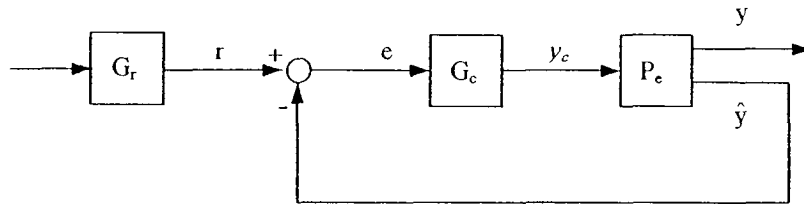


Figure 3-20: Equivalent Plant with Observer

It is easy to show that the state space representation of this system is given by

$$\begin{aligned} \dot{x}_e &= \begin{bmatrix} \mathbf{A} & \mathbf{B} \mathbf{C}_a & \mathbf{0}_{n \times n_o} \\ \mathbf{0}_{n_a \times n} & \mathbf{A}_a & \mathbf{0}_{n_a \times n_o} \\ \mathbf{G} \mathbf{C}_z & \mathbf{G} \mathbf{D}_z \mathbf{C}_a & (\mathbf{A}_o - \mathbf{G} \mathbf{C}_z) \end{bmatrix} x_e + \begin{bmatrix} \mathbf{B} \mathbf{D}_a \mathbf{K}_b \\ \mathbf{B}_a \mathbf{K}_b \\ \mathbf{B}_o \mathbf{K}_b + \mathbf{G} \mathbf{D}_z \mathbf{D}_a \mathbf{K}_b \end{bmatrix} y_c \\ y &= \begin{bmatrix} \mathbf{C}_y & \mathbf{0}_{m_y \times (n_a + n_o)} \end{bmatrix} x_e + \begin{bmatrix} \mathbf{D}_y \mathbf{K}_b \end{bmatrix} y_c \\ \hat{y} &= \begin{bmatrix} \mathbf{0}_{m_y \times n} & \mathbf{0}_{m_y \times n_a} & \mathbf{C}_o \end{bmatrix} x_e \end{aligned} \quad x_e = \begin{bmatrix} x \\ x_a \\ \hat{x} \end{bmatrix} \quad (3.12)$$

It is instructive to now examine the transfer function  $\frac{\hat{y}}{y_c}(s)$  and compare it to both the

original nominal plant transfer function with no actuator and the plant with the actuator

For the MIMO case, the transfer functions of interest are the ones from the control outputs to their corresponding output variable. Since a square system is assumed, this direct correspondence will always exist. The cross-coupling transfer functions are not needed here

### 3.3.1 Observer-Based Design, SISO Case

Consider the F-16 SISO system given in Section 3.2.1 with a second order actuator  $\frac{\delta}{\delta_c}(s) = \frac{20^2}{s^2 + 2 \cdot 0.7 \cdot 20 s + 20^2}$ . Recall the controlled feedback variable is pitch rate,  $q$ . The Bode plots of the nominal system and the nominal system with the actuator are shown in the Figure 3-21. While this plot does not show anything surprising, there are two things to point out when considering a sliding mode controller for this system. First, the relative order of the nominal plant is 1. Therefore, if the actuator dynamics are neglected, the order of a traditional 1-SMC sliding manifold has to be 0 (1 degree less than the relative degree of the controlled state). Unfortunately, the real system has the actuator, so the actual relative degree of the system is 3. Therefore, the SMC can not be guaranteed to stabilize the system with the actuator. Second, if the actuator is included in the design, the sliding manifold would need to be 2<sup>nd</sup> order. While an SMC could be designed to stabilize this system, the second derivative of the pitch rate would be required. Now, compare the estimated output from the equivalent system shown above with the nominal plant output. The observer poles are arbitrary selected to be very fast, ( $\lambda = -500, -501$ ). The resulting Bode plots are shown in Figure 3-22.

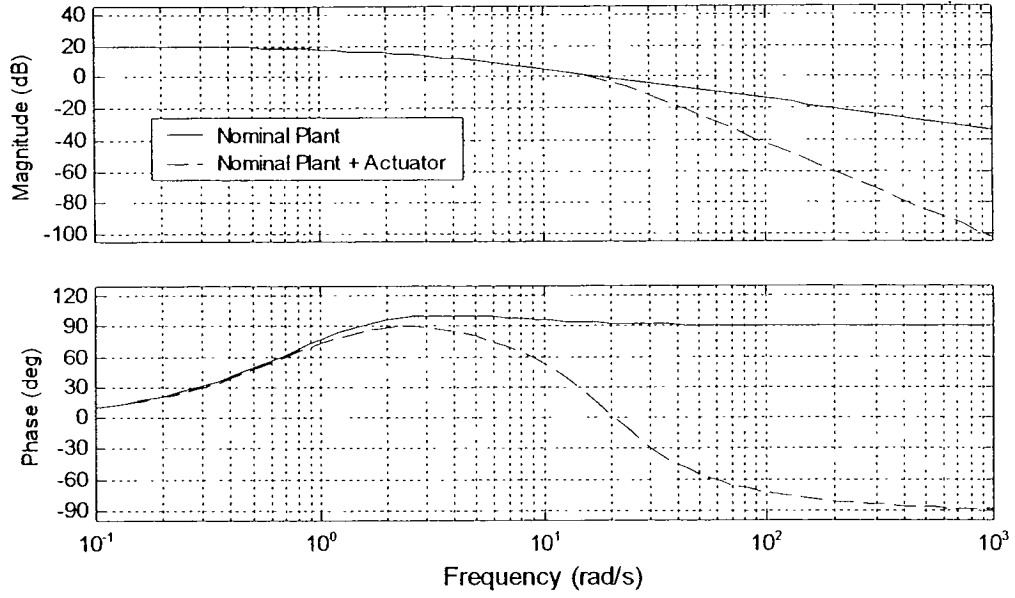


Figure 3-21: F-16 Bode Plots,  $\frac{y}{y_c}$  Nominal System and Actuator

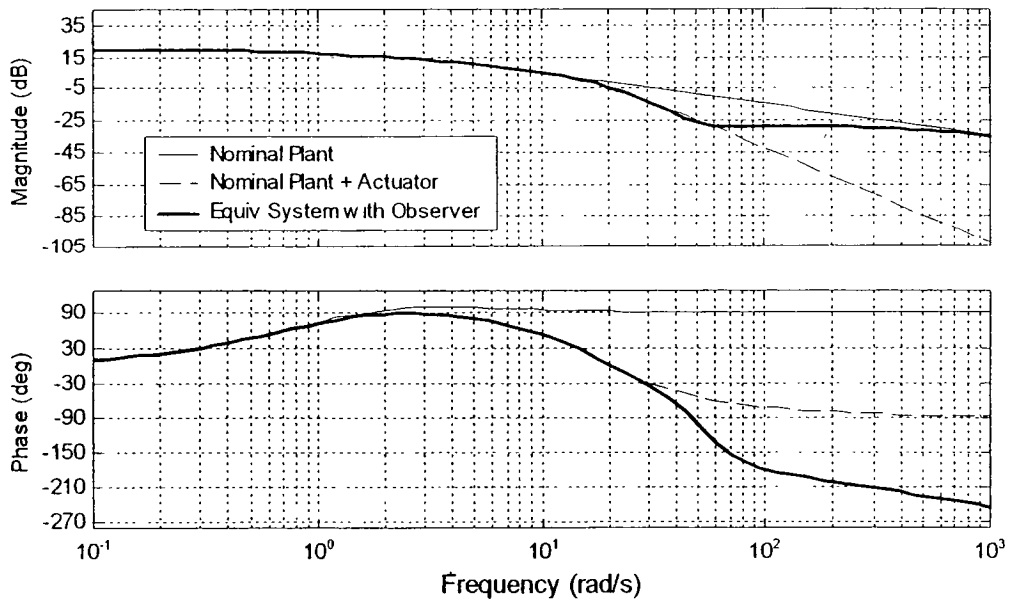
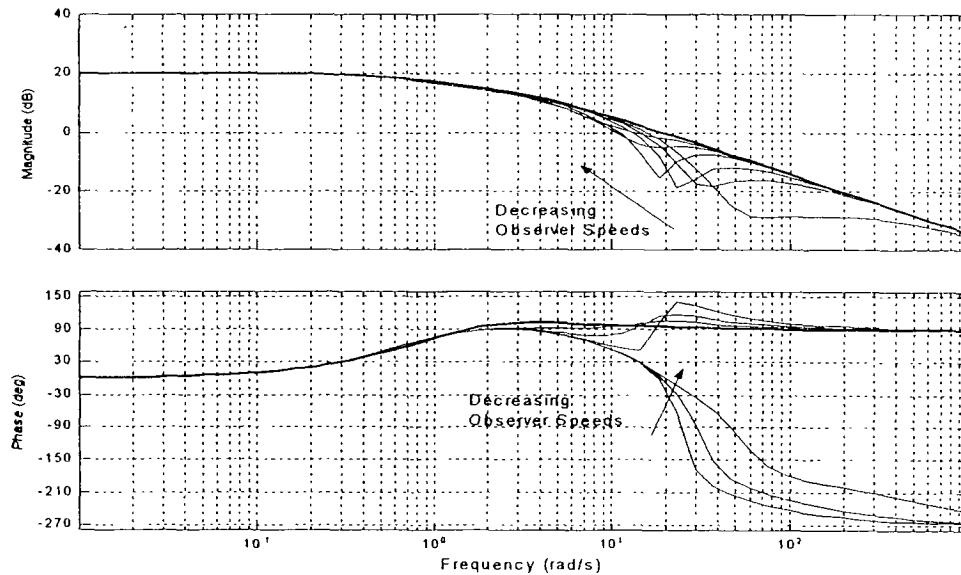


Figure 3-22: F-16 Bode Plots,  $\frac{\hat{y}}{y_c}$  Observer System Output

Since the controller is operating on the estimated state, the behavior of this transfer function is of particular interest. At frequencies below the bandwidth of the actuator, the observer state will follow that of the actual plant+actuator response. At higher frequencies, the magnitude of the observer state will approach that of the nominal state, but with a large increase in phase lag. This system, including the observer, cannot be stabilized by the SMC. However, an interesting observation can be made. The estimated state signal once again has the same relative order as the original system. As long as the nominal plant used in the observer has the same relative order as the nominal system plant, this will always be the case. Since it is critical to know the relative order of the plant for which the SMC is to be designed, using an observer provides a large benefit. This is also encouraging because the knowledge of the actual order of the actuator dynamics is no longer needed. In addition, no measurement of actuator output is necessary. However, just using an observer does not guarantee system stability. The observer must be tuned such that the effects of the actuator are attenuated before being fed back to the SMC. Now, consider slowing down the observer.

The Bode plots in Figure 3-23 show the results for observer frequencies of 500, 100, 50, 20, 10, 5, and 1 rad/s. On the magnitude plots, the effect of decreasing the observer speed is to cause the plots to approach that of the nominal system with no actuators. In general, the differences between the two cannot be completely eliminated, but they can be minimized to a degree depending on the relative dominant frequencies of the actuators and the plant. On the phase plots, note there is an observer speed below which the phase does not exhibit the large lag. In general, the observer poles must be

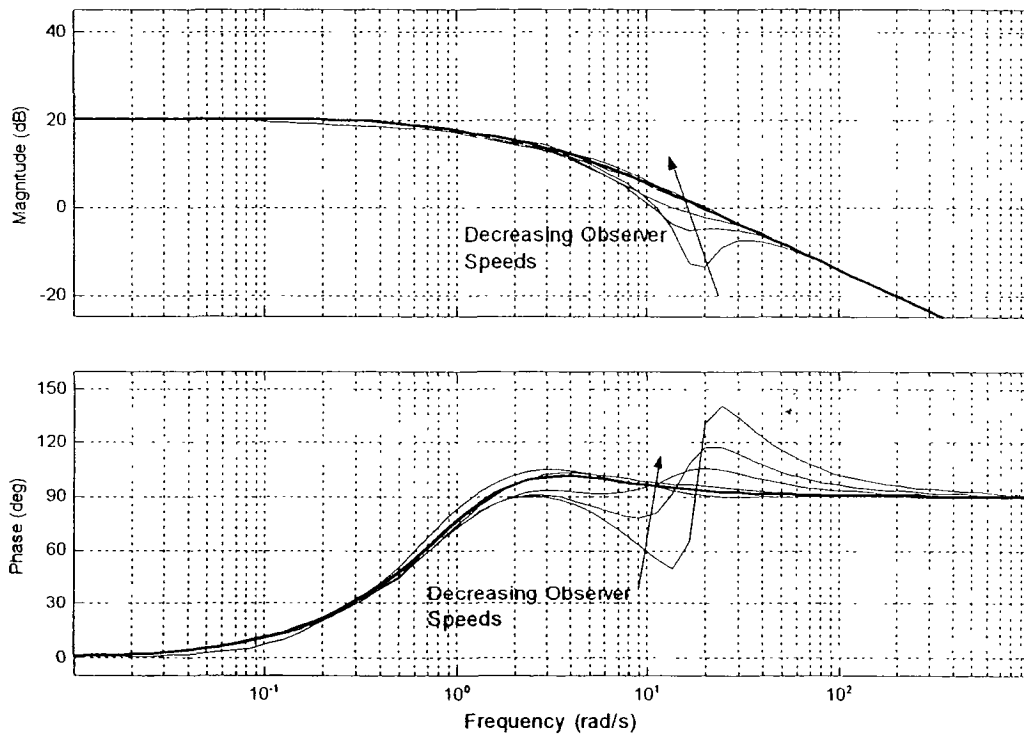


**Figure 3-23: F-16 Bode Plots,  $\frac{\hat{y}}{y_c}$  Various Observer Speeds**

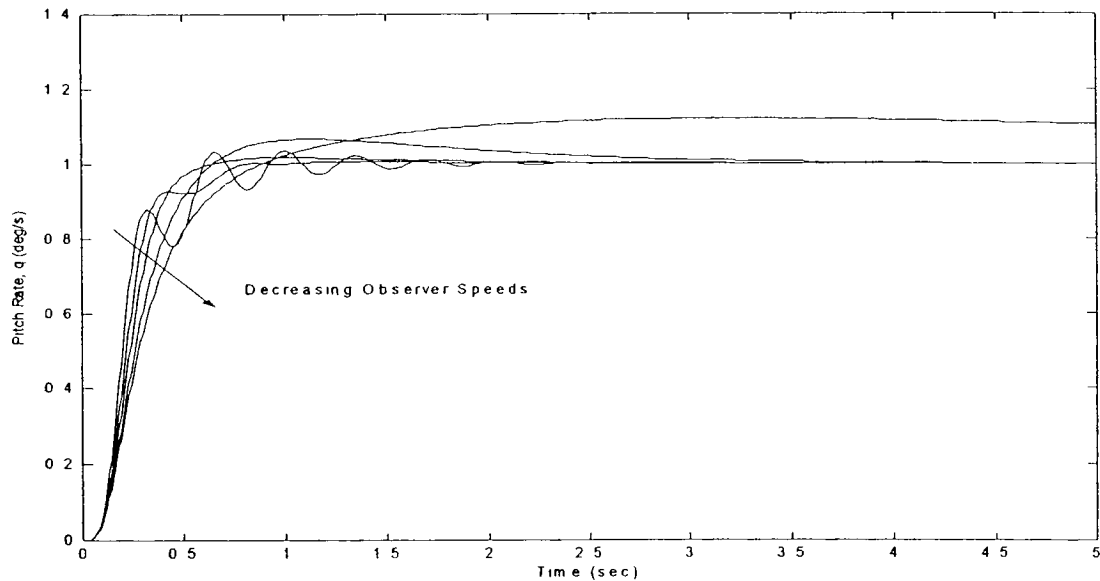
below this frequency in order for the SMC to stabilize the system. The phase lag/lead shape near the bandwidth of the actuator is common and results in a characteristic lead/lag shape in the closed loop. These Bode plots are very useful for determining the appropriate observer gains during the design process. First, design the SMC for the nominal plant neglecting the actuator dynamics. Next, include the actuator dynamics and examine the Bode plots of the equivalent system with the observer. Start with observer speeds near the bandwidth of the actuator and decrease the observer speeds until further reduction does not produce any further benefit. Double-check the results by examining a step response of the controlled variable of interest.

As an example, consider again the F-16 SISO pitch rate tracking problem with the actuator defined above. The SMC is already designed. Now tune the observer

Observer speeds of 20, 10, 5, 1 and 0.1 rad/s are tried. The Bode plots and resulting closed-loop step responses are shown in Figure 3-24 and Figure 3-25. There is almost no difference on the Bode plots between observer poles at 1 and 0.1. Based on the Bode plots alone, observer poles at 1.0 appear to be the best choice. This design tends to give too much overshoot; however, and the final choice of 5 is made based on the actual step responses.



**Figure 3-24: F-16 Bode Plots,  $\frac{\hat{y}}{y_c}$  Choosing Observer Speed**



**Figure 3-25: F-16 Pitch Rate Step Responses, Various Observer Speeds**

### 3.3.2 Observer-Based Design, MIMO Case

Assuming the system is square and feedback linearizable, the controlled outputs can be decoupled and independently managed by the controller. In light of the desire to shape the observer feedback loop appropriately for the SMC, it logically follows that an independent observer may be needed for each feedback channel. Indeed, simulation has indicated that this is the case, especially when the feedback variables have sufficiently different time-scales. The MIMO case then becomes simply a set of independent SISO cases, and the approach outlined above is used for each feedback channel. Parameter coupling can still be somewhat of a problem, so some care must be given to ensure the observer for one channel does not cause adverse interaction with another channel. An example of this is seen later in the ICE aircraft application.

Consider, now, a system with multiple observers (in this case, three),

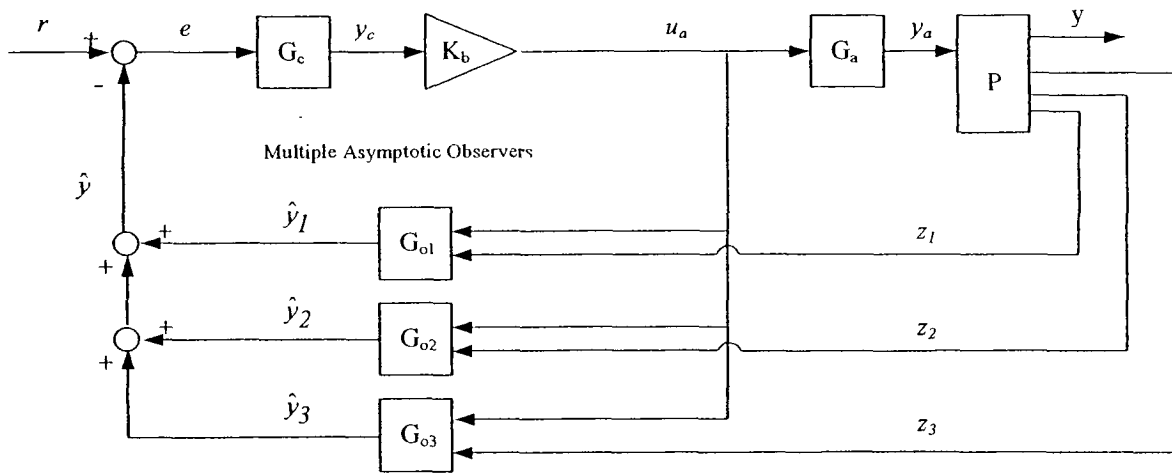


Figure 3-26: Multiple Observer-Based SMC Block Diagram

with the following state space definitions:

$$\begin{aligned} x \in \mathcal{R}^n, \quad x_a \in \mathcal{R}^{n_a}, \quad x_c \in \mathcal{R}^{n_c}, \quad x_r \in \mathcal{R}^{n_r}, \quad \hat{x}_{o1} \in \mathcal{R}^{n_{o1}}, \quad \hat{x}_{o2} \in \mathcal{R}^{n_{o2}}, \quad \hat{x}_{o3} \in \mathcal{R}^{n_{o3}} \\ y \in \mathcal{R}^{m_y}, \quad y_a \in \mathcal{R}^m, \quad y_c \in \mathcal{R}^{m_y}, \quad y_r \in \mathcal{R}^{m_y}, \quad \hat{y}_1 \in \mathcal{R}^{m_y}, \quad \hat{y}_2 \in \mathcal{R}^{m_y}, \quad \hat{y}_3 \in \mathcal{R}^{m_y} \\ z_1 \in \mathcal{R}^{m_{z1}}, \quad z_2 \in \mathcal{R}^{m_{z2}}, \quad z_3 \in \mathcal{R}^{m_{z3}}, \quad \hat{y} \in \mathcal{R}^{m_y} \end{aligned} \quad (3.13)$$

#### Linear Plant

$$\begin{aligned} \dot{x} &= \mathbf{A}x + \mathbf{B}y_a \\ y &= \mathbf{C}_y x + \mathbf{D}_y y_a \\ z_1 &= \mathbf{C}_{z1} x + \mathbf{D}_{z1} y_a \\ z_2 &= \mathbf{C}_{z2} x + \mathbf{D}_{z2} y_a \\ z_3 &= \mathbf{C}_{z3} x + \mathbf{D}_{z3} y_a \end{aligned}$$

#### Actuators

$$\begin{aligned} \dot{x}_a &= \mathbf{A}_a x_a + \mathbf{B}_a \mathbf{K}_b y_c \\ y_a &= \mathbf{C}_a x_a + \mathbf{D}_a \mathbf{K}_b y_c \end{aligned}$$

#### Reference Model

$$\begin{aligned} \dot{x}_r &= \mathbf{A}_r x_r + \mathbf{B}_r r_p \\ y_r &= \mathbf{C}_r x_r + \mathbf{D}_r r_p \end{aligned}$$

#### Observer 1

$$\begin{aligned} \dot{\hat{x}}_1 &= (\mathbf{A}_{o1} - \mathbf{G}_1 \mathbf{C}_{z1}) \hat{x}_1 + \mathbf{B}_{o1} \mathbf{K}_b y_c + \mathbf{G}_1 z_1 \\ \hat{y}_1 &= \mathbf{C}_{o1} \hat{x}_1 \end{aligned}$$

$\mathbf{C}_{o1} \in \mathcal{R}^{m_y \times n}$  with zeros in the rows corresponding to states not output by Observer 1.  $\mathbf{G}_1$  = Observer gains

Observer 2

$$\begin{aligned}\dot{\hat{x}}_2 &= (\mathbf{A}_{o2} - \mathbf{G}_2 \mathbf{C}_{z2}) \hat{x}_2 + \mathbf{B}_{o2} \mathbf{K}_b y_c + \mathbf{G}_2 z_2 \\ \hat{y}_2 &= \mathbf{C}_{o2} \hat{x}_2\end{aligned}$$

$\mathbf{C}_{o2} \in \mathfrak{R}^{m_y \times n}$  with zeros in the rows corresponding to states not output by Observer 2  $\mathbf{G}_2 =$  Observer gains

Observer 3

$$\begin{aligned}\dot{\hat{x}}_3 &= (\mathbf{A}_{o3} - \mathbf{G}_3 \mathbf{C}_{z3}) \hat{x}_3 + \mathbf{B}_{o3} \mathbf{K}_b y_c + \mathbf{G}_3 z_3 \\ \hat{y}_3 &= \mathbf{C}_{o3} \hat{x}_3\end{aligned}$$

$\mathbf{C}_{o3} \in \mathfrak{R}^{m_y \times n}$  with zeros in the rows corresponding to states not output by Observer 3  $\mathbf{G}_3 =$  Observer gains

Output Feedback

$$\hat{y} = \hat{y}_1 + \hat{y}_2 + \hat{y}_3$$

Again, an equivalent plant in which the control distribution, actuators, nominal plant, and observers lumped together as shown in Figure 3-20 can be expressed as

$$\begin{aligned}\dot{x}_e &= \mathbf{A}_e x_e + \mathbf{B}_e y_c \\ y &= \begin{bmatrix} \mathbf{C}_y & \mathbf{0}_{m_y \times (n_a + n_{o1} + n_{o2} + n_{o3})} \end{bmatrix} x_e + \begin{bmatrix} \mathbf{D}_y \mathbf{K}_b \end{bmatrix} y_c \\ \hat{y} &= \mathbf{C}_e x_e\end{aligned} \quad x_e = \begin{bmatrix} x \\ x_a \\ \hat{x}_1 \\ \hat{x}_2 \\ \hat{x}_3 \end{bmatrix} \quad (3.14)$$

where

$$\mathbf{A}_e = \begin{bmatrix} \mathbf{A} & \mathbf{B} \mathbf{C}_a & \mathbf{0}_{n \times n_{o1}} & \mathbf{0}_{n \times n_{o2}} & \mathbf{0}_{n \times n_{o3}} \\ \mathbf{0}_{n_a \times n} & \mathbf{A}_a & \mathbf{0}_{n_a \times n_{o1}} & \mathbf{0}_{n_a \times n_{o2}} & \mathbf{0}_{n_a \times n_{o3}} \\ \mathbf{G}_1 \mathbf{C}_{z1} & \mathbf{G}_1 \mathbf{D}_{z1} \mathbf{C}_a & (\mathbf{A}_{o1} - \mathbf{G}_1 \mathbf{C}_{z1}) & \mathbf{0}_{n_{o1} \times n_{o2}} & \mathbf{0}_{n_{o1} \times n_{o3}} \\ \mathbf{G}_2 \mathbf{C}_{z2} & \mathbf{G}_2 \mathbf{D}_{z2} \mathbf{C}_a & \mathbf{0}_{n_{o2} \times n_{o1}} & (\mathbf{A}_{o2} - \mathbf{G}_2 \mathbf{C}_{z2}) & \mathbf{0}_{n_{o2} \times n_{o3}} \\ \mathbf{G}_3 \mathbf{C}_{z3} & \mathbf{G}_3 \mathbf{D}_{z3} \mathbf{C}_a & \mathbf{0}_{n_{o3} \times n_{o1}} & \mathbf{0}_{n_{o3} \times n_{o2}} & (\mathbf{A}_{o3} - \mathbf{G}_3 \mathbf{C}_{z3}) \end{bmatrix}$$

$$\mathbf{B}_e = \begin{bmatrix} \mathbf{B} \mathbf{D}_a \mathbf{K}_b \\ \mathbf{B}_a \mathbf{K}_b \\ \mathbf{B}_{o1} \mathbf{K}_b + \mathbf{G}_1 \mathbf{D}_{z1} \mathbf{D}_a \mathbf{K}_b \\ \mathbf{B}_{o2} \mathbf{K}_b + \mathbf{G}_2 \mathbf{D}_{z2} \mathbf{D}_a \mathbf{K}_b \\ \mathbf{B}_{o3} \mathbf{K}_b + \mathbf{G}_3 \mathbf{D}_{z3} \mathbf{D}_a \mathbf{K}_b \end{bmatrix}$$

$$\mathbf{C}_e = \begin{bmatrix} \mathbf{0}_{m_y \times n} & \mathbf{0}_{m_y \times n_a} & \mathbf{C}_{o1} & \mathbf{C}_{o2} & \mathbf{C}_{o3} \end{bmatrix}$$

Again, this system gives the designer the ability to look at the  $\frac{\hat{y}}{y_c}(s)$  transfer

functions and tune the observers as needed

### 3.3.3 Observers with Failed Plants

In general, it is seen that slowing down the observer helps mitigate the effects of parasitic dynamics. Consider now the behavior of the observer when the actual plant is significantly different than the nominal plant. In this case, it is assumed that the observer continues to use the nominal model in its calculations while the actual plant has suffered some failure. The same  $\frac{\hat{y}}{y_c}(s)$  transfer functions used for tuning the observer provide useful insight here. The Bode plots in Figure 3-27 show the SISO F-16 example. The nominal system and a failed system (a 50% loss of horizontal tail area) are shown. The actuator dynamics are neglected. Also shown is the equivalent system assuming a very fast observer ( $\lambda = -500, -501$ ). Note that at low frequencies, the observed state closely matches that of the actual failed plant. However, the observed state then transitions to the nominal system and matches the nominal system at frequencies above the observer frequency. This implies that as long as the observed state is close to the actual state around the closed-loop bandwidth, the controller will exhibit acceptable performance.

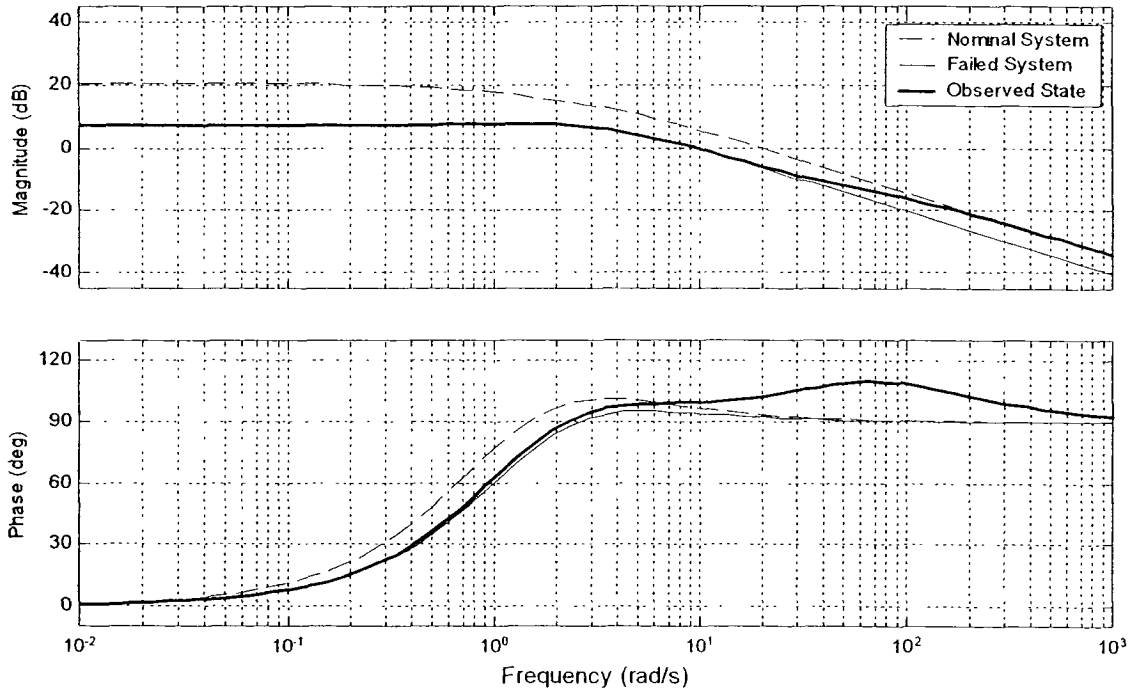
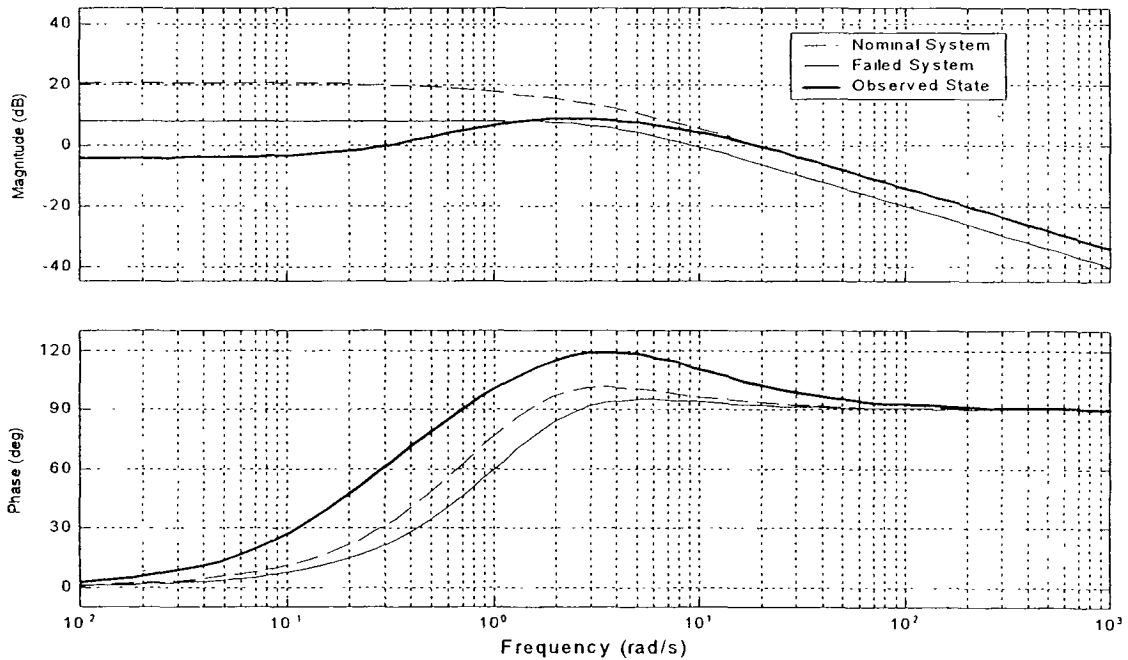


Figure 3-27: F-16 Bode Plots, Nominal Plant  $\frac{y}{y_c}$ , Failed Plant  $\frac{y_{fail}}{y_c}$ , Fast Observer  $\frac{\hat{y}}{y_c}$

Next, consider slowing the observer down to the speed determined earlier as optimum for reducing the effects of the parasitic dynamics ( $\lambda = -5, -6$ ). Again, the observer follows the nominal system at frequencies above the observer frequency. Below that frequency, the observed state follows neither. The result in the closed loop is very poor tracking and a steady state error.



**Figure 3-28:** F-16 Bode Plots, Nominal Plant  $\frac{y}{y_c}$ , Failed Plant  $\frac{y_{fail}}{y_c}$ , Slow Observer  $\frac{\hat{y}}{y_c}$

These results lead to the conclusion that a very fast observer is desired for robustness to system parameter changes. Unfortunately, fast observers do not help eliminate the effects of the actuator. Therefore, these competing design objectives must either be somehow balanced, or another method of dealing with parasitic dynamics must be sought.

### 3.4 Model Reference Hedging

Observer-based SMC helps deal with the problem of unmodeled parasitic dynamics. However, the addition of the observer does not directly address the issue of control saturation. The observer does help with rate saturation to some degree because

of phase lag reductions at medium to high frequencies. However, position saturation is still an issue—especially when the system does not have redundant control effectors. Initially, in an attempt to deal with control saturation, a method called model reference hedging is pursued. The concept of hedging has been successfully demonstrated in a dynamic inversion design approach.<sup>134</sup> The concept in words is this. “The reference model is moved backwards (hedged) by an estimate of the amount the plant did not move due to system characteristics the control designer does not want the adaptive control element to ‘know’ about.”<sup>134</sup> The actual accelerations are subtracted from the expected accelerations (assuming no actuators). This difference represents the amount of desired acceleration which was not achieved due to the actuators and should capture nonlinear saturation of the actual actuators. This difference is then subtracted from the reference model acceleration. Since all this is done in a dynamic inversion setting, these accelerations are pseudo-commands for the dynamic inversion controller, and Johnson *et al.* call this “Pseudo-Control Hedging.” The concept has great merit and is very successful in their work.

In order to employ this method in an SMC design, some modification to the actual implementation is required. Rather than subtracting the acceleration difference from the reference model pseudo command, the following approach is used. The actual controlled variable output is subtracted from the expected output (through a nominal system with no actuators). This signal ( $y_h$ ) represents the amount of unachieved performance due to the actuator. This passes through a hedge gain ( $K_h$ ) and is subtracted directly from the model reference states as shown below.

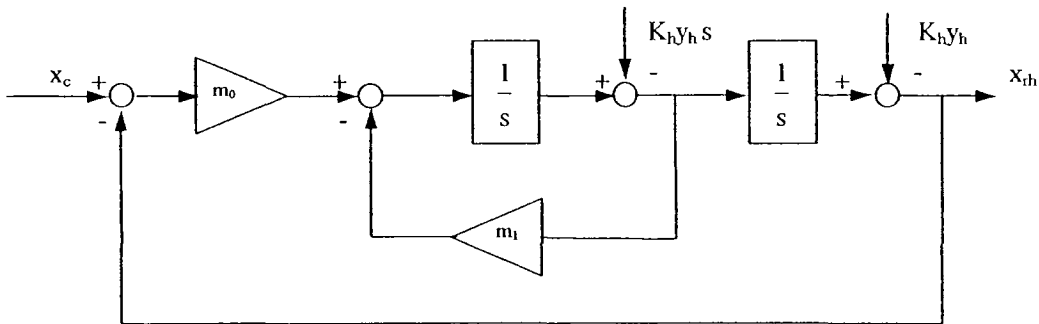


Figure 3-29: 2<sup>nd</sup> Order Hedged Reference Model

If a 3<sup>rd</sup> order reference model is used, the hedge signal enters the reference model as shown below.

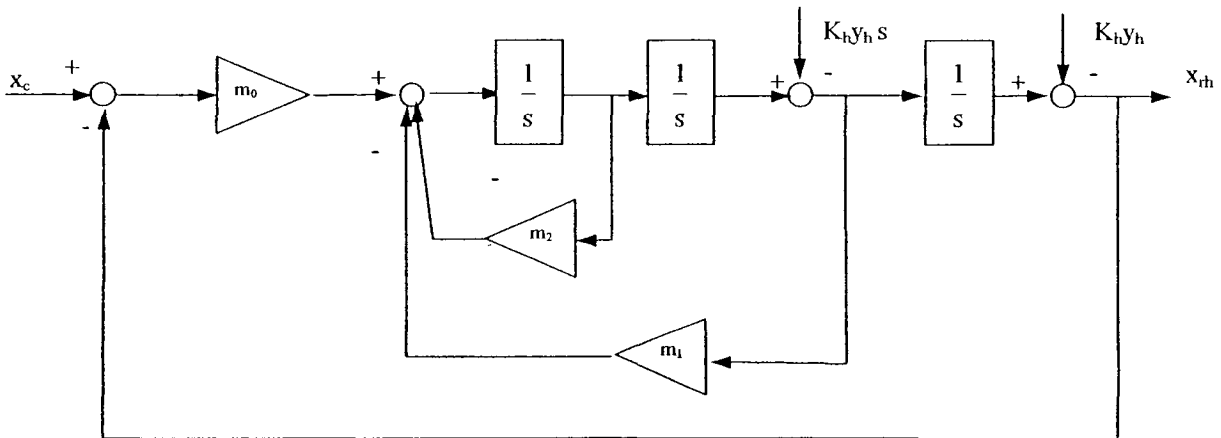
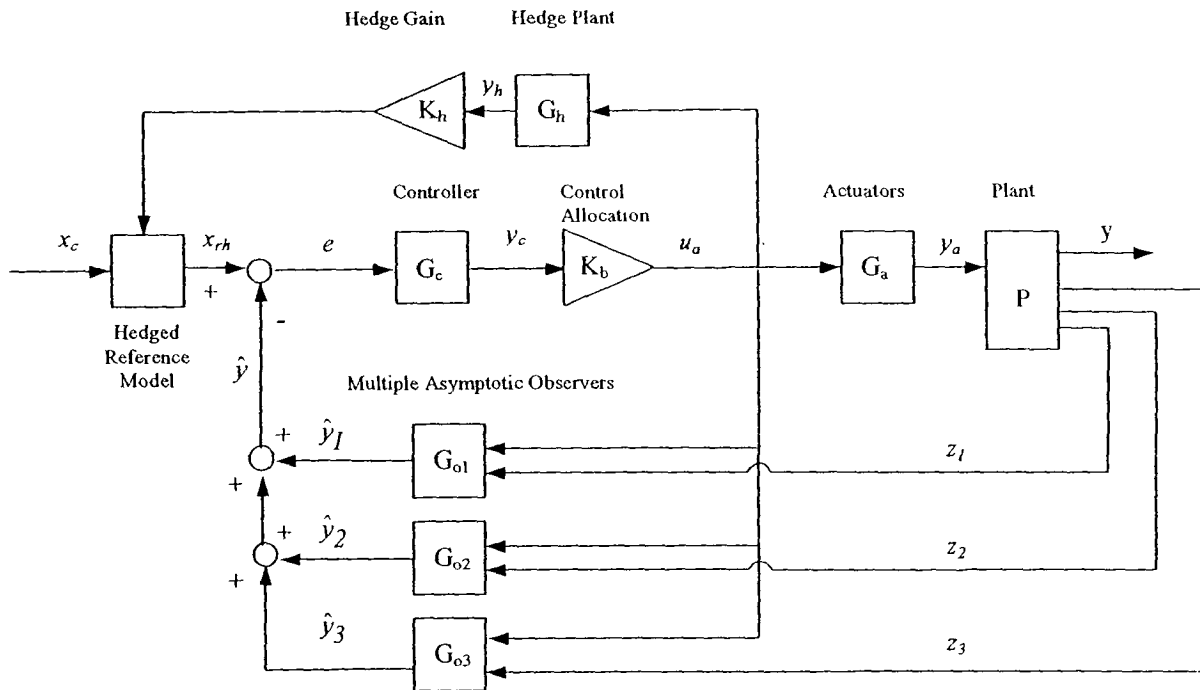


Figure 3-30: 3<sup>rd</sup> Order Hedged Reference Model

In order to investigate how hedging affects the system, an analytical expression for the system with hedging included is needed. Consider, initially, a model architecture as shown below.

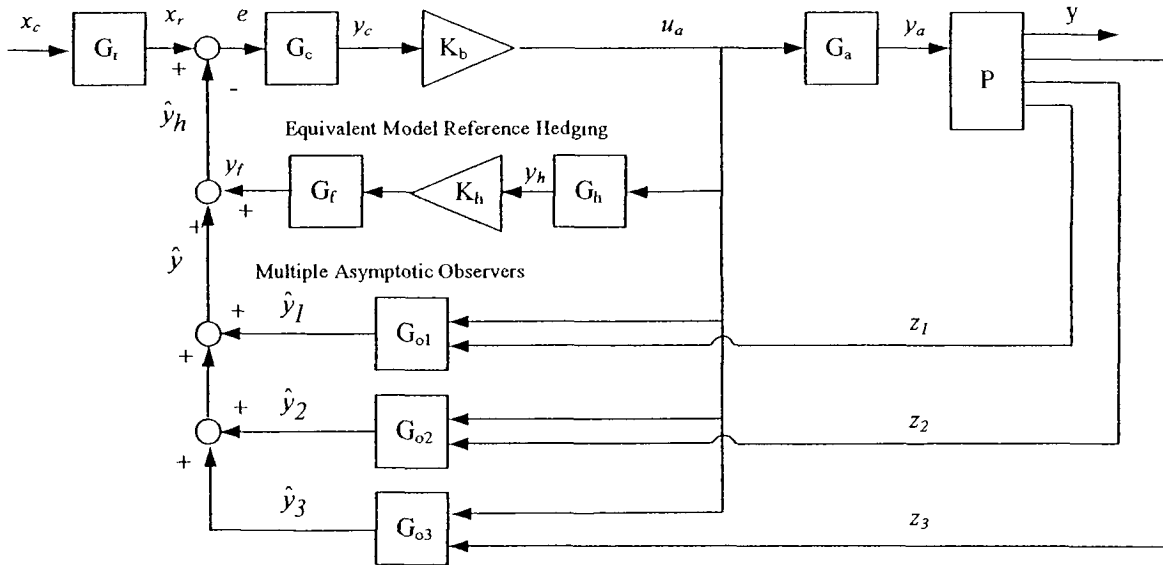


**Figure 3-31: Hedged System Architecture**

In this system, the hedge plant,  $G_h$ , is simply the nominal plant model (assuming it is stable). The subsystem block labeled “Hedged Reference Model” is the subsystem shown in either Figure 3-29 or Figure 3-30. Note that hedging occurs on individual control variable channels, so it is possible to write the transfer function for the hedged reference model. It can be shown that this transfer function (for a 2<sup>nd</sup> order reference model) is given by

$$\begin{aligned}
 x_{rh} &= \left( \frac{m_0}{s^2 + m_1 s + m_0} \right) x_c - \left( \frac{2s^2 + m_1 s}{s^2 + m_1 s + m_0} \right) K_h y_h \\
 &\equiv G_f(s) x_c - G_f(s) K_h y_h
 \end{aligned} \tag{3.15}$$

This indicates that the hedged reference signal consists of two parts, a reference model part and a hedge signal passing through a “hedge filter,”  $G_f$ . With this definition, the block diagram can be redrawn as:



**Figure 3-32: Equivalent Hedged System Architecture**

Next, define the following state space representations for the given system:

$$\begin{aligned}
 &x \in \mathcal{R}^n, \quad x_a \in \mathcal{R}^{n_a}, \quad x_c \in \mathcal{R}^{n_c}, \quad x_r \in \mathcal{R}^{n_r}, \quad x_h \in \mathcal{R}^{n_h}, \quad x_f \in \mathcal{R}^{n_f}, \quad \hat{x}_{o1} \in \mathcal{R}^{n_{o1}}, \quad \hat{x}_{o2} \in \mathcal{R}^{n_{o2}}, \quad \hat{x}_{o3} \in \mathcal{R}^{n_{o3}} \\
 &y \in \mathcal{R}^{m_y}, \quad y_a \in \mathcal{R}^m, \quad y_c \in \mathcal{R}^{m_y}, \quad y_r \in \mathcal{R}^{m_y}, \quad y_h \in \mathcal{R}^{m_y}, \quad y_f \in \mathcal{R}^{m_y}, \quad \hat{y}_1 \in \mathcal{R}^{m_y}, \quad \hat{y}_2 \in \mathcal{R}^{m_y}, \quad \hat{y}_3 \in \mathcal{R}^{m_y} \\
 &z_1 \in \mathcal{R}^{m_{z1}}, \quad z_2 \in \mathcal{R}^{m_{z2}}, \quad z_3 \in \mathcal{R}^{m_{z3}}, \quad \hat{y}_h \in \mathcal{R}^{m_y}
 \end{aligned}$$

#### Actual Linear Plant

$$\begin{aligned}
 \dot{x} &= \mathbf{A} x + \mathbf{B} y_a \\
 y &= \mathbf{C}_y x + \mathbf{D}_y y_a \\
 z_1 &= \mathbf{C}_{z1} x + \mathbf{D}_{z1} y_a \\
 z_2 &= \mathbf{C}_{z2} x + \mathbf{D}_{z2} y_a \\
 z_3 &= \mathbf{C}_{z3} x + \mathbf{D}_{z3} y_a
 \end{aligned}$$

#### Reference Model

$$\begin{aligned}
 \dot{x}_r &= \mathbf{A}_r x_r + \mathbf{B}_r y_c \\
 y_r &= \mathbf{C}_r x_r + \mathbf{D}_r y_c
 \end{aligned}$$

#### Actuators

$$\begin{aligned}
 \dot{x}_a &= \mathbf{A}_a x_a + \mathbf{B}_a \mathbf{K}_b y_c \\
 y_a &= \mathbf{C}_a x_a + \mathbf{D}_a \mathbf{K}_b y_c
 \end{aligned}$$

#### Linear Compensator

$$\begin{aligned}
 \dot{x}_c &= \mathbf{A}_c x_c + \mathbf{B}_c e \\
 y_c &= \mathbf{C}_c x_c + \mathbf{D}_c e
 \end{aligned}$$

#### Hedge Plant

$$\begin{aligned}
 \dot{x}_h &= \mathbf{A}_h x_h + \mathbf{B}_h \mathbf{K}_b y_c \\
 y_h &= \mathbf{C}_h x_h + \mathbf{D}_h \mathbf{K}_b y_c
 \end{aligned}$$

#### Hedge Filter

$$\begin{aligned}
 \dot{x}_f &= \mathbf{A}_f x_f + \mathbf{B}_f \mathbf{K}_h y_h \\
 y_f &= \mathbf{C}_f x_f + \mathbf{D}_f \mathbf{K}_h y_h
 \end{aligned}$$

Observer 1

$$\begin{aligned}\dot{\hat{x}}_1 &= (\mathbf{A}_{o1} - \mathbf{G}_1 \mathbf{C}_{z1}) \hat{x}_1 + \mathbf{B}_{o1} \mathbf{K}_b y_c + \mathbf{G}_1 z_1 \\ \hat{y}_1 &= \mathbf{C}_{o1} \hat{x}_1\end{aligned}$$

$\mathbf{C}_{o1} \in \mathfrak{R}^{m \times n}$  with zeros in the rows corresponding to states not output by Observer 1.  $\mathbf{G}_1 =$  Observer gains

Observer 2

$$\begin{aligned}\dot{\hat{x}}_2 &= (\mathbf{A}_{o2} - \mathbf{G}_2 \mathbf{C}_{z2}) \hat{x}_2 + \mathbf{B}_{o2} \mathbf{K}_b y_c + \mathbf{G}_2 z_2 \\ \hat{y}_2 &= \mathbf{C}_{o2} \hat{x}_2\end{aligned}$$

$\mathbf{C}_{o2} \in \mathfrak{R}^{m \times n}$  with zeros in the rows corresponding to states not output by Observer 2.  $\mathbf{G}_2 =$  Observer gains

Observer 3

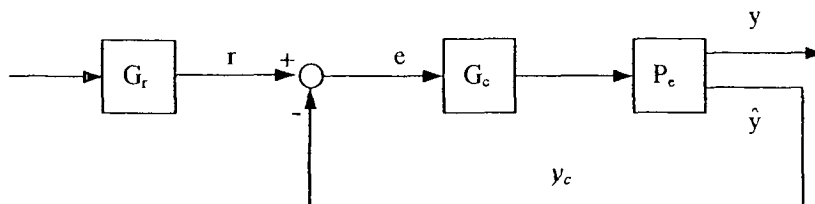
$$\begin{aligned}\dot{\hat{x}}_3 &= (\mathbf{A}_{o3} - \mathbf{G}_3 \mathbf{C}_{z3}) \hat{x}_3 + \mathbf{B}_{o3} \mathbf{K}_b y_c + \mathbf{G}_3 z_3 \\ \hat{y}_3 &= \mathbf{C}_{o3} \hat{x}_3\end{aligned}$$

$\mathbf{C}_{o3} \in \mathfrak{R}^{m \times n}$  with zeros in the rows corresponding to states not output by Observer 3.  $\mathbf{G}_3 =$  Observer gains

Output Feedback

$$\hat{y}_h = \hat{y}_1 + \hat{y}_2 + \hat{y}_3 + y_f$$

Again, this can be cast into an equivalent system in which the control distribution, actuators, nominal plant, observer, and equivalent hedge are lumped together as shown below.



**Figure 3-33: Equivalent Plant with Observer and Hedge**

The equivalent system is defined in state space as

$$\begin{aligned}
 \dot{x}_e &= \mathbf{A}_e x_e + \mathbf{B}_e y_c \\
 y &= \begin{bmatrix} \mathbf{C}_y & \mathbf{0}_{m_y \times (n_a + n_{o1} + n_{o2} + n_{o3} + n_f + n_h)} \end{bmatrix} x_e + \begin{bmatrix} \mathbf{D}_y \mathbf{K}_b \end{bmatrix} y_c \\
 \hat{y}_h &= \mathbf{C}_e x_e + \mathbf{D}_e y_c
 \end{aligned}
 \quad x_e = \begin{bmatrix} x \\ x_a \\ \hat{x}_1 \\ \hat{x}_2 \\ \hat{x}_3 \\ x_f \\ x_h \end{bmatrix} \quad (3.16)$$

where

$$\mathbf{A}_e = \begin{bmatrix} \mathbf{A} & \mathbf{B} \mathbf{C}_a & \mathbf{0}_{n \times n_{o1}} & \mathbf{0}_{n \times n_{o2}} & \mathbf{0}_{n \times n_{o3}} & \mathbf{0}_{n \times n_f} & \mathbf{0}_{n \times n_h} \\ \mathbf{0}_{n_a \times n} & \mathbf{A}_a & \mathbf{0}_{n_a \times n_{o1}} & \mathbf{0}_{n_a \times n_{o2}} & \mathbf{0}_{n_a \times n_{o3}} & \mathbf{0}_{n_a \times n_f} & \mathbf{0}_{n_a \times n_h} \\ \mathbf{G}_1 \mathbf{C}_{z1} & \mathbf{G}_1 \mathbf{D}_{z1} \mathbf{C}_a & (\mathbf{A}_{o1} - \mathbf{G}_1 \mathbf{C}_{z1}) & \mathbf{0}_{n_{o1} \times n_{o2}} & \mathbf{0}_{n_{o1} \times n_{o3}} & \mathbf{0}_{n_{o1} \times n_f} & \mathbf{0}_{n_{o1} \times n_h} \\ \mathbf{G}_2 \mathbf{C}_{z2} & \mathbf{G}_2 \mathbf{D}_{z2} \mathbf{C}_a & \mathbf{0}_{n_{o2} \times n_{o1}} & (\mathbf{A}_{o2} - \mathbf{G}_2 \mathbf{C}_{z2}) & \mathbf{0}_{n_{o2} \times n_{o3}} & \mathbf{0}_{n_{o2} \times n_f} & \mathbf{0}_{n_{o2} \times n_h} \\ \mathbf{G}_3 \mathbf{C}_{z3} & \mathbf{G}_3 \mathbf{D}_{z3} \mathbf{C}_a & \mathbf{0}_{n_{o3} \times n_{o1}} & \mathbf{0}_{n_{o3} \times n_{o2}} & (\mathbf{A}_{o3} - \mathbf{G}_3 \mathbf{C}_{z3}) & \mathbf{0}_{n_{o3} \times n_f} & \mathbf{0}_{n_{o3} \times n_h} \\ \mathbf{0}_{n_f \times n} & \mathbf{0}_{n_f \times n_a} & \mathbf{0}_{n_f \times n_{o1}} & \mathbf{0}_{n_f \times n_{o2}} & \mathbf{0}_{n_f \times n_{o3}} & \mathbf{A}_f & \mathbf{B}_f \mathbf{K}_h \mathbf{C}_h \\ \mathbf{0}_{n_h \times n} & \mathbf{0}_{n_h \times n_a} & \mathbf{0}_{n_h \times n_{o1}} & \mathbf{0}_{n_h \times n_{o2}} & \mathbf{0}_{n_h \times n_{o3}} & \mathbf{0}_{n_h \times n_f} & \mathbf{A}_h \end{bmatrix}$$

$$\mathbf{B}_e = \begin{bmatrix} \mathbf{B} \mathbf{D}_a \mathbf{K}_b \\ \mathbf{B}_a \mathbf{K}_b \\ \mathbf{B}_{o1} \mathbf{K}_b + \mathbf{G}_1 \mathbf{D}_{z1} \mathbf{D}_a \mathbf{K}_b \\ \mathbf{B}_{o2} \mathbf{K}_b + \mathbf{G}_2 \mathbf{D}_{z2} \mathbf{D}_a \mathbf{K}_b \\ \mathbf{B}_{o3} \mathbf{K}_b + \mathbf{G}_3 \mathbf{D}_{z3} \mathbf{D}_a \mathbf{K}_b \\ \mathbf{B}_f \mathbf{K}_h \mathbf{D}_h \mathbf{K}_b \\ \mathbf{B}_h \mathbf{K}_b \end{bmatrix}$$

$$\mathbf{C}_e = \begin{bmatrix} \mathbf{0}_{m_y \times n} & \mathbf{0}_{m_y \times n_a} & \mathbf{C}_{o1} & \mathbf{C}_{o2} & \mathbf{C}_{o3} & \mathbf{C}_f & \mathbf{D}_f \mathbf{K}_h \mathbf{C}_h \end{bmatrix}$$

$$\mathbf{D}_e = \mathbf{D}_f \mathbf{K}_h \mathbf{D}_h \mathbf{K}_b$$

Now the effects of hedging can be examined on the Bode plots of the transfer functions  $\frac{\hat{y}_h}{y_c}(s)$  as is done with the observer. For the sake of illustration, consider a SISO model of the F-18/HARV longitudinal system for a pitch rate tracking task. Details for the system are given later in Section 4.5. The important aspects of the system for this discussion are that the nominal plant is stable and has a relative order of 1 for pitch rate; it has second order actuator dynamics; and it has a single observer which is very fast ( $\lambda = -1000, -1001$ ). The observer ensures the SMC sees a relative order of 1, however, it is running too fast to eliminate the instability caused by the parasitic dynamics of the actuators. Note, the F-16 model used in previous illustrations cannot be used here because it has an unstable plant—which causes yields an unstable hedge signal.

The Bode plots below show the nominal system and the  $\frac{\hat{y}_h}{y_c}(s)$  feedback signal. Also shown is the transfer function  $K_h \cdot G_h(s) \cdot G_f(s)$  which is the hedge signal. In this example the hedge gain is very low to show the system behavior with no hedging. Note the large phase lag. The SMC designed for this system cannot stabilize it. In this example, the hedge plant,  $G_h$ , is simply the nominal system open loop transfer function for pitch rate,  $q$ . The hedge filter,  $G_f$ , is the transfer function defined earlier in Eqn. (3.15).

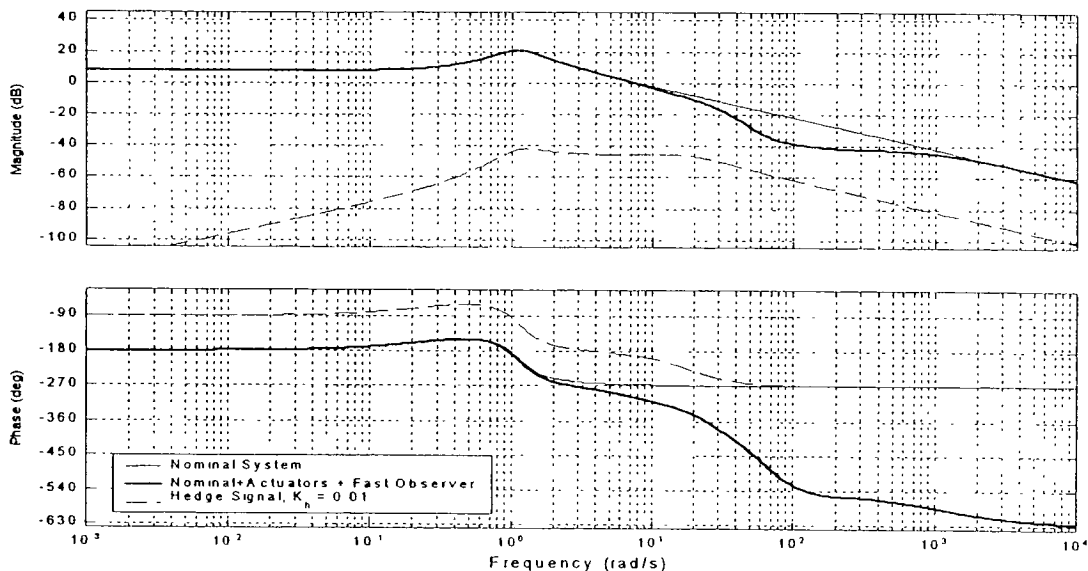


Figure 3-34: System with Hedging, Bode Plots  $\frac{\hat{y}_h}{y_c}$ ,  $K_h=0.01$

Next, increase the hedge gain to see its effect on the system. This is shown in the Bode plots below. Of course, increasing hedge gain does not change the loop shape of the hedge signal—it simply shifts its magnitude curve vertically. As Figure 3-32 indicates, the hedge signal is additive to the observer signal. Therefore, as it approaches the observer magnitude curve from below, it increases the magnitude of this latter curve. The result is that the large drop-off in the magnitude curve (due to the actuators) is reduced. Note, also, that the phase no longer has the characteristic increase in phase lag. This system is stable and has acceptable tracking performance.

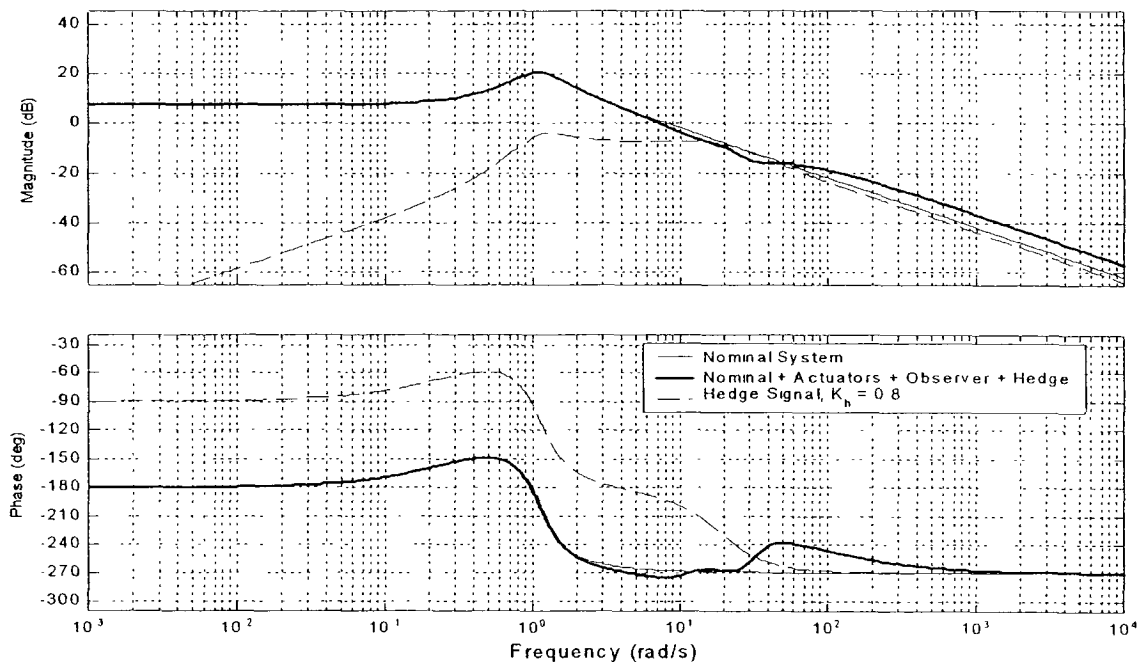


Figure 3-35: System with Hedging, Bode Plots  $\frac{\hat{y}_h}{y_c}$ ,  $K_h=0.8$

The hedge plant and the observer plant have the same relative order. This means that when the hedge gain is large enough to eliminate the drop-off in the magnitude curve, the additive effect of the hedge signal is too large at high frequencies. Note how the  $\frac{\hat{y}_h}{y_c}(s)$  magnitude curve is above the nominal system at high frequencies. This can result in overshoot in the closed loop response. If the hedge signal had additional roll-off at high frequencies, this effect could be eliminated.

After examining several different systems, it is noted that the hedge signal has basically the same loop shape for each system. It resembles a derivative at low frequencies; it peaks; and it rolls off at the relative order of the plant at high frequencies.

This is not surprising considering the hedge filter has the same form in all cases—it looks like a high-pass filter. All real plants have a high frequency roll-off. When these two are placed in series, the result is this characteristic “hump” shape. The question then is this: can the same beneficial effects of hedging be achieved with a simplified “equivalent hedge” transfer function? This is highly desired because, in its current form, hedging can only be used with a stable plant

Consider a hedge filter of the form (a high-pass filter).

$$G_f(s) = \frac{s}{s + a_f} \quad (3.17)$$

And a hedge plant of the form (a low-pass filter):

$$G_h(s) = \frac{b_h}{s^2 + a_h s + b_h} \quad (3.18)$$

The hedge plant,  $G_h$ , in Eqn (3.18) has relative order 2 and is intended to be used with a system with a relative order of 1. The extra pole is added in order to have the additional high frequency roll-off, which is noted as being desirable in the previous discussion. This appears to be a good rule. The hedge plant should be one relative degree higher than the nominal system plant. Figure 3-36 shows a comparison of this simplified hedge model ( $K_h G_h G_f$ ) with a hedge signal using the nominal plant. In general, the simplified model can be designed to be fairly close to the original hedge system. In addition, desirable high frequency roll-off is obtained and lightly damped zeros are eliminated. Note that since the simplified models operate on individual pseudo-command channels, the input to the hedge plant is simply  $y_c$  (instead of  $\mathbf{B}_k y_c$ ). In other words, the take-off

point for the input to the hedge model in the block diagram in Figure 3-32 moves to a position before the control distribution block. The appropriate changes to the state space matrices (Eqn. ( 3.13 )) are easily made.

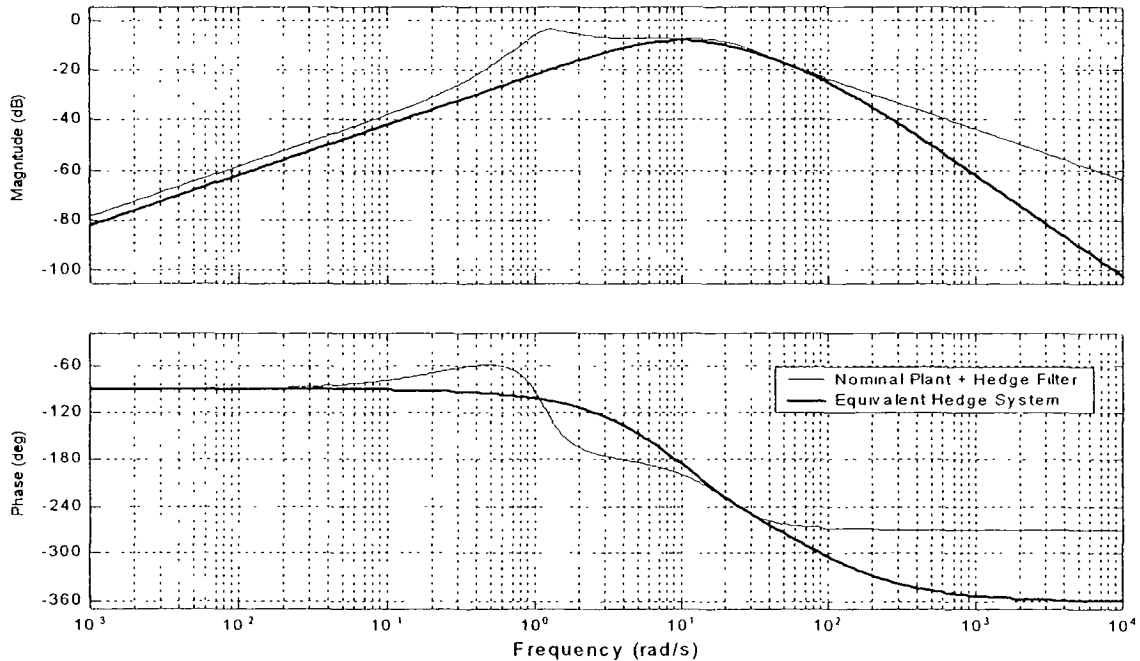


Figure 3-36: Simplified Hedge System,  $\frac{y_f}{u_a}$

Consider now, using this simplified hedge system with the F-18/HARV model demonstrated above. The results are shown in Figure 3-37. Compare this plot with the original hedge scheme results in Figure 3-35. The results here are very good. In fact these results are better than the original hedge scheme. The observed state being fed back is very close to the original nominal plant with no actuators.

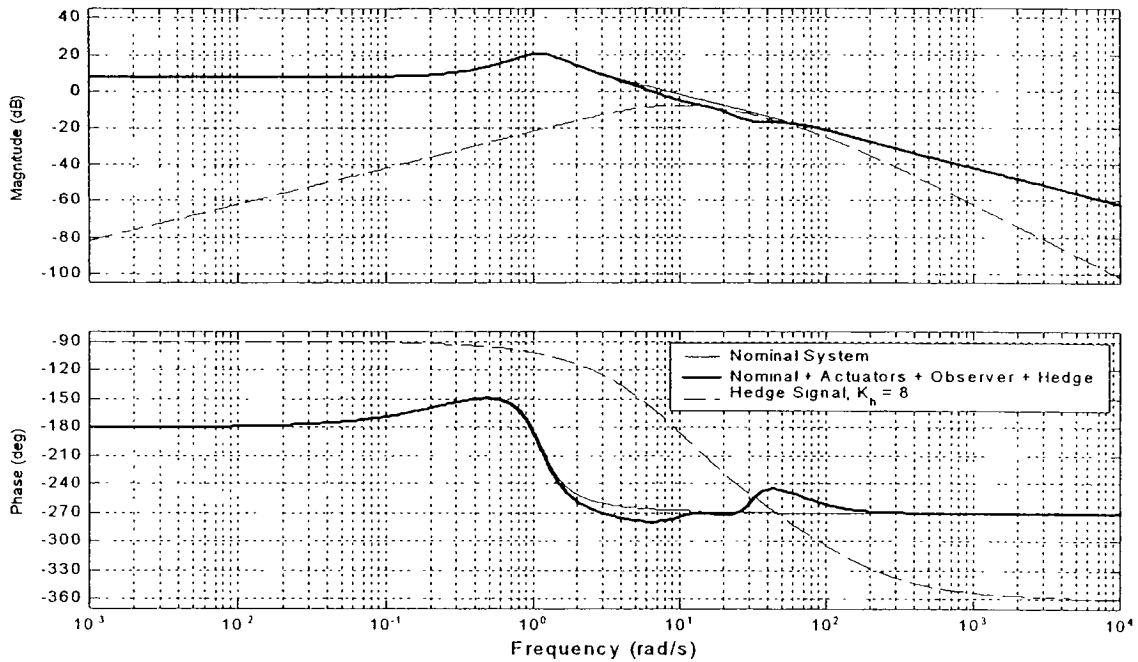


Figure 3-37: System with Simplified Hedging, Bode Plots  $\frac{\hat{y}_h}{y_c}$ ,  $K_h=8.0$

### 3.4.1 Creating the Hedge Model

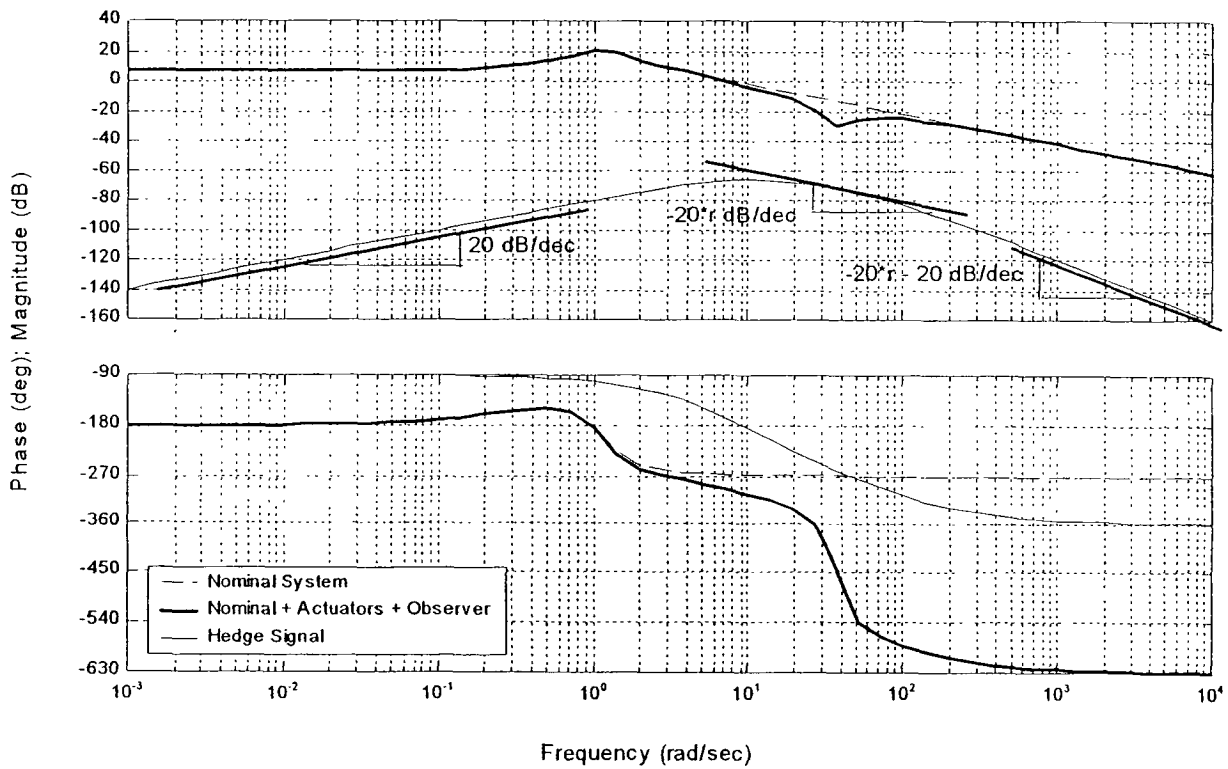
The following technique is proposed for creating the hedge model. Begin by plotting the Bode plots of  $\frac{\hat{y}_h}{y_c}(s)$  and the nominal system as before with zero hedge gain.

The basic form of the desired hedge model loop shape is as follows:

- +20 dB/dec slope at low frequencies
- $-20 \cdot r$  dB/dec slope at frequencies where the actuators distort the magnitude curve ( $r$  = relative degree of nominal system with no actuators)
- $-20 \cdot r - 20$  dB/dec slope at high frequencies

This shape can be accomplished (for a system with relative degree 1) using the hedge plant and hedge filter given in Eqns ( 3.17 )and ( 3.18 ) with the pole in the hedge filter at the high frequency end of the magnitude distortion and the two poles of the hedge plant at the low frequency end of the distortion. For example, in the F-18/HARV example given above, the hedge filter and hedge plant are  $G_r(s) = \frac{s}{s+100}$  and

$G_h(s) = \frac{100}{s^2 + 20s + 100}$ . This is illustrated below in Figure 3-38.



**Figure 3-38: Creating the Hedge Model,  $\frac{\hat{y}_h}{y_c}$**

Obviously, the selection procedure of the pole locations for the hedge system is not exact. Some tuning is usually required. However, the basic rules of thumb given above are a good starting place. Some key factors which affect the optimum pole placement of the hedge system include: system plant parameters, actuator dynamics, and observer speed. Once the hedge system loop shape is set, adjust the hedge gain as required.

### 3.4.2 Selecting Hedge Gain

Note that the hedge gain in the simplified hedge model shown above is much higher than that in the original hedge approach ( $K_h = 8.0$  instead of 0.8). The magnitude of the hedge gain required is a function of the bandwidth of the hedge plant and filter. Higher bandwidth hedge systems require lower hedge gains; lower bandwidth hedge systems require higher hedge gains. In general, it is better to have a lower bandwidth hedge system because the larger range of acceptable hedge gains makes the overall system less sensitive to hedge gain—thus easier to design and potentially easier to implement an adaptive hedge scheme.

If the observer is very fast, or if no observer is used, there is a minimum hedge gain which will stabilize the system. Using this method of examining the Bode plots of  $\frac{\hat{y}_h}{y_c}(s)$ , it is easy to determine the minimum hedge gain. Examining the Bode plots will also give an indication of the upper limit for acceptable hedge gain. In general, if the hedge signal moves the magnitude plot of  $\frac{\hat{y}_h}{y_c}(s)$  above the nominal plant magnitude plot, the closed-loop system will have unacceptable overshoot and phase lag. This can lead to instability if outer control loops are closed around the SMC system. The

To illustrate the time domain effect of increasing hedge gain on the F-18/HARV system, see Figure 3-40. This plot shows unit step responses for pitch rate. Hedge gains used are  $K_h = 1.0, 8.0, 15.0, 20.0$ . As can be seen, when the hedge gain is too low, oscillations due to the interaction of the SMC and the parasitic dynamics are a problem. If the hedge gain is reduced below this, the system will be unstable. When the hedge gain is too high, tracking is slower and has more overshoot. This confirms the design choice of  $K_h = 8.0$  from the Bode plots in Figure 3-37 and Figure 3-39. Once again, the

Figure 3-39: System with Simplified Hedging, Bode Plots  $\frac{Y_c}{Y_h}, K_h=20.0$

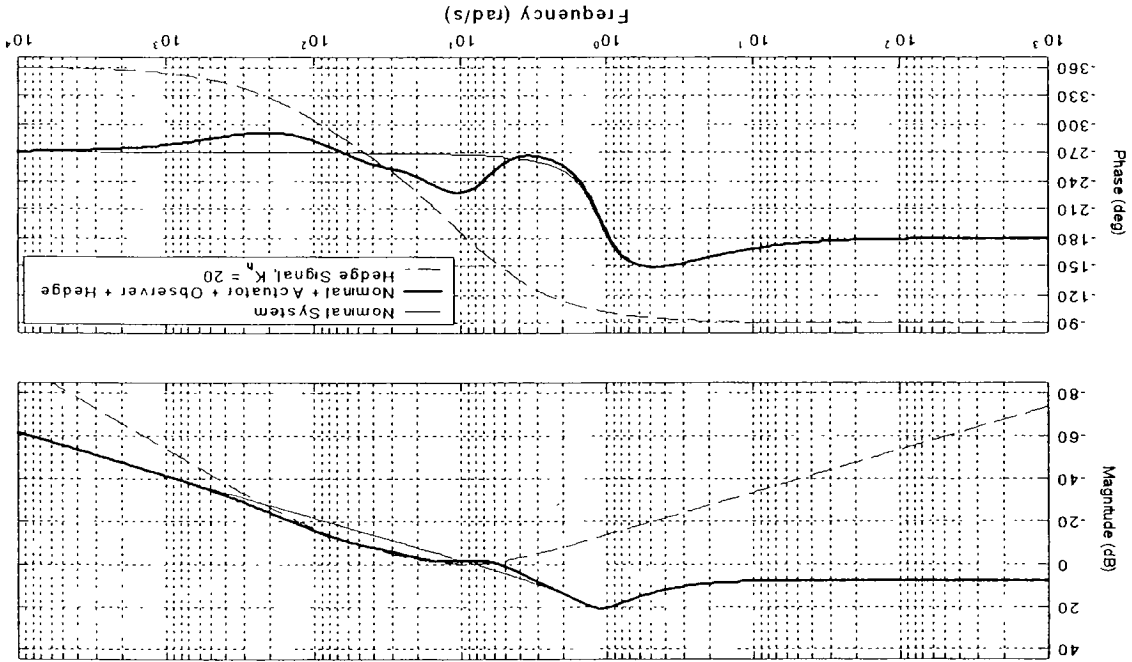
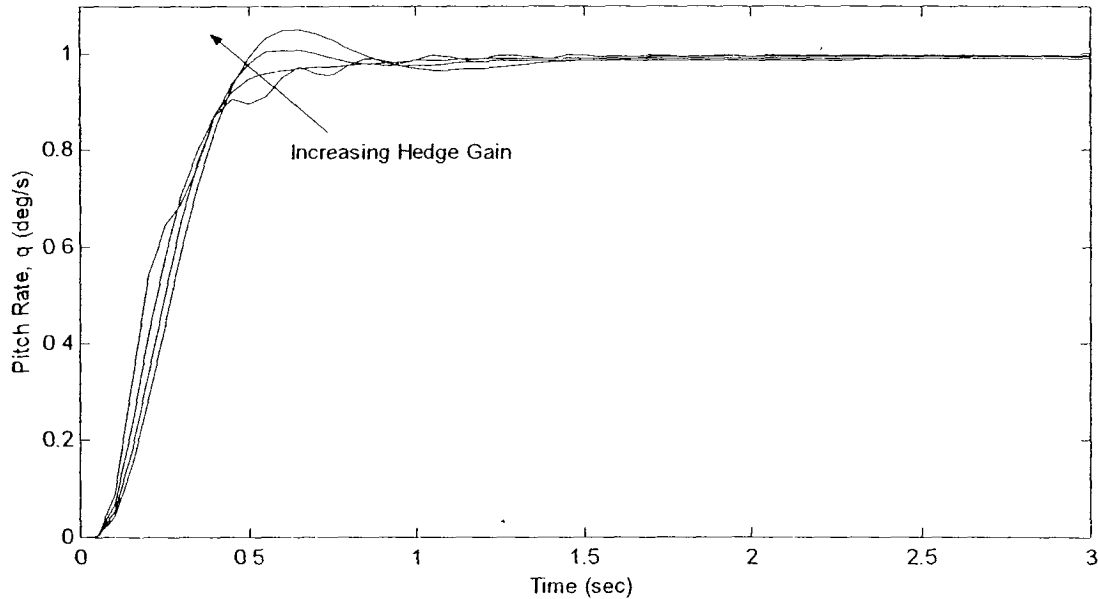


Figure 3-39.

previous example is run with a hedge gain of  $K_h = 20$  to illustrate. Results are shown in

use of Bode plots of  $\frac{\hat{y}_h}{y_c}(s)$ , combined with time domain step responses of the SMC inner loop control variables provides a useful tool for choosing hedge gains.

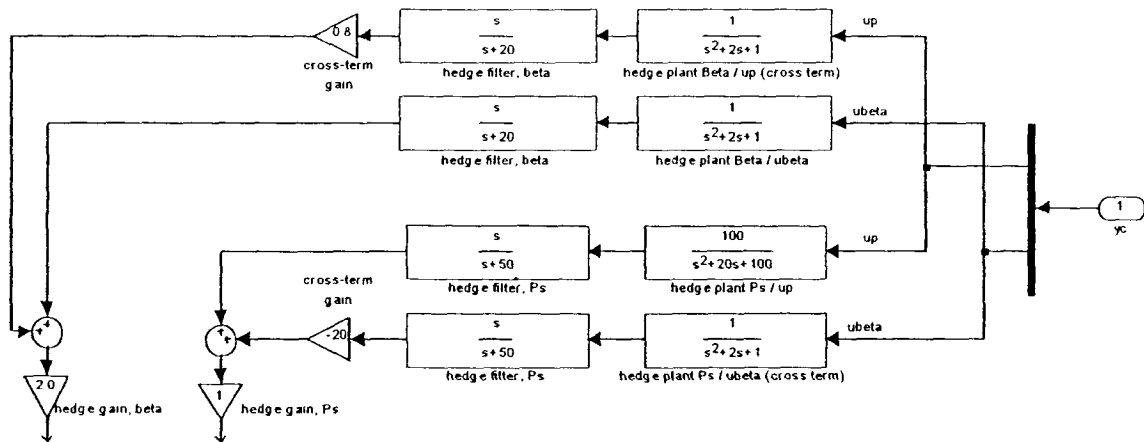


**Figure 3-40: System with Simplified Hedging, Step Responses**

### 3.4.3 Hedging in MIMO Systems

Since the control variables are decoupled by the controller, it is a simple matter to treat each channel independently and design a hedge model for each separate channel. However, recall that with the initial concept of hedging, the control output fed into a nominal model of the plant. This means that the original hedge signal included not only the primary variable transfer function, but it also included the effects of all the cross-coupled transfer functions as well. For example, in a lateral directional model (with roll rate,  $p$ ; and sideslip angle,  $\beta$ ), the primary transfer function for roll rate would be roll rate to roll-rate-command,  $\frac{p}{u_p}$ . The cross-coupled transfer function would be roll rate to

$\beta$ -command,  $\frac{P}{u_\beta}$  When using the simplified hedge plant as introduced in Section 3.4 1, the effects of the cross-coupling are lost. Unfortunately, if the effects of cross-coupling are strong, the interaction of commands of one channel with the unmodeled parasitic dynamics can lead to instability in another channel. Therefore, in MIMO applications, the cross-coupled transfer functions need to be examined. If necessary, a hedge model for the cross-coupling term can be designed and the feedback loop properly shaped. The same guidelines introduced above are also used for the cross-coupled hedge models. This cross-term hedge signal is then added to the primary hedge signal. For example, see the hedge model shown in Figure 3-41. This shows the hedge model for a lateral-directional system in which stability axis roll rate,  $P_s$ , and sideslip,  $\beta$ , are the control variables. The cross-coupled terms are included.



**Figure 3-41: Hedge Model Example with Cross-Coupled Terms**

Examples of hedging with cross-coupling are given later in an F-18/HARV and a tailless fighter aircraft application. The potential effects of neglecting these cross-coupled terms are also shown.

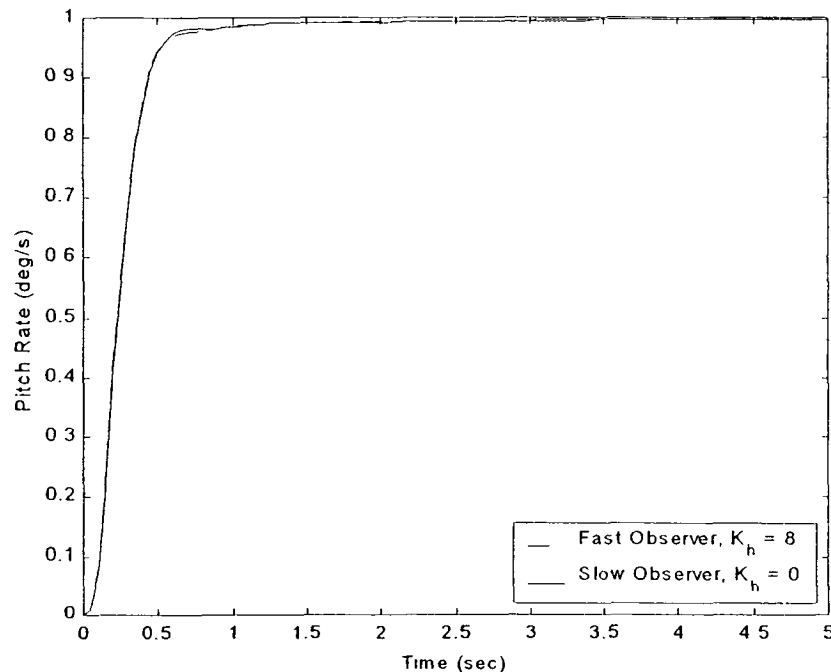
#### 3.4.4 Observer Gains and Hedging with Failed Plants

Recall from Section 3.3.3 that robustness to failures of the system plant and tolerance of parasitic dynamics present competing objectives when choosing observer gains. Fast observers are more robust to system parameter variations, but they do not eliminate the adverse interaction of the SMC and parasitic dynamics. Slow observers enable the SMC to operate in the face of parasitic dynamics, but they provide poor robustness to system parameter changes. Some trade-offs must be made when designing the observer.

The use of hedging can sometimes help meet both objectives. Since the hedge system contains no nominal system model, it is less sensitive to system parameter variations. The basic loop shape of the hedge system is always the same. Therefore, as long as the parameter variations do not significantly change the location of the distortion in the  $\frac{\hat{y}_h}{y_c}(s)$  Bode magnitude curve, the design hedge system poles will provide the correct hedge loop shape for the failed system. With the correct hedge system loop shape, the effects of the parasitic dynamics can be mitigated with the correct hedge gain. After a system failure, the hedge gain will probably need to be adjusted using some kind of adaptive mechanism.

This is encouraging and means that it is possible to run the observer with fast eigenvalues. In fact, one may be tempted to eliminate the observer altogether and use

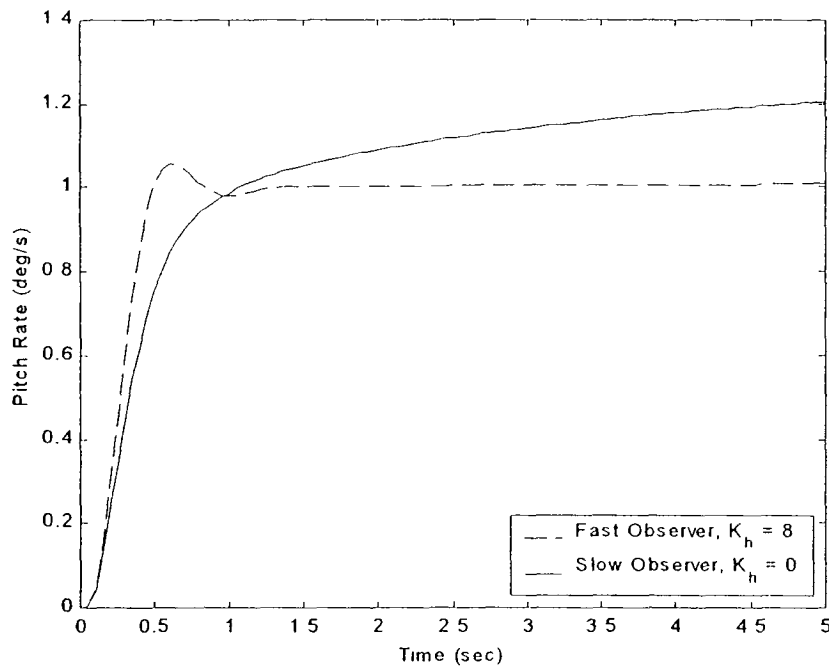
only hedging. In some cases, this is true. However, in general, hedging alone is not the best answer. To illustrate the effects of observer speed and hedging, consider several different types of failures: plant parameter variations (changes to system state space  $\mathbf{A}$  and  $\mathbf{B}$  matrices), actuator bandwidth variations; and pure time delay. The following set of figures use the F-18/HARV SISO longitudinal pitch rate tracking model introduced above and given in detail in Section 4.5. All use the same SMC and include actuator dynamics.



**Figure 3-42: F-18/HARV Step Response, Nominal System, Nominal Actuators, No Time Delay**

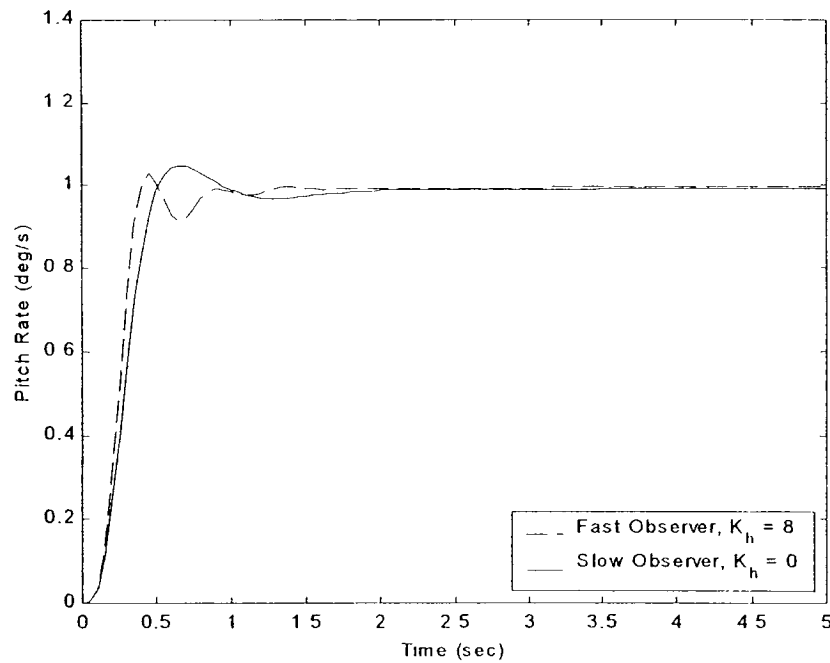
Figure 3-42 shows the nominal system step response assuming a “fast” observer with hedging and a “slow” observer with no hedging. In all the following cases, “Fast Observer” means observer poles at  $\lambda = -100, -101$ ; and “Slow Observer” means observer poles at  $\lambda = -4, -5$ . While the SMC alone cannot stabilize the system when actuators are

included, the observer-based SMC and the hedged SMC model both stabilize the system as illustrated in Figure 3-42. Note that they provide equally good performance. The question, then, is: which will provide the most robustness to system failures? Figure 3-43 shows the same SMC, observer, and hedge systems with a “failed” system plant.



**Figure 3-43: F-18/HARV Step Response, FAILED System, Nominal Actuators, No Time Delay**

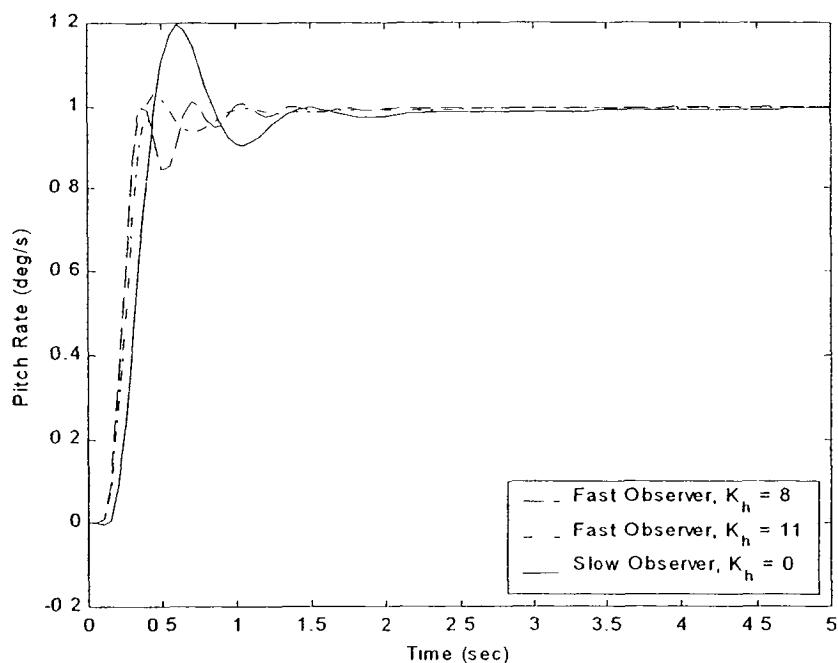
The failure is a 50% loss of horizontal tail area (which affects the system state space  $\mathbf{A}$  and  $\mathbf{B}$  matrices). As can be seen in Figure 3-43, the hedged system is much more robust than the system with the slow observer. While this tends to be true in the case of system variations, it is not true if the actuator dynamics change. For example, Figure 3-44 shows the results for a nominal plant and failed actuators. The actuator failures are a 50% reduction in the actuator bandwidths.



**Figure 3-44: F-18/HARV Step Response, Nominal System, FAILED Actuators, No Time Delay**

As can be seen, in this case the slow observer has better performance than the hedged system. This is because the location of the distortion in the  $\frac{\hat{y}_h}{y_c}(s)$  Bode magnitude curve occurs at a lower frequency and the hedge signal loop shape is incorrect for the failed system. Varying the hedge gain does little to help. The hedge system poles require tuning for the new condition.

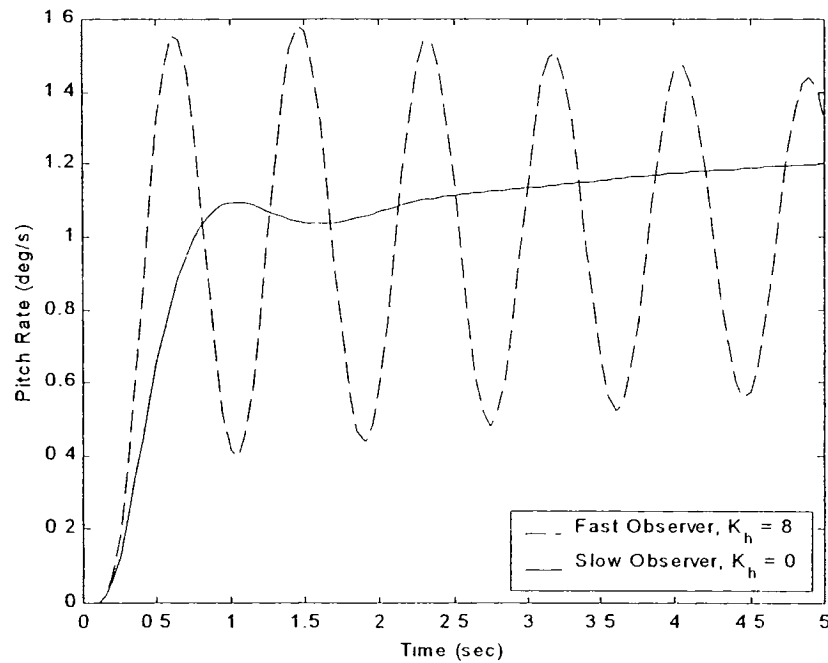
Next, consider the case of a nominal plant and actuators and a pure time delay. A 50 ms time delay is inserted between the controller and the actuators. For the simulation, a second order Pade approximation is used.



**Figure 3-45: F-18/HARV Step Response, Nominal System, Nominal Actuators, 50 mS Time Delay**

In this case, neither the slow observer nor the hedged system with a fast observer provide responses comparable to that of the nominal system. The slow observer has 20% overshoot, and the hedged model is too oscillatory. As illustrated, increasing the hedge gain eliminates some of the oscillations, but changing the hedge gain alone can not restore the desired performance. The addition of a time delay has the effect of moving the location of the distortion in the  $\frac{\hat{y}_h}{y_c}(s)$  Bode magnitude curve to a lower frequency. Again, this type of failure requires tuning of the hedge model poles.

Finally, consider a case that combines all three types of failures. Figure 3-46 shows the case of a failed plant, 50% reduction in actuator bandwidths, and a 50 ms time delay. Results are clearly unacceptable.



**Figure 3-46: F-18/HARV Step Response, FAILED System, FAILED Actuators, 50 mS Time Delay**

As illustrated, the slow observer system is unstable, the hedged system is highly oscillatory. In order for the slow observer system to be effective, the plant model used in the observer needs to be adjusted. In order for the hedged system to be effective, the hedge model poles need to be tuned. Hedge gain alone will not help.

The conclusion here is that design trade-offs need to be made based on the types of failures expected. In general, hedging provides more robustness to plant variations. Slow observers provide more robustness to actuator bandwidth variations and time delays. If a system is to be robust to all three types of failures, the observer should be moderately fast and hedging should be included. In addition, the hedge model can be tuned such that there is a wider separation between the low and high frequency poles in the hedge model ( $b_f$  and  $a_h$  in Eqns ( 3.18 ) and ( 3.17 ) ) than is required for the nominal

system. This results in a hedge model which provides degraded performance in the nominal case but is more robust to actuator variations and time delays.

#### 3.4.5 A Hedge By Any Other Name

It is worth noting that the hedging method proposed no longer resembles the concept of hedging given in the initial reference work.<sup>134</sup> Note in Figure 3-32 that all the hedge signal dynamics occur parallel to the observer loop and no longer enter the reference model. The hedging method here is really a form of observer loop shaping. In fact, it is recognized that this approach is very similar to Loop Transfer Recovery (LTR) as used in Linear Quadratic Gaussian (LQG) control. An LQG controller combines an optimal regulator (LQR) with an optimal observer (Kalman filter) and can result in arbitrarily poor stability margins.<sup>135</sup> LTR is a method by which optimality of the observer is traded for increased stability margins. The hedge signal used here also has the effect of “tuning down” the observer at certain frequencies in order to recover desirable stability margins.

It can also be shown that the hedge system is attempting to invert the actuator dynamics. This is why it is so dependent on the actuator bandwidths. When viewed in this light, one could argue that this is simply another form of an SMC prefilter-type design. In order to prevent confusion, the method presented here should probably be given a different name. On the other hand, recall that if the hedge signal enters the reference model as originally illustrated in Figure 3-29 (which is supposed to implement the intent of hedging<sup>134</sup>), the final method being proposed is exactly equivalent. Therefore, this analysis has illustrated in the frequency domain why model reference hedging works and how to proceed with the design. There are two advantages of this

approach. First, the actuator states are not required as they are in pseudo-command hedging.<sup>134</sup> Second, if the simplified hedge plant is used, the model of the nominal system is not required.

### 3.5 Robustness Issues

So far, the effects of asymptotic observers and model reference hedging on an SMC system have been investigated, and design procedures for synthesizing these models have been offered. General observations about performance and robustness are made via application examples and inferences from frequency domain Bode plots. A key issue which remains unanswered is a formal quantitative statement about overall system robustness. There are several difficulties which hinder the derivation of such a proof. These are introduced below.

#### 3.5.1 Difficulties with SMC Robustness Proofs

##### 3.5.1.1 Practical design issues with standard Lyapunov proofs

Almost all robustness proofs for SMC involve the use of Lyapunov stability criteria to guarantee global attractiveness of the sliding manifold (i.e. the reaching condition). A classic simple example of how such a proof proceeds is given in *The Control Handbook*.<sup>92</sup> Consider the following nonlinear plant:

$$\begin{aligned}\dot{x} &= A(x)x + B u(x) \\ &= \begin{bmatrix} 0 & 1 \\ -\frac{\sin(x_1)}{x_1} & 0 \end{bmatrix} \begin{bmatrix} x_1 \\ x_2 \end{bmatrix} + \begin{bmatrix} 0 \\ 1 \end{bmatrix} u(x)\end{aligned}$$

The sliding manifold is given by

$$\sigma(x) = [s_1 \ s_2] x$$

A variable structure control law is used

$$u(x) = k_1(x) x_1 + k_2(x) x_2$$

where

$$k_i(x) = \begin{cases} \alpha_i(x), & \text{if } \sigma(x) x_i > 0 \\ \beta_i(x), & \text{if } \sigma(x) x_i < 0 \end{cases}$$

A candidate Lyapunov function is selected

$$V(t, x, s) = \frac{1}{2} \sigma^2(x)$$

The Lyapunov stability criteria requires the derivative of the Lyapunov function to be strictly negative, so

$$\begin{aligned} \dot{V} &= \sigma(x) \frac{d\sigma}{dt} = \sigma(x) [s_1 \quad s_2] \dot{x} \\ &= \sigma(x) x_1 \left[ s_2 \left( k_1(x) - \frac{\sin(x_1)}{x_1} \right) \right] + \sigma(x) x_2 [s_1 + s_2 k_2(x)] < 0 \end{aligned}$$

The control law parameters which satisfy the negative definite condition are

$$\begin{aligned} \alpha_1(x) &< \min_{x_1} \left[ \frac{\sin(x_1)}{x_1} \right]; & \beta_1(x) &> \max_{x_1} \left[ \frac{\sin(x_1)}{x_1} \right] \\ \alpha_2(x) &< -\left( \frac{s_1}{s_2} \right); & \beta_2(x) &> -\left( \frac{s_1}{s_2} \right) \end{aligned} \quad (3.19)$$

If the control law constants are selected such that (3.19) is satisfied, the sliding mode is guaranteed.

Note that the criteria in (3.19) only accounts for maximum excursions of the state variables and the (known) nonlinearities in the system. It does not account for any other parameter variations. A common method to include parameter variations is to write the state space system as

$$\dot{x} = (\mathbf{A} + \Delta\mathbf{A})x + (\mathbf{B} + \Delta\mathbf{B})u$$

where  $\Delta\mathbf{A}$  and  $\Delta\mathbf{B}$  are unknown, bounded, smooth perturbations. There are several examples of works which approach the problem in this manner.<sup>63-66</sup> The analysis proceeds as above; however, it becomes extremely involved. In the end, bounds for the control law parameters which guarantee the reaching condition are found in terms of maximum state excursions and norms of the perturbation parameterizations.

These types of proofs are necessary to complete a full analytical treatment of SMC robustness, however, they are not entirely practical. The example given above from *The Control Handbook* is a simple pendulum for which all the possible states of the system are known (and bounded). In general, for an aircraft application, the maximum excursions of all the states (and potentially their derivatives) are unknown and could be practically unbounded. Further, parameterizing all potential failure events is a difficult task. Norms of the perturbation matrices for the state parameters is common. However, parameterizing actuator failures is especially difficult due to the nonlinear nature of the failure modes. From a practical standpoint, these issues make even this traditional approach to proving robustness very difficult.

### 3.5.1.2 Boundary layers

The Lyapunov analyses discussed above are generally applied to the pure sliding mode problem. The SMC control law is derived to guarantee the sliding motion, and once on the sliding mode, the system is invariant to matched uncertainty. When a boundary layer is included, pseudo-sliding takes place, and the invariance property is lost. It is possible to perform the Lyapunov analysis using a boundary layer in the control law definition. In this case, stability to the boundary layer surface (rather than

the sliding manifold) is guaranteed. However, a question which remains is “How robust is the system inside the boundary layer?” The system can be made arbitrarily close to invariant by decreasing the boundary layer width, but it is not clear how much robustness is retained when practically useful boundary layer widths are used. Further, boundary layer thickness appears to have competing robustness objectives. On one hand, very small boundary layers make the system more robust to plant parameter variations. On the other hand, large boundary layers make the system more robust to unmodeled parasitic dynamics. So, even if a complete formal Lyapunov stability proof is performed, the measure of robustness is not exactly known when a boundary layer is employed.

### 3.5.1.3 Matching conditions

Another difficulty with SMC robustness proofs is the issue of matching conditions. The system is shown to be invariant to matched uncertainties when on the sliding surface. However, an issue which is not usually addressed is robustness to variations in the unmatched parameters. There are two recent works which provide design approaches for systems with unmatched uncertainties;<sup>136,137</sup> however, a formal treatment of robustness to unmatched uncertainties in a traditional SMC setting has not been found. There are two interesting observations concerning matching conditions which have been noted in the process of this research. First, matching conditions change depending on the state space selected. Second, if parasitic dynamics are neglected in the design, matching conditions vary with the bandwidth of the neglected dynamics. Each of these is illustrated in turn.

First, the state variables chosen affect which parameters are matched and which are unmatched. Consider again the simple system introduced in Section 3.1, Figure 3-4, pg. 87. By lumping the actuator with the plant, the resulting state space variables appear in phase variable form:

$$\begin{bmatrix} \dot{x}_1 \\ \dot{x}_2 \end{bmatrix} = \begin{bmatrix} 0 & 1 \\ -pa & -(p+a) \end{bmatrix} \begin{bmatrix} x_1 \\ x_2 \end{bmatrix} + \begin{bmatrix} 0 \\ k \end{bmatrix} \mathbf{u} \quad (3.20)$$

$$y = \begin{bmatrix} 1 & 0 \end{bmatrix} \begin{bmatrix} x_1 \\ x_2 \end{bmatrix}$$

By inspection, it is expected that the parameters  $p$ ,  $k$ , and  $a$  are matched because they lie in the row of the control input. The sliding manifold is defined in terms of the state variables ( $x_1$ =plant output;  $x_2$ =derivative of plant output):

$$\sigma = m x_2 + x_1 \quad (3.21)$$

The equivalent control is found

$$\mathbf{u}_{eq} = \left( \frac{m(p+a)-1}{mpk} \right) x_2 + \left( \frac{a}{k} \right) x_1 \quad (3.22)$$

Using this equivalent control, the closed loop, unforced response is determined

$$\begin{bmatrix} \dot{x}_1 \\ \dot{x}_2 \end{bmatrix} = \begin{bmatrix} 0 & 1 \\ 0 & -\frac{1}{m} \end{bmatrix} \begin{bmatrix} x_1 \\ x_2 \end{bmatrix} \quad (3.23)$$

with eigenvalues at  $\lambda = 0, -\frac{1}{m}$ . Indeed, as noted before, this system is invariant to changes in parameters  $p$ ,  $k$ , and  $a$ .

Next, consider the same system; but instead of writing the state variables in phase variable form, write the states with the actuator and plant in series

$$\begin{bmatrix} \dot{x} \\ \dot{x}_a \end{bmatrix} = \begin{bmatrix} -a & k \\ 0 & -p \end{bmatrix} \begin{bmatrix} x \\ x_a \end{bmatrix} + \begin{bmatrix} 0 \\ p \end{bmatrix} u \quad (3.24)$$

$$y = \begin{bmatrix} 1 & 0 \end{bmatrix} \begin{bmatrix} x \\ x_a \end{bmatrix}$$

By inspection, it is expected that the parameter  $p$  is matched, and the parameters  $k$  and  $a$  are unmatched. The sliding manifold is defined in terms of the state variables ( $x$ =plant output,  $x_a$ =actuator output):

$$\sigma = m x_a + x \quad (3.25)$$

The equivalent control is found

$$u_{eq} = \frac{a x - k x_a}{m p} + x_a \quad (3.26)$$

Using this equivalent control, the closed loop, unforced response is determined

$$\begin{bmatrix} \dot{x} \\ \dot{x}_a \end{bmatrix} = \begin{bmatrix} -a & k \\ \frac{a}{m} & -\frac{k}{m} \end{bmatrix} \begin{bmatrix} x \\ x_a \end{bmatrix} \quad (3.27)$$

with eigenvalues at  $\lambda = 0, -\left(a + \frac{k}{m}\right)$ . The closed loop response is a function of both  $a$  and  $k$ . This system is not invariant to these unmatched parameters. This shows that when the sliding manifold is defined in terms of different state variables, invariance can be lost and system robustness is affected. The work of Chan, *et al.*,<sup>136</sup> takes advantage of this by defining a subspace where unmatched parameters become matched--resulting

in a new sliding manifold on which invariance is achieved. Another work defines the existence of sliding surfaces in terms of Linear Matrix Inequalities.<sup>137</sup> The conclusion of this observation is that care must be given to the selection of state variables. In this work, by specifying the system architecture to be square, all the key system parameters are matched. However, there can still be uncontrolled states which remain unmatched, and robustness to changes in these parameters is not clear.

A second observation is that matching conditions vary with the bandwidth of parasitic dynamics when these dynamics are neglected in the design. Consider a second order plant model (with no actuator).

$$\begin{aligned} \begin{bmatrix} \dot{x}_1 \\ \dot{x}_2 \end{bmatrix} &= \begin{bmatrix} 0 & 1 \\ -a_1 & -a_2 \end{bmatrix} \begin{bmatrix} x_1 \\ x_2 \end{bmatrix} + \begin{bmatrix} 0 \\ k \end{bmatrix} u \\ y &= \begin{bmatrix} 1 & 0 \end{bmatrix} \begin{bmatrix} x_1 \\ x_2 \end{bmatrix} \end{aligned} \quad (3.28)$$

The sliding manifold is defined in terms of the state variables ( $x_1$ =plant output;  $x_2$ =derivative of plant output):

$$\sigma = m x_2 + x_1 \quad (3.29)$$

The equivalent control is found

$$u_{eq} = \frac{1}{k} \left( a_1 x_1 + \left( a_2 - \frac{1}{m} \right) x_2 \right) \quad (3.30)$$

Using this equivalent control, the closed loop, unforced response is determined

$$\begin{bmatrix} \dot{x}_1 \\ \dot{x}_2 \end{bmatrix} = \begin{bmatrix} 0 & 1 \\ 0 & -\frac{1}{m} \end{bmatrix} \begin{bmatrix} x_1 \\ x_2 \end{bmatrix} \quad (3.31)$$

with eigenvalues at  $\lambda = 0, -\frac{1}{m}$ . As expected, the system is invariant to changes in  $a_1$ ,  $a_2$ , and  $k$ . Now, a first order actuator model,  $\frac{p}{s+p}$ , is placed in series with the plant, resulting in the following state space system.

$$\begin{bmatrix} \dot{x}_1 \\ \dot{x}_2 \\ \dot{x}_a \end{bmatrix} = \begin{bmatrix} 0 & 1 & 0 \\ -a_1 & -a_2 & k \\ 0 & 0 & -p \end{bmatrix} \begin{bmatrix} x_1 \\ x_2 \\ x_a \end{bmatrix} + \begin{bmatrix} 0 \\ 0 \\ p \end{bmatrix} u \quad (3.32)$$

$$y = \begin{bmatrix} 1 & 0 & 0 \end{bmatrix} \begin{bmatrix} x_1 \\ x_2 \\ x_a \end{bmatrix}$$

The actuator dynamics were not included in the design, but consider driving the “actual” system in (3.32) with the control derived for the system in (3.28). The equivalent control in (3.30) is not capable of maintaining the sliding mode because of the unmodeled disturbance, so a traditional discontinuous control element is included in the feedback control law.

$$u = \frac{1}{k} \left( a_1 x_1 + \left( a_2 - \frac{1}{m} \right) x_2 \right) - \rho \operatorname{sgn}(\sigma) \quad (3.33)$$

Further, in order to analyze this system using linear methods, replace the signum function with a boundary layer in which the limits of the saturation function are never reached. The approximated linear control takes the form

$$u \approx \frac{1}{k} \left( a_1 x_1 + \left( a_2 - \frac{1}{m} \right) x_2 \right) - \frac{\rho}{\varepsilon} (m x_2 + x_1) \quad (3.34)$$

The closed loop, unforced response is then given by

$$\begin{bmatrix} \dot{x}_1 \\ \dot{x}_2 \\ \dot{x}_a \end{bmatrix} = \begin{bmatrix} 0 & 1 & 0 \\ -a_1 & -a_2 & k \\ \frac{p}{k}a_1 - \frac{p\rho}{\varepsilon} & \frac{p}{k}\left(a_2 - \frac{1}{m}\right) - \frac{p\rho m}{\varepsilon} & -p \end{bmatrix} \begin{bmatrix} x_1 \\ x_2 \\ x_a \end{bmatrix} \quad (3.35)$$

The characteristic equation for this system is

$$s^3 + (a_2 + p)s^2 + \left(\frac{p}{m} + \frac{p\rho mk}{\varepsilon} + a_1\right)s + \frac{p\rho k}{\varepsilon} = 0 \quad (3.36)$$

First of all, notice that by neglecting the actuator and using the control law derived for the nominal plant, the resulting system is not invariant to either the plant parameters or the actuator parameters. The relative values of the plant parameters and actuator parameters can result in oscillatory behavior and instability. Unfortunately, it is invalid to consider the system behavior as the bandwidth of the actuator,  $p$ , approaches zero because the assumption of a linear control becomes invalid. The system, with a discontinuous control element in the control law, quickly becomes unstable as  $p$  is reduced; while the continuous control law results in closed loop eigenvalues at the locations of the nominal plant. However, as  $p$  is increased, the linear assumption holds and it can be shown that the closed loop eigenvalues approach:  $\lambda = -\frac{1}{m}; -\frac{\rho km}{\varepsilon}; -\infty$ .

In fact, if the system is exactly on the sliding mode, the eigenvalues as  $p \rightarrow \infty$  are  $\lambda = -\frac{1}{m}; 0; -\infty$ , which is exactly the same result as obtained when there was no

actuator. In conclusion, actuator bandwidth affects the matching conditions. On the low frequency side, matching conditions are lost and instability occurs. On the high

frequency side, matching conditions are regained and invariance is approached in the limit.

### 3.5.2 Difficulties with Hybrid Nature of the Observer-based SMC

As discussed, proving robustness is difficult for the sliding mode controller. The nonlinear control necessitates the use of Lyapunov analyses which are problematic in a practical sense; boundary layers introduce an unknown amount of robustness degradation; and there are questions surrounding robustness to unmatched uncertainties. Now add an asymptotic observer with hedging. The classical linear tools for analyzing the robustness of the observer cannot be used due to the nonlinear controller. The already difficult methods of analyzing the SMC become intractable due to the addition of an entire closed-loop feedback structure in the SMC feedback path. The controller never “sees” the actual plant outputs, so it is no longer clear which parameters are matched, if any.

## 3.6 Robustness Summary

It is clearly unsatisfying to offer a design approach for which quantitative measures of robustness are not known—especially when the main goal of the method is to handle large scale failures. All efforts to quantify the robustness have turned up empty due to the issues described above. However, experience has shown that the SMC approach provides superior robustness and deserves continued development. While the formal robustness proofs are left for another, attention is now given to the development of a practical design procedure and application examples which demonstrate the SMC’s robustness.

# Chapter 4

---

## Design Procedure

### 4.1 Interpretation of Linear SMC Design in the Frequency Domain

Considering a linear plant or vehicle model, the SMC system including boundary layers can be interpreted as a linear system and analyzed in the frequency domain. That is, classical loop-shaping principles can be applied to the design, both in terms of choosing appropriate sliding manifolds and in evaluating the characteristics of the final SMC configuration. Note that, if a boundary layer is employed, and the boundary layer thickness is selected such that the limits of the saturation element are never reached, the control law is essentially a high gain linear controller. For example, consider a sliding function of the form

$$\sigma = c_1 \dot{e} + c_0 e + c_{-1} \int e dt \quad (4.1)$$

and an SMC control law (with a boundary layer)

$$u = \rho \operatorname{sat} \left( \frac{\sigma}{\varepsilon} \right) \quad (4.2)$$

If the saturation element always operates in the linear region, the feedback control law in the Laplace domain looks like a PID controller:

$$u(s) = \frac{\rho}{\varepsilon} \sigma = \frac{\rho}{\varepsilon} \left( c_1 s + c_0 + \frac{c_{-1}}{s} \right) e(s) \quad (4.3)$$

This fact can be used to help choose both the sliding function constants ( $c_{-1}$ ,  $c_0$ , and  $c_1$ ) and the control law gain ( $\rho/\varepsilon$ ). This interpretation of the sliding function allows the use of familiar loop shaping techniques and provides insight into the behavior of the controller.

The full closed-loop system including the reference model, linear compensator, actuators, plant, observer(s), and hedge is given in state space by

$$\begin{aligned} \dot{x}_{CL} &= \mathbf{A}_{CL} x_{CL} + \mathbf{B}_{CL} u_p \\ y &= \begin{bmatrix} \mathbf{C}_y & \mathbf{0} \\ \mathbf{0}_{m_y \times (n_a + n_{ol} + n_{o2} + n_{o3} + n_f + n_h + n_c + n_r)} \end{bmatrix} x_{CL} \end{aligned} \quad x_{CL} = \begin{bmatrix} x_e \\ x_c \\ x_r \end{bmatrix} \quad (4.4)$$

where

$$\mathbf{A}_{CL} = \begin{bmatrix} \mathbf{A}_e - \mathbf{B}_e \mathbf{D}_e \mathbf{S} \mathbf{C}_e & \mathbf{B}_e \mathbf{C}_e - \mathbf{B}_e \mathbf{D}_e \mathbf{S} \mathbf{D}_e \mathbf{C}_e & \mathbf{B}_e \mathbf{D}_e \mathbf{S} \mathbf{C}_r \\ -\mathbf{B}_e \mathbf{S} \mathbf{C}_e & \mathbf{A}_e - \mathbf{B}_e \mathbf{S} \mathbf{D}_e \mathbf{C}_e & \mathbf{B}_e \mathbf{S} \mathbf{C}_r \\ \mathbf{0}_{n_r \times n_{ro}} & \mathbf{0}_{n_r \times n_e} & \mathbf{A}_r \end{bmatrix}$$

$$\mathbf{B}_{CL} = \begin{bmatrix} \mathbf{B}_e \mathbf{D}_e \mathbf{S} \mathbf{D}_r \\ \mathbf{B}_e \mathbf{S} \mathbf{D}_r \\ \mathbf{B}_r \end{bmatrix}$$

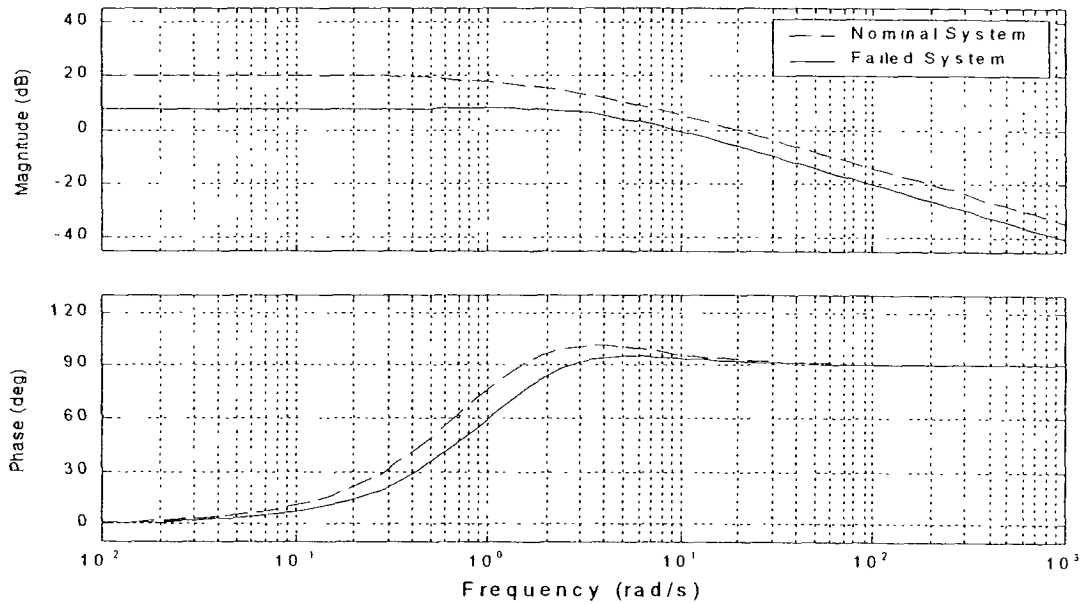
$\mathbf{S} \equiv (\mathbf{I}_m + \mathbf{D}_e \mathbf{D}_c)^{-1}$ ; and all e-subscripted variables are defined in Eqn ( 3.16 ).

## 4.2 Instantaneous Adaptation

One can rightly argue that, in treating the SMC as a linear high gain controller as introduced in Section 4.1, the system should no longer be called a sliding mode system. No true sliding mode is ever achieved, and all the properties associated with the sliding mode are lost. If the system is nothing more than a linear one, why not use classical linear design techniques for which design methods and robustness bounds are well

known? There are several answers to this question. First of all, it is common practice to still treat this as an SMC. While this is a very unsatisfying response, it is true. When applying SMC to real systems with physical actuators, a continuous control signal is almost always sought. Since an infinite frequency switching is required to maintain the sliding mode, none of the researchers who employ a boundary layer truly have a sliding mode system. They really only have a high gain linear controller. Yet, these controllers are still referred to in the literature as sliding mode controllers. Another reason is that the sliding manifold provides known error dynamics for the system. While a pseudo-sliding only provides asymptotic convergence to the sliding manifold, it nevertheless is converging to a known dynamic response. A third and more important reason is that this observer-based system with a pseudo-sliding mode is actually adapting to parameter changes. It instantaneously adjusts the gain and crossover frequency of the equivalent linear controller. A conventional linear controller (designed by loop shaping, for example) does not do this.

In order to illustrate this phenomenon, consider again the F-16 SISO longitudinal system from Section 3.2.1. Figure 4-1 shows the Bode plots of the pitch-rate to pitch-rate-command transfer function for the nominal system and a failed system. The system failure is a 50% loss of horizontal tail area (resulting in changes to the plant **A** and **B** state space matrices). Notice that the failure results in a gain reduction in the open-loop system transfer function.

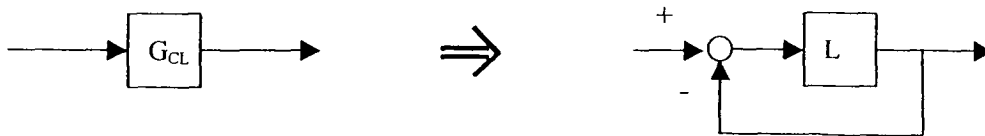


**Figure 4-1: Bode Plots, F-16 Pitch Rate  $\frac{q}{q_c}$ , Nominal and Failed Plants**

An observer-based SMC with hedging is designed for the nominal model. The SMC control law is  $u_c = -30 \text{sat}\left(\frac{\sigma}{1}\right)$ ,  $\sigma = 1(q_r - \hat{q}) + 20 \int (q_r - \hat{q}) d\tau$ . The observer poles are

at  $\lambda = -500, -501$ . The hedge system is  $-50 \left( \frac{64}{s^2 + 16s + 64} \right) \left( \frac{s}{s + 300} \right)$ . Using

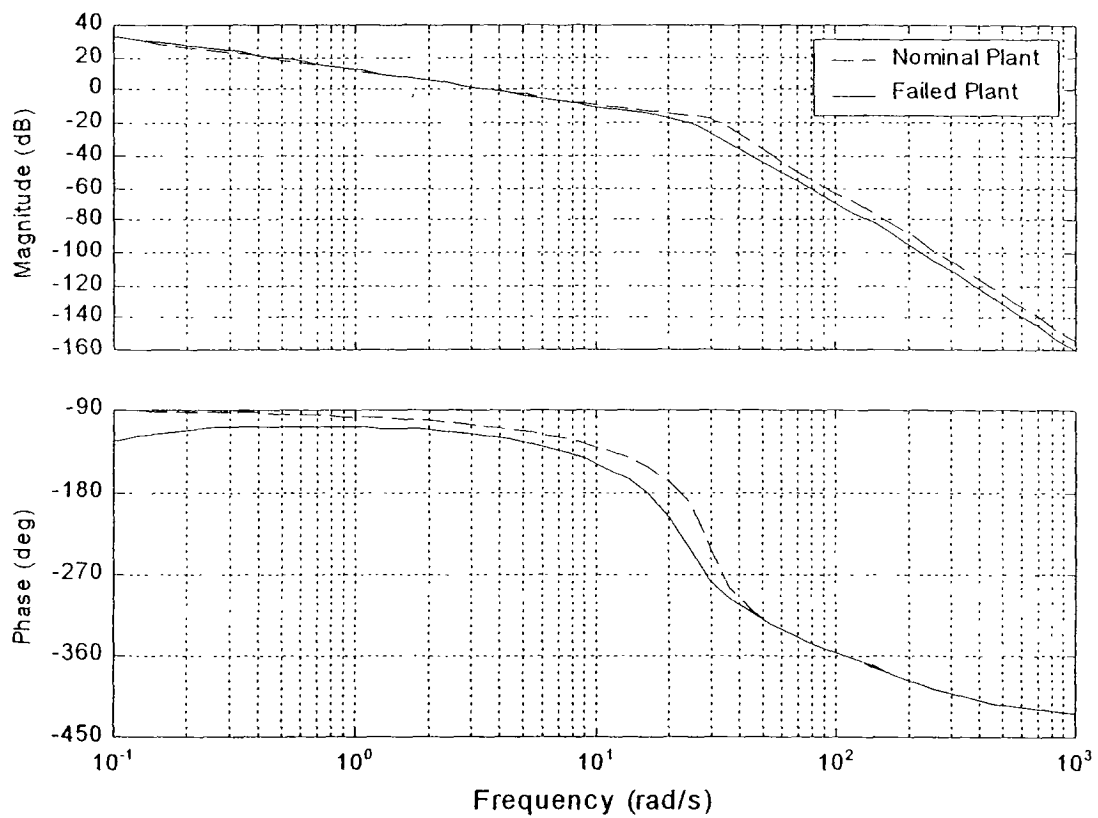
Eqn (4.7), the closed loop transfer function,  $G_{CL}(s)$ , is determined for both the nominal and failed cases. Next, determine the equivalent unity feedback loop transmission as illustrated below.



The unity feedback loop transmission,  $L$ , is given simply as

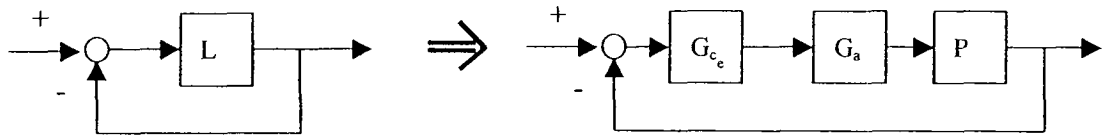
$$L(s) = \frac{G_{cl}(s)}{1 - G_{cl}(s)} \quad (45)$$

The resulting Bode plots of the equivalent unity feedback loop transmissions for the nominal and failed cases are shown in Figure 4-2.



**Figure 4-2: Bode Plots, F-16 Equivalent Unity Feedback Loop Transmission**

Note, first of all, the desirable  $\frac{K}{s}$  characteristic at the crossover frequency. Note also, that both the nominal and failed systems look almost identical at crossover. Indeed, both systems have very good (almost identical) tracking performance. Consider, next, the determination of an equivalent serial compensator as illustrated below.



where  $G_a(s)$  is the actuator and  $P(s)$  is the system plant (nominal or failed). The element  $G_c(s)$  then represents a serial compensator which is equivalent to the combined effects of the (linear) SMC, observer, and hedge. It can be calculated as

$$G_c(s) = \frac{L(s)}{G_a(s) P(s)} \quad (46)$$

This equivalent serial compensator is calculated for the nominal and failed systems. The results are shown in the Bode plots in Figure 4-3. First of all, note that the two compensators are different. This means that the observer-based SMC has changed. Note also that the equivalent serial compensator for the failed case has an increased gain to compensate for the lower gain of the failed system. So, the controller is varying in a manner that tends to compensate for the changes in the vehicle dynamics. This behavior is attributable to the presence of the observer(s) in the feedback loop. Of course, the changes are instantaneous.

One last observation is of interest. Consider using the nominal equivalent serial compensator with the failed plant and compare the results with using the "adapted" equivalent serial compensator with the failed plant. This is analogous to designing a loop shaped compensator which does not change with the varying system parameters. The open loop transfer functions of  $(G_c \cdot G_a \cdot P_{fail})$  and  $(G_c^{adapted} \cdot G_a \cdot P_{fail})$  are shown in

Figure 4-3: Bode Plots, F-16 Equivalent Serial Compensator,  $G_c$  and  $G_c^{adapted}$

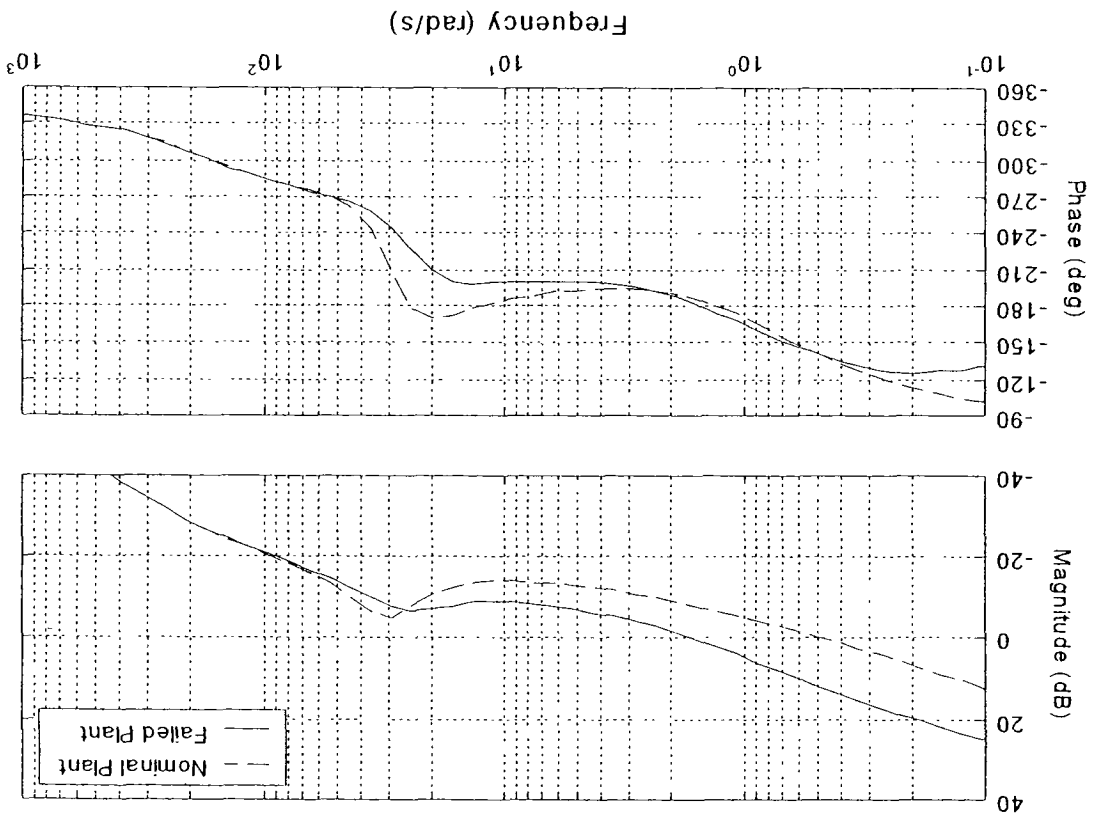
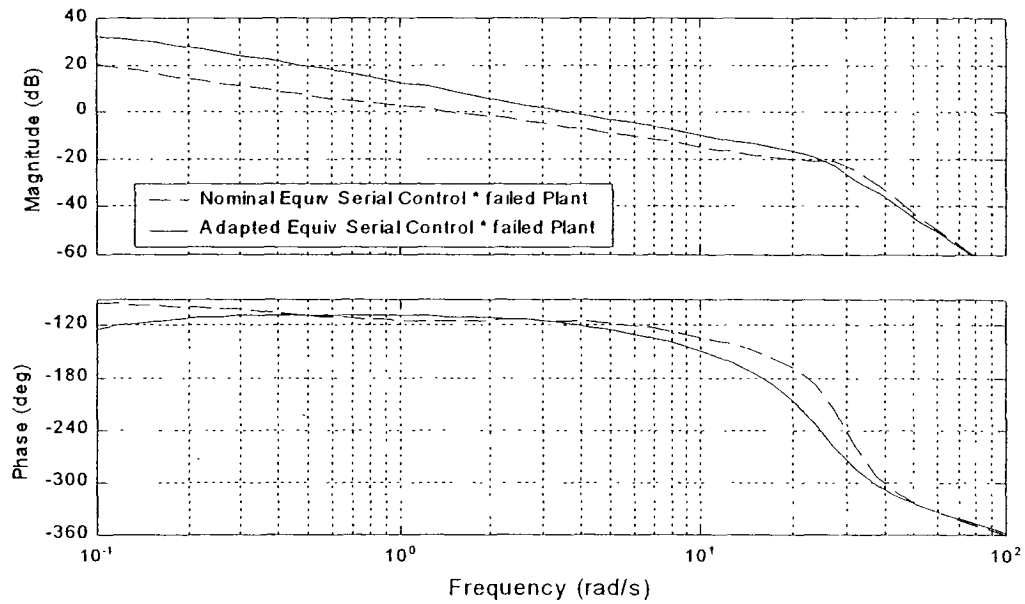


Figure 4-4. The “adapted” equivalent serial compensator is superior. It has a considerably higher crossover frequency with little degradation in stability margins.



**Figure 4-4: Bode Plots, Nominal Equiv Serial Compensator with Failed Plant**

### 4.3 Design Procedure Summary

A proposed SMC design methodology can now be offered. A step-by-step procedure is given, followed by three application examples of increasing complexity. Recalling that the objectives of SMC design are finding appropriate sliding surfaces and switching logic, the procedure to be described approaches this problem from a frequency-domain based, model-reference approach.

- (1) The vehicle model is obtained, along with an estimate of the frequency beyond which parasitic dynamics (or unstructured uncertainties) are likely to come into play. This frequency is referred to as the limit frequency in this discussion. Actuator dynamics are not included in the nominal plant model.
- (2) A reference model is chosen for each control variable channel. Since piloted flight control is of interest in the present application, this reference model should be selected with an eye towards Level I handling qualities with no pilot-induced oscillation (PIO) tendencies. This can be accomplished based upon a pilot model-based handling qualities and PIO prediction technique.<sup>138</sup> An example is available.<sup>43</sup>
- (3) The desired feedback structure of the control system is determined with a square system architecture. For example, if a pitch-rate command flight control system is desired, then pitch rate ( $q_c$ ) becomes the output of the reference model, and estimated pitch rate ( $\hat{q}$ ) is fed back to the SMC system from the observer. System error is then defined as  $e(t) = q_c(t) - \hat{q}(t)$ . Special care must be given to ensure the dynamics of the uncontrolled variables remain stable. This assumption is analogous to the minimum phase assumption used in feedback linearization.<sup>66</sup> Also, if there are redundant control effectors for the desired moments/pseudo-commands, a control distribution matrix must be defined. This research considers only static control allocation. Simple ganging is used in the first two examples. A pseudo-inverse method is used in the third application.

(4) The sliding manifold,  $\sigma$ , is chosen based upon the following principles:

a)  $\sigma$  is derived from a tracking error expression as

$$\sigma = e(t)^{p-1} + K_{p-2}e(t)^{p-2} + K_0e(t) + K_{-1}\int e(t) dt \quad (4.7)$$

where  $p$  is the relative order of the system, i.e., the number of times the vehicle output must be differentiated for the input to appear. Note that the  $(p-1)^{\text{st}}$  derivative of the error signal is included in the definition of  $\sigma$ . An integral term also appears in Eqn (4.7) to counter the steady-state bias often created with the use of a boundary layer.

b) Recognizing that a boundary layer is to be implemented, the control law is expressed as a linear transfer function as discussed earlier.

$$\begin{aligned} u(s) &= \frac{\rho}{\varepsilon} \sigma \\ &= K_{\rho} \left( s^{p-1} + K_{p-2}s^{p-2} + K_0 + \frac{K_{-1}}{s} \right) e(s) \end{aligned} \quad (4.8)$$

The parameters  $K_i$  are chosen to provide desirable properties in the frequency domain. This means creating a loop transmission with broad  $K/s$ -like characteristics around crossover.<sup>139</sup> This will always be possible since enough derivatives are included in Eqn.(4.3) to create exact  $K/s$  characteristics beyond a certain frequency (at least as high as the limit frequency). Parasitic

dynamics are deliberately excluded in this formulation. This step will involve obtaining an estimate of  $K_p$ , as this value will determine the crossover frequency of the loop transmission. This crossover frequency is selected to provide acceptable stability margins as obtained from a Bode plot of the loop transmission but using a value of  $K_p$  at least as large as the largest amplitude limit of any of the control effectors. The latter criterion is included to accommodate maximum trim positions of the control effectors. As opposed to typical designs involving loop shaping, very high crossover frequencies may result from this step. Indeed these frequencies may be well beyond the limit frequency. This result is of no immediate concern. If a MIMO system is being designed, a classic sequential loop closure technique is used, thereby sequentially and independently determining the coefficients for each sliding manifold.

- (5) Using the  $K_i$ 's just determined in the definition of the sliding function, the existence of a sliding mode is verified in the inner loops using a true SMC. This step is completed without the observer, actuators, reference model or pilot model, i.e., assuming that no outer-loop is being utilized. If necessary,  $\rho$  is increased until sliding behavior is created. The initial value of  $\rho = K_p$  obtained in step (4b) should be considered a lower limit in this process. While an analytical approach to determine  $\rho$  is certainly possible here, a more expedient route of establishing the sliding mode using a computer simulation of the system

is also possible. Near perfect tracking in the face of large parameter variations should be observed. The control signal, however, will exhibit very high frequency switching

- (6) A boundary layer is included in the controller by replacing the signum function  $\text{sign}(\sigma)$  with the saturation function  $\text{sat}\left(\frac{\sigma}{\varepsilon}\right)$ . While maintaining an approximate constant  $\frac{p}{\varepsilon} = K_p$ , increase the boundary layer thickness,  $\varepsilon$ , until no high frequency switching is evident. Again, a simulation of the SMC system is a convenient way of finding this  $\varepsilon$ . Near-perfect tracking (with a continuous control signal) in the face of large parameter variations should be observed.
- (7) Parasitic dynamics are included in the model. The SMC controller will very likely be unstable at this juncture
- (8) An asymptotic observer is created for each control variable channel as discussed in Section 3.3.
- (9) If desired, a hedge model is designed as described in Section 3.4
- (10) The frequency domain characteristics of the open and closed-loop SMC system with observer, boundary layer and reference model are examined to ensure that stability of the linear system is in evidence.

#### 4.4 Task-Dependent Analytical Handling Qualities Assessment

The goal of the research described herein involves the stability and performance robustness of flight control systems associated with damaged aircraft/actuators. With the exception of uninhabited vehicles, all these aircraft will be under piloted control. Thus,

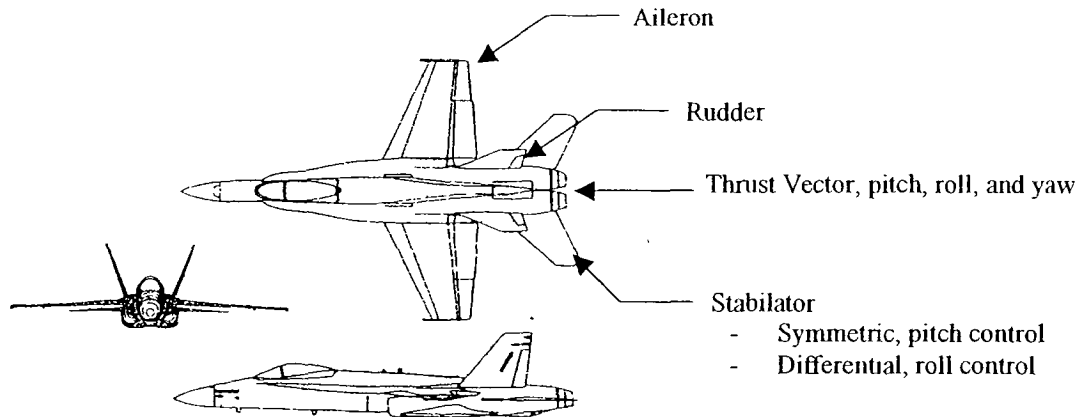
an analysis of the predicted handling qualities of damaged aircraft/actuators with the SMC systems is of considerable importance in determining the utility the proposed design methodology. Space does not allow a detailed description of the handling qualities assessment technique to be utilized here. Several key works provide a description of the pilot-model based assessment tool that can be used.<sup>43,138,140</sup> Using the handling qualities level and PIO levels discussed therein, task-oriented handling qualities and PIO levels can be predicted using the Structural model of the human pilot.

In this pilot modeling approach, a Handling Qualities Sensitivity Function (HQSF)--defined as the magnitude of a transfer function obtained from the pilot model--is obtained. The magnitude is plotted on linear amplitude vs. frequency axes and compared with bounds delineating handling qualities Levels 1 - 3. The predicted handling qualities level is determined by the minimum level bound violated by the HQSF.

A similar plot involving the power spectral density of a proprioceptive signal in the pilot model is used to delineate predicted PIO levels. PIO "levels" are defined relative to a six-point PIO rating (PIOR) scale<sup>138</sup> with PIOR = 1 meaning no PIO tendencies and PIOR = 6 meaning very PIO prone.

It should be emphasized that once a suitable pilot model has been chosen for the nominal or undamaged vehicle, it is not altered when pilot/vehicle performance is predicted for the damaged vehicle. The design examples to be discussed next include these handling qualities and PIO assessments.

#### 4.5 Application Example: F-18/HARV Longitudinal SISO Model



The F-18 High Angle-of-Attack Research Vehicle (HARV) is a modified pre-production-model F-18 Hornet used by NASA Dryden Flight Research Center for high angle of attack studies. The aircraft completed 385 research flights during a three-phase program from 1978 to 1996. Key modifications included a multi-axis thrust vectoring system, advanced flight control laws, and movable strakes.<sup>141</sup> The only special feature utilized in the models which follow is the thrust vectoring system.

The linearized longitudinal short period approximation for the nominal F-18/HARV at the flight condition,  $M = 0.6$ ,  $h = 30\text{k ft}$ , straight and level, is given in state space as<sup>142</sup>

$$\begin{bmatrix} \dot{\alpha} \\ \dot{q} \end{bmatrix} = \begin{bmatrix} -0.5088 & 0.9940 \\ -1.1310 & -0.2804 \end{bmatrix} \begin{bmatrix} \alpha \\ q \end{bmatrix} + \begin{bmatrix} -0.9277 & -0.01787 \\ -6.575 & -1.525 \end{bmatrix} \begin{bmatrix} \delta_{\text{stab}} \\ \delta_{\text{TV}} \end{bmatrix} \quad (4.9)$$

where:  $\alpha \equiv$  angle of attack (deg),  $q \equiv$  pitch rate (deg/s),  $\delta_{\text{stab}} \equiv$  stabilator deflection (deg), and  $\delta_{\text{TV}} \equiv$  pitch thrust vector deflection (deg).

The failure for the longitudinal model of the F-18/HARV is defined as a 50% loss of stabilator area. This will be referred to as the plant failure. Later, actuator failures

will also be defined. An approximate state space representation of this failed system at the same flight condition can be given by

$$\begin{bmatrix} \dot{\alpha} \\ \dot{q} \end{bmatrix} = \begin{bmatrix} -0.48 & 0.997 \\ -0.39 & -0.182 \end{bmatrix} \begin{bmatrix} \alpha \\ q \end{bmatrix} + \begin{bmatrix} -0.4639 & -0.01787 \\ -3.2875 & -1.525 \end{bmatrix} \begin{bmatrix} \delta_{stab} \\ \delta_{TV} \end{bmatrix} \quad (4.10)$$

The healthy actuator dynamics and limits are given in Table 4-1

	Dynamics	Amplitude Limit	Rate Limit
<b>Stabilator</b>	$\frac{(30)^2}{(s^2 + 2 \cdot 0.707 \cdot 30s + 30^2)}$	$\pm 30$ deg	60 deg/s
<b>Pitch Thrust Vector</b>	$\frac{(20)^2}{(s^2 + 2 \cdot 0.6 \cdot 20s + 20^2)}$	$\pm 30$ deg	60 deg/s

**Table 4-1: F-18/HARV Longitudinal Actuator Dynamics and Limits**

A pitch rate tracking control system is desired. The next step in the design process is to define a reference model. For this application, the following reference model is chosen.<sup>40</sup>

$$G_r(s) = \frac{q_r}{q_c}(s) = \frac{100}{(s+5)(s+20)} \quad (4.11)$$

Next, the desired square system feedback architecture is defined. This is given in Figure 4-5. The inner loop is a pitch rate feedback loop which is controlled by the SMC. A pilot closes an outer loop to control the Euler pitch angle.

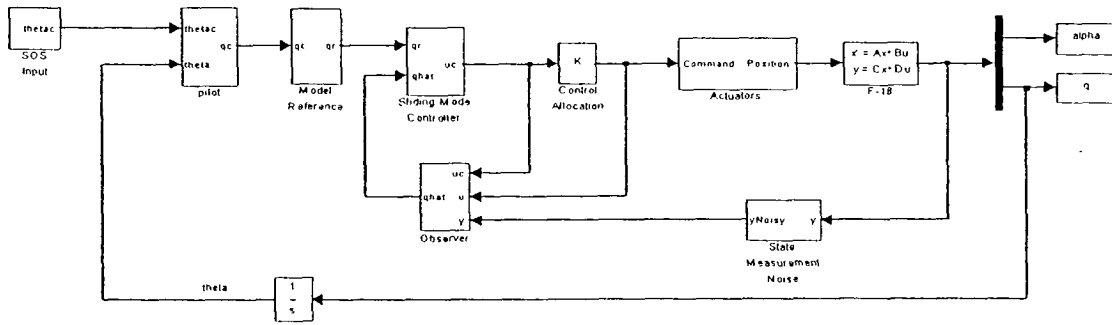


Figure 4-5: F-18/HARV Longitudinal System Block Diagram

The controller to be designed commands pitch rate. This demand is allocated to the two control effectors using an arbitrary ganging method. The control distribution matrix is defined as<sup>40</sup>

$$B_k = \begin{bmatrix} 1 \\ 1 \end{bmatrix} \quad (4.12)$$

The pitch-attitude command profile is a sum-of-sines profile which gives a random-like tracking task with frequencies representative of those encountered by a pilot<sup>143</sup>

$$\theta_c(t) = \xi \sum_{i=1}^7 A_i \sin(\omega_i t) \quad (4.13)$$

The overall amplitude gain is  $\xi = 5$ . The sum-of-sines parameters are given in Table 4-2. In addition, the pitch-attitude signal is introduced in exponential fashion by multiplying the sum-of-sines signal by a unit step passed through a filter of  $\frac{0.8}{s + 0.8}$ .

This results in a continuous, zero-mean, random-like signal with a zero initial condition.

$i$	$A_i$	$\omega_i$
1	-1.00	0.19947
2	1.00	0.49867
3	1.00	0.89760
4	0.50	1.39626
5	-0.20	2.39359
6	0.20	4.19970
7	-0.08	8.97598

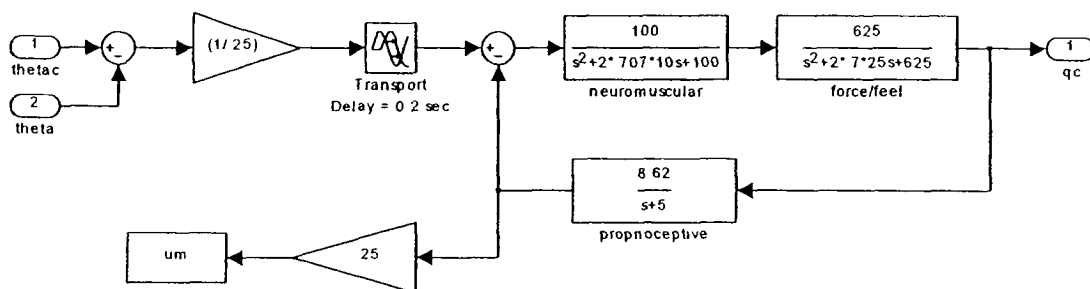
**Table 4-2: Sum-of-Sines Parameters**

The measured states are angle of attack,  $\alpha$ , and pitch rate,  $q$ . The state measurement noise for each channel is assumed to be band-limited white noise filtered by

$$\frac{100}{s^2 + 20s + 100}$$

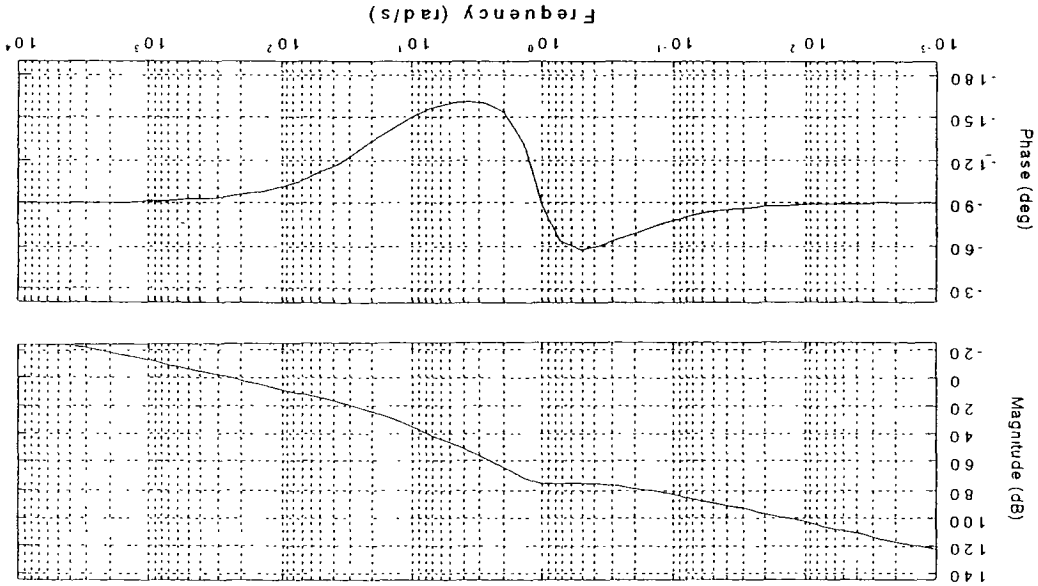
The RMS value of the noise is approximately 0.5 deg/s.

Assuming the inner loop SMC provides the desired model reference tracking, the apparent system model that the pilot “sees” is the model reference. Therefore, the pilot model,<sup>138,144,145</sup> based on the reference model given, is shown below.



**Figure 4-6: Pilot Model for F-18/HARV Pitch Angle Tracking Task**

Figure 4-7: q Loop Transmission of Compensator\*Plant, F-18/HARV



This gives one zero to place and a gain to set during the loop-shaping design. These values are chosen to be  $K_p = -30$ ,  $K_0 = 1$ , and  $K_{-1} = 20$ . The negative value of  $K_p$  is due to the sign convention of actuators. The resulting forward loop transmission of the

$$u^c(s) = K_p \left( \frac{s}{K_0 s + K_{-1}} \right) \quad (4.15)$$

form as

The control law, assuming the use of a boundary layer, then can be expressed in linear

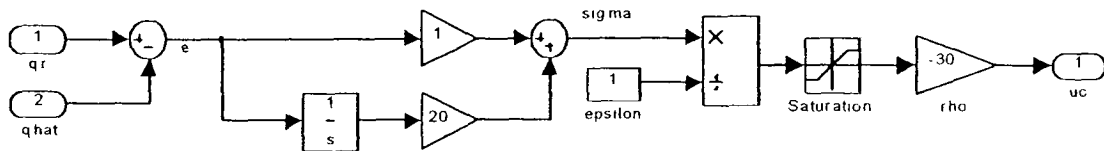
$$\sigma = K_0 e + K_{-1} \int e dt; \quad e = q_r - \hat{q} \quad (4.14)$$

of the sliding manifold is

actuators) has a relative order of 1 for the pitch rate output variable. Therefore, the form

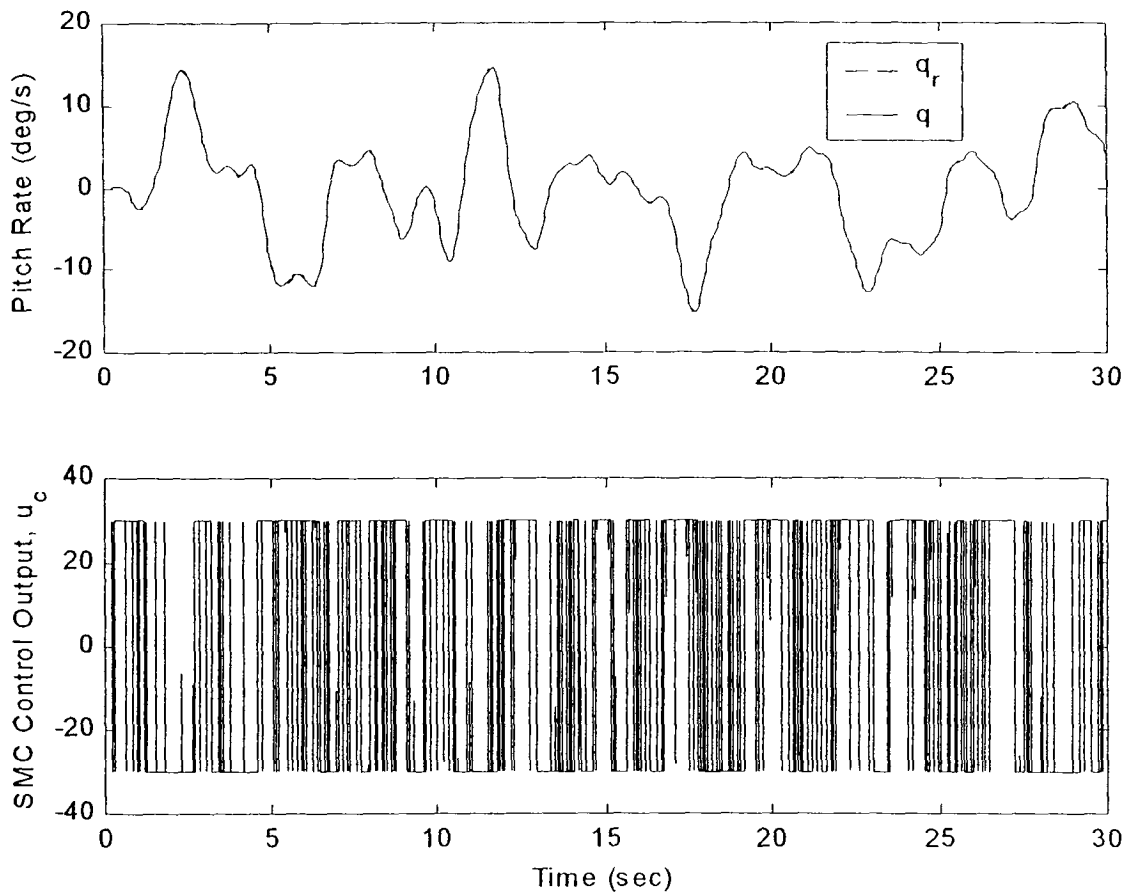
The next step is to define the desired sliding manifold. The system (without

compensator and plant with these values is shown in Figure 4-7. Note the desired  $\frac{K}{s}$  shape at crossover. The crossover frequency is about  $\omega = 250$  rad/s. The initial design of the SMC is complete and is shown in Figure 4-8.



**Figure 4-8: SMC Pitch Rate Controller for F-18/HARV**

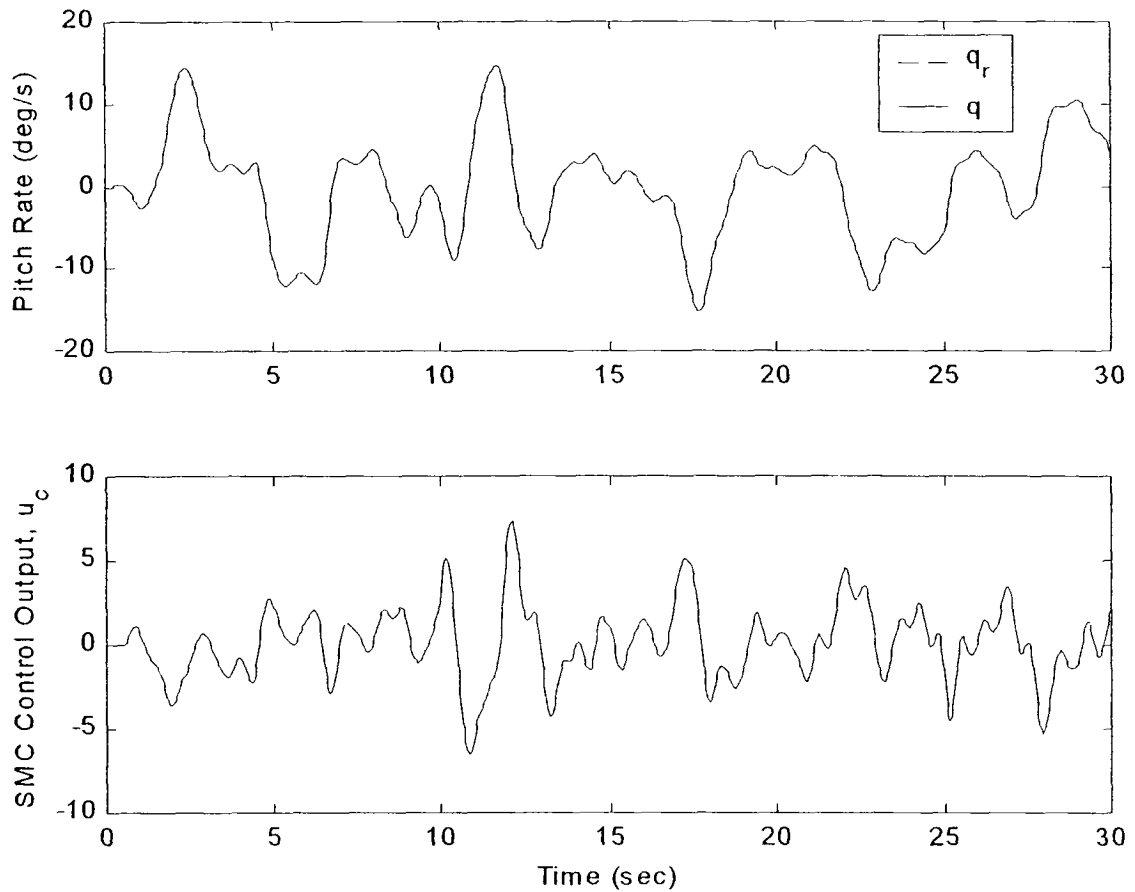
The fifth step in the design process is to verify that the SMC is working properly. Either replace the saturation element in Figure 4-8 with a signum function or make the boundary layer very small ( $\epsilon \approx 0.0001$ ). Figure 4-9 shows the time response for the inner loop pitch rate tracking of the SMC with a boundary layer of  $\epsilon = 0.0001$ . The Simulink<sup>®</sup> simulation is run with an ODE2 solver using a fixed time step of  $\Delta t = 0.0005$  sec. A system plant failure occurs at  $t = 10$  sec.



**Figure 4-9: F-18/HARV Inner Loop SMC Pitch Rate Tracking**

As expected, the SMC performs very well and is invariant to the system parameter changes. The control output shows the classic high frequency switching. Note, if a signum function was actually used, this plot would exhibit the expected near infinite frequency switching.

Next, the boundary layer is increased until a continuous control signal is achieved. For this model,  $\varepsilon = 0.1$  is the approximate minimum boundary layer thickness that will result in a continuous control signal. The resulting time history of the inner loop tracking (with a failure at  $t = 10$  sec) is shown in Figure 4-10.

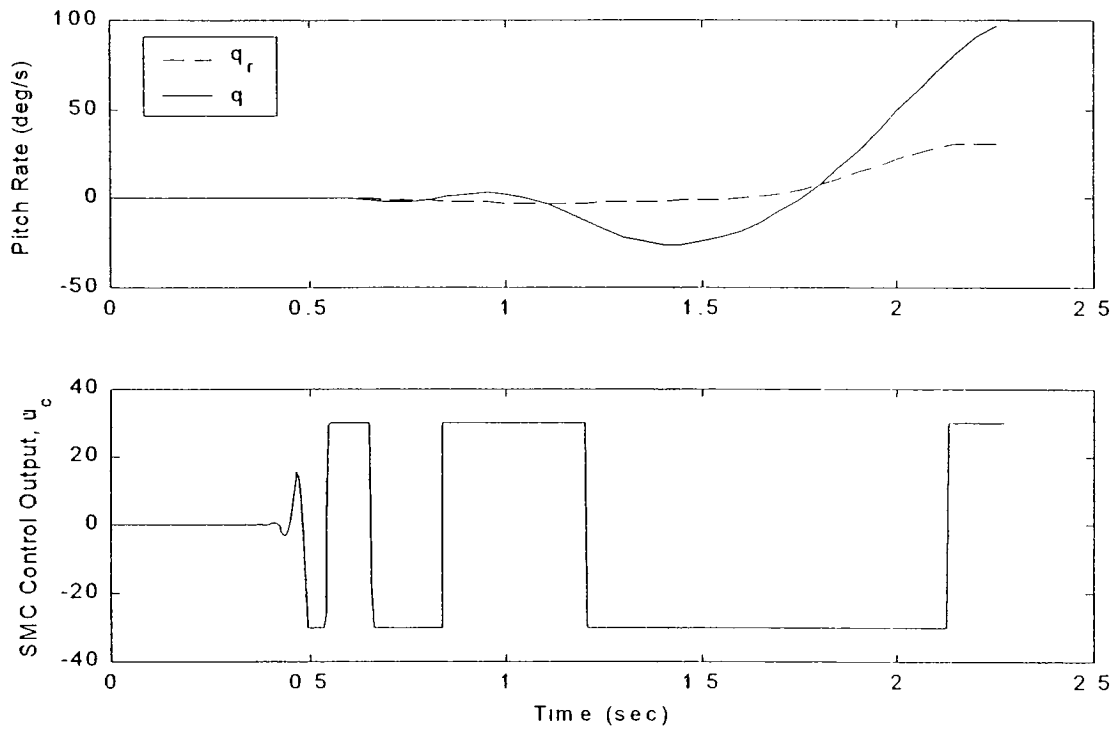


**Figure 4-10: F-18/HARV Inner Loop SMC Pitch Rate Tracking with Boundary Layer**

Although not apparent, the tracking performance is degraded slightly by increasing the boundary layer thickness. The performance is still excellent, even in the face of a large system failure. More importantly, the control signal is now continuous. During the design process, the boundary layer thickness,  $\epsilon$ , is varied without changing the SMC gain,  $\rho$ , which appears to be contrary to the guidance given in Section 4.3, Step 6 (of trying to maintain a constant  $K_p = \frac{\rho}{\epsilon}$ ) This is because the amplitude limits on the

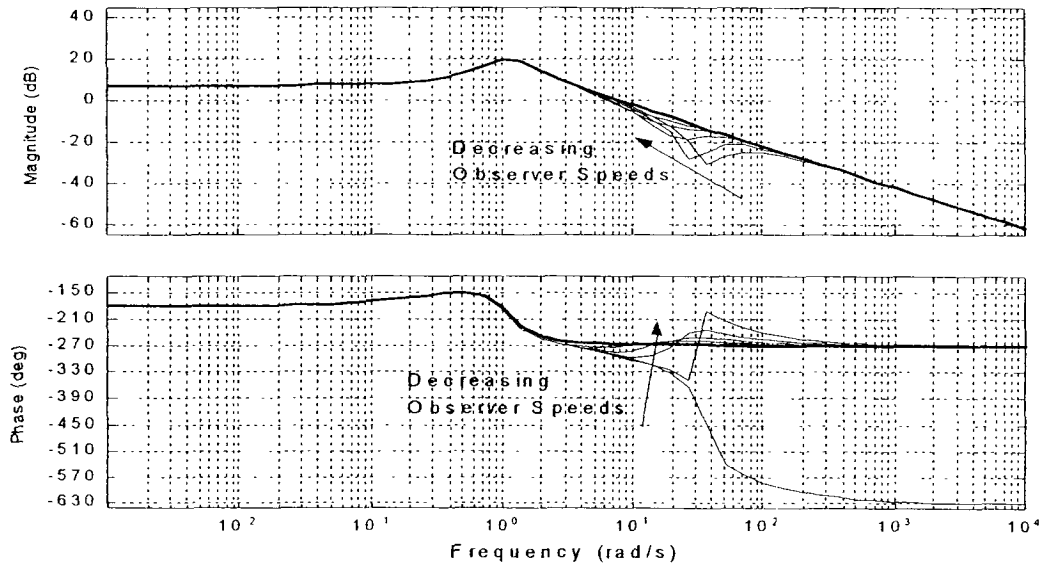
actuators are  $\pm 30$ . The magnitude of  $\rho$  should always be equal to or greater than the maximum expected actuator amplitude limit. Therefore, in this case,  $|\rho|$  can not be reduced below 30. In addition, as long as  $\varepsilon$  is less than 1, the transmission loop crossover will be at least as high as that designed for. Therefore, decreasing  $\varepsilon$  below 1 without varying  $\rho$  is usually acceptable. If  $\varepsilon$  is increased above 1,  $\rho$  should be increased accordingly to try to maintain an approximately constant  $K_p = \frac{\rho}{\varepsilon}$ . In practice, the easiest way to identify the minimum boundary layer thickness is to begin with  $\rho = K_p$  and  $\varepsilon = 1$ . Then decrease  $\varepsilon$  (leaving  $\rho$  alone) until the undesired switching begins. It is rare that  $\varepsilon$  needs to be greater than 1 for the nominal design.

The SMC design is now complete, the resulting tracking performance is remarkably good, and the system is (nearly) invariant to system parameter changes. The next step is the inclusion of the actuators. This is the point where sliding mode methods falter. Figure 4-11 shows the inner loop tracking results with the actuators now included. The system (without plant failure) goes unstable in less than a second.



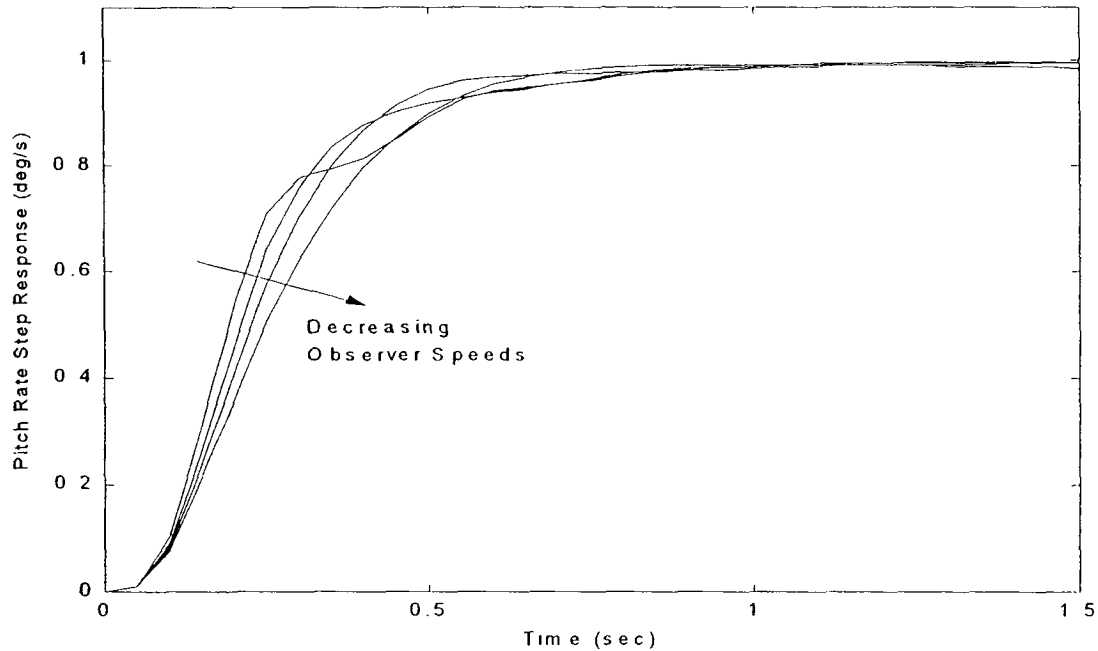
**Figure 4-11: F-18/HARV Inner Loop SMC Pitch Rate Tracking, Actuators Included**

The next steps are to design the observer and hedge models. As introduced in Section 3.3, the Bode plots of the equivalent plant/observer with unity feedback ( $\frac{\hat{q}}{u_c}$ ) are examined for varying observer speeds (with no hedging). Observer speeds of 100, 50, 20, 10, 5, and 1 rad/s are tried. The Bode plots are shown in Figure 4-12.



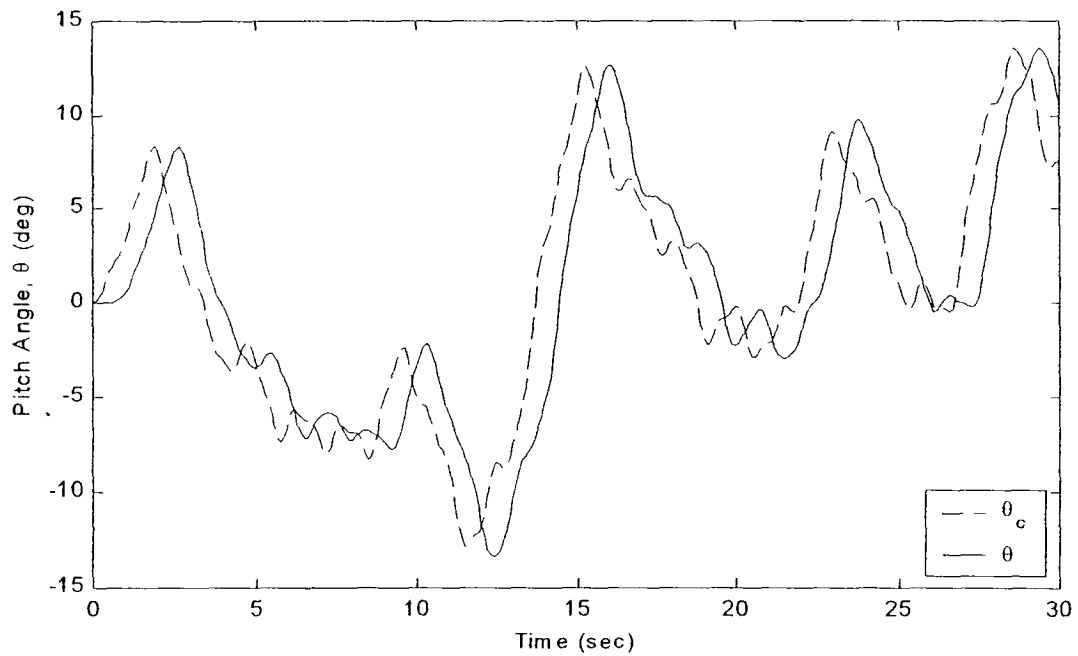
**Figure 4-12: Bode Plots, F-18/HARV Pitch Rate  $\frac{\hat{q}}{u_c}$ , Various Observer Speeds**

As shown on the Bode plots, observer speeds of 50 and 100 rad/s result in an unstable system. The unit step response for the inner loop with observer speeds of 20, 10, 5, and 1 rad/s are given in Figure 4-13. Based on the Bode plots and the unit step response plots alone, a good choice for the observer speed is between 5 and 10 rad/s.

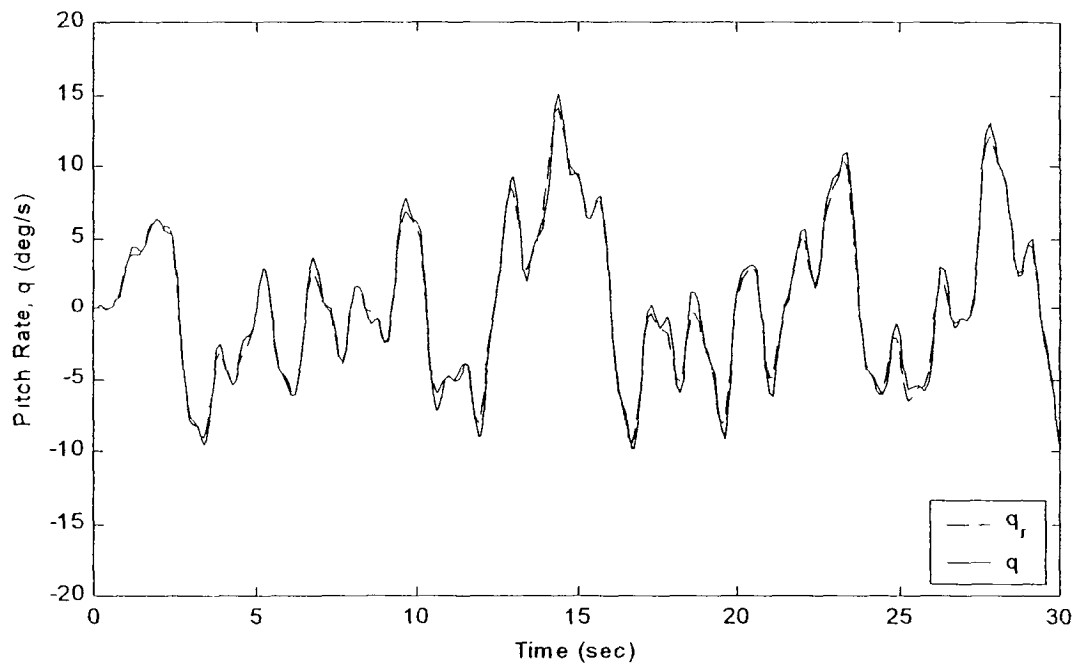


**Figure 4-13: Unit Step Response, F-18/HARV Pitch Rate, Various Observer Speeds**

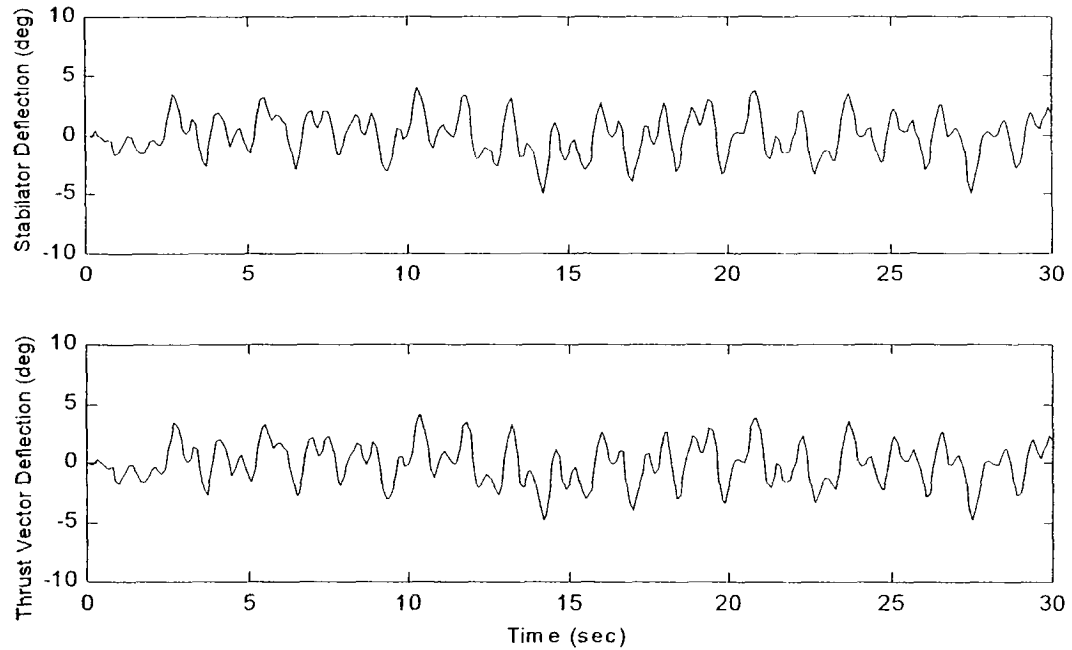
Observer poles of  $\lambda = -7, -8$  are selected, and the design (with no hedging) is complete. Now exercise the full system with measurement noise and the pilot in the loop. The outer loop pitch angle tracking performance for the nominal vehicle is shown in Figure 4-14. Performance is very good. The large time delay between the commanded pitch angle and the achieved pitch angle is almost entirely due to the pilot. Note in Figure 4-15 that the inner loop tracking is also very good. Of course, with the actuators and observer now included, the SMC does not give the almost perfect tracking achieved before. Figure 4-16 and Figure 4-17 show the actuator deflections and rates, respectively. No limits are hit. As shown in Figure 4-18 and Figure 4-19, Level I handling qualities are expected with no adverse PIO tendencies.



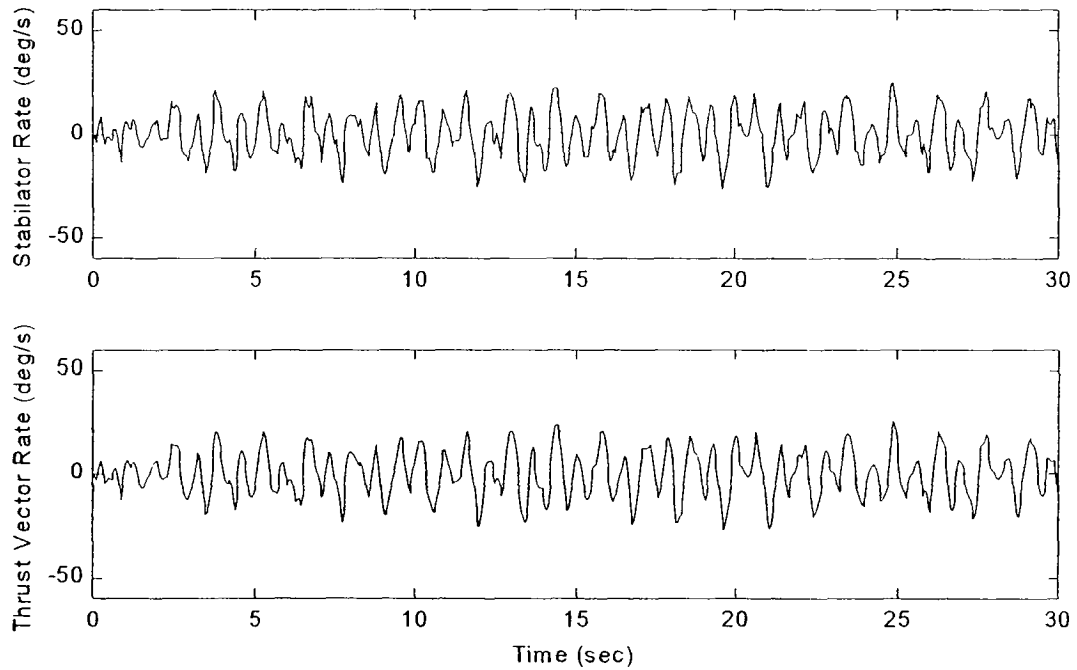
**Figure 4-14: Outer Loop Tracking, Nominal F-18/HARV, with Actuators, Observer, and Noise**



**Figure 4-15: Inner Loop Tracking, Nominal F-18/HARV, with Actuators, Observer, and Noise**



**Figure 4-16: Actuator Deflections, Nominal F-18/HARV, with Observer and Noise**



**Figure 4-17: Actuator Rates, Nominal F-18/HARV, with Observer and Noise**

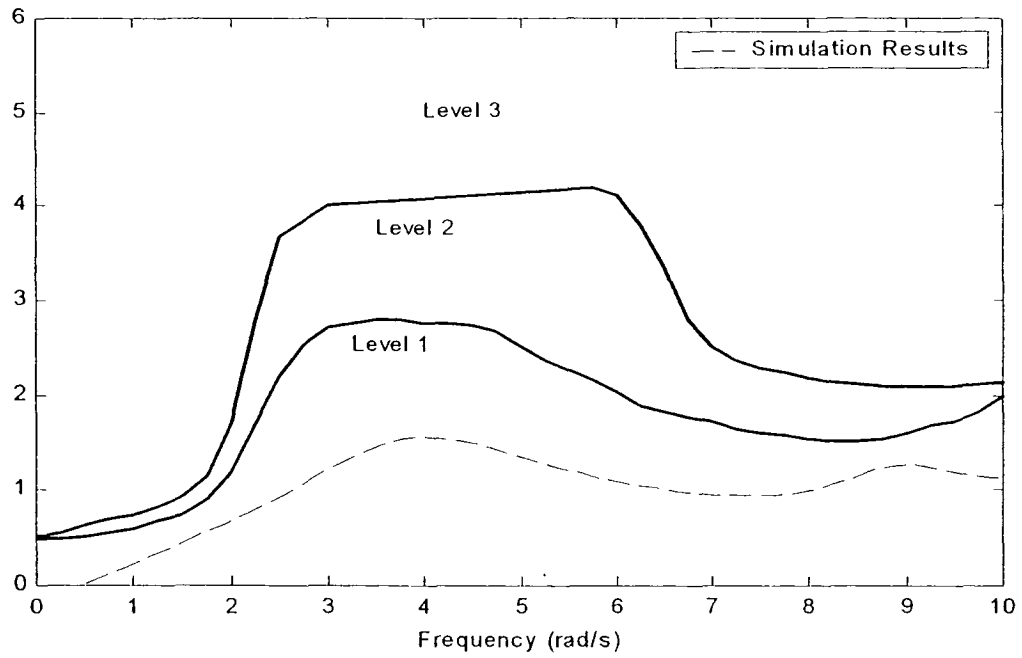


Figure 4-18: Nominal F-18/HARV Handling Qualities Assessment,  $\theta$  Tracking Task

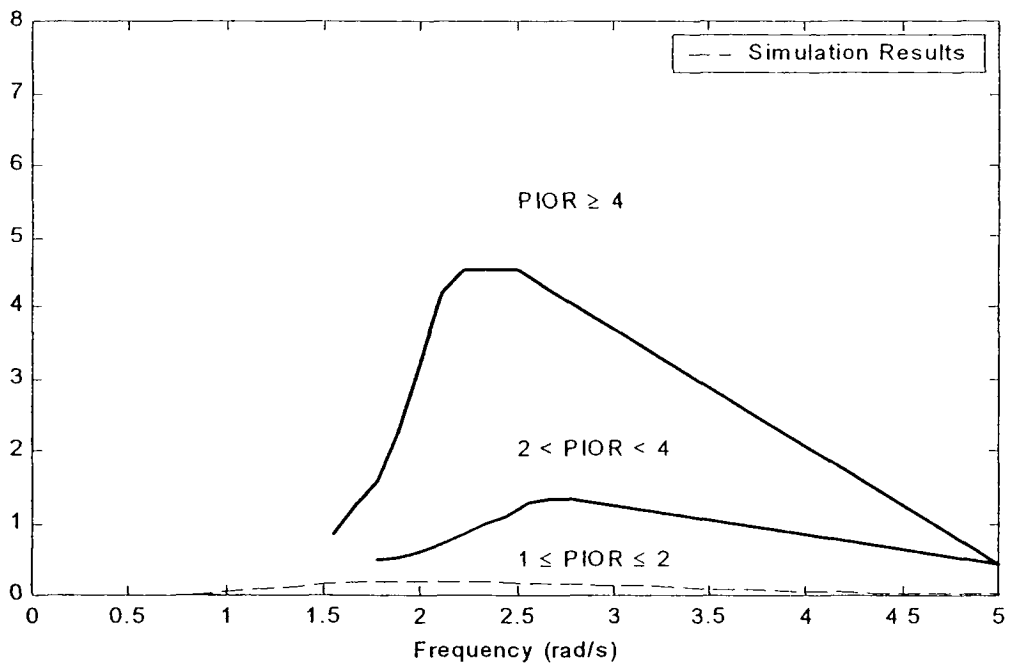
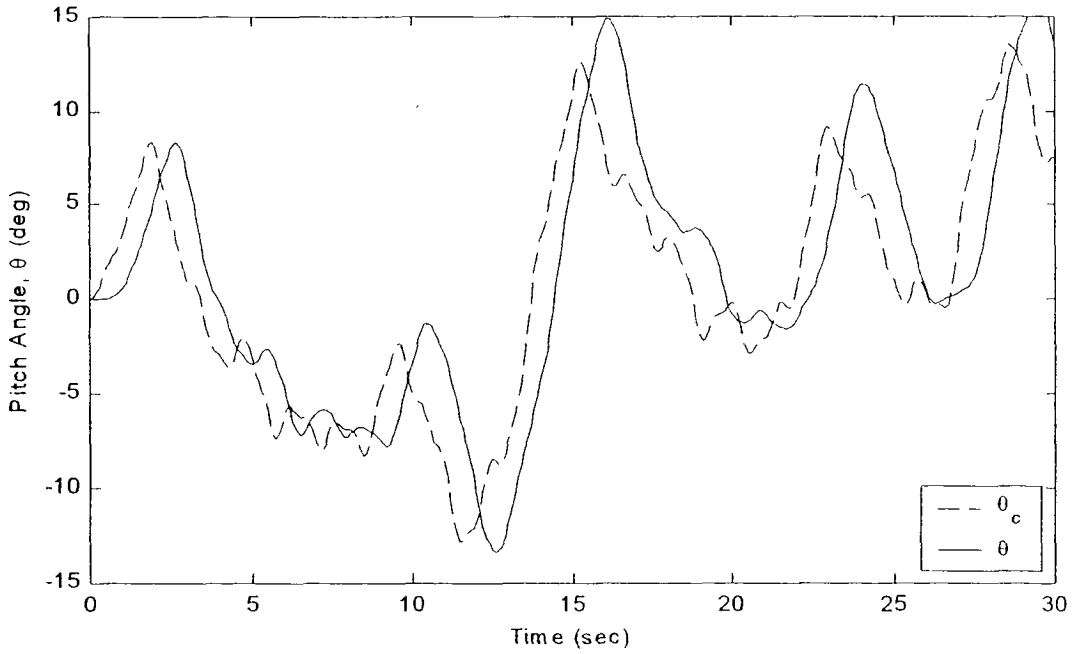


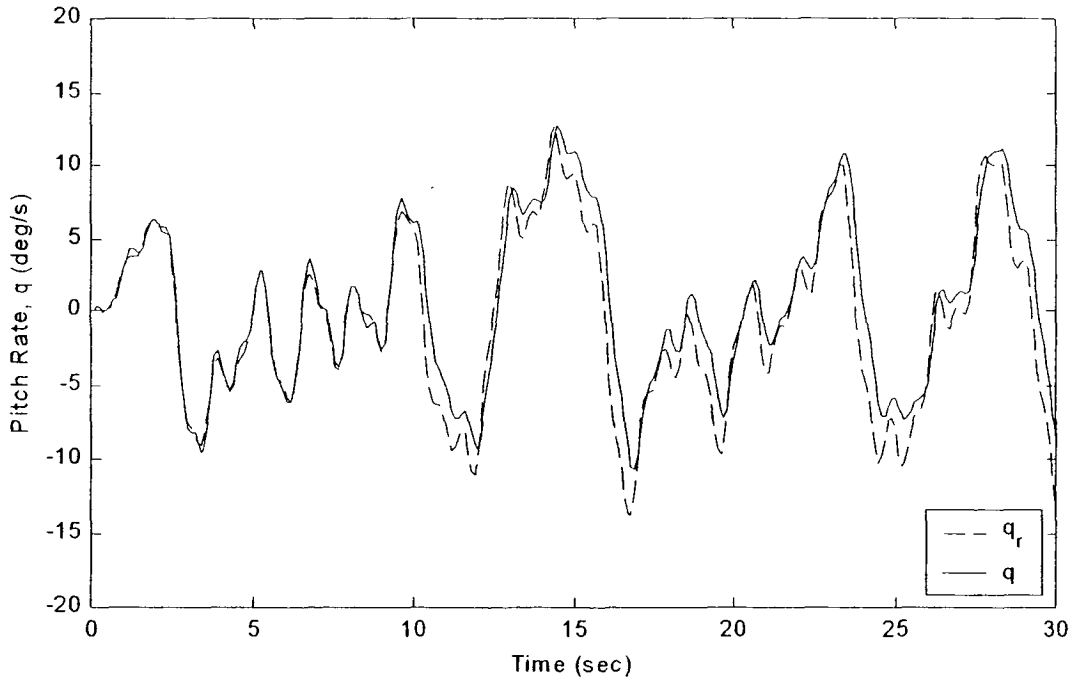
Figure 4-19: Nominal F-18/HARV PIO Assessment,  $\theta$  Tracking Task

Next, exercise this control system with a vehicle failure. The failure used in the following simulations is defined as a plant failure (50% loss of horizontal tail area) plus a thrust vector hard-over of  $\delta_{TV} = -3$  deg. Initially, the simulation starts with a healthy vehicle. Then, at  $t = 10$  sec, the system experiences a sudden “unknown” failure. No changes are made to the control law or observer after the failure.

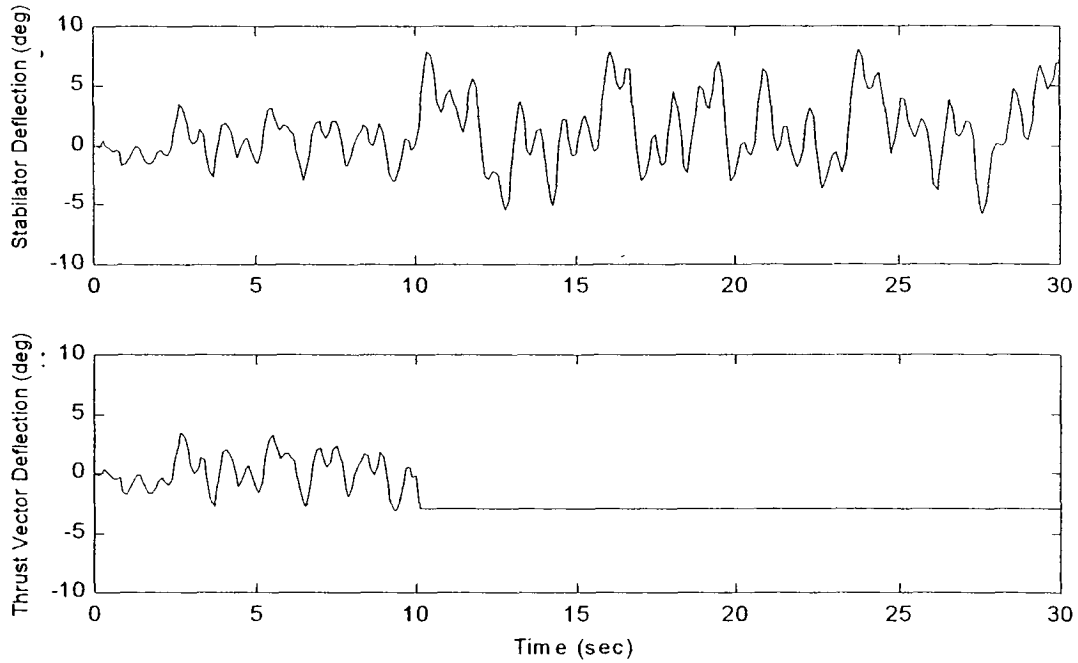
Figure 4-20 shows the outer loop pitch angle tracking performance. Figure 4-21 shows the inner loop pitch rate tracking performance. After the failure, the inner loop tracking is noticeably degraded, although it is still relatively good. The degradation of the inner loop performance results in degraded outer loop performance. Figure 4-22 and Figure 4-23 show the actuator deflections and rates. Note the stabilator is working much harder after the failure. Still no limits are reached. Even though the tracking performance is degraded, Figure 4-24 and Figure 4-25 predict Level II handling qualities (almost Level I) and no adverse PIO tendencies. This is actually remarkably good considering the severity of the failure.



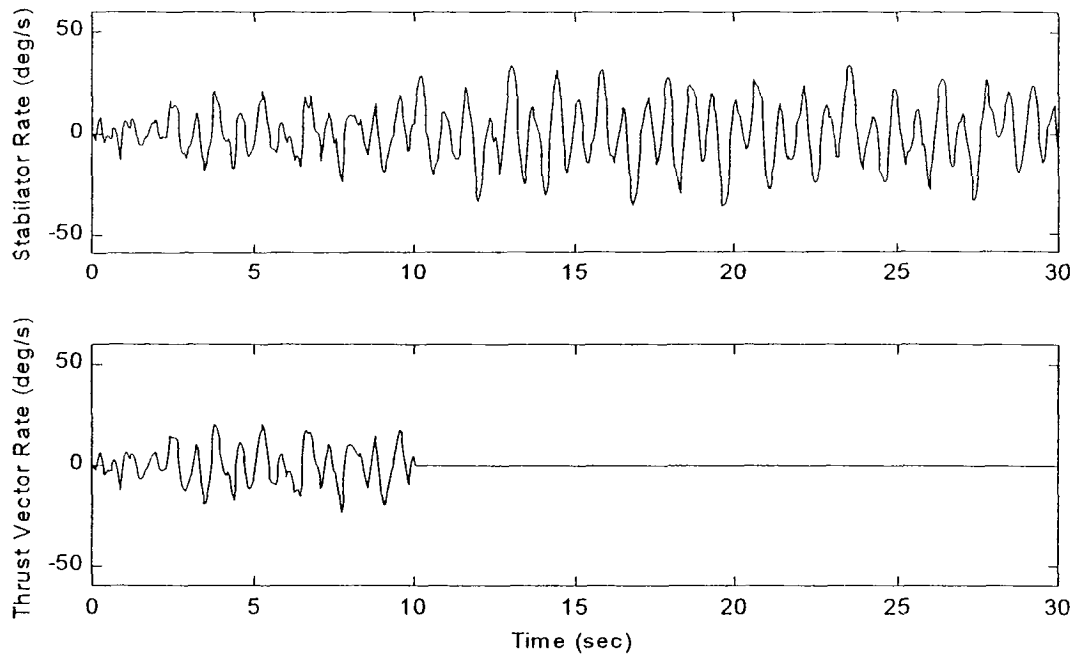
**Figure 4-20: Outer Loop Tracking ( $\theta$ ), F-18/HARV, with SMC, Actuators, Observer, and Noise, Failure at  $t = 10$  sec**



**Figure 4-21: Inner Loop Tracking ( $q$ ), F-18/HARV, with SMC, Actuators, Observer, and Noise, Failure at  $t = 10$  sec**



**Figure 4-22: Actuator Deflections, F-18/HARV, with SMC, Observer, and Noise, Failure at  $t = 10$  sec**



**Figure 4-23: Actuator Rates, F-18/HARV, with SMC, Actuators, Observer, and Noise, Failure at  $t = 10$  sec**

Figure 4-25: Failed F-18/HARV, PIO Assessment,  $\theta$  Tracking Task

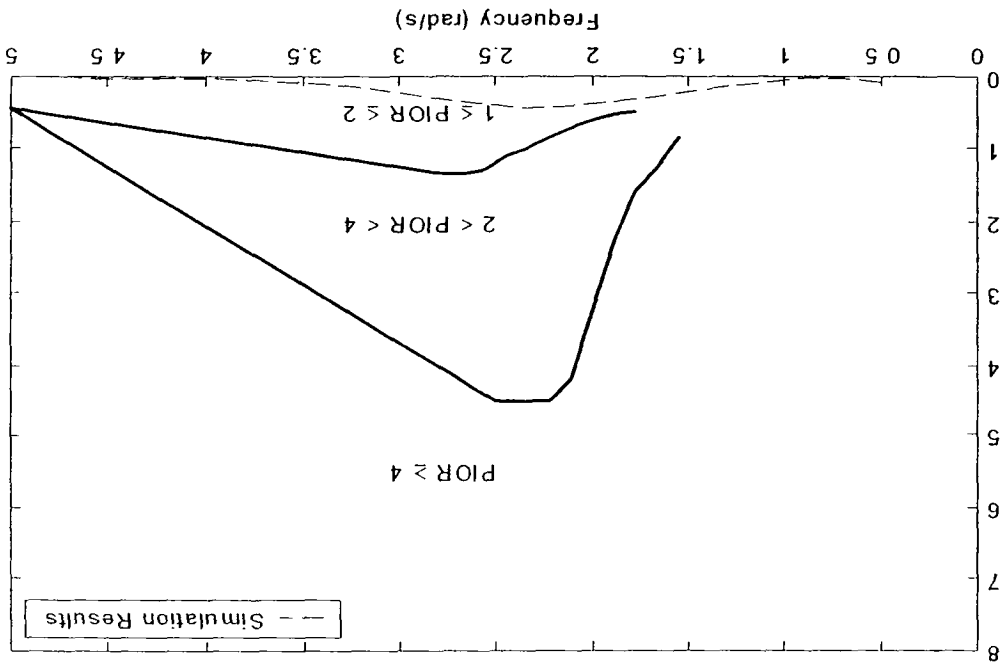
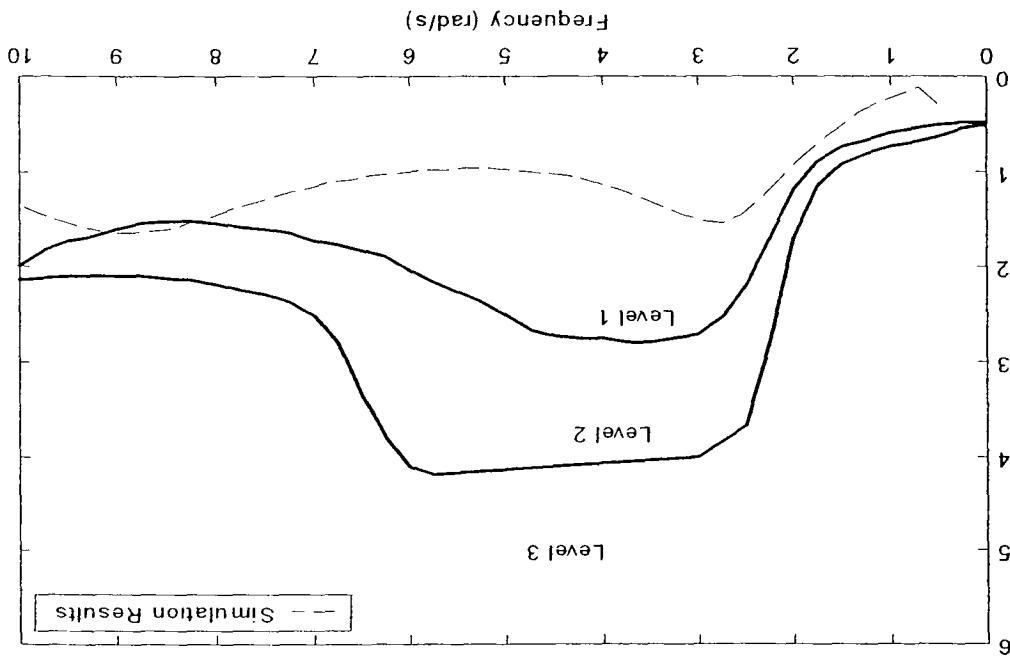


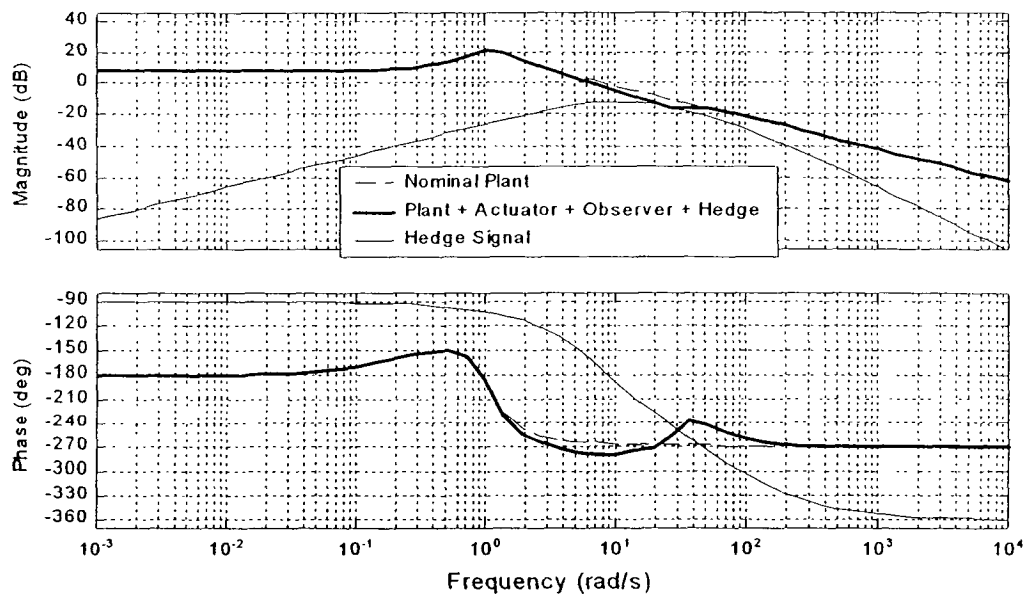
Figure 4-24: Failed F-18/HARV, Handling Qualities Assessment,  $\theta$  Tracking Task



As discussed earlier, the slow observer can result in noticeably reduced robustness to plant parameter changes. Therefore, the observer gains are increased to help deal with this failure. This, however, results in adverse interaction between the SMC and parasitic dynamics. With a fast observer, hedging is required. The methods described in Section 3.4 are used to redesign the observer speed and build the hedge model. The final values chosen are

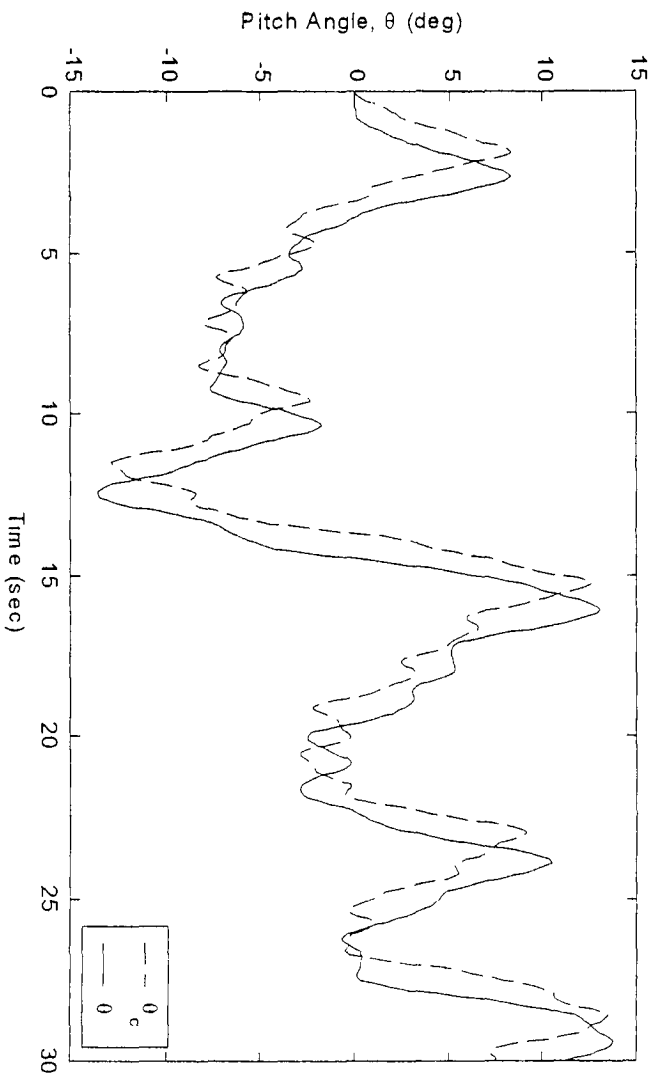
$$\text{Observer poles: } \lambda = -50, -51; \quad \text{Hedge model: } -5 \left( \frac{s}{s+100} \right) \left( \frac{100}{s^2 + 20s + 100} \right)$$

and the resulting design Bode plots are shown in Figure 4-26.

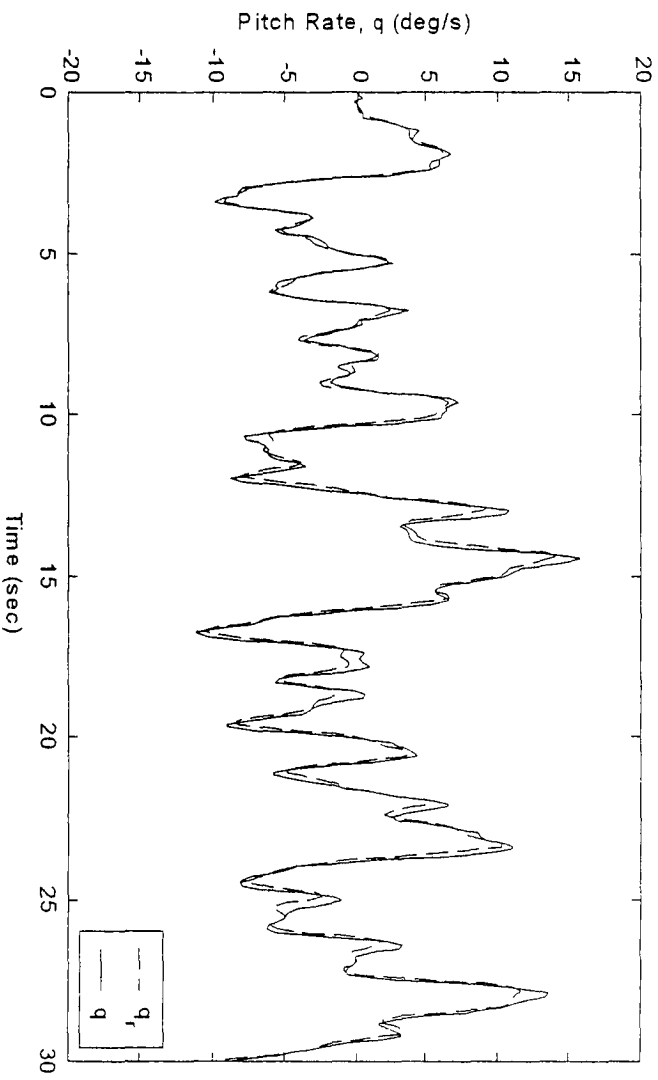


**Figure 4-26: Bode Plots  $\frac{\hat{q}_h}{u_c}$ , F-18/HARV Pitch Rate Observer & Hedge Design**

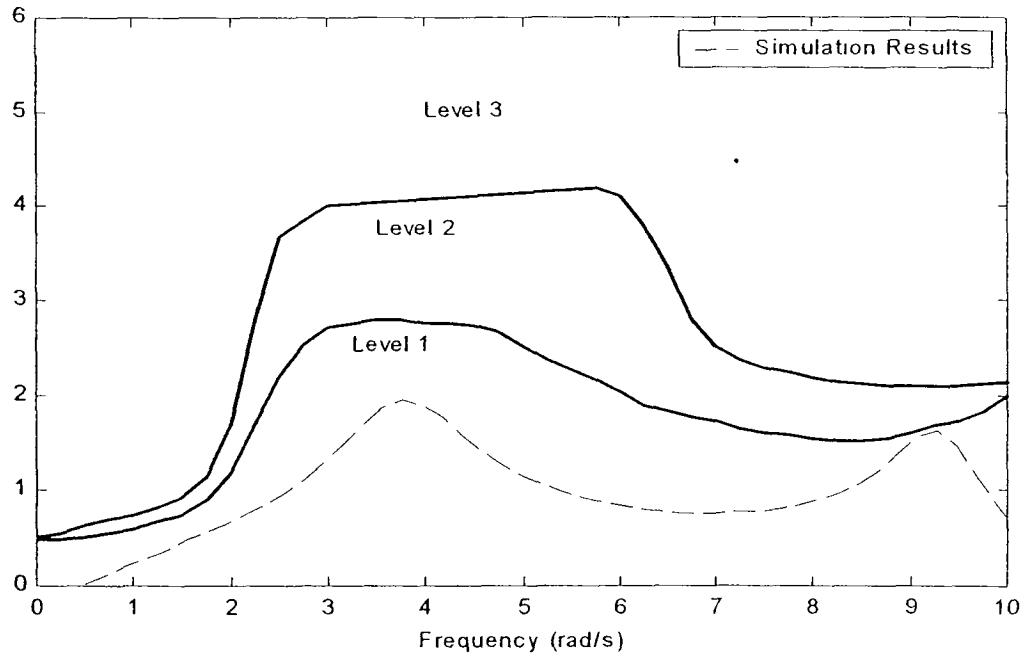
Figure 4-27 and Figure 4-28 show the tracking performance with this new design. Again the plant failure plus thrust vector hard-over occurs at  $t = 10$  sec. Figure 4-29 and Figure 4-30 show the handling qualities and PIO bounds for the failed system.



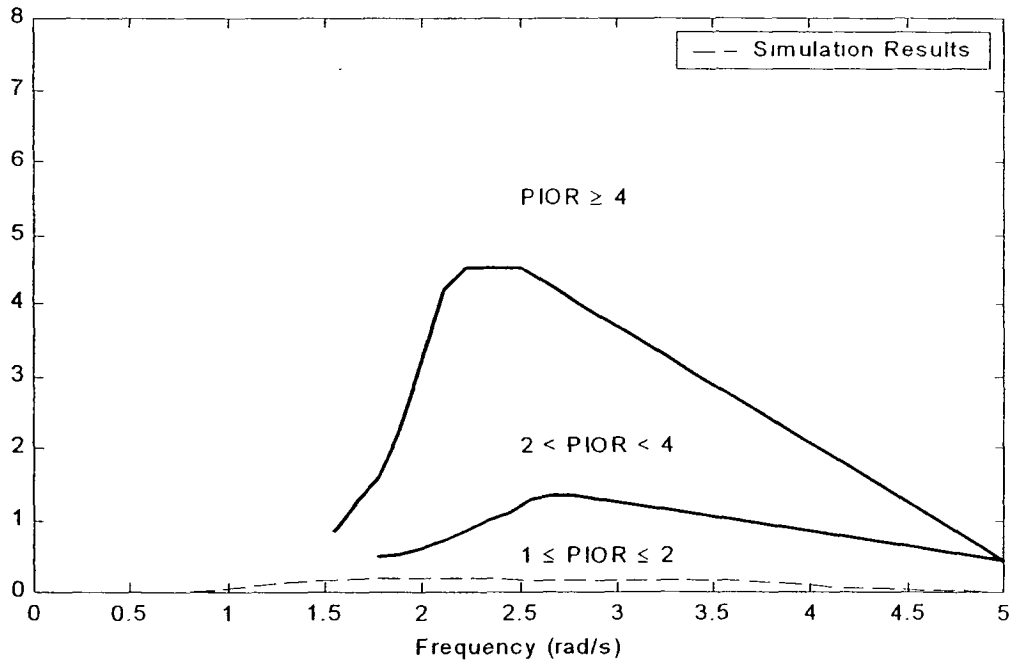
**Figure 4-27: Outer Loop Tracking, F-18/HARV, with SMC, Actuators, Observer, Hedging, and Noise, Failure at  $t = 10$  sec**



**Figure 4-28: Inner Loop Tracking, F-18/HARV, with SMC, Actuators, Observer, Hedging, and Noise, Failure at  $t = 10$  sec**



**Figure 4-29: Failed F-18/HARV, Handling Qualities Assessment,  $\theta$  Tracking Task, With Hedging**



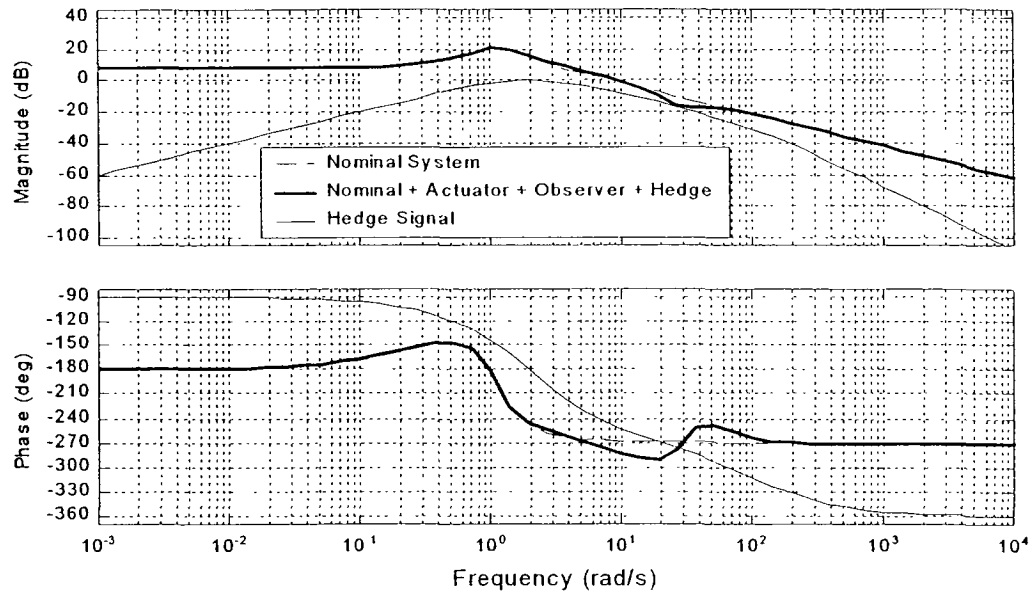
**Figure 4-30: Failed F-18/HARV, PIO Assessment,  $\theta$  Tracking Task, With Hedging**

This design, with the faster observer and hedge model included is clearly superior to the slow observer design for this particular failure. With this design and failure, tracking is almost as good as the nominal case, and Level I handling qualities are predicted.

As seen in Figure 4-26, the hedge model for this system is designed to work well with the known linear actuators. The portion of the hedge signal on the Bode magnitude plot which needs to have the  $-20$  dB/dec slope is fairly narrow—just enough to remove the effects of the actuators. Unfortunately, if the actuator dynamics slow down (by changing bandwidth or by reaching rate limits), or if a pure time delay is introduced, the hedge model shown above will not be able to stabilize the system. A slower observer will help with robustness to changes in actuator dynamics but will result in lower robustness to system parameter changes. Therefore, a compromise is sought. Consider slowing down the observer to reduce the amount of hedging needed and also changing the hedge signal loop shape. Create a hedge signal loop shape with a broader region of  $-20$  dB/dec slope. Since slower actuator dynamics are of concern (not faster), extend the region of  $-20$  dB/dec slope toward lower frequencies. For example, consider the following observer and hedge systems.

$$\text{Observer poles: } \lambda = -40, -41; \quad \text{Hedge model: } -100 \left( \frac{s}{s+100} \right) \left( \frac{4}{s^2 + 4s + 4} \right)$$

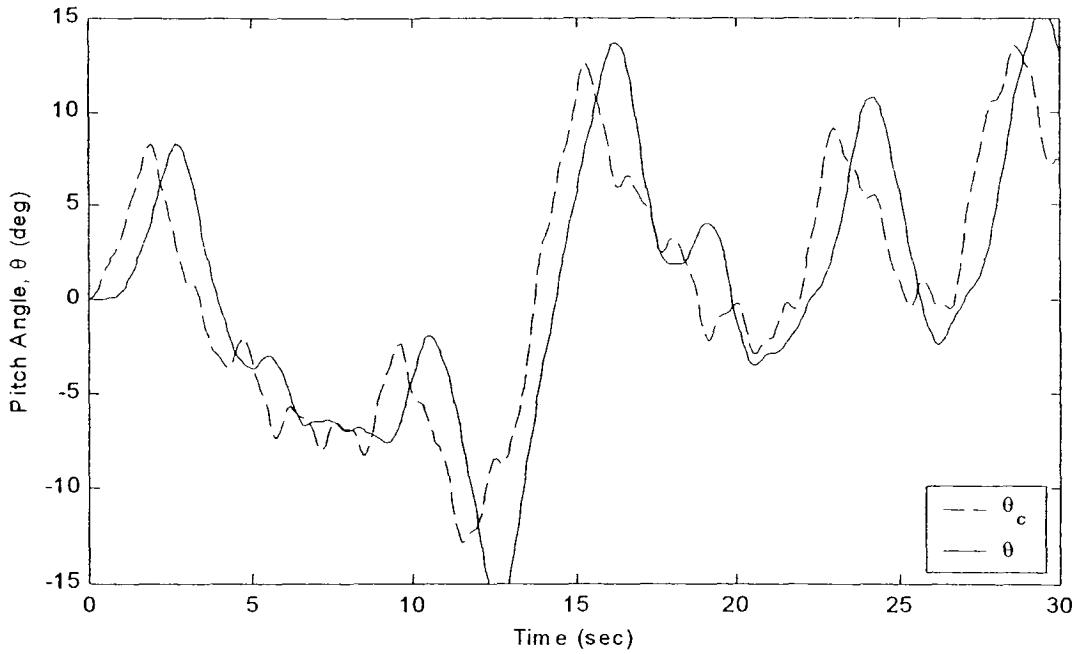
The resulting design Bode plots are shown in Figure 4-31. As seen in Figure 4-31, the effects of the actuator dynamics are not removed as well as they are in the previous design. The hedge gain could be increased to help remove the distortion in the Bode magnitude plot; however, since the hedge loop shape has such a broad region



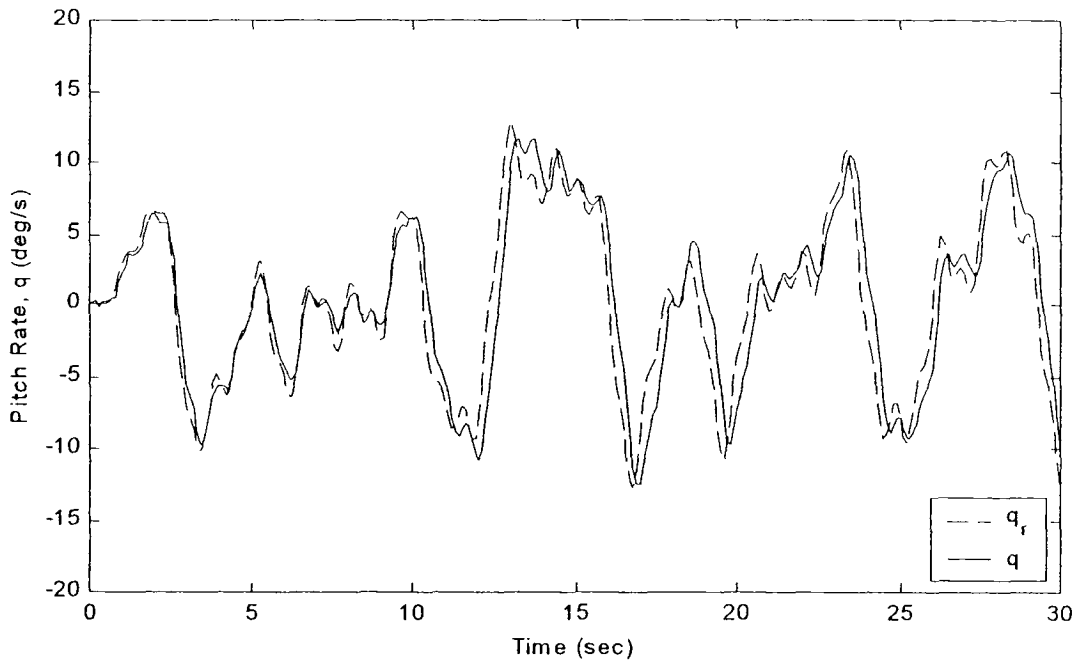
**Figure 4-31: Bode Plots  $\frac{\hat{q}_h}{u_c}$ , F-18/HARV Modified Observer & Hedge Design**

of -20 dB/dec slope, any more increase in hedge gain will cause the low frequency portion of the  $\frac{\hat{q}_h}{u_c}(s)$  Bode magnitude plot to move above the desired nominal plot. This results in unacceptable overshoot in the nominal case. Overall, this design appears to be a reasonable compromise. The nominal case with this new design has very slightly degraded performance and still has Level I handling qualities.

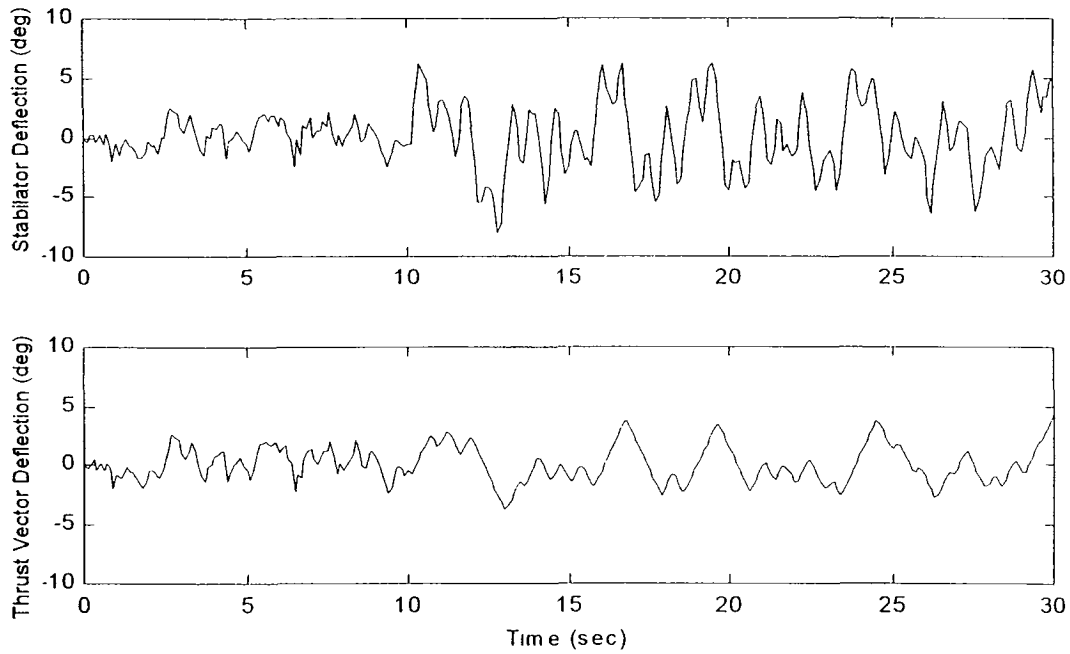
Consider a new failure condition (Failure #2) as follows: failed plant; stabilator rate limit = 30 deg/s; thrust vector rate limit = 6 deg/s; thrust vector bandwidth = 10 rad/s; and a 50 ms time delay in both actuators. The simulation results with a failure at  $t = 10$  sec follow.



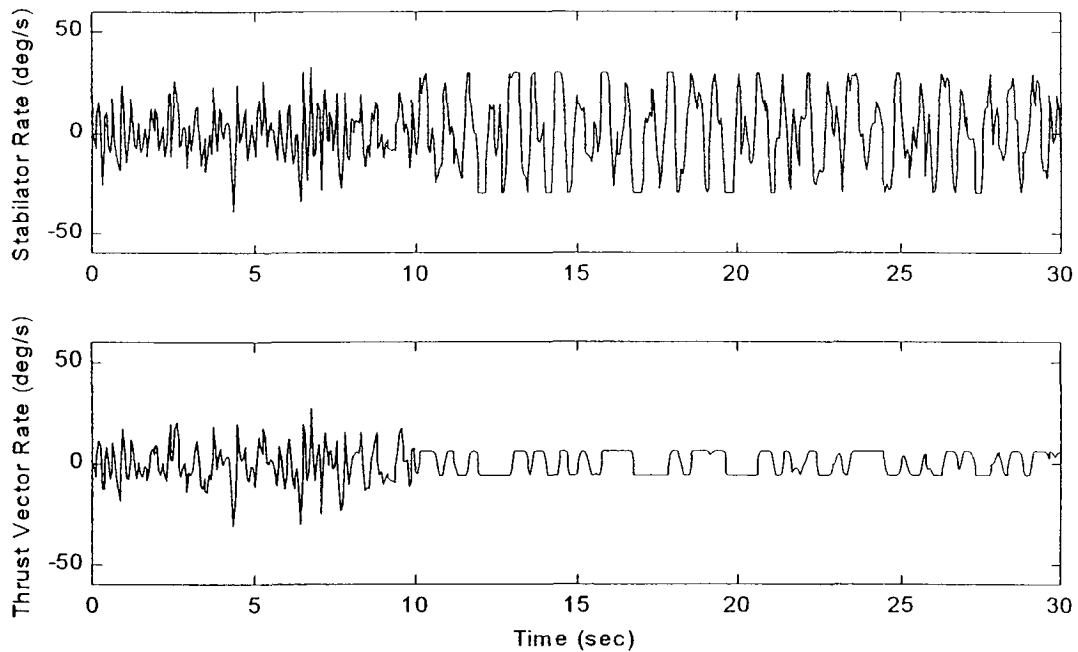
**Figure 4-32: Outer Loop Tracking, Failed F-18/HARV, with SMC, Actuators, Observer, Hedging, and Noise, (Failure #2)**



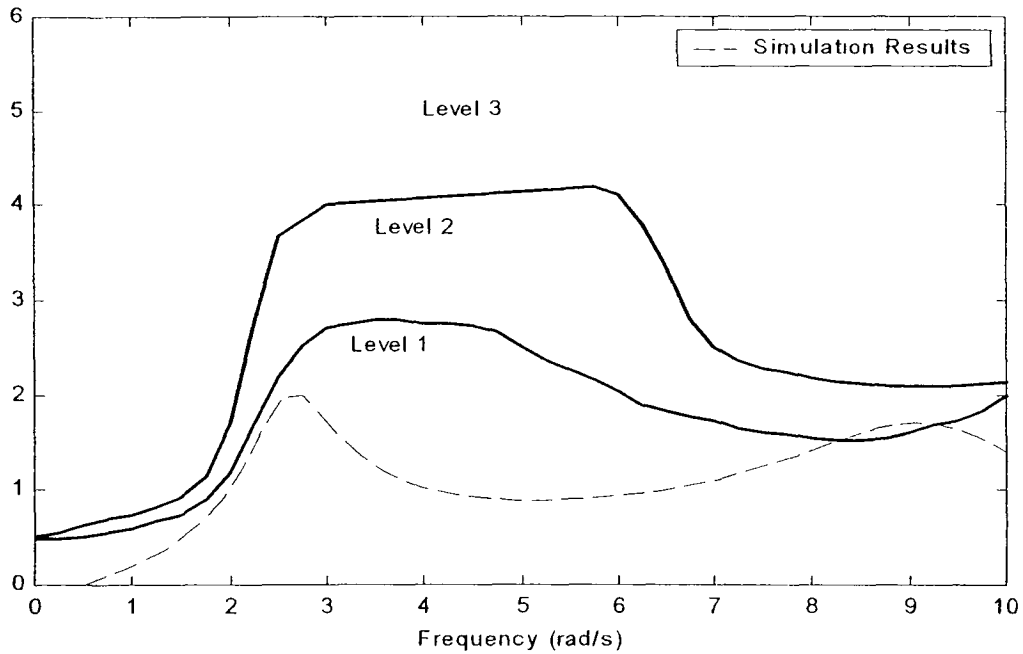
**Figure 4-33: Inner Loop Tracking, Failed F-18/HARV, with SMC, Actuators, Observer, Hedging, and Noise, (Failure #2)**



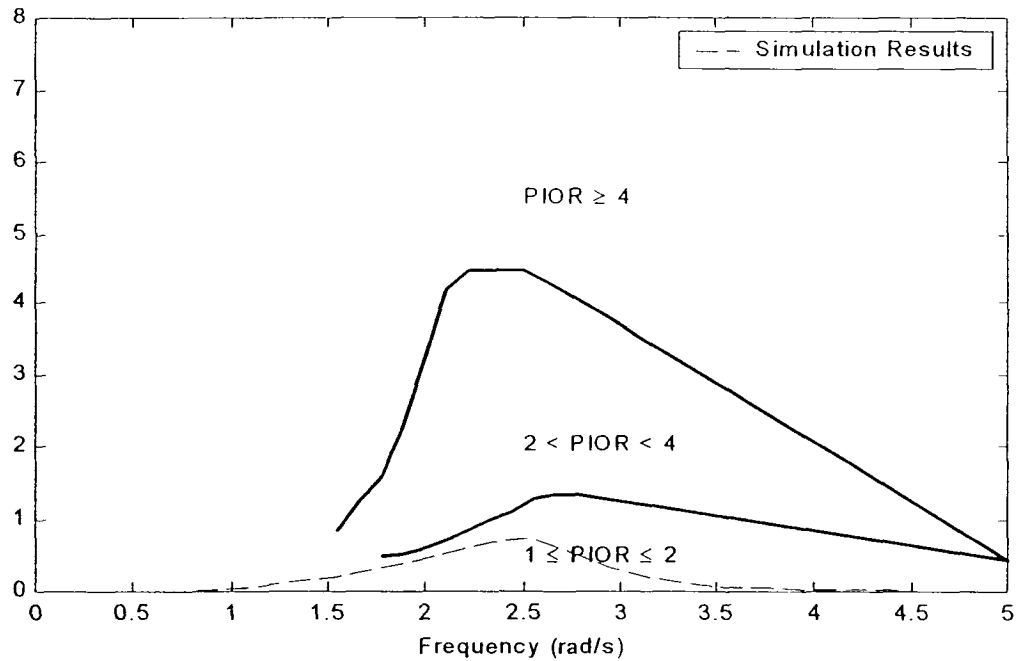
**Figure 4-34: Actuator Deflections, Failed F-18/HARV, with SMC, Observer, Hedging, and Noise, (Failure #2)**



**Figure 4-35: Actuator Rates, Failed F-18/HARV, with SMC, Observer, Hedging, and Noise, (Failure #2)**



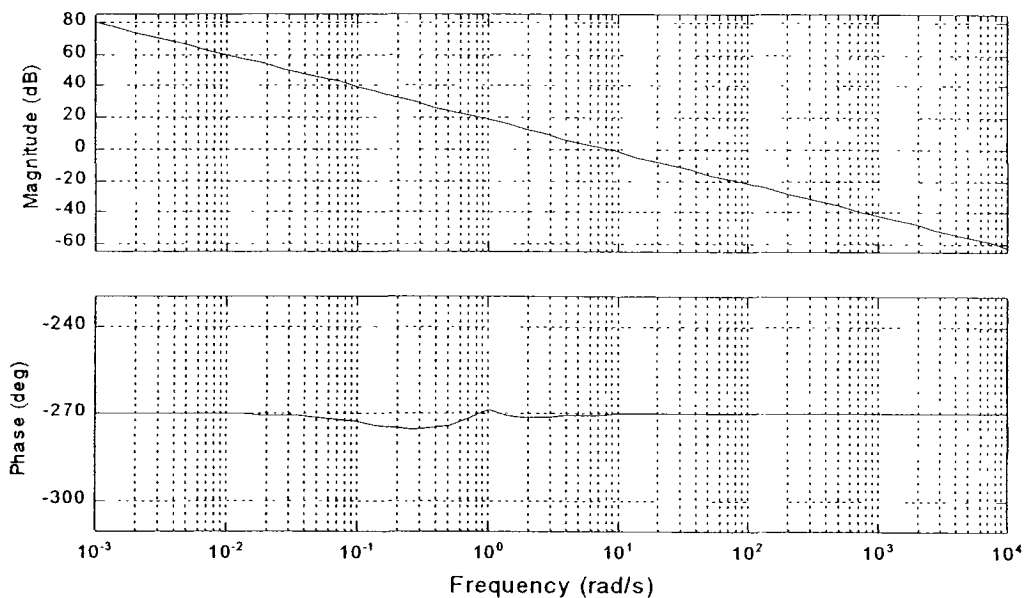
**Figure 4-36: Failed F-18/HARV Handling Qualities Assessment,  $\theta$  Tracking Task, With Hedging (Failure #2)**



**Figure 4-37: Failed F-18/HARV PIO Assessment,  $\theta$  Tracking Task, With Hedging (Failure #2)**

Several points are worth noting. The tracking performance is degraded after the failure, but the system remains stable. In fact, Level II handling qualities (almost Level I) are predicted. This is very encouraging considering the severity of the failure and the fact that the thrust vector is in almost constant rate saturation and the stabilator hits its reduced rate limits.

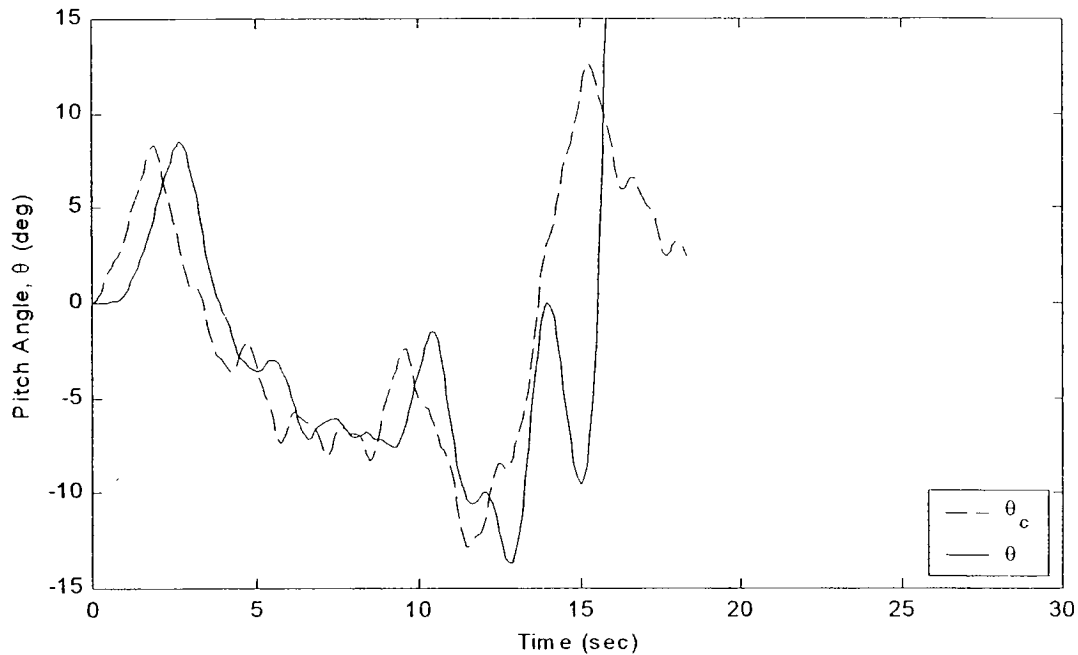
For comparison, consider a loop shaped design. Using classic loop shaping techniques, a controller is designed:  $G_c = -2.5 \left( \frac{s^2 + 0.8s + 1.2}{s(s + 0.3)} \right)$ . The resulting forward loop transmission,  $G_c(s)P(s)$ , with no actuators is given in Figure 4-38.



**Figure 4-38: Bode Plots, F-18/HARV Pitch Rate Loop Transmission for Loop Shaped Design**

As expected, this results in excellent tracking and Level I handling qualities for the nominal case. These plots are not given here, but they are essentially the same as the

SMC design results. This design is remarkably robust. In fact, for Failure #1, this loop shaped design does almost as well as the SMC design. However, this design can not handle Failure #2 as illustrated in Figure 4-39. Failure occurs at  $t = 10$  sec.

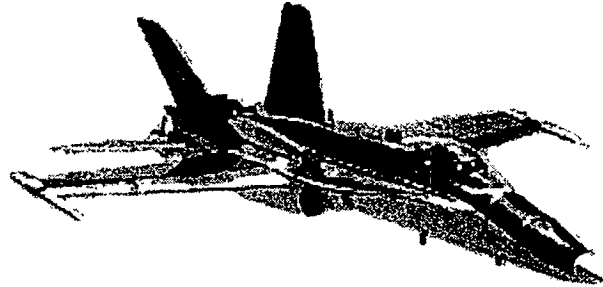


**Figure 4-39: Outer Loop Tracking ( $\theta$ ) for Loop-Shaped Controller, Failed F-18/HARV, with Actuators and Noise, (Failure #2)**

In conclusion, an SMC controller is designed for a SISO system with limited bandwidth actuators and is found to be superior to a classically designed system for a class of failures. Design tradeoffs are made in the observer and hedge models which help make the system more robust to different types of failures. Next, a basic MIMO system design is demonstrated

#### 4.6 Application Example: F-18/HARV Lat-Dir MIMO Model

The linearized lateral directional (Lat-Dir) state space model for the F-18/HARV<sup>142</sup> at the flight condition,  $M = 0.2$ ,  $h = 10\text{k ft}$ , straight and level,  $\alpha_{trim} = 29.7\text{ deg}$ , is given in Eqn.



(4.16). Note this low speed, high angle of attack, flight condition is a very demanding flight condition with extreme yaw/roll coupling.

$$\begin{bmatrix} \dot{\beta} \\ \dot{p} \\ \dot{r} \end{bmatrix} = \begin{bmatrix} -0.05904 & 0.4959 & -0.8703 \\ -5.513 & -0.9391 & 0.6655 \\ 0.06838 & 0.02632 & -0.1038 \end{bmatrix} \begin{bmatrix} \beta \\ p \\ r \end{bmatrix} + \begin{bmatrix} 0.005629 & 0.005764 & 0.003685 & 0 & 0.0904 \\ 1.879 & 1.328 & 0.02922 & 0.6754 & 0.217 \\ -0.1092 & -0.09645 & -0.08404 & 0.006811 & -2.974 \end{bmatrix} \begin{bmatrix} \delta_{DT} \\ \delta_{AI} \\ \delta_{RU} \\ \delta_{RTV} \\ \delta_{YTV} \end{bmatrix} \quad (4.16)$$

where

$\beta \equiv$  sideslip angle (deg),  $p \equiv$  roll rate (deg/s),  $r \equiv$  yaw rate (deg/s),  $\delta_{DT} \equiv$  differential tail deflection (deg),  $\delta_{AI} \equiv$  aileron deflection (deg),  $\delta_{RU} \equiv$  rudder deflection (deg),  $\delta_{RTV} \equiv$  roll thrust vector deflection (deg), and  $\delta_{YTV} \equiv$  yaw thrust vector deflection (deg).

The failure for the lateral-directional model of the F-18/HARV is defined as:

$$\begin{aligned} \mathbf{A}_{\text{fail}} &= 2.0 \mathbf{A} \\ \mathbf{B}_{\text{fail}} &= 0.75 \mathbf{B} \end{aligned} \quad (4.17)$$

where  $\mathbf{A}$  is the state plant matrix and  $\mathbf{B}$  is the control power matrix in Eqn (4.16).

This will be referred to as the plant failure. Later, actuator failures will also be defined.

This failure is not intended to represent an actual physical failure. It simply gives a 100% change in the system A-matrix and a 25% reduction in all actuator control power derivatives.

The healthy actuator dynamics and limits are given below.<sup>142</sup>

	Dynamics	Amplitude Limit	Rate Limit
Differential Tail	$\frac{(30)^2}{(s^2 + 2 \cdot 0.707 \cdot 30s + 30^2)}$	$\pm 17.5$ deg	60 deg/s
Aileron	$\frac{(75)^2}{(s^2 + 2 \cdot 0.6 \cdot 75s + 75^2)}$	$\pm 27.5$ deg	100 deg/s
Rudder	$\frac{(72)^2}{(s^2 + 2 \cdot 0.69 \cdot 72s + 72^2)}$	$\pm 30$ deg	100 deg/s
Roll Thrust Vector	$\frac{(20)^2}{(s^2 + 2 \cdot 0.6 \cdot 20s + 20^2)}$	$\pm 30$ deg	60 deg/s
Yaw Thrust Vector	$\frac{(20)^2}{(s^2 + 2 \cdot 0.6 \cdot 20s + 20^2)}$	$\pm 30$ deg	60 deg/s

**Table 4-3: F-18/HARV Lat/Dir Actuator Dynamics and Limits**

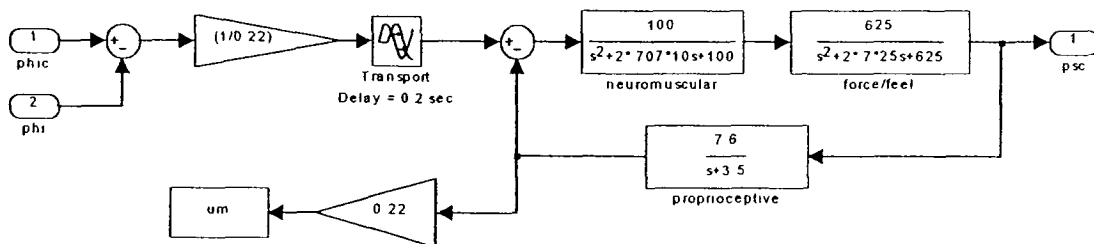


$$\mathbf{B}_k = \begin{bmatrix} 0 & 0.6 \\ 0 & 1 \\ 1 & 0 \\ 0 & 0.6 \\ 0.6 & 0 \end{bmatrix} \quad (4.19)$$

The input command profile for roll angle is a sum-of-sines function defined in Eqn. (4.13). The sum-of-sines parameters are those given in Table 4-2, and the overall amplitude gain in Eqn. (4.13) is  $\xi = 6$ .

The measured states are sideslip,  $\beta$ ; roll rate,  $p$ ; and yaw rate,  $r$ . The state measurement noise for each channel is assumed to be band-limited white noise filtered by  $\frac{100}{s^2 + 20s + 100}$  and multiplied by a gain. Roll and yaw rate noise have a gain of 0.1414, resulting in an RMS noise value of approximately 0.07 deg/s. The sideslip noise has a gain of 0.0707, resulting in an RMS noise value of approximately 0.035 deg.

Assuming the inner loop SMC provides the desired model reference tracking, the apparent system model that the pilot “sees” is the model reference. Therefore, the pilot model,<sup>138,144,145</sup> based on the reference model given, is shown below.



**Figure 4-41: Pilot Model for F-18/HARV Roll Angle Tracking Task**

The next step is to define the desired sliding manifolds. The system (without actuators) has a relative order of 1 for both roll rate and sideslip. Therefore, the form of the sliding manifolds are

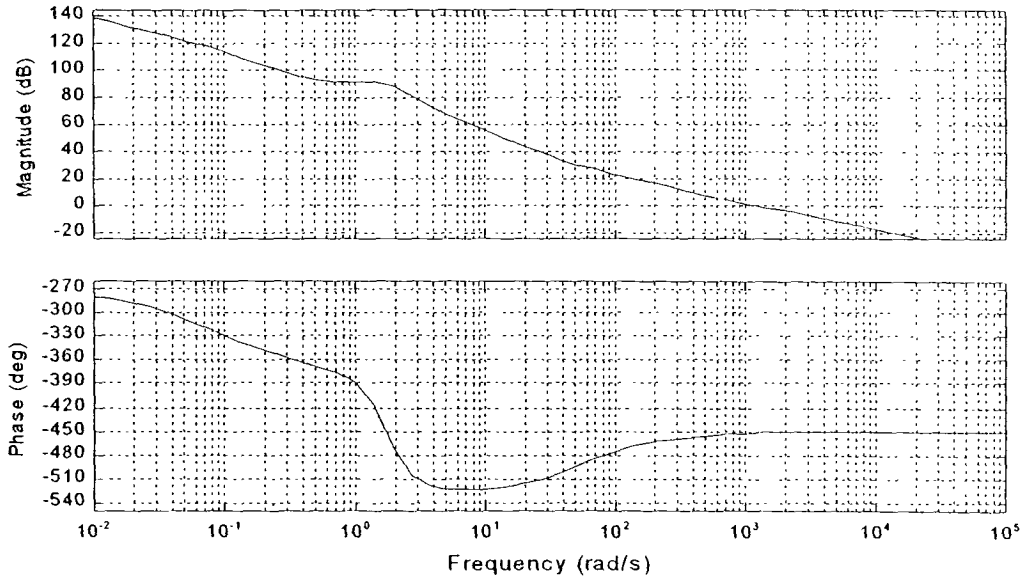
$$\sigma = K_0 e + K_{-1} \int e \, d\tau; \quad e = \left\{ \beta_r - \hat{\beta}, p_r - \hat{p} \right\}^T \quad (4.20)$$

The control laws, assuming the use of a boundary layer, then can be expressed in linear form as

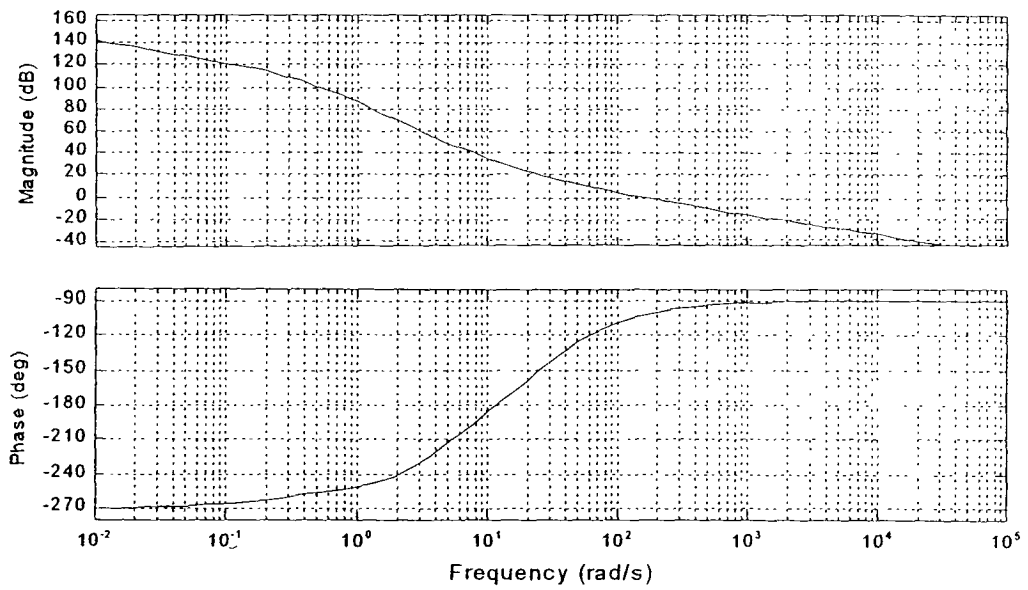
$$\begin{aligned} u_{c\beta}(s) &= K_{\rho\beta} \left( \frac{K_{0\beta}s + K_{-1\beta}}{s} \right) \\ u_{cp}(s) &= K_{\rho p} \left( \frac{K_{0p}s + K_{-1p}}{s} \right) \end{aligned} \quad (4.21)$$

This gives one zero to place and a gain to set for each loop during the loop-shaping design. Since the roll rate is a higher bandwidth loop, begin with this loop first. Assuming the beta loop is left open, the values chosen for the p-loop are  $K_{\rho p} = 500$ ,  $K_{0p} = 1$ , and  $K_{-1p} = 50$ . The resulting forward p-loop transmission of the compensator and plant (no actuators) with these values is shown in Figure 4-42. Note the desired  $\frac{K}{s}$  shape at crossover. The crossover frequency is about  $\omega = 1000$  rad/s.

Using a standard sequential loop closure technique, the p-loop is closed and the  $\beta$ -loop is designed. The values chosen for the  $\beta$ -loop are  $K_{\rho\beta} = 3000$ ,  $K_{0\beta} = 1$ , and  $K_{-1\beta} = 5$ . The resulting forward  $\beta$ -loop transmission of the compensator and effective plant with the p-loop closed is shown in Figure 4-43. Note the desired  $\frac{K}{s}$  shape at crossover. The crossover frequency is about  $\omega = 200$  rad/s.

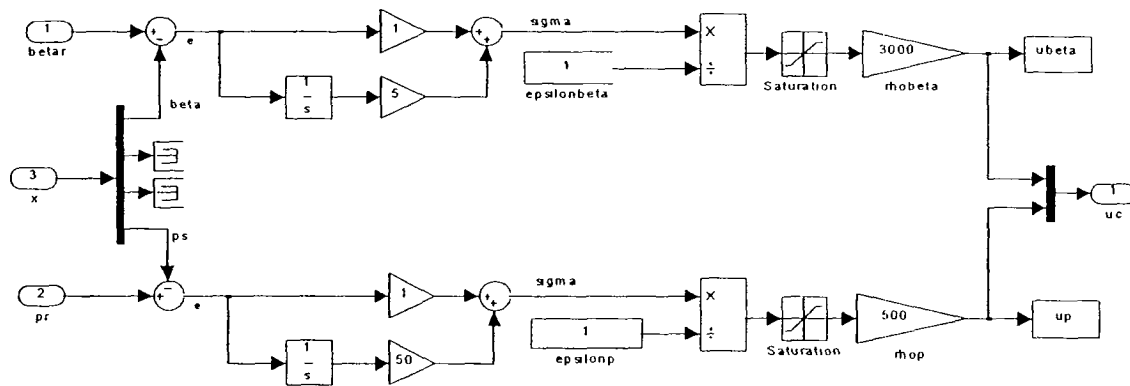


**Figure 4-42:  $\beta$ -Loop Transmission of Compensator\*Plant, F-18/HARV,  $\beta$ -Loop Open**



**Figure 4-43:  $\beta$ -Loop Transmission of Compensator\*Effective Plant, F-18/HARV,  $p$ -Loop Closed**

The initial design of the SMC is complete and is shown in Figure 4-44.

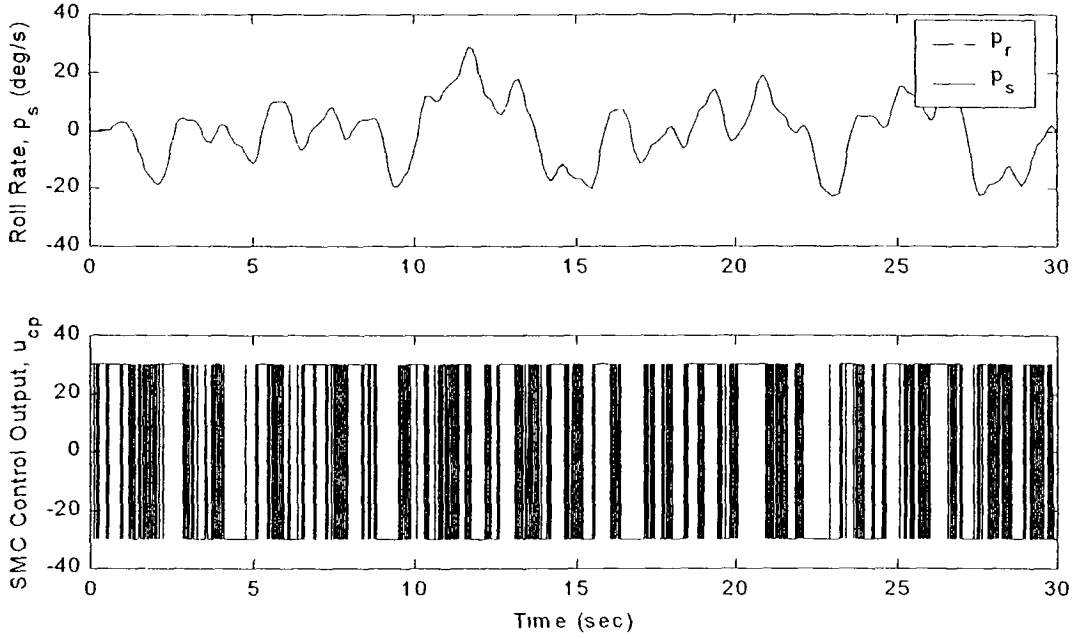


**Figure 4-44: SMC Roll Rate and Sideslip Angle Controller for F-18/HARV**

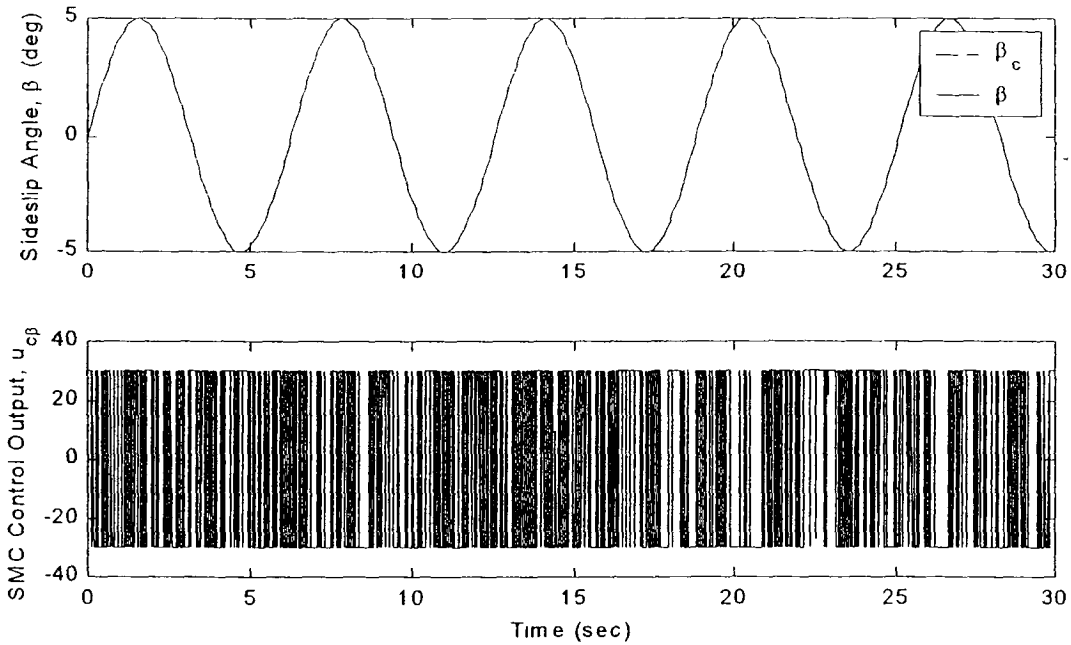
The fifth step in the design process is to verify that the SMC is working properly. Either replace the saturation elements in Figure 4-44 with a signum function or make the boundary layer very small. Figure 4-45 and Figure 4-46 show the time responses for the inner loop  $p_s$  and  $\beta$  tracking of the SMC with a boundary layer of  $\varepsilon = 0.000001$ . The Simulink<sup>®</sup> simulation is run with an ODE2 solver using a fixed time step of  $\Delta t = 0.0005$  sec. A system plant failure occurs at  $t = 10$  sec. Although the  $\beta$  input will be a constant zero for the final system, a simple sine wave is used here to verify decoupled tracking of  $p_s$  and  $\beta$ . Notice that, in this case, the SMC gain,  $\rho$ , is reduced for the very low value of  $\varepsilon$ . Sometimes, when the SMC gain is very high, the numerics of the solution become unstable. One solution is to reduce the simulation time step. Another solution is to reduce  $\rho$ . It may not be possible to reduce  $\rho$  in a manner such that

$$K_\rho = \frac{\rho}{\varepsilon} = \text{constant because, as discussed in Section 2.1.6, there is a minimum } \rho \text{ which}$$

will stabilize the system for a pure SMC. The actual value of  $\rho$  used here is not critical since a much larger boundary layer will be employed.



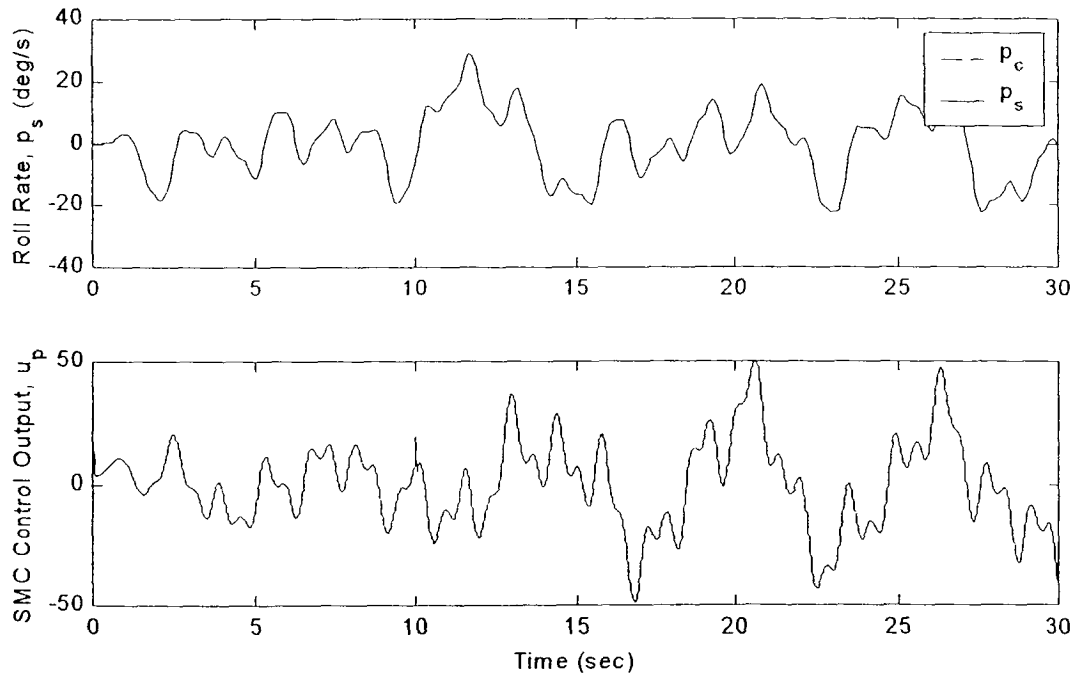
**Figure 4-45: F-18/HARV Inner Loop SMC Roll Rate Tracking**



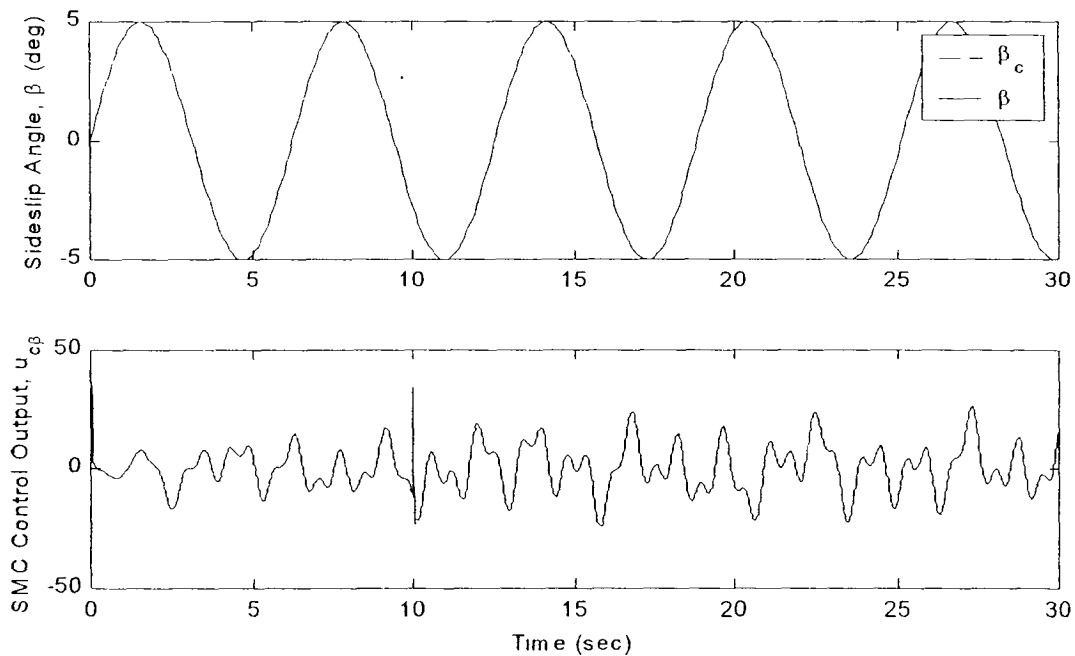
**Figure 4-46: F-18/HARV Inner Loop SMC  $\beta$  Tracking**

As expected, the SMC performs very well and is invariant to the system parameter changes. The control output shows the classic high frequency switching. Note, also that the controller achieves decoupled tracking of  $p_s$  and  $\beta$ , as desired. Considering the high level of yaw/roll coupling at this flight condition, the decoupled tracking performance of this controller is remarkable

Next, the boundary layer is increased until a continuous control signal is achieved. For this model,  $\varepsilon = 1$  is chosen for both channels. The resulting time history of the inner loop tracking for  $p_s$  and  $\beta$  is shown in Figure 4-47 and Figure 4-48.



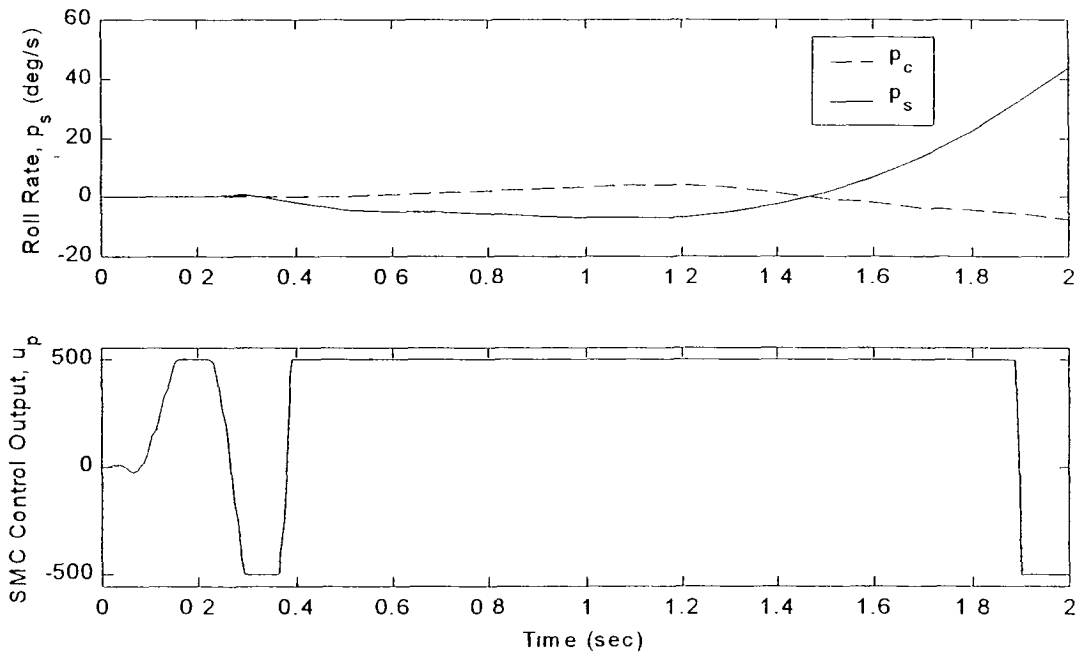
**Figure 4-47: F-18/HARV Inner Loop SMC Roll Rate Tracking with Boundary Layer**



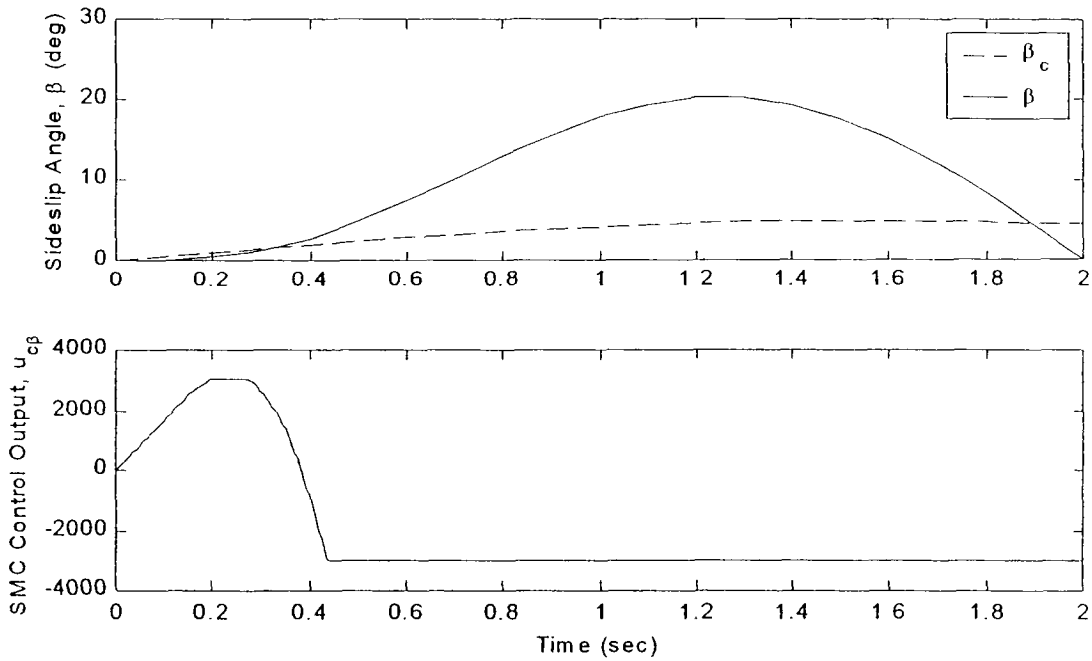
**Figure 4-48: F-18/HARV Inner Loop SMC  $\beta$  Tracking with Boundary Layer**

Again, the performance is excellent, even in the face of a large system failure. Also, the control signal is now continuous. Note the large spike in the control signal at the time of failure and the increased overall magnitude of the required control signal after the failure.

The SMC design is now complete, the resulting tracking performance is remarkably good, and the system is (nearly) invariant to system parameter changes. The next step is the inclusion of the actuators. Figure 4-49 and Figure 4-50 show the inner loop tracking results with the actuators now included. As expected, the nominal system goes unstable in less than half a second.

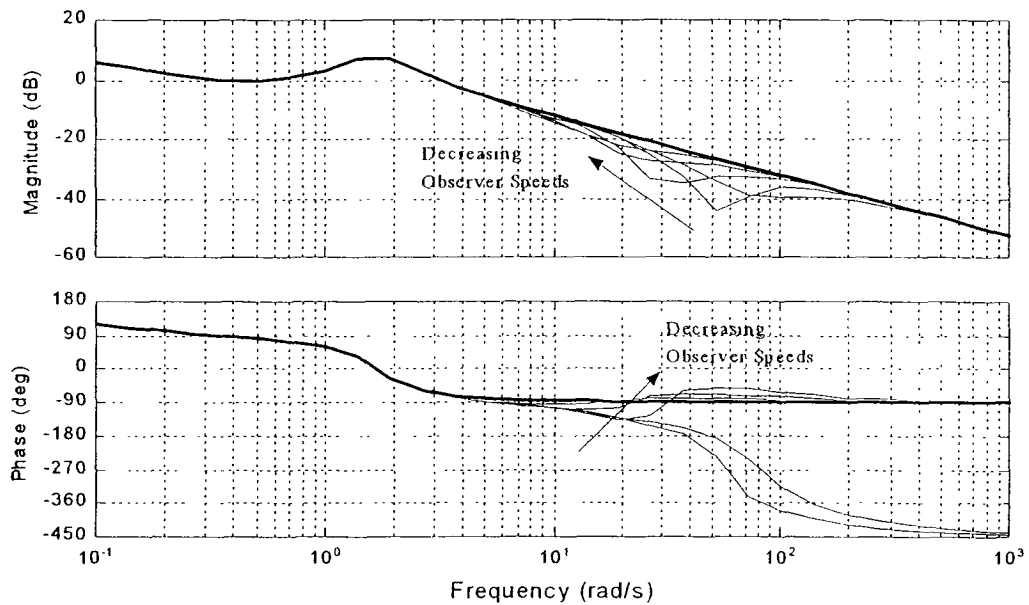


**Figure 4-49: Inner Loop  $p$ -Tracking, Nominal F-18/HARV, SMC with Actuators**



**Figure 4-50: Inner Loop  $\beta$ -Tracking, Nominal F-18/HARV, SMC with Actuators**

The next steps are to design the observers and hedge models. As introduced in Section 3.3, the individual Bode plots of the equivalent plant/observer transfer functions with unity feedback ( $\frac{\hat{p}}{u_{cp}}$  and  $\frac{\hat{\beta}}{u_{c\beta}}$ ) are examined for varying observer speeds (with no hedging). Observer speeds of 100, 50, 20, 10, 5, and 1 rad/s are tried. The Bode plots for  $p_s$  and  $\beta$  are shown in Figure 4-51 and Figure 4-52 respectively.



**Figure 4-51: Bode Plots,  $\frac{\hat{p}}{u_{cp}}$ , F-18/HARV, Various Observer Speeds**

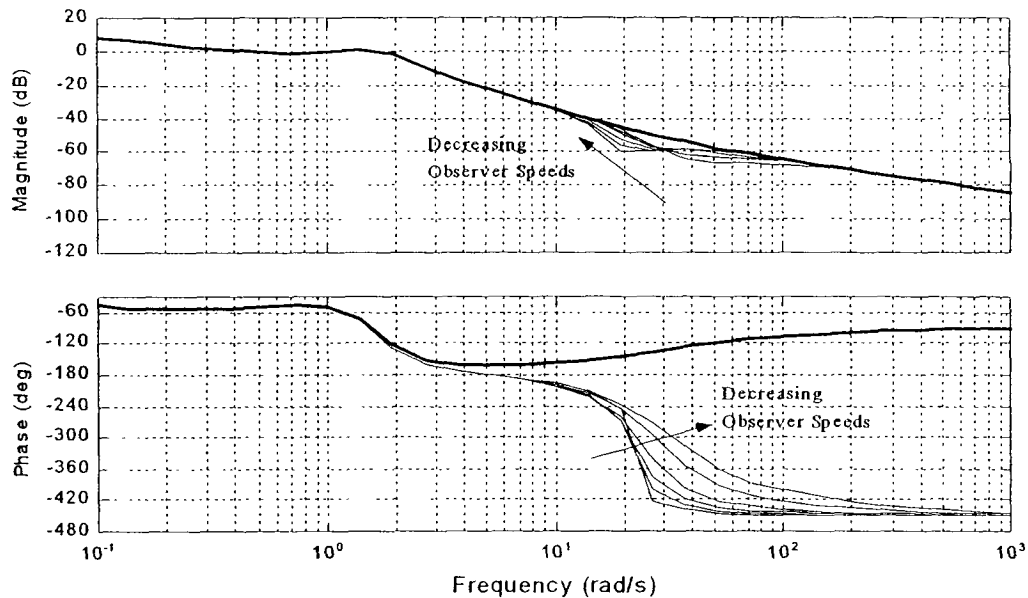


Figure 4-52: Bode Plots,  $\frac{\hat{\beta}}{u_{c\beta}}$ , F-18/HARV, Various Observer Speeds

As shown on the Bode plots, observer speeds of 50 and 100 rad/s in the p-loop result in an unstable system. Also, it is clear that the observer for the  $\beta$ -loop can not be slowed down enough to stabilize the system. Hedging is required for this system, at least in the  $\beta$ -loop.

Before designing the hedge models, the transfer functions of the cross-coupled variables are examined. The Bode plots of the open loop transfer functions for the nominal plant are given below. Figure 4-53 shows the stability axis roll rate transfer functions (roll-rate to roll-rate-command, and roll-rate to  $\beta$ -command). Figure 4-54 shows the sideslip angle transfer functions ( $\beta$  to  $\beta$ -command, and  $\beta$  to roll-rate-command).

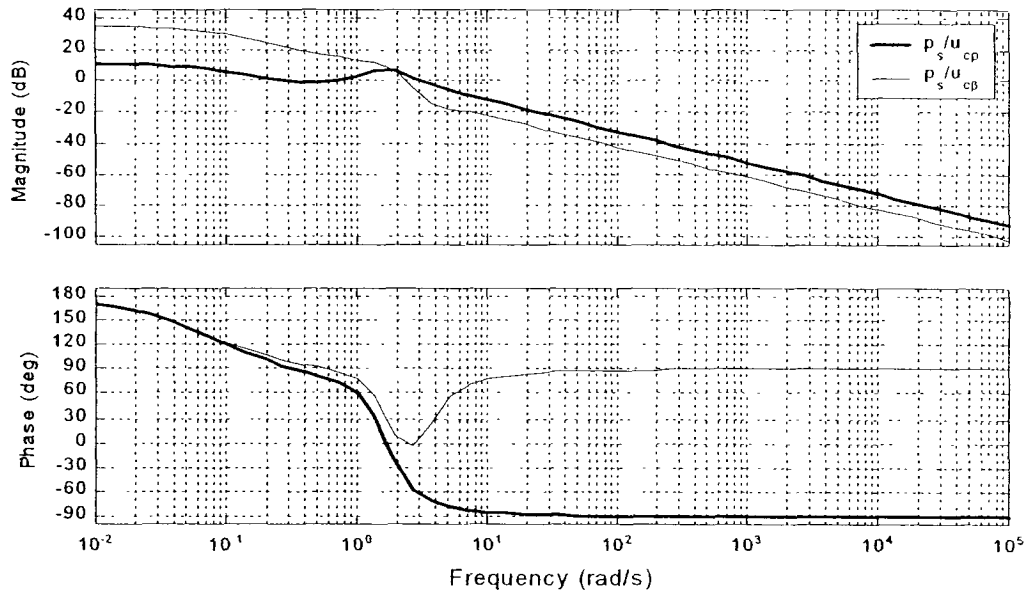


Figure 4-53: Bode Plots,  $\frac{p}{u_{cp}}$  and  $\frac{p}{u_{c\beta}}$ , F-18/HARV Nominal Vehicle

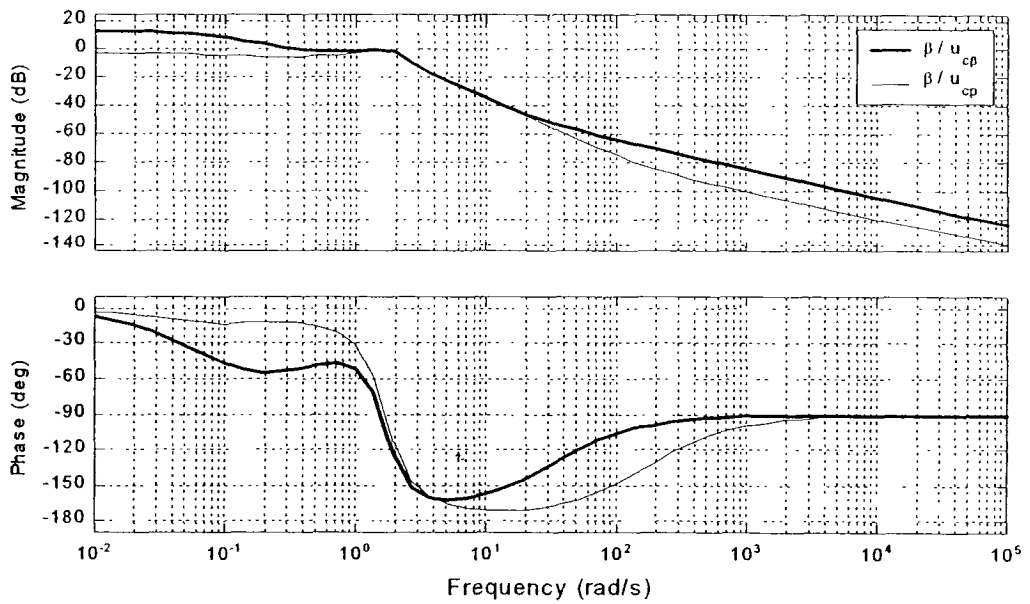


Figure 4-54: Bode Plots,  $\frac{\beta}{u_{cp}}$  and  $\frac{\beta}{u_{c\beta}}$ , F-18/HARV Nominal Vehicle

Very strong coupling is seen. The Bode magnitude plots of the cross-coupled transfer functions are of the same order of magnitude as the primary transfer functions. It is expected, therefore, that cross-coupled hedging models may be required. Following the design procedures outlined in Section 3.4, the following parameters are chosen for the observer and hedging models.

Channel	Observer Poles
$p_s$	$\lambda = -10, -11, -12$
$\beta$	$\lambda = -10, -11, -12$
Hedge Model	
$\frac{p_h}{u_{cp}}$	$\left(\frac{s}{s+50}\right)\left(\frac{100}{s^2+20s+100}\right)$
$\frac{\beta_h}{u_{c\beta}}$	$\left(\frac{s}{s+20}\right)\left(\frac{1}{s^2+2s+1}\right)$
$\frac{p_h}{u_{c\beta}}$	$-20\left(\frac{s}{s+50}\right)\left(\frac{1}{s^2+2s+1}\right)$ cross term
$\frac{\beta_h}{u_{cp}}$	$0.8\left(\frac{s}{s+20}\right)\left(\frac{1}{s^2+2s+1}\right)$ cross term
Hedge Gain	
$p_s$	1.0
$\beta$	2.0

**Table 4-4: Observer and Hedge Models for Lateral Directional F-18/HARV**

The resulting design Bode plots are shown below.

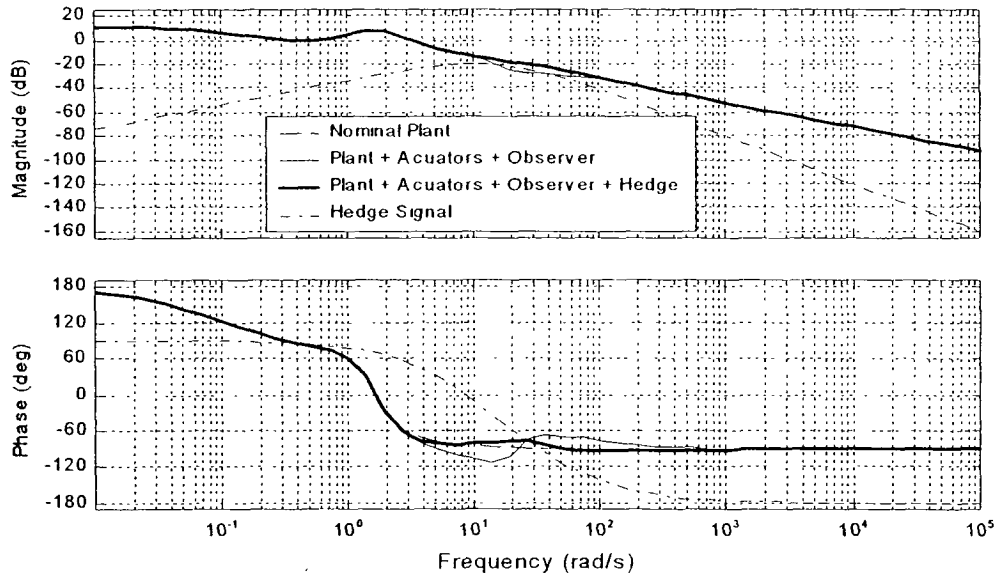


Figure 4-55: Bode Plots,  $\frac{\hat{p}_h}{u_{cp}}$ , F-18/HARV Hedge Design

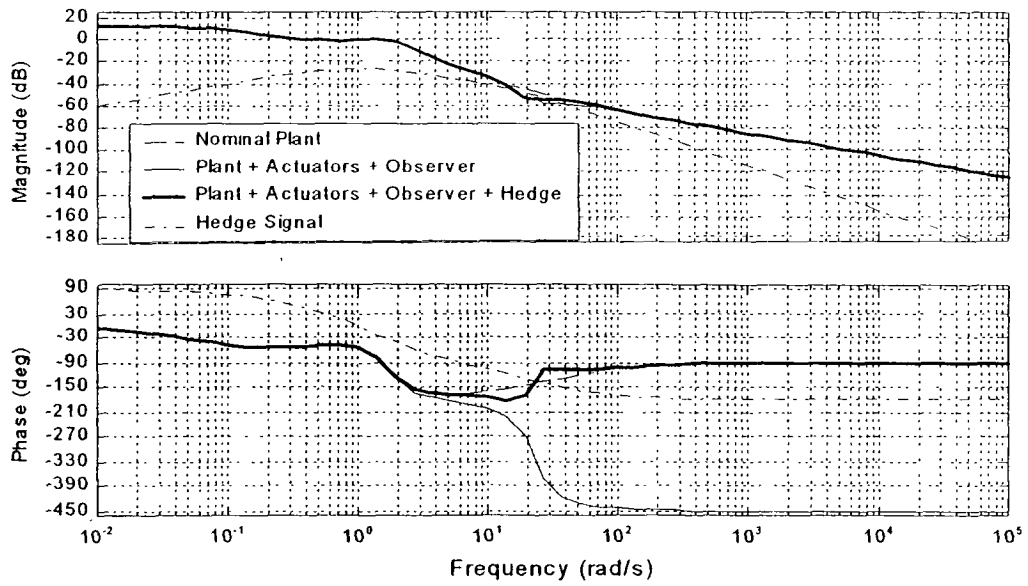
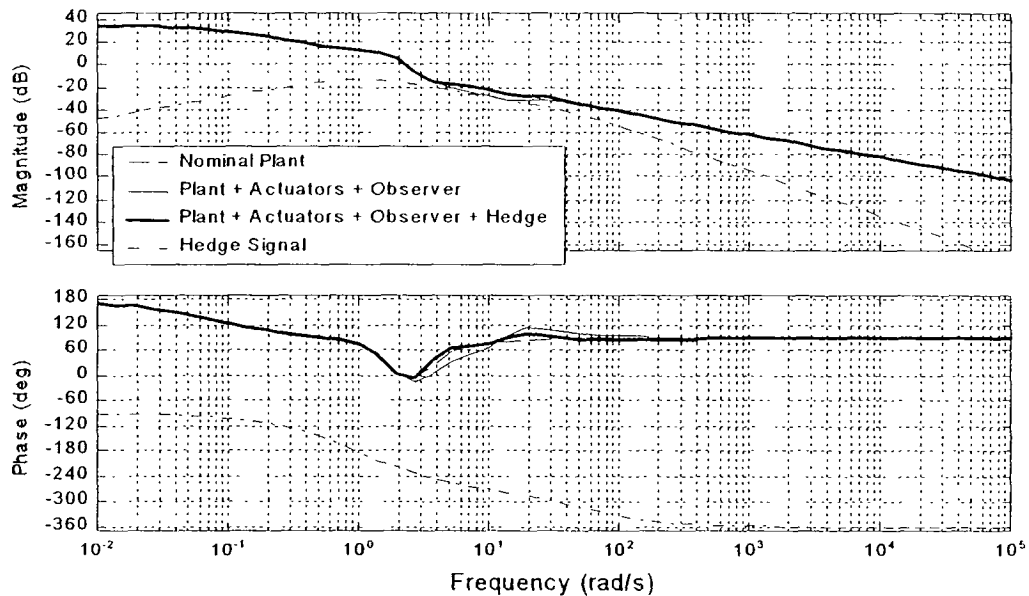


Figure 4-56: Bode Plots,  $\frac{\hat{\beta}_h}{u_{c\beta}}$ , F-18/HARV Hedge Design

Note from Figure 4-55 that the p-loop is stable without hedging if the observer is run at 10 rad/s. Hedging helps some but is not required for the nominal model. Figure 4-56 shows that the  $\beta$ -loop is unstable without hedging. The hedging used on this channel stabilizes the system and provides a desirable feedback loop shape.

Next, consider the cross-coupling hedge models. Figure 4-57 shows the p to  $\beta$ -command hedge design. As can be seen, hedging helps some but is probably not required.



**Figure 4-57: Bode Plots,  $\frac{\hat{p}_h}{u_{c\beta}}$  (cross term), F-18/HARV Hedge Design**

Figure 4-58 shows the  $\beta$  to p-command hedge design. In this case, the effect of the p-command on  $\beta$  is strong enough to require hedging. The hedge model chosen provides a desirable feedback loop shape for this cross-coupled channel

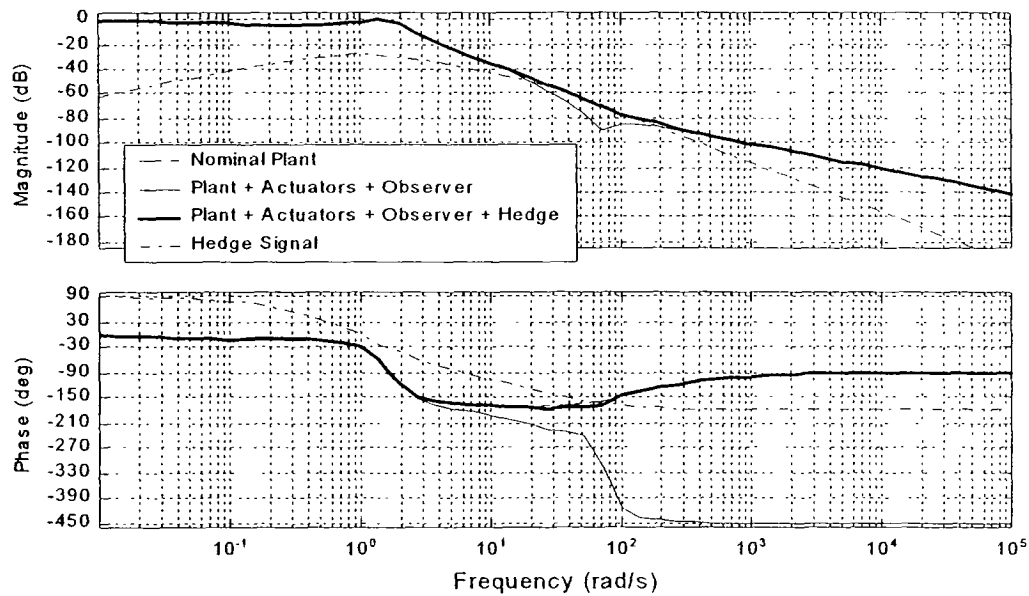
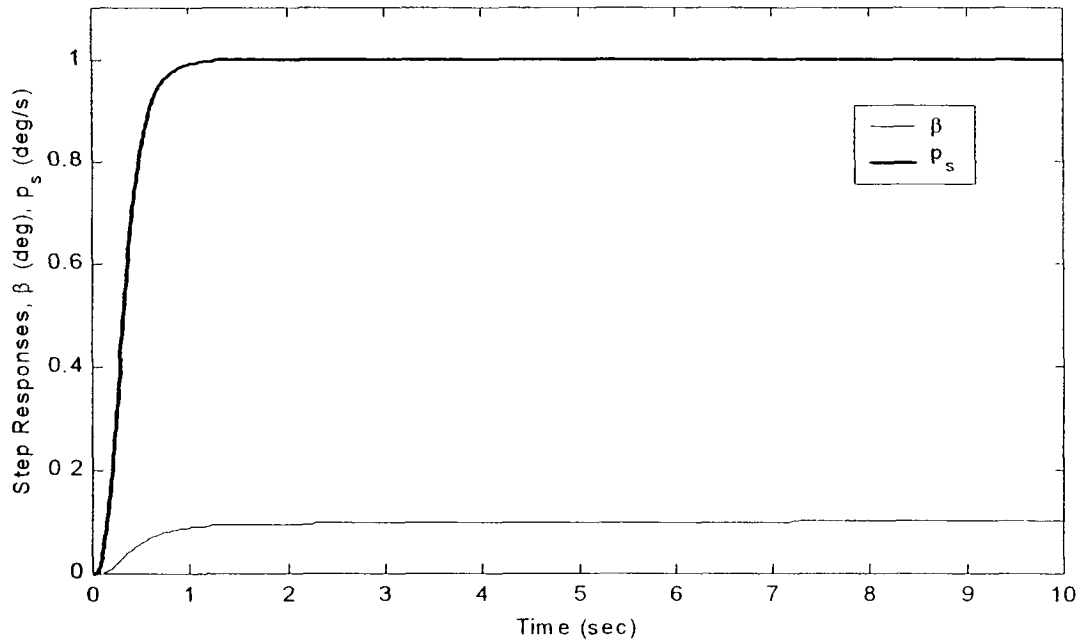
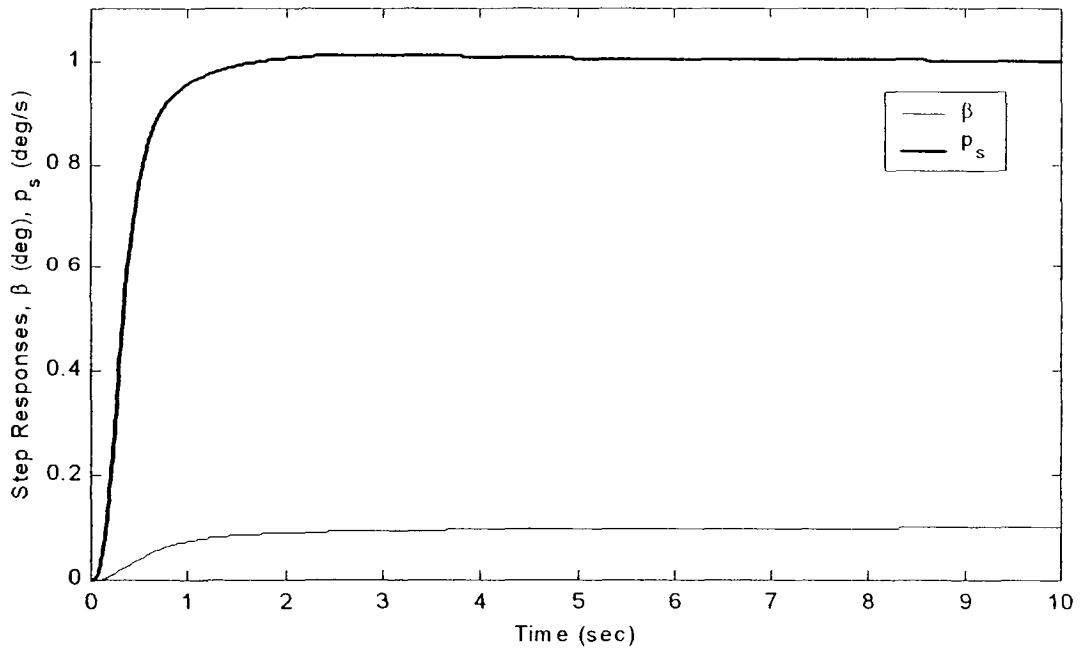


Figure 4-58: Bode Plots,  $\frac{\hat{\beta}_h}{u_{cp}}$  (cross term), F-18/HARV Hedge Design

With the observer and hedge models designed, the system is now tested. First the step responses for the inner loop are examined. The step responses for the inner loop with the given observer and hedge models are shown below. The roll rate command is a unit step, while the  $\beta$  command is a step of 0.1. The two steps are commanded simultaneously in order to test the effects of cross-coupling. Figure 4-59 shows the results if the cross-coupled hedging models are neglected. Figure 4-60 includes the cross-coupled hedging models.



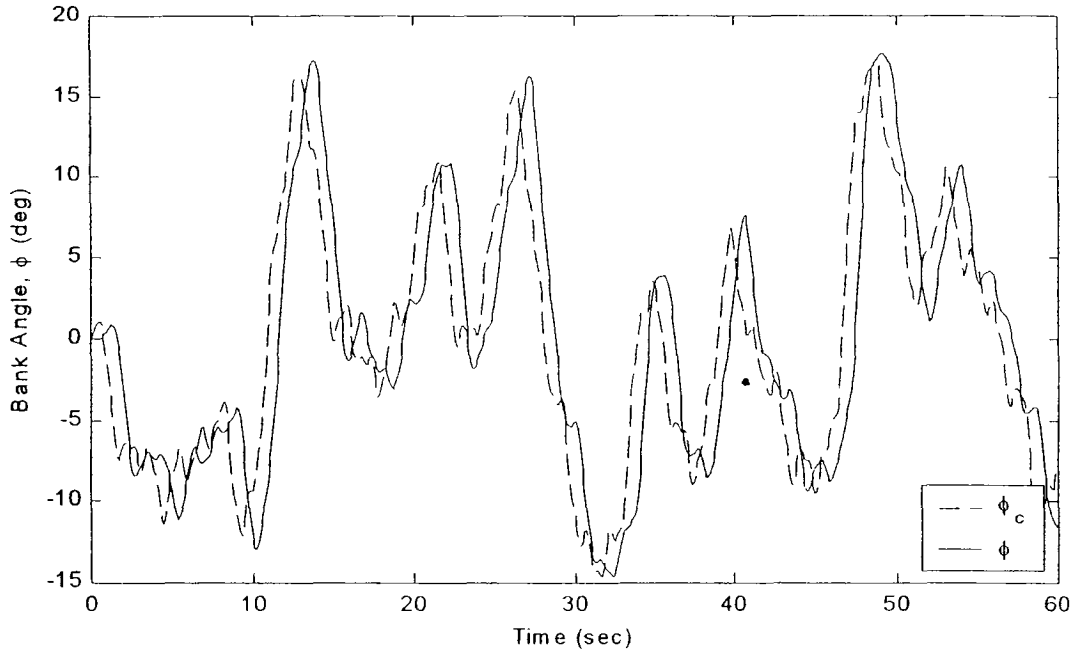
**Figure 4-59: Step Response for  $p$  and  $\beta$ , F-18/HARV, no Cross-Coupled Hedging**



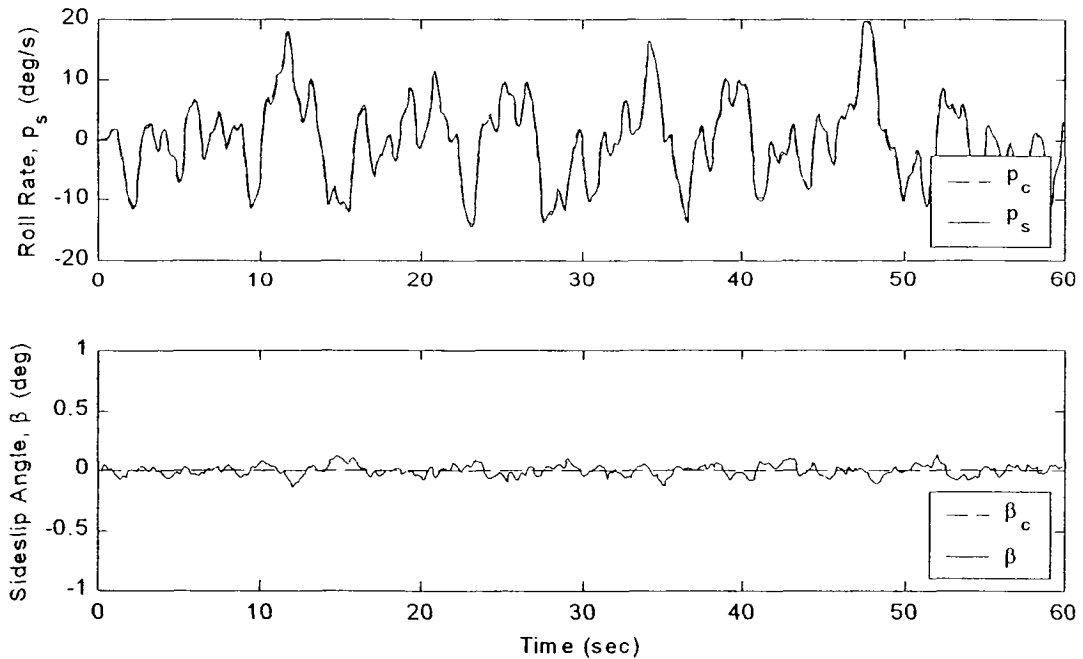
**Figure 4-60: Step Response for  $p$  and  $\beta$ , F-18/HARV, with Cross-Coupled Hedging**

For the nominal model, the step responses in Figure 4-59 and Figure 4-60 indicate that neglecting the cross-coupled hedge models yields slightly better results. It is seen later, however, that including the cross-coupled hedge models increases the system robustness to variations in the actuator dynamics and reduces the activity in the  $\beta$  channel. Unless specified, all the following results use the coupled hedge models.

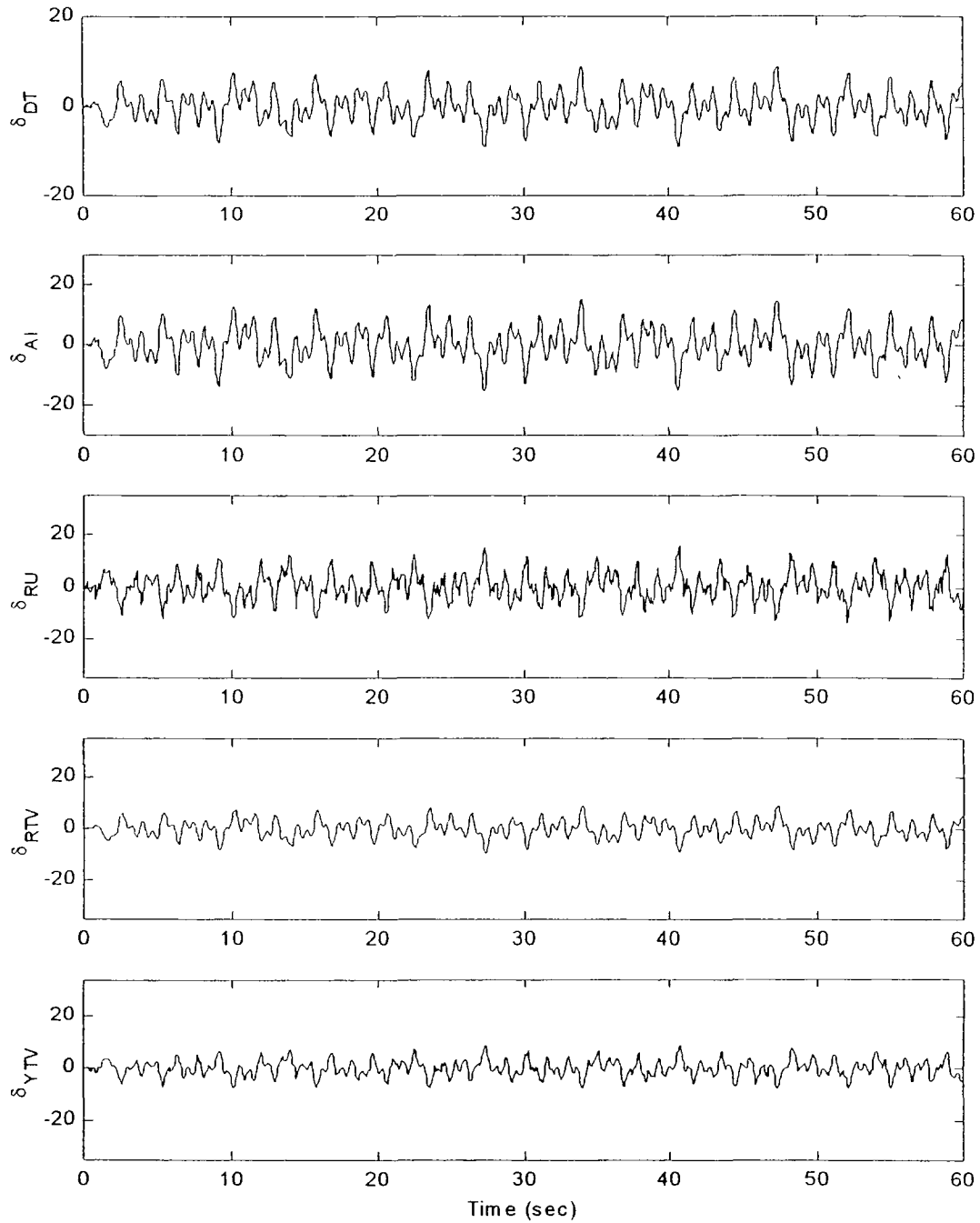
Now exercise the full system with measurement noise and the pilot in the loop. The outer loop bank angle tracking performance for the nominal vehicle is shown in Figure 4-61. Performance is very good. The large time delay between the commanded roll angle and the achieved roll angle is almost entirely due to the pilot. Note in Figure 4-62 that the inner loop tracking is very good. Of course, with the actuators and observer now included, the SMC does not give the almost perfect tracking achieved with the plant only. There is still essentially decoupled control of  $p_s$  and  $\beta$ , although  $\beta$  is not exactly zero. Considering the aggressive roll rates and the addition of state noise,  $\beta$  is acceptably small. Figure 4-63 and Figure 4-64 show the actuator deflections and rates, respectively. No position limits are reached, although there is some minor rate limiting in the rudder and yaw thrust vector. As shown in Figure 4-65 and Figure 4-66, Level I handling qualities are expected for the bank angle tracking task with no adverse PIO tendencies.



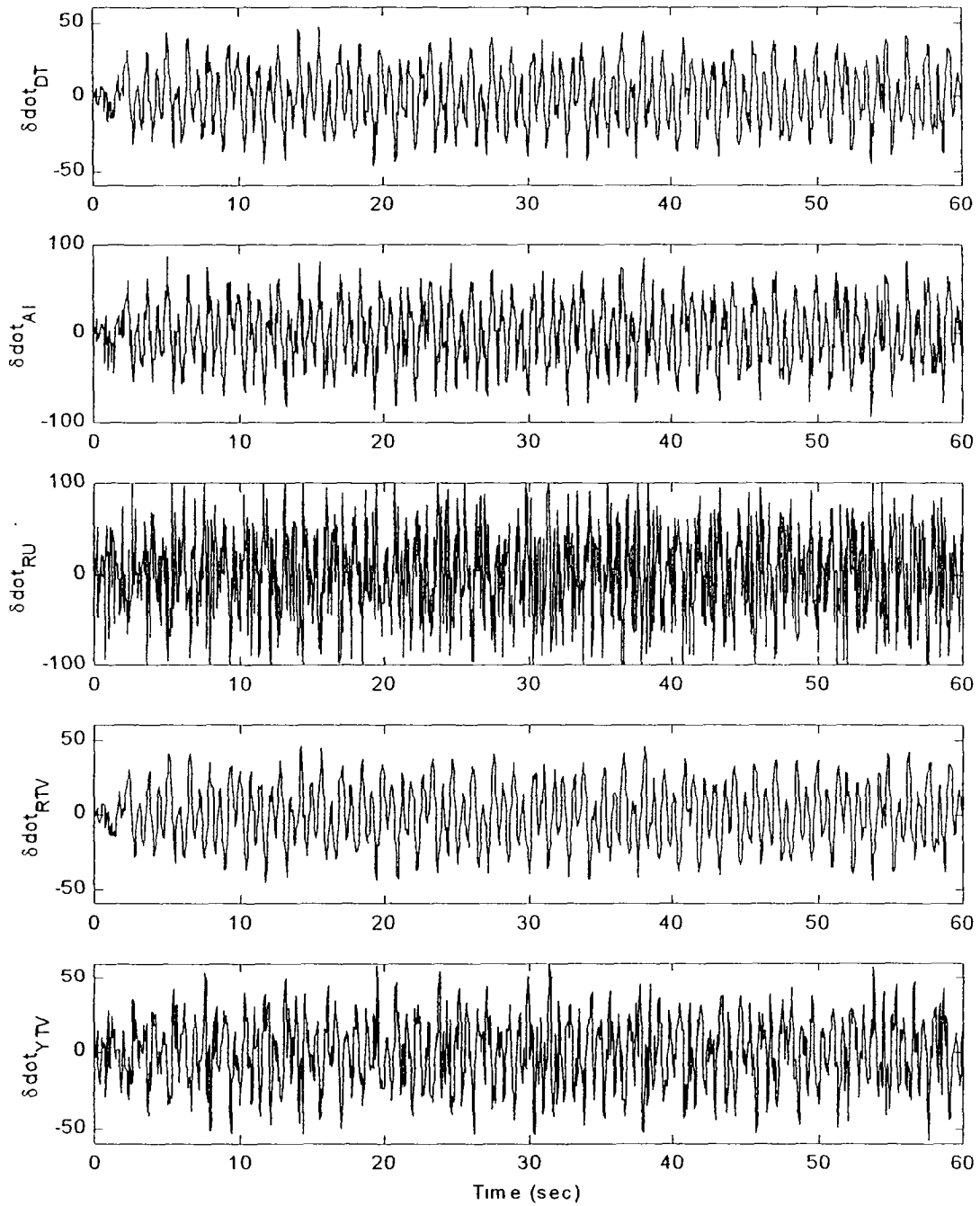
**Figure 4-61: Outer Loop Tracking ( $\phi$ ), Nominal F-18/HARV, with SMC, Actuators, Observers, Hedging, and Noise**



**Figure 4-62: Inner Loop Tracking ( $p_s$  and  $\beta$ ), Nominal F-18/HARV, with SMC, Actuators, Observers, Hedging, and Noise**



**Figure 4-63: Actuator Deflections, Nominal F-18/HARV, with SMC, Observers, Hedging and Noise**



**Figure 4-64: Actuator Rates, Nominal F-18/HARV, with SMC, Observers, Hedging and Noise**

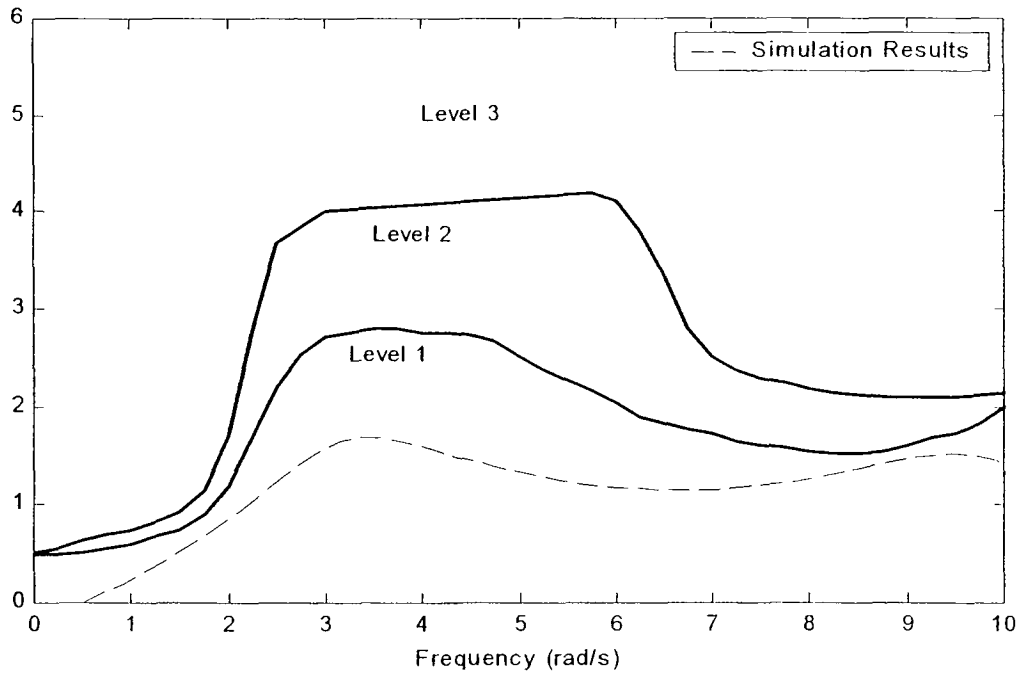


Figure 4-65: Nominal F-18/HARV Handling Qualities Assessment,  $\phi$  Tracking Task

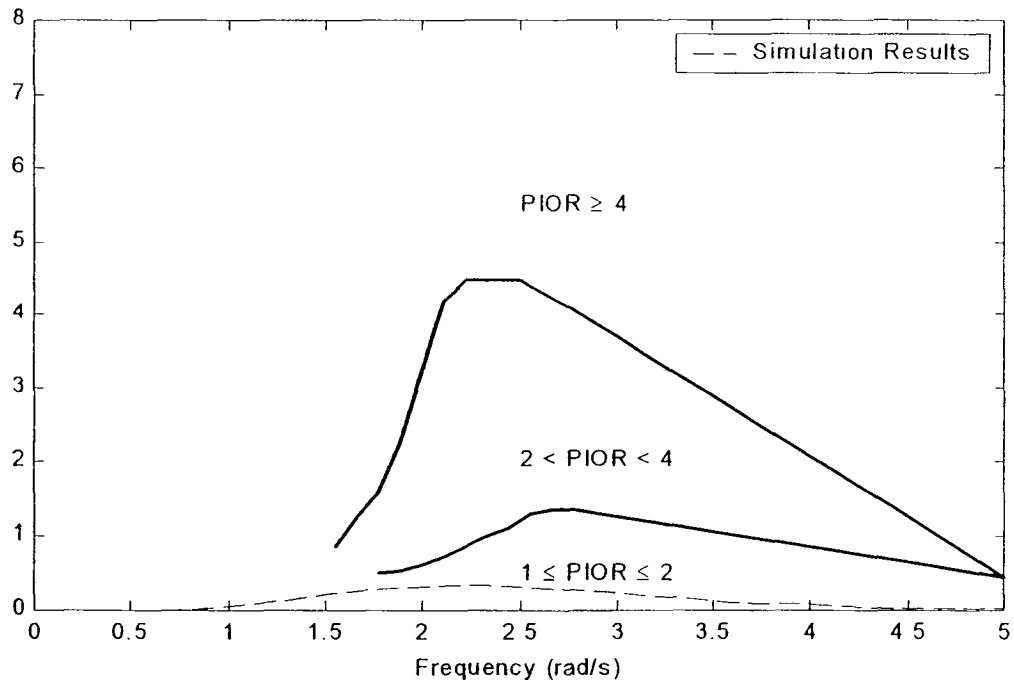
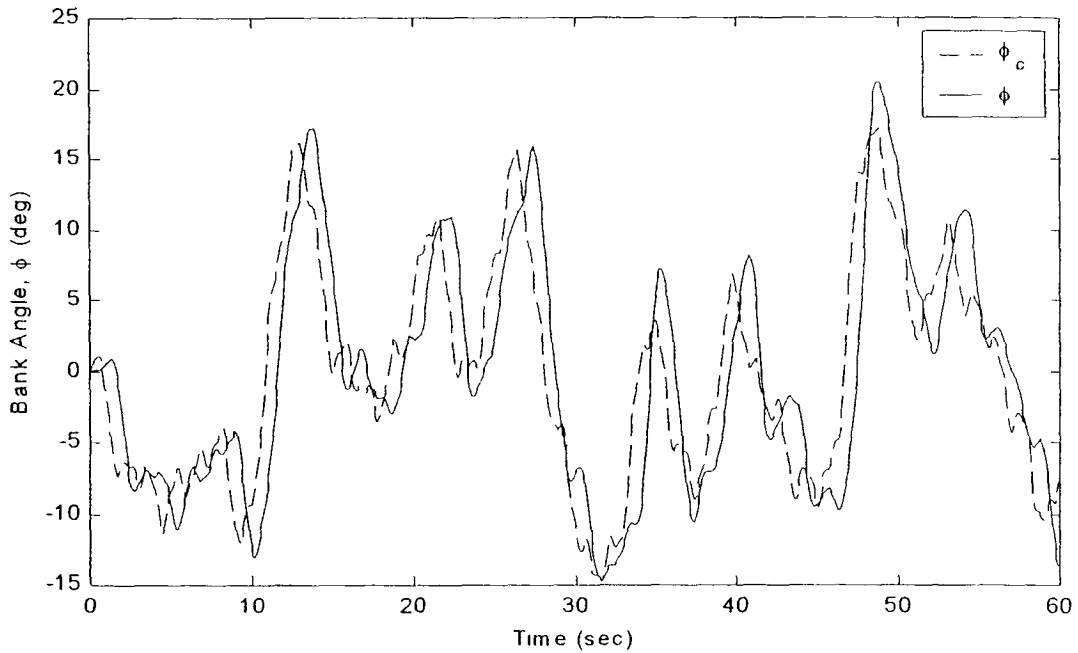


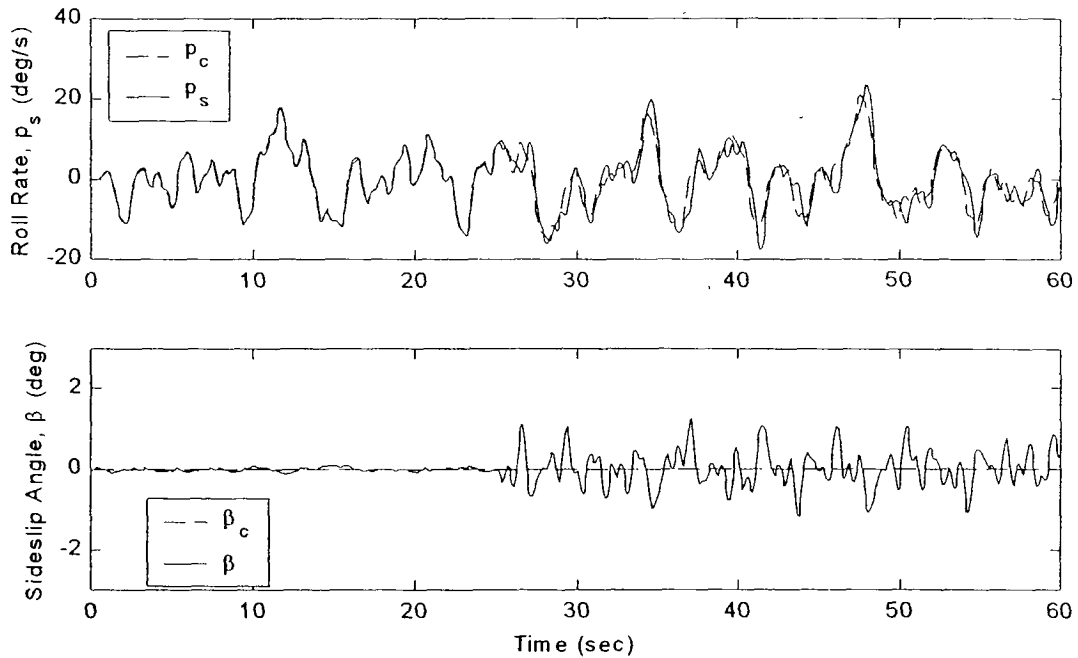
Figure 4-66: Nominal F-18/HARV PIO Assessment,  $\phi$  Tracking Task

In order to compare performance of a failed vehicle with other types of designs, two different failures are defined. Failure #1 is defined as follows: failed plant, failed yaw and roll thrust vectors (max deflection = 15 deg, max rate = 30 deg/s, 50 ms time delay). This is a dramatic failure: 100% change in plant parameters, 25% reduction in effectiveness of all controls, a 50% reduction in thrust vector limits, and a sizeable time delay.

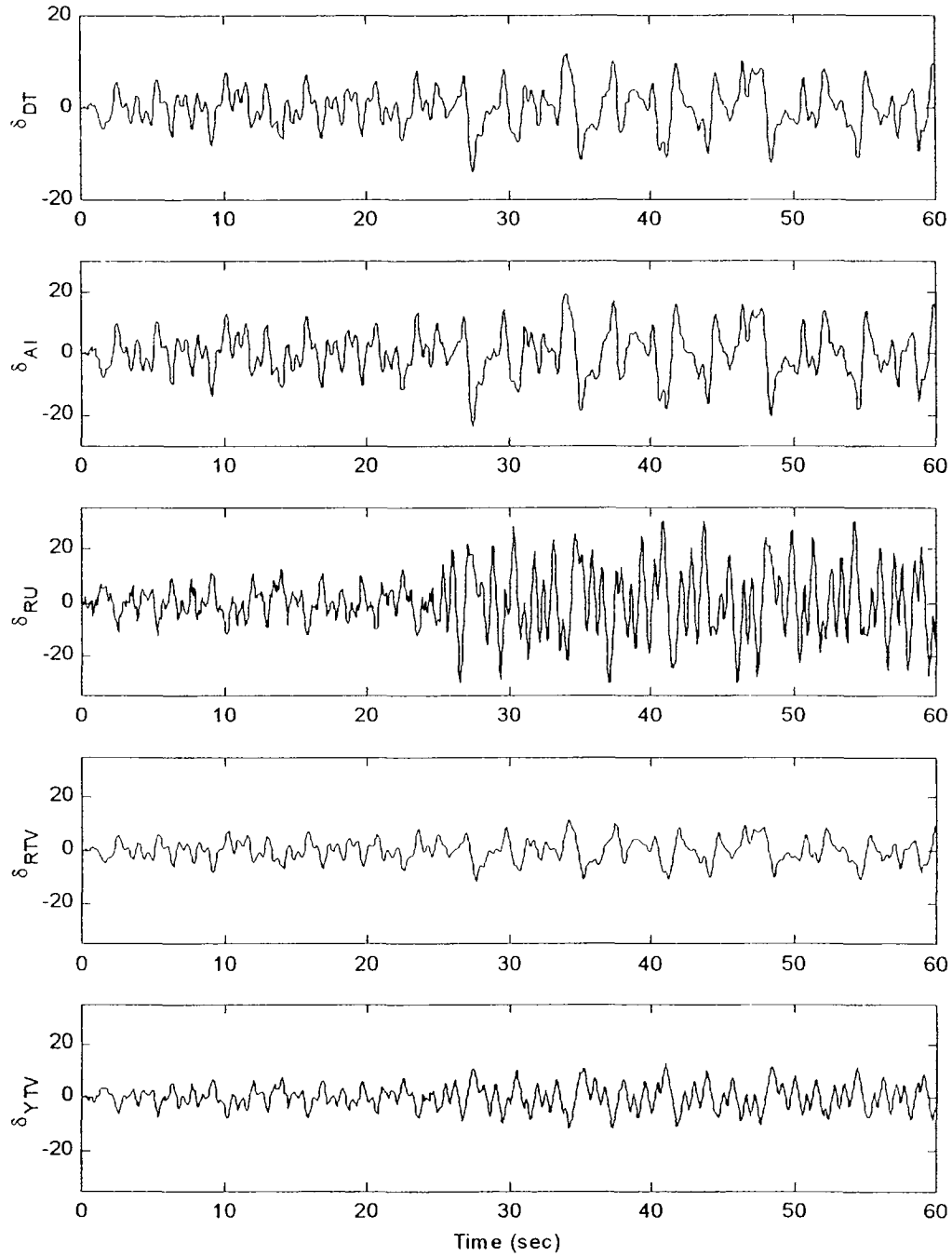
The Simulink<sup>®</sup> simulation results are shown below. The simulation starts with a nominal vehicle followed by a failure which occurs at  $t = 25$  sec. Figure 4-67 shows the outer loop bank angle tracking performance. Tracking is degraded after the failure, but the system remains stable. Figure 4-68 shows the inner loop tracking.  $\beta$  excursions change from negligible (before the failure) to a maximum value of about 1 deg (after the failure). Figure 4-69 shows the actuator deflections. No position limits are encountered, although the rudder is very near its limit. Figure 4-70 gives the actuator rates. The yaw thrust vector, roll thrust vector, and rudder are in almost constant rate saturation after the failure. The differential tail and ailerons also reach their rate limits occasionally after the failure. This would seem to indicate that the system is on the edge of its maximum achievable performance. Figure 4-71 and Figure 4-72 indicate that a Level II handling qualities rating is expected and PIO tendencies are low. Given the severity of the failure, the demands of the flight condition, and the fact that all the control effectors are operating at their limits, it is doubtful that any control system could achieve Level I handling qualities for this condition.



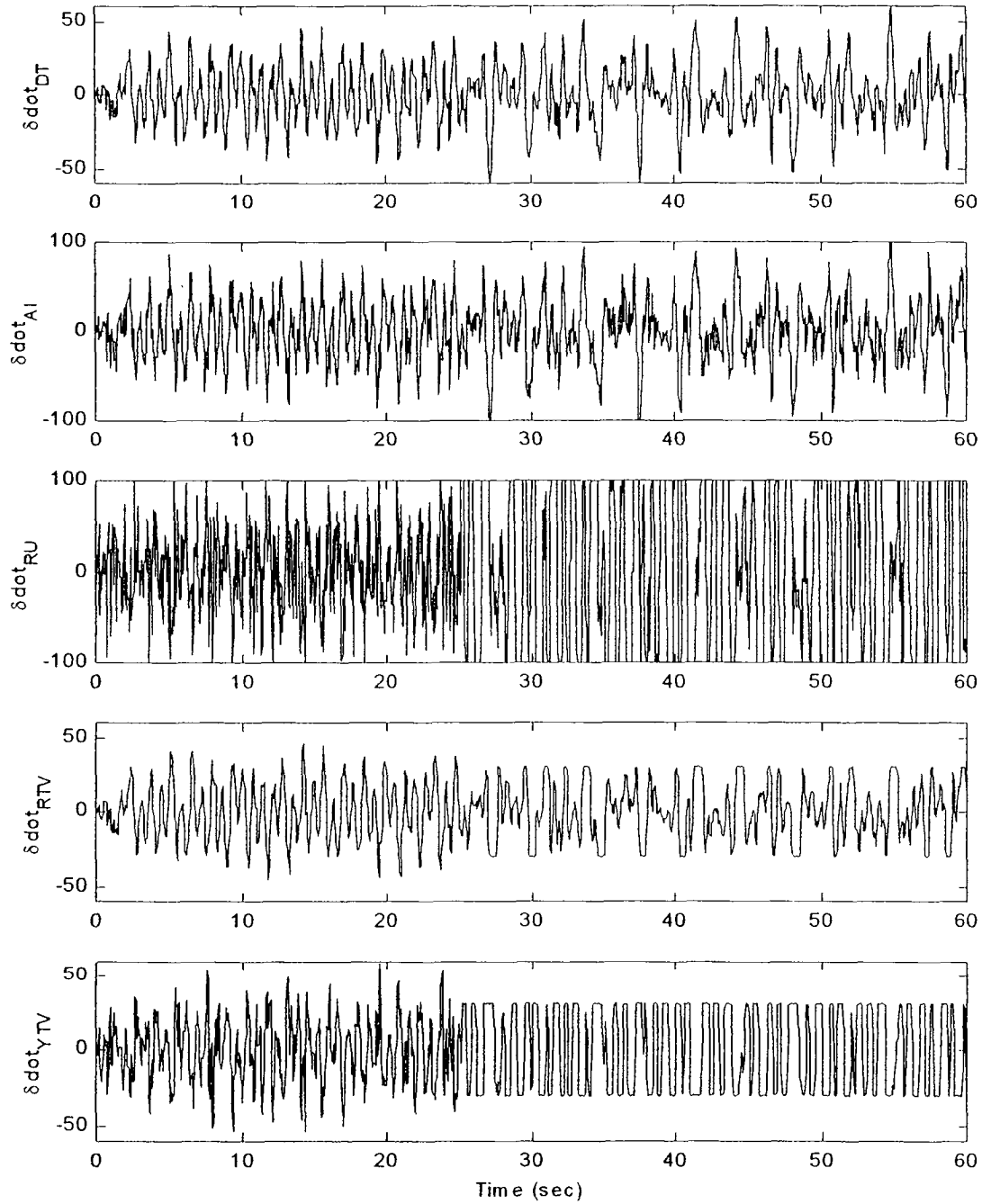
**Figure 4-67: Outer Loop Tracking ( $\phi$ ), F-18/HARV, with SMC, Actuators, Observer, Hedging, and Noise, Failure #1 at  $t = 25$  sec**



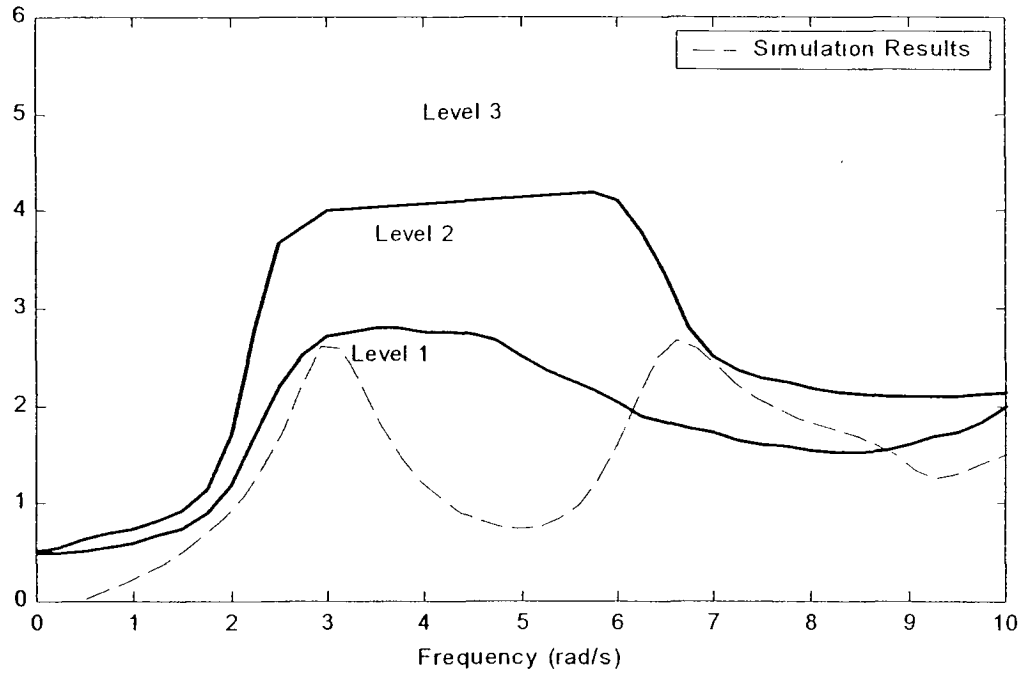
**Figure 4-68: Inner Loop Tracking ( $p_s$  and  $\beta$ ), F-18/HARV, with SMC, Actuators, Observer, Hedging, and Noise, Failure #1 at  $t = 25$  sec**



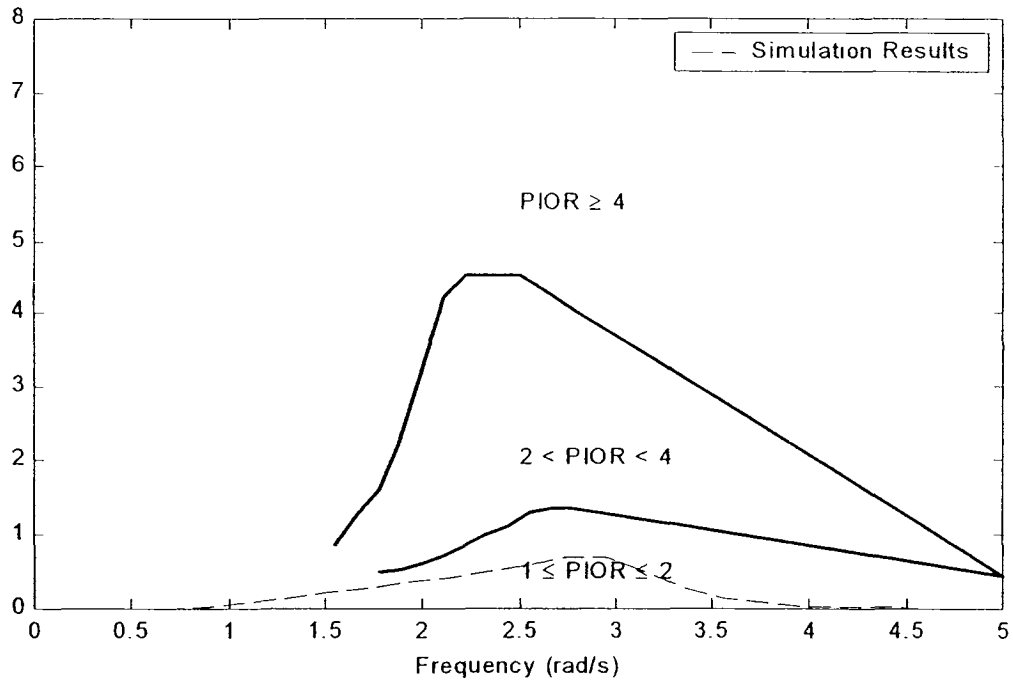
**Figure 4-69: Actuator Deflections, F-18/HARV, with SMC, Observer, Hedging, and Noise, Failure #1 at  $t = 25$  sec**



**Figure 4-70: Actuator Rates, F-18/HARV, with SMC, Actuators, Observer, Hedging, and Noise, Failure #1 at  $t = 25$  sec**



**Figure 4-71: F-18/HARV, Failure #1, Handling Qualities Assessment,  $\phi$  Tracking Task**

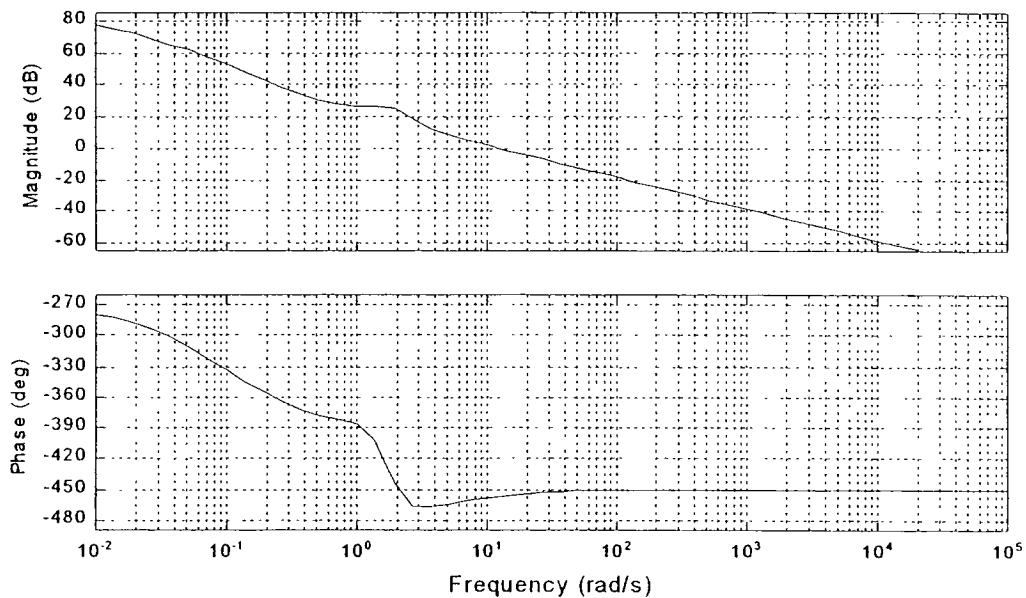


**Figure 4-72: F-18/HARV, Failure #1, PIO Assessment,  $\phi$  Tracking Task**

In order to compare these results to a well-known design approach, a classical loop shaped controller is designed. The first loop to design is the p-loop (with the  $\beta$ -loop

open). The roll rate control transfer function selected is  $G_{p_s}(s) = 5.0 \left( \frac{s^2 + 3s + 2.25}{s^2 + 0.5s} \right)$ .

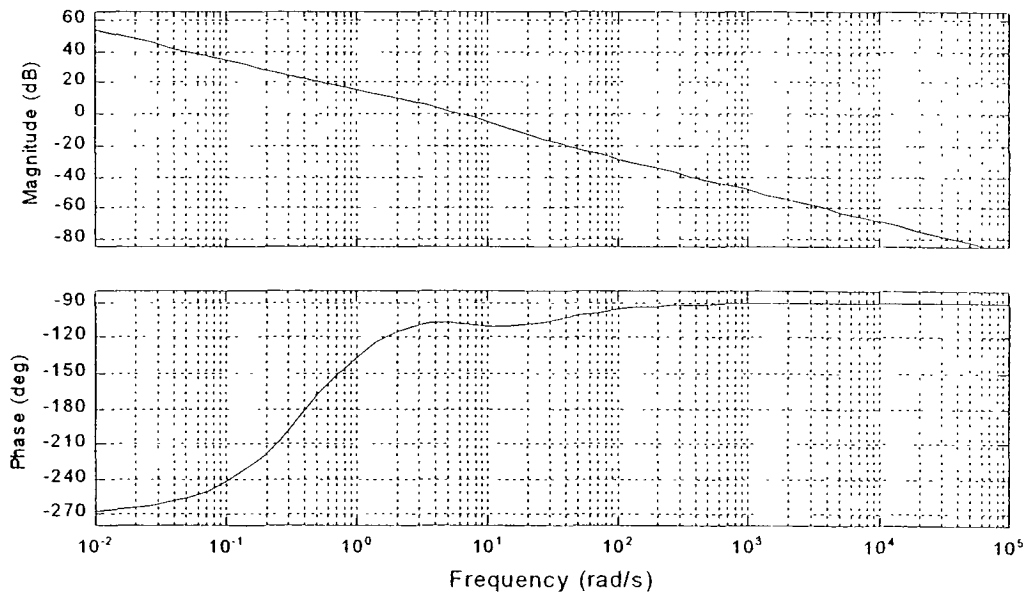
The resulting loop transmission for the control and plant is shown in Figure 4-73. This gives a crossover frequency of about  $\omega = 10$  rad/s.



**Figure 4-73: Bode Plots, F-18/HARV Roll Rate Loop Transmission for Loop Shaped Design,  $\beta$ -Loop Open**

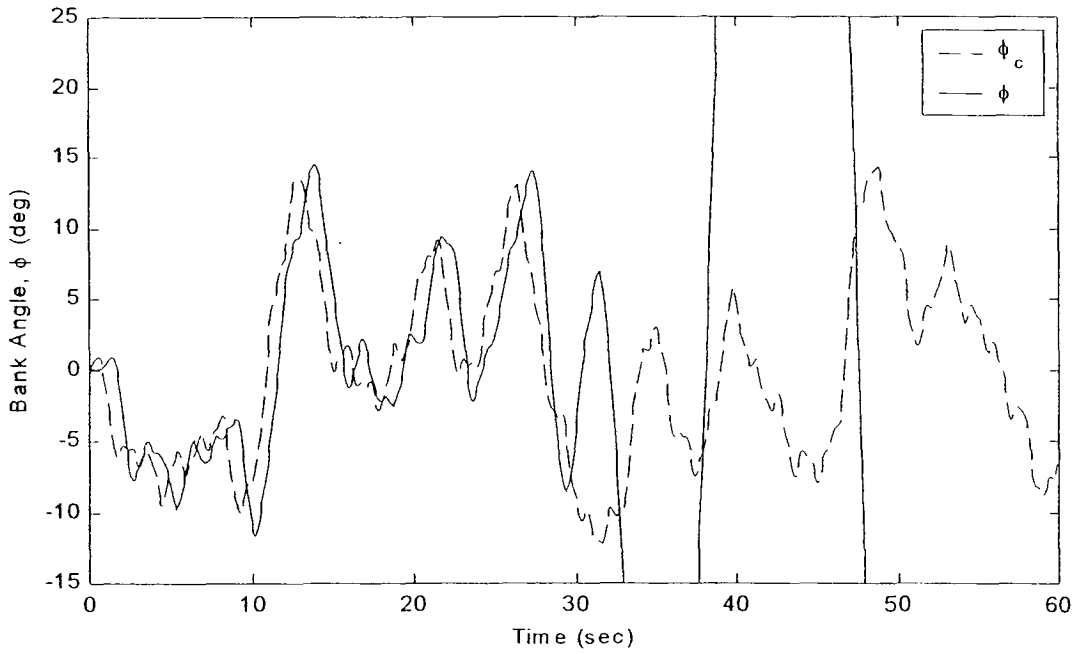
With the p-loop closed, the  $\beta$ -loop is designed:  $G_{\beta}(s) = 63.0 \left( \frac{s^2 + 0.9s + 0.2}{s^2 + 20s} \right)$ . The

resulting loop transmission of the  $\beta$  controller and effective plant is shown in Figure 4-74. The crossover frequency for  $\beta$  is about  $\omega = 5$  rad/s.

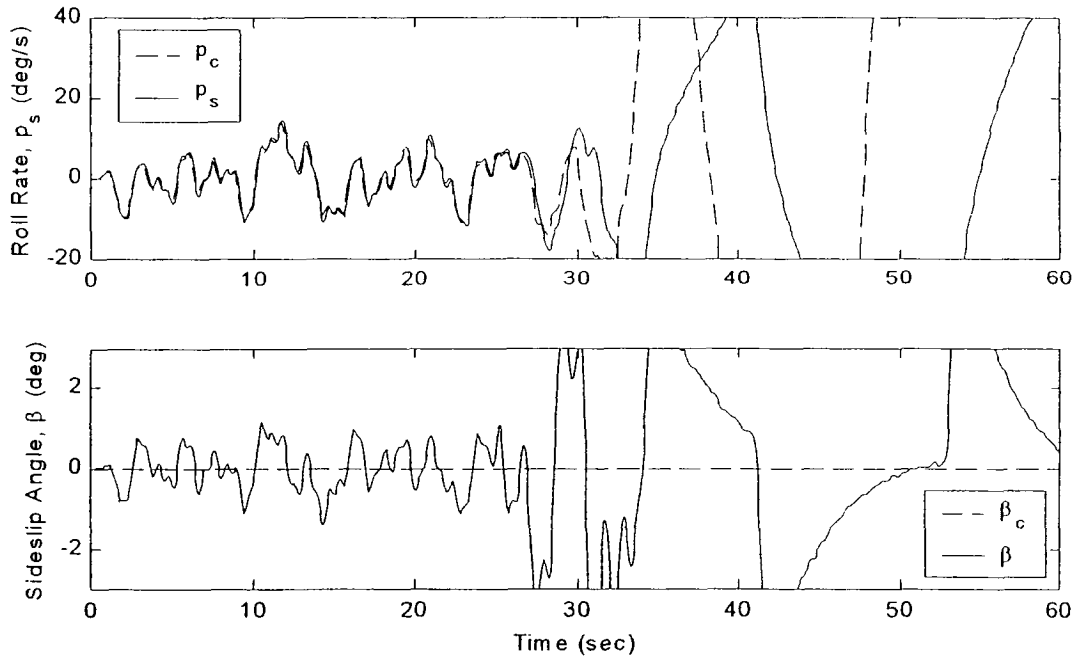


**Figure 4-74: Bode Plots, F-18/HARV  $\beta$  Loop Transmission for Loop Shaped Design, p-Loop Closed**

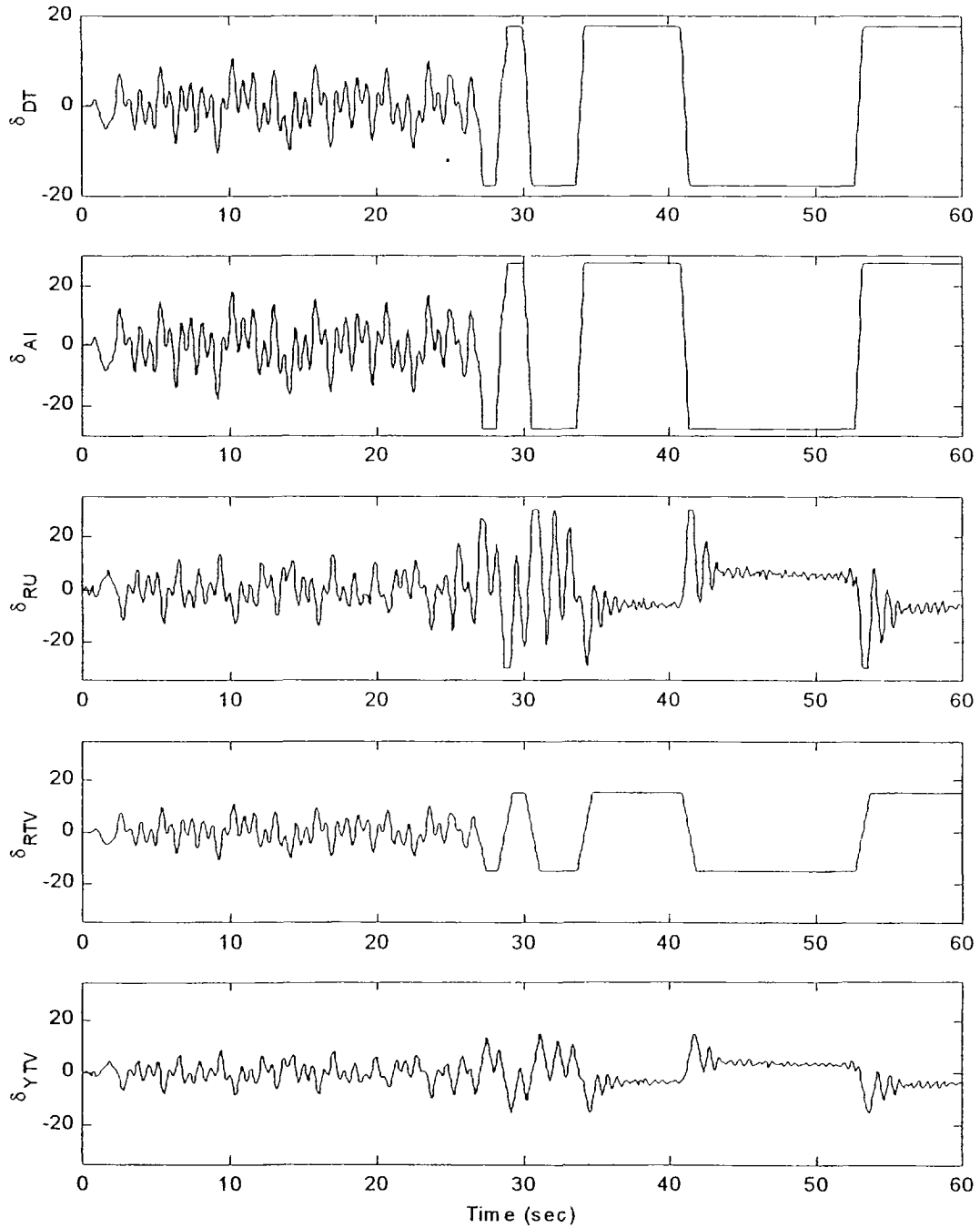
This design results in excellent tracking in the nominal case. Although not shown here, the nominal tracking performance is comparable to the SMC design and gives Level I handling qualities. Next, this design is exercised with a system failure (Failure #1) at time  $t = 25$  sec. Figure 4-75 shows the outer loop bank angle tracking performance. The system goes unstable immediately after the failure. Figure 4-76 shows that the inner loop variables are unstable after the failure. Figure 4-77 and Figure 4-78 show that all the actuators are driven to their limits.



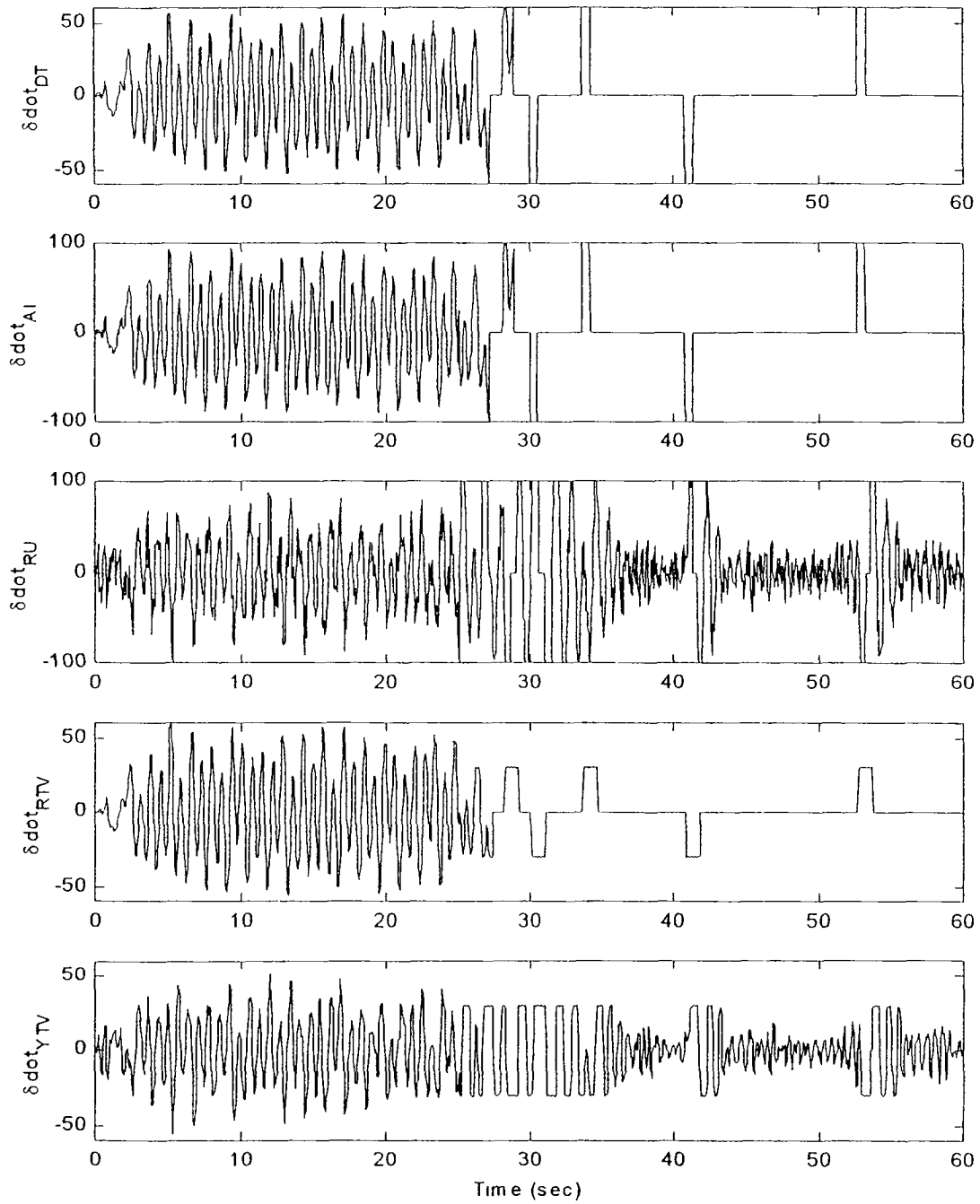
**Figure 4-75: Outer Loop Tracking ( $\phi$ ), F-18/HARV, with Loop Shaped Controller, Actuators, and Noise, Failure #1 at  $t = 25$  sec**



**Figure 4-76: Inner Loop Tracking ( $p_s$  and  $\beta$ ), F-18/HARV, with Loop Shaped Controller, Actuators, and Noise, Failure #1 at  $t = 25$  sec**

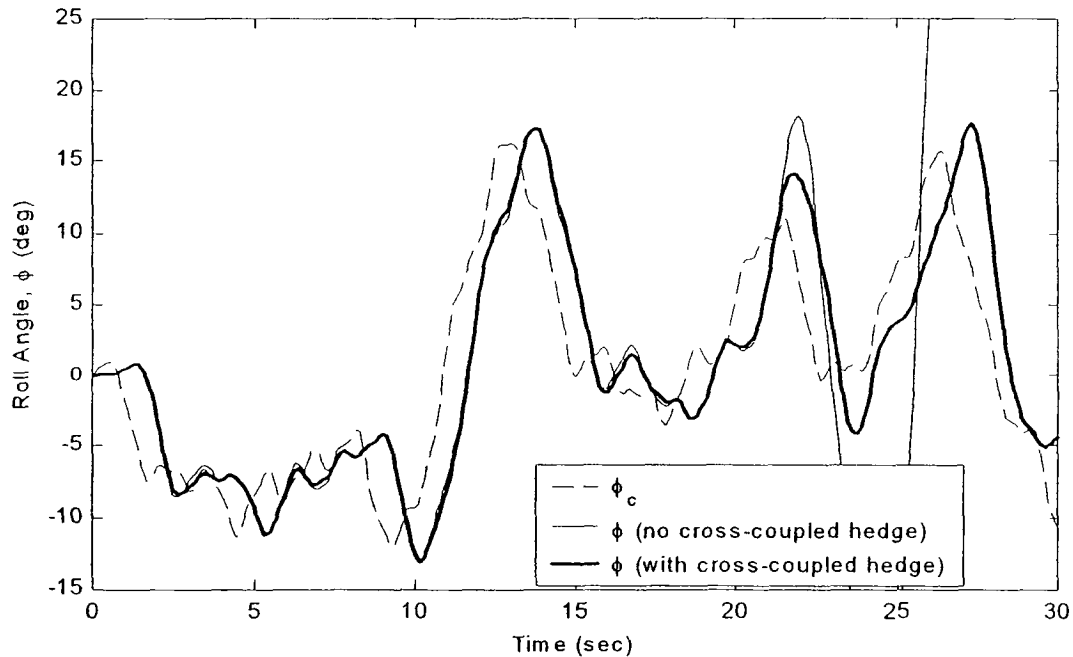


**Figure 4-77: Actuator Deflections, F-18/HARV, with Loop Shaped Controller and Noise, Failure #1 at  $t = 25$  sec**



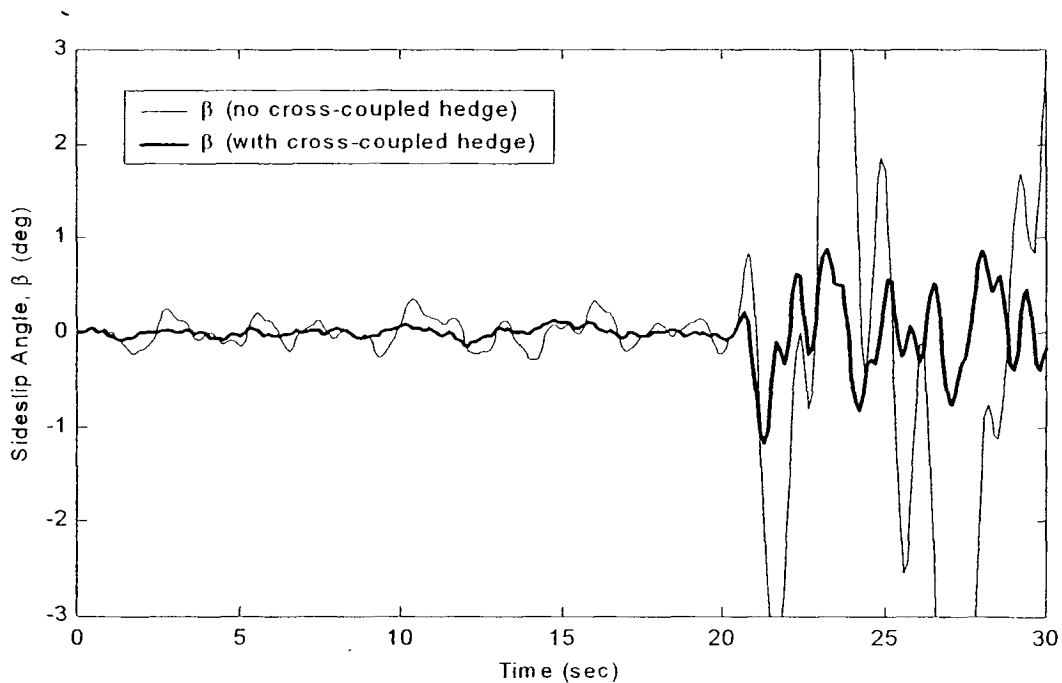
**Figure 4-78: Actuator Rates, F-18/HARV, with Loop Shaped Controller and Noise, Failure #1 at  $t = 25$  sec**

This flight condition and failure provide an excellent example to illustrate the effects of cross-coupled hedging. In all the previous examples, the SMC design included hedging of the cross-coupled terms. It was noted that, in the nominal case, excluding the cross-coupled terms results in slightly better inner loop performance (see Figure 4-59 and Figure 4-60). However, when the actuator dynamics change (as they do in this failure case), the effects of the cross-coupled transfer functions can become significant. Consider a direct comparison of including the cross-coupled hedge models and excluding them. Figure 4-79 shows the roll angle tracking performance for these two cases. Failure #1 occurs at  $t = 20$  sec.



**Figure 4-79: Outer Loop Tracking ( $\phi$ ), SMC with and without Cross-Coupled Hedging**

Figure 4-80 shows the  $\beta$  tracking performance.

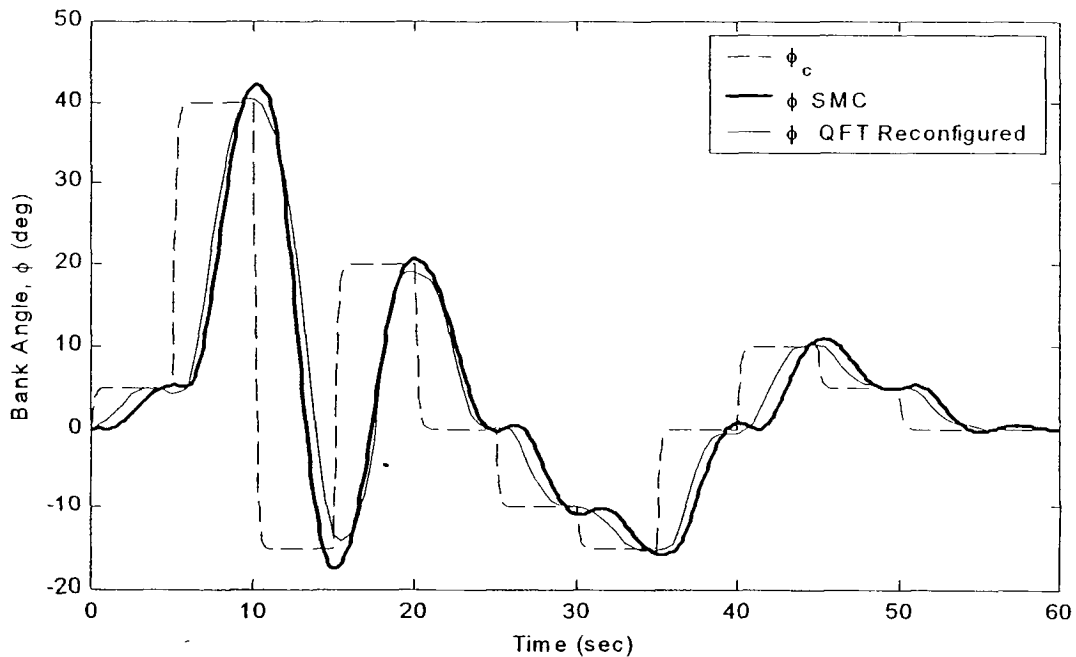


**Figure 4-80: Inner Loop Tracking ( $\beta$ ), SMC with and without Cross-Coupled Hedging**

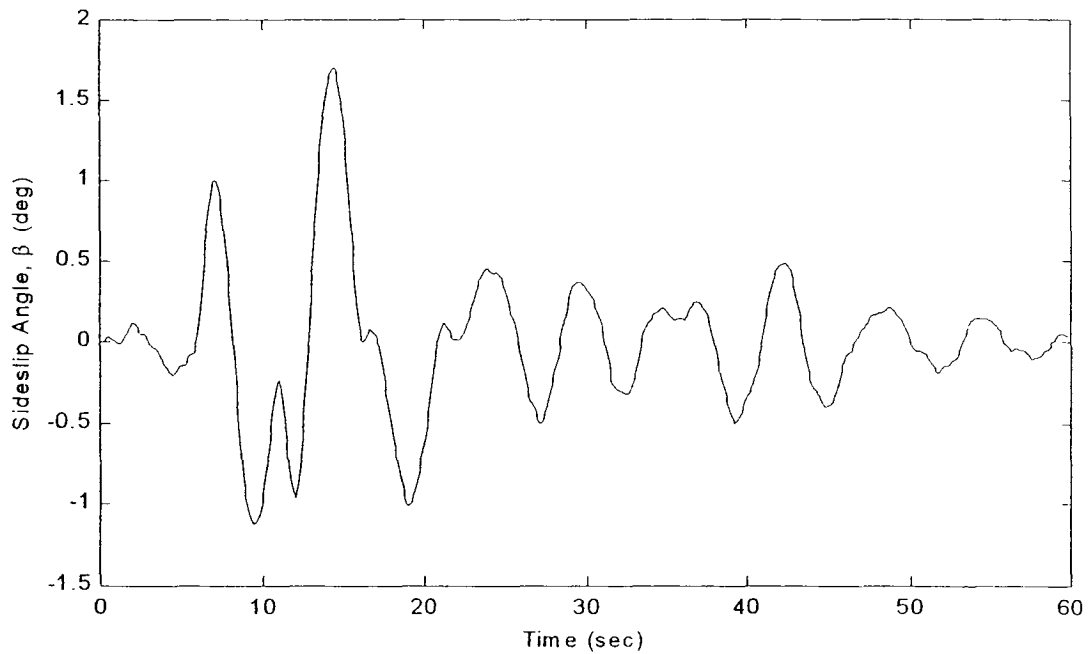
Several points are worthy of mention. First of all, while the roll rate tracking is essentially the same for both cases in the nominal system, the hedge model with no cross-coupling results in an unstable system in the failed case. Further, the cross-coupled hedge model provides much better  $\beta$  tracking even in the nominal case. Sideslip excursions are an order of magnitude less. It is concluded that if the nominal system has strong cross-coupling, hedging of these cross-coupled channels should be considered.

Next, to compare this SMC controller with another reconfigurable controller, a new failure condition is used. Failure #2 is defined as follows: nominal plant, 90% reduction in yaw thrust vector effectiveness (gain = 0.1, position limits =  $\pm 3.0$  deg, rate limits =  $\pm 6.0$  deg/sec). This is a failure used in a previous work.<sup>146</sup> In order to directly

compare results, the same input signal is also used. The input is a series of steps filtered by  $\left(\frac{100}{s^2 + 20s + 100}\right)\left(\frac{1}{s^2 + 2s + 1}\right)$ . In the reference work, the reconfigurable design approach utilizes dynamic inversion, QFT, and least-mean square adaptive filtering<sup>146</sup>. The control laws take about 10 to 20 seconds to converge to their reconfigured states. The results in Figure 4-81 show the fully reconfigured QFT model<sup>146</sup> and the SMC design developed here. Figure 4-82 shows the corresponding tracking for  $\beta$  with the SMC controller.



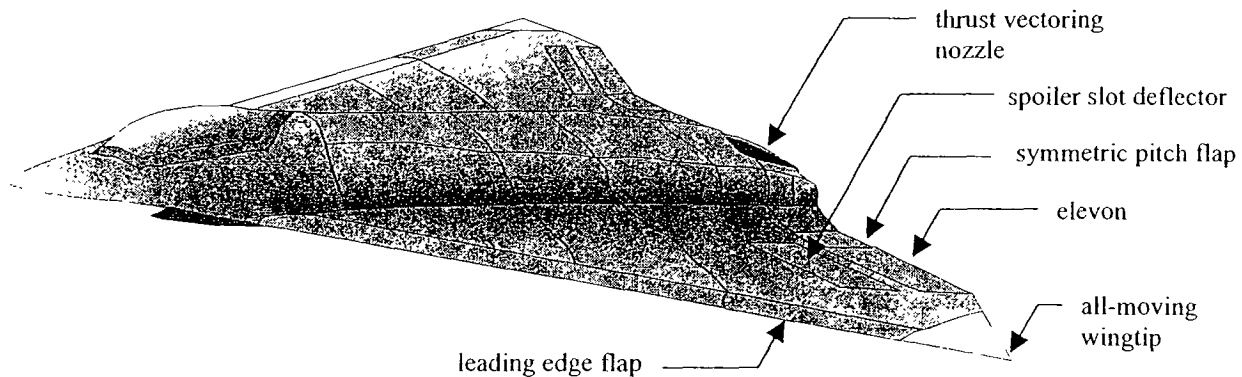
**Figure 4-81: Outer Loop Tracking ( $\phi$ ), F-18/HARV, SMC vs Reconfigured QFT, Failure #2 at  $t = 0$  sec**



**Figure 4-82:  $\beta$  Tracking, F-18/HARV, SMC, Failure #2 at  $t = 0$  sec**

The inner loop tracking, actuator position, and actuator rate plots do not add anything to this comparison, so they are not shown. As seen in Figure 4-81, the observer-based SMC with hedging provides very comparable tracking results to the fully reconfigured QFT system.<sup>146</sup> More importantly, the SMC accomplishes this with no adaptation time. Additionally, the control architecture of reconfigurable QFT system<sup>146</sup> is considerably more complex than the design developed here.

#### 4.7 Application Example: ICE MIMO 6-DOF Model



**Figure 4-83: Innovative Control Effectors (ICE) Aircraft**

The Innovative Control Effectors (ICE) aircraft is developed by Lockheed under an Air Force Research Laboratories (AFRL) sponsored program and is the vehicle of choice for many controls applications in the current literature.<sup>18,19,21,25,48,56,66,79,80,110,147</sup> It is a single engine, multi-role, supersonic, tailless fighter aircraft in the 38,000 lb (gross takeoff weight) class. It has a 65 degree sweep delta wing and an internal weapons carriage bay. The configuration incorporates all-aspect low observable technologies and is sized for a 1,100 nautical mile air-to-ground mission.<sup>25</sup> As illustrated in Figure 4-83, the conventional control effectors include elevons, symmetric pitch flaps, and outboard leading edge flaps. The innovative control effectors include pitch and yaw thrust vectoring, all moving tips, and spoiler slot deflectors. The all moving tips and spoiler slot deflectors have zero lower deflections limits.

The static aerodynamic force and moment data were collected by NASA Langley Research Center and AFRL using wind tunnel tests with a 1/18<sup>th</sup> scale model. Additional wind tunnel tests during Phase II of the ICE program provide updated data

for simulation models.<sup>25</sup> There are strong multi-axis effects and highly nonlinear interactions between the close-coupled control surfaces. The full nonlinear simulation of the ICE vehicle is proprietary; however, linearized models at various flight conditions (which do not include nonlinear effector interactions) are made available to this research directly from the NASA Langley Research Center.

The flight condition used for this application design is. 1g, wings-level,  $M = 0.3$ ,  $h = 15,000$  ft. The linearized model for this flight condition in state space is given by

$$\mathbf{A} = \begin{bmatrix} 0.005957049 & 0.03198734 & -1.330975822 & -0.545071629 & -0.001257882 & 0 & 0 & 0 \\ -0.063377426 & -0.586254141 & 5.373673826 & -0.135005804 & -0.001903204 & 0.000232091 & 5.74854E-05 & 0 \\ -0.052181448 & 0.081703751 & -0.594369479 & 0 & 0.011258699 & 0.001753944 & 0.000434425 & 0 \\ 0 & 0 & 1 & 0 & 0 & 0 & 0 & 0 \\ 3.32155E-07 & 8.215E-08 & 0 & 0 & 0.011094111 & 1.331849864 & -5.373457339 & 0.54507129 \\ 8.50045E-06 & 2.10115E-06 & 0 & 0 & -1.220701747 & -0.607006478 & 0.395148765 & 0 \\ -2.90151E-06 & -7.15713E-07 & 0 & 0 & -0.126260979 & 0.002970324 & 0.02064623 & 0 \\ 0 & 0 & 0 & 0 & 0 & 1 & 0.247684519 & 0 \end{bmatrix}$$

$$\mathbf{B}^T = \begin{bmatrix} -0.005969294 & -0.267968418 & -1.385041358 & 0 & -0.009123567 & 2.411735136 & 0.037657455 & 0 \\ -0.005969294 & -0.267968418 & -1.385041358 & 0 & 0.009123567 & -2.411735136 & -0.037657455 & 0 \\ -0.004085579 & -0.230586355 & -1.20225331 & 0 & 0 & 0 & 0 & 0 \\ -0.014173739 & -0.084039328 & -0.352069164 & 0 & -0.000248489 & 0.536897487 & -0.05609334 & 0 \\ -0.014173739 & -0.084039326 & -0.352069164 & 0 & 0.000248489 & -0.536903664 & 0.0560923 & 0 \\ -0.02523841 & 0.111216392 & 0.266496208 & 0 & 0.021932906 & -1.196261818 & -0.123503836 & 0 \\ -0.025238416 & 0.111216392 & 0.266496208 & 0 & -0.021932906 & 1.196261818 & 0.123503836 & 0 \\ 0.011499932 & 0.09704284 & 0.233406726 & 0 & -0.028900689 & -0.985320208 & 0.185896833 & 0 \\ 0.011499932 & 0.09704284 & 0.233406726 & 0 & 0.028900689 & 0.985320208 & -0.185896833 & 0 \\ -1.1804E-05 & -0.123946616 & -1.731151121 & 0 & 0 & 0 & 0 & 0 \\ 0 & 0 & 0 & 0 & 0.123946616 & -0.066733456 & -1.227324384 & 0 \end{bmatrix}$$

$$\mathbf{C} = \begin{bmatrix}
 0.970669032 & 0.240419692 & 0 & 0 & 0 & 0 & 0 & 0 \\
 -0.043428009 & 0.17533598 & 0 & 0 & 0 & 0 & 0 & 0 \\
 0 & 0 & 1 & 0 & 0 & 0 & 0 & 0 \\
 0 & 0 & 0 & 1 & 0 & 0 & 0 & 0 \\
 0 & 0 & 0 & 0 & 0.180634155 & 0 & 0 & 0 \\
 0 & 0 & 0 & 0 & 0 & 0.970669034 & 0.240419689 & 0 \\
 0 & 0 & 0 & 0 & 0 & -0.240419689 & 0.970669034 & 0 \\
 0 & 0 & 0 & 0 & 0 & 0 & 0 & 1 \\
 0.000185151 & 0.000994198 & 0 & 0 & -3.90962E-05 & 0 & 0 & 0 \\
 1.03237E-08 & 2.55331E-09 & 0 & 0 & 0.000344816 & 2.71661E-05 & 6.72862E-06 & 0 \\
 0.001969834 & 0.018221363 & 0 & 0 & 5.91535E-05 & -7.21362E-06 & -1.7867E-06 & 0
 \end{bmatrix}$$

$$\mathbf{D}^T = \begin{bmatrix}
 0 & 0 & 0 & 0 & 0 & 0 & 0 & 0 & -0.000185532 & -0.00028357 & 0.008328726 \\
 0 & 0 & 0 & 0 & 0 & 0 & 0 & 0 & -0.000185532 & 0.00028357 & 0.008328726 \\
 0 & 0 & 0 & 0 & 0 & 0 & 0 & 0 & -0.000126984 & 0 & 0.007166854 \\
 0 & 0 & 0 & 0 & 0 & 0 & 0 & 0 & -0.000440534 & -7.72328E-06 & 0.002612026 \\
 0 & 0 & 0 & 0 & 0 & 0 & 0 & 0 & -0.000440534 & 7.72328E-06 & 0.002612026 \\
 0 & 0 & 0 & 0 & 0 & 0 & 0 & 0 & -0.000784435 & 0.000681697 & -0.003456716 \\
 0 & 0 & 0 & 0 & 0 & 0 & 0 & 0 & -0.000784435 & -0.000681697 & -0.003456716 \\
 0 & 0 & 0 & 0 & 0 & 0 & 0 & 0 & 0.000357429 & -0.000898262 & -0.003016188 \\
 0 & 0 & 0 & 0 & 0 & 0 & 0 & 0 & 0.000357429 & 0.000898262 & -0.003016188 \\
 0 & 0 & 0 & 0 & 0 & 0 & 0 & 0 & -3.669E-07 & 0 & 0.003852384 \\
 0 & 0 & 0 & 0 & 0 & 0 & 0 & 0 & 0 & 0.003852384 & 0
 \end{bmatrix}$$

The state vector is defined as.

$$\mathbf{x}^T = [u \quad w \quad qb \quad \text{theta} \quad v \quad pb \quad rb \quad \text{phi}]$$

where

$u$   $\equiv$  velocity along body x-axis (ft/s),  $w$   $\equiv$  velocity along body z-axis (ft/s),  $qb$   $\equiv$  body axis pitch rate (deg/s),  $\text{theta}$   $\equiv$  Euler pitch angle (deg),  $\text{betaw}$   $\equiv$  sideslip angle (deg),  $v$   $\equiv$  velocity along body y-axis (ft/s),  $pb$   $\equiv$  body axis roll rate (deg/s),  $rb$   $\equiv$  body axis yaw rate (deg/s),  $\text{phi}$   $\equiv$  Euler bank angle (deg).

The output vector is defined as

$$y^T = [\text{vel} \quad \text{alphaw} \quad \text{qb} \quad \text{theta} \quad \text{betaw} \quad \text{ps} \quad \text{rs} \quad \text{phi} \quad \text{axcg} \quad \text{aycg} \quad \text{azcg}]$$

where

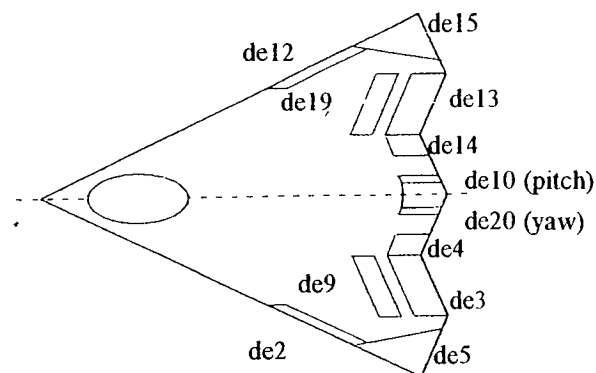
vel  $\equiv$  true airspeed (ft/s), alphaw  $\equiv$  angle of attack (deg), qb  $\equiv$  body axis pitch rate (deg/s), theta  $\equiv$  Euler pitch angle (deg), betaw  $\equiv$  sideslip angle (deg), ps  $\equiv$  stability axis roll rate (deg/s), rs  $\equiv$  stability axis yaw rate (deg/s), phi  $\equiv$  Euler bank angle (deg), axcg  $\equiv$  longitudinal acceleration at c.g. (g's), aycg  $\equiv$  lateral acceleration at c.g. (g's), azcg  $\equiv$  normal acceleration at c.g. (g's)

The control vector is defined as

$$u^T = [\text{de3} \quad \text{de13} \quad \text{de4} \quad \text{de5} \quad \text{de15} \quad \text{de9} \quad \text{de19} \quad \text{de2} \quad \text{de12} \quad \text{de10} \quad \text{de20}]$$

where (see Figure 4-84)

de3/de13  $\equiv$  left/right elevon deflection (deg), de4  $\equiv$  symmetric pitch flap deflection (deg), de5/de15  $\equiv$  left/right all moving tip deflection (deg), de9/de19  $\equiv$  left/right spoiler slot deflector angle (deg), de2/de12  $\equiv$  left/right outboard leading edge flap deflection (deg), de10  $\equiv$  pitch nozzle deflection (deg), de20  $\equiv$  yaw nozzle deflection (deg).



**Figure 4-84: ICE Control Deflection Definitions**

The healthy actuator dynamics and limits are given in Table 4-5.

	Dynamics	Amplitude Limit	Rate Limit
<b>Elevon</b>	$\frac{(40)(100)}{(s+40)(s+100)}$	$\pm 30$ deg	150 deg/s
<b>Symmetric Pitch Flap</b>	$\frac{(40)(100)}{(s+40)(s+100)}$	$\pm 30$ deg	50 deg/s
<b>All Moving Tip</b>	$\frac{(40)(100)}{(s+40)(s+100)}$	[0, 60] deg	150 deg/s
<b>Spoiler-Slot Deflector</b>	$\frac{(40)(100)}{(s+40)(s+100)}$	[0, 60] deg	150 deg/s
<b>Leading Edge Flap</b>	$\frac{(17.828)(100)}{(s+17.828)(s+100)}$	$\pm 40$ deg	40 deg/s
<b>Pitch/Yaw Thrust Vectoring</b>	$\frac{(37.168)(41.3)}{(s+37.186)(s+41.3)}$	$\pm 15$ deg	60 deg/s

**Table 4-5: ICE Actuator Dynamics and Limits**

A control system which tracks roll rate, angle of attack and sideslip is desired. The next step in the design process is to define a reference model. For this application, the following reference models are chosen:

$$G_{\alpha}(s) = \frac{\alpha_r}{\alpha_c}(s) = \frac{100}{(s^2 + 20s + 100)}$$

$$G_p(s) = \frac{p_r}{p_c}(s) = \frac{100}{(s^2 + 20s + 100)} \quad (4.22)$$

$$G_{\beta}(s) = \frac{\beta_r}{\beta_c}(s) = \frac{100}{(s^2 + 25s + 100)}$$

Next, the desired square system feedback architecture is defined. This is given in Figure 4-85. The inner loop has an angle of attack, roll rate, and a sideslip angle feedback loop which are controlled by the SMC. A zero sideslip is commanded; and a pilot closes an outer loop to control the angle of attack and Euler roll angle.

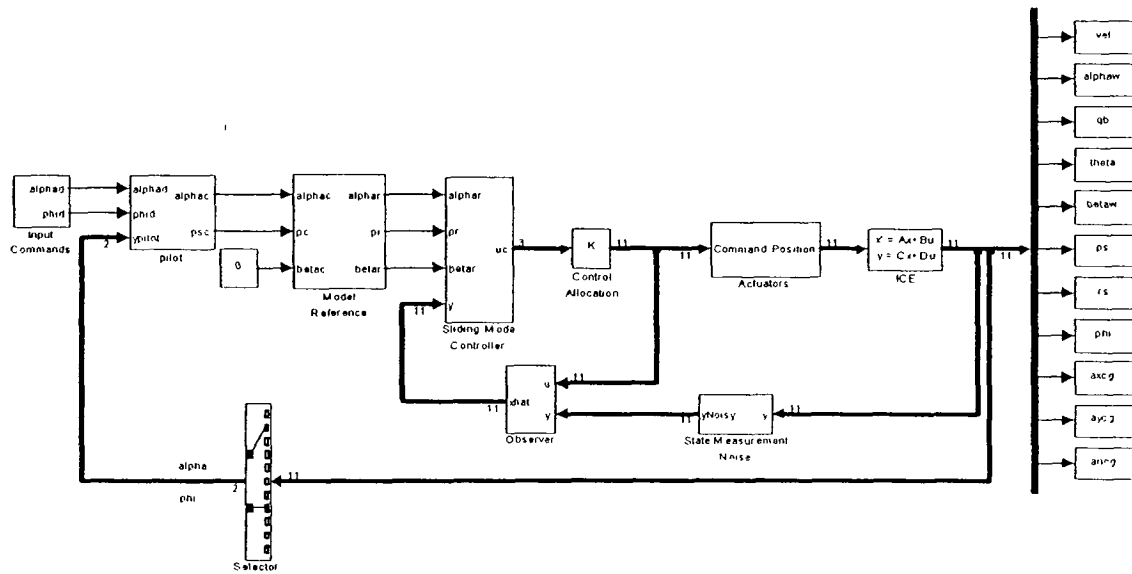


Figure 4-85: ICE System Block Diagram

The controller to be designed outputs commands for angle of attack, stability axis roll rate, and side slip angle. These demands are allocated to the eleven control effectors using a pseudo-inverse approach (see Eqn ( 1.23 )). If the preferred actuator positions are assumed to be zero, the solution to the control allocation problem using a pseudo-inverse is

$$B_k = W_u^{-1} B^T (B W_u^{-1} B^T)^{-1} \tag{ 4.23 }$$

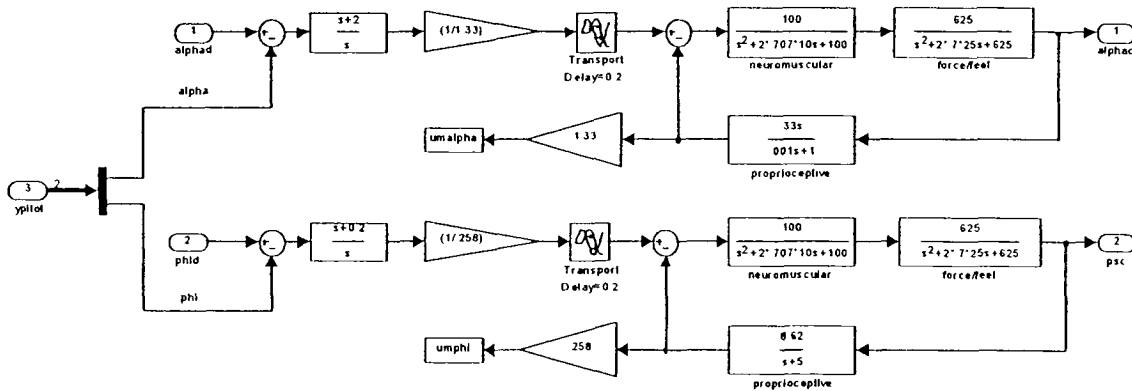
With weighting matrix,  $W_u = \text{diag}[2,2,1,1,1,1,1,1,1,1,1]$ , and the spoilers artificially removed from the pitch channel, the control distribution used in the design is

$$\mathbf{B}_k = \begin{bmatrix} -0.773 & 0.107 & -0.097 \\ -0.773 & -0.107 & 0.097 \\ -1.33 & 0 & 0 \\ -0.485 & 0.048 & 0.055 \\ -0.485 & -0.048 & -0.055 \\ 0 & -0.104 & 1.06 \\ 0 & 0.104 & -1.06 \\ 0.560 & -0.0920 & -1.73 \\ 0.560 & 0.0920 & 1.73 \\ -0.715 & 0 & 0 \\ 0 & 0.01 & 6.87 \end{bmatrix} \quad (4.24)$$

The input command profiles for angle of attack and roll angle are sum-of-sines functions defined in Eqn. ( 4.13 ). The sum-of-sines parameters are those given in Table 4-2. The overall amplitude gain in Eqn. ( 4.13 ) for the  $\alpha$ -channel is  $\xi = 5$ . The overall amplitude gain for the  $\phi$ -channel is  $\xi = 10$ . Additionally, the  $i = 1,7$  sine functions for the  $\phi$ -channel have phase offsets of  $\left( i \cdot \frac{\pi}{4} \right)$  in order to prevent correlation with the  $\alpha$ -channel.

The measured variables include the full output vector given above. The measurement noise for each channel is assumed to be band-limited white noise filtered by  $\frac{100}{s^2 + 20s + 100}$  and multiplied by a gain. All variables except  $\alpha$  and  $\beta$  have a noise gain of 0.1414, resulting in an RMS noise value of approximately 0.07 deg/s.  $\alpha$  and  $\beta$  have a noise gain of 0.0707, resulting in an RMS noise value of approximately 0.035 deg.

Assuming the inner loop SMC provides the desired model reference tracking, the apparent system models that the pilot “sees” are the model references. Therefore, the pilot models,<sup>138,144,145</sup> based on the reference models given, are shown below



**Figure 4-86: Pilot Models for ICE Angle of Attack and Roll Angle Tracking Tasks**

The next step is to define the desired sliding manifolds. The system (without actuators) has a relative order of 1 for all three control variables. Therefore, the form of the sliding manifolds are

$$\sigma = K_0 e + K_{-1} \int e \, d\tau, \quad e = \{(\alpha_r - \hat{\alpha}), (p_r - \hat{p}), (\beta_r - \hat{\beta})\}^T \quad (4.25)$$

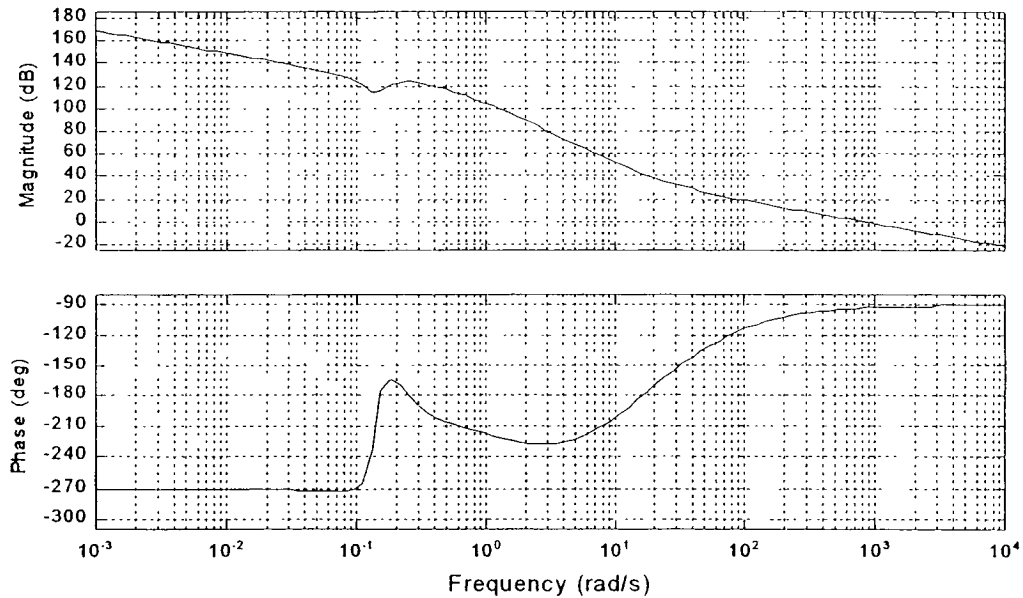
The control laws, assuming the use of a boundary layer, then can be expressed in linear form as

$$\begin{aligned} u_{c\alpha}(s) &= K_{p\alpha} \left( \frac{K_{0\alpha} s + K_{-1\alpha}}{s} \right) \\ u_{c\phi}(s) &= K_{p\phi} \left( \frac{K_{0\phi} s + K_{-1\phi}}{s} \right) \\ u_{c\beta}(s) &= K_{p\beta} \left( \frac{K_{0\beta} s + K_{-1\beta}}{s} \right) \end{aligned} \quad (4.26)$$

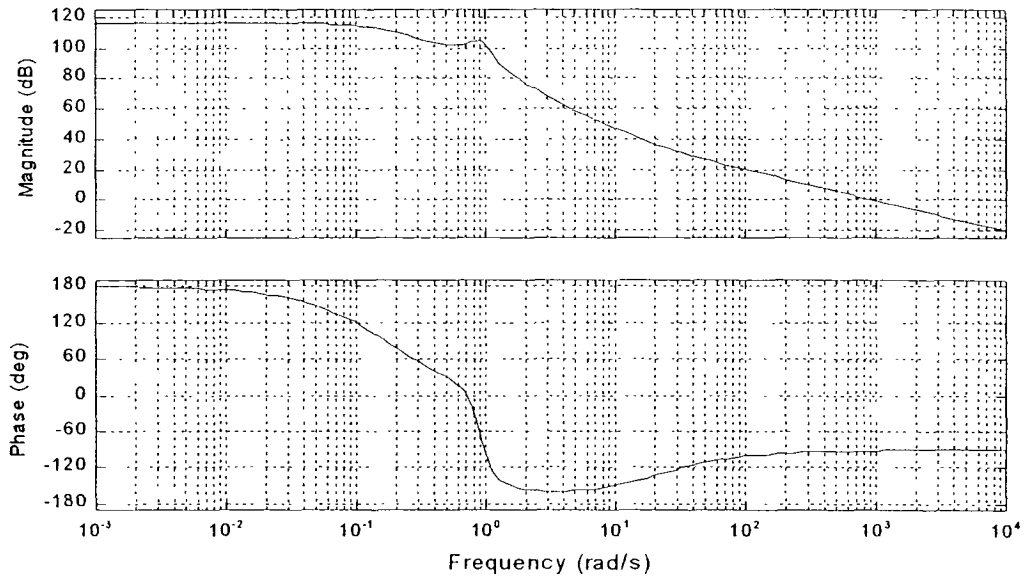
This gives one zero to place and a gain to set for each loop during the loop-shaping design. Using a traditional sequential loop shaping technique, the parameters of Eqn. (4.26) are determined--with roll rate being the first loop to close, followed by  $\alpha$ ;

then  $\beta$ . The designed manifolds are given in Eqn. ( 4.27 ), and the design Bode plots are shown below. A crossover frequency of  $\omega = 1000$  rad/s is set for each channel.

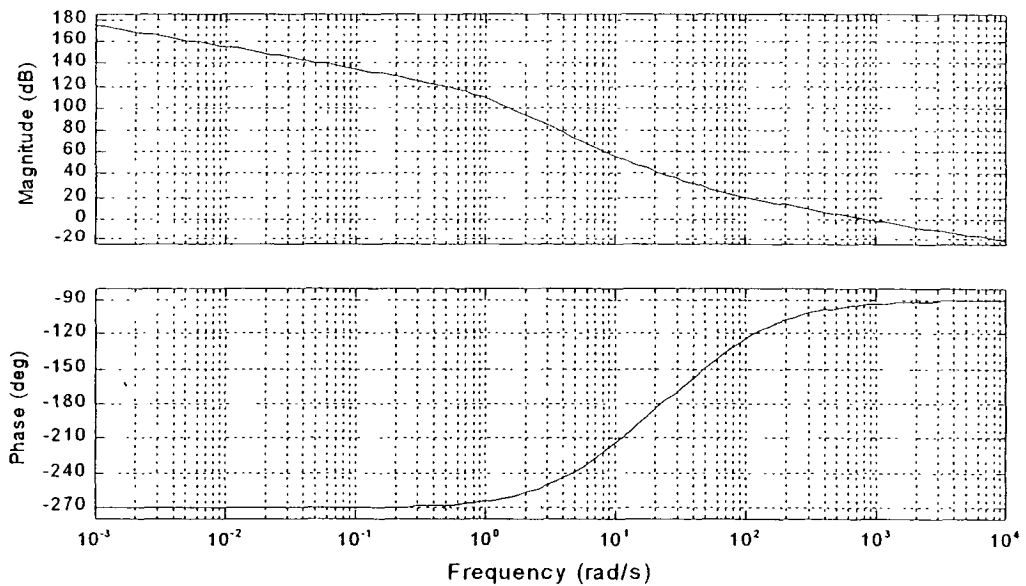
$$\begin{aligned} u_{c\alpha}(s) &= 5000 \left( \frac{s+10}{s} \right) \\ u_{cp}(s) &= 1000 \left( \frac{s+20}{s} \right) \\ u_{c\beta}(s) &= 5000 \left( \frac{s+10}{s} \right) \end{aligned} \quad (4.27)$$



**Figure 4-87: ICE  $\alpha$ -Loop Transmission of Compensator\*Plant,  $p$ -Loop Open,  $\beta$ -Loop Open**

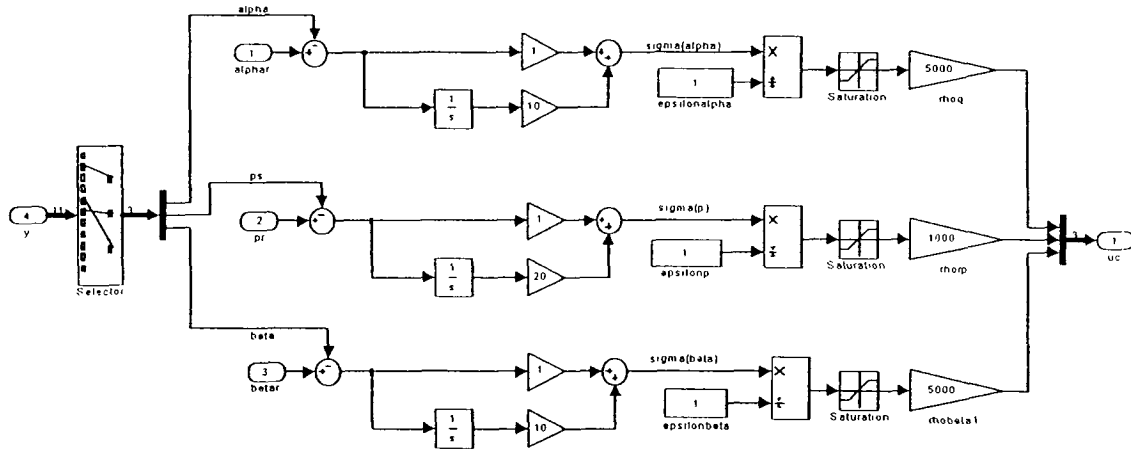


**Figure 4-88: ICE p-Loop Transmission of Compensator\*Effective Plant,  $\alpha$ -Loop Closed,  $\beta$ -Loop Open**



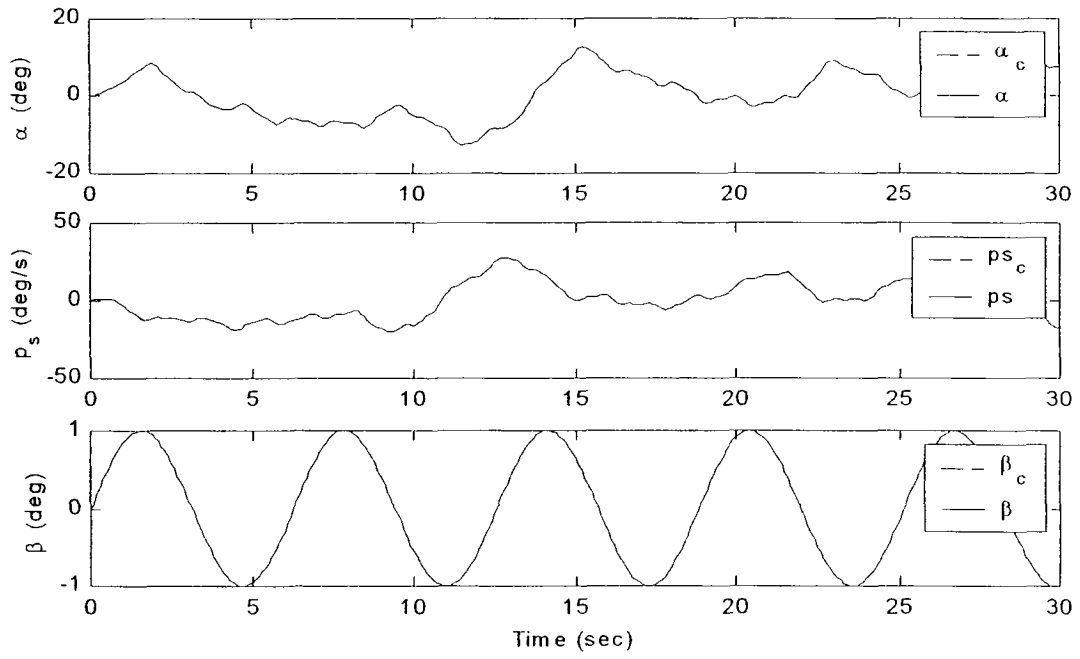
**Figure 4-89: ICE  $\beta$ -Loop Transmission of Compensator\*Effective Plant,  $\alpha$ -Loop Closed, p-Loop Closed**

The initial design of the SMC is complete and is shown in Figure 4-90

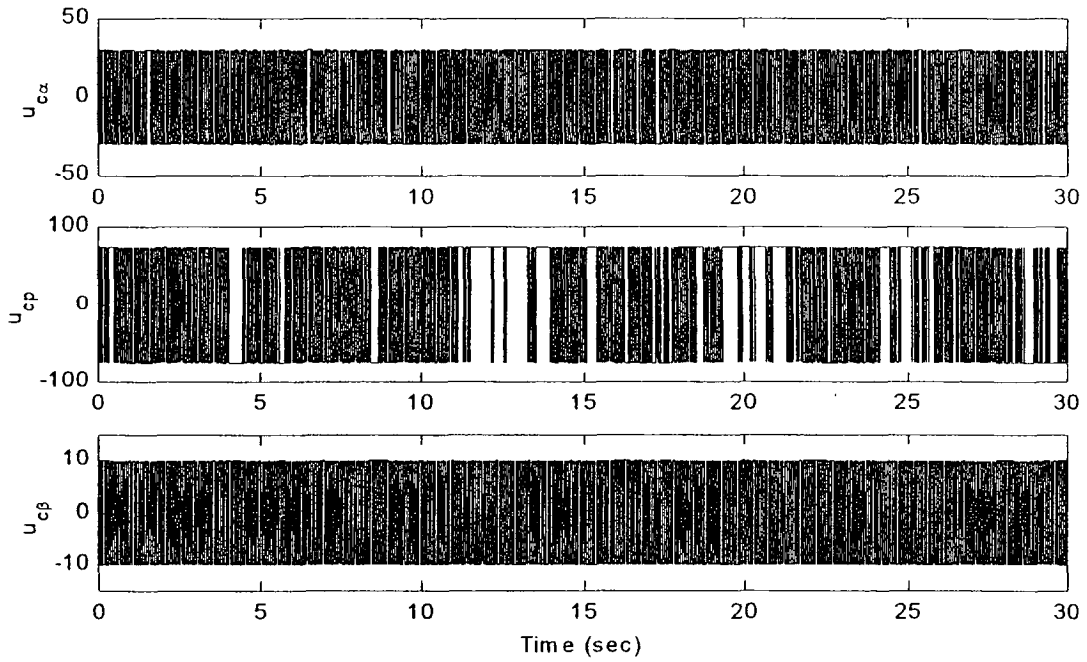


**Figure 4-90: SMC Controller for ICE**

The fifth step in the design process is to verify that the SMC is working properly. Either replace the saturation elements in Figure 4-90 with a signum function or make the boundary layer very small. Figure 4-91 and Figure 4-92 show the SMC inner loop tracking of the control variables and the SMC control effort. This Simulink<sup>®</sup> simulation is run with signum functions in the SMC and a time step of  $\Delta t = 0.0005$  sec. A system plant failure occurs at  $t = 10$  sec. Although the  $\beta$  input will be a constant zero for the final simulation, a simple sine wave is used here to verify decoupled tracking of  $\alpha$ ,  $p_s$ , and  $\beta$ .



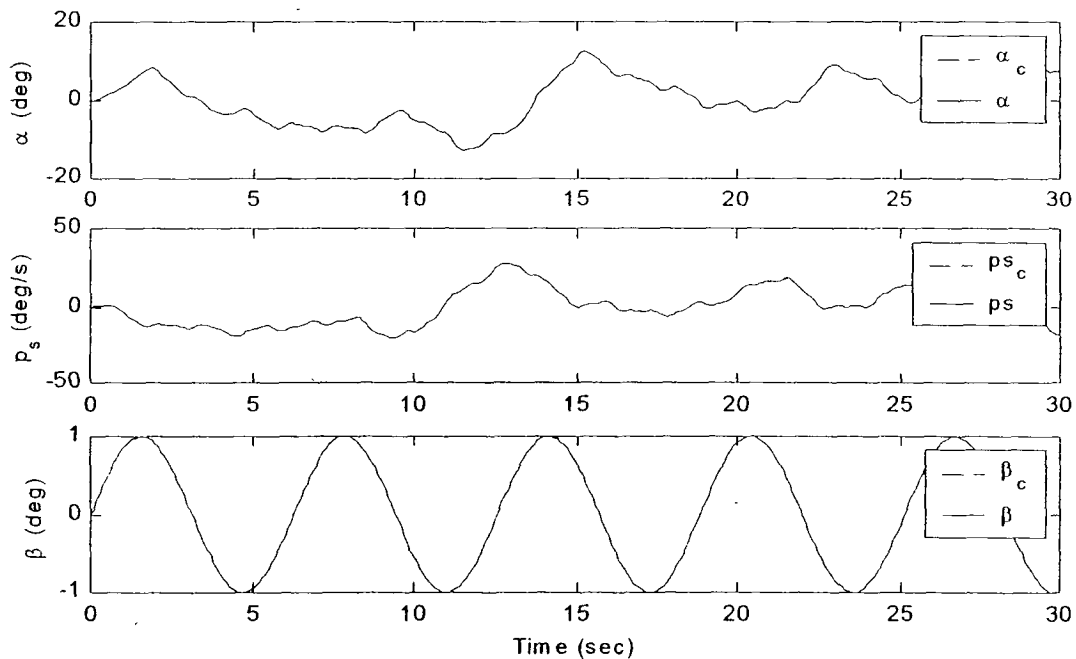
**Figure 4-91: ICE Inner Loop SMC Tracking**



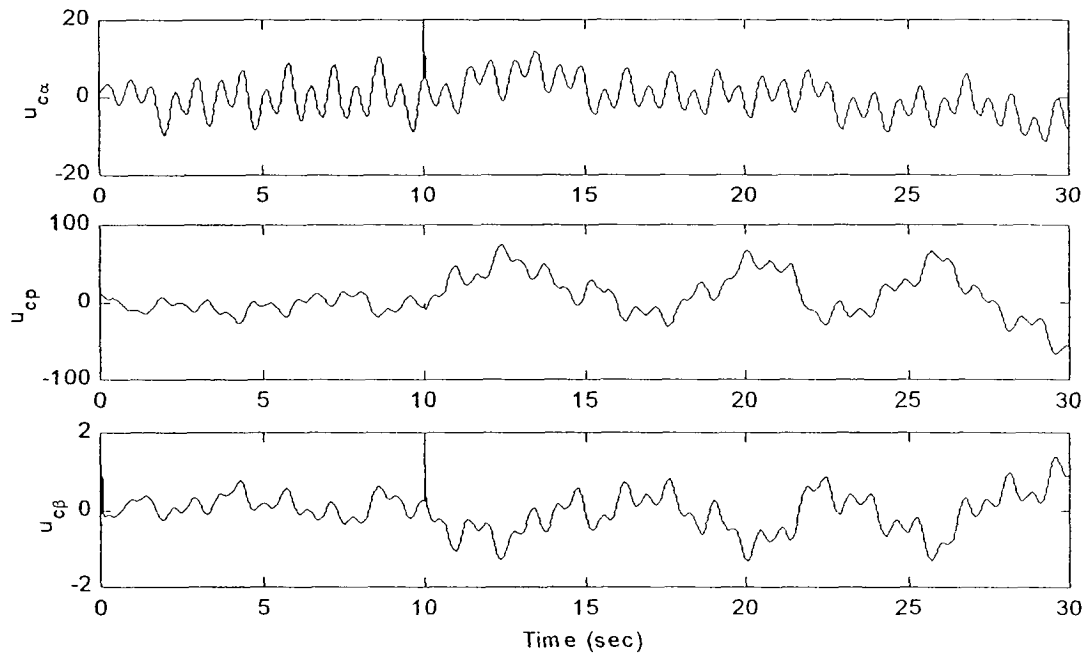
**Figure 4-92: ICE Inner Loop SMC Control Outputs**

As expected, the SMC performs very well and is invariant to the system parameter changes. The control output shows the classic high frequency switching. Note, also that the controller achieves decoupled tracking of  $\alpha$ ,  $p_s$  and  $\beta$ , as desired.

Next, the boundary layer is increased until a continuous control signal is achieved. For this model,  $\varepsilon = 1$  is chosen for all three channels. The resulting time history of the inner loop tracking of  $\alpha$ ,  $p_s$  and  $\beta$  is shown in Figure 4-93. The corresponding SMC control efforts are shown in Figure 4-94. Again, the performance is excellent, even in the face of a large system failure. Also, the control signal is now continuous. Note the large spike in the control signal at the time of failure and the increased overall magnitude of the required control signal after the failure.

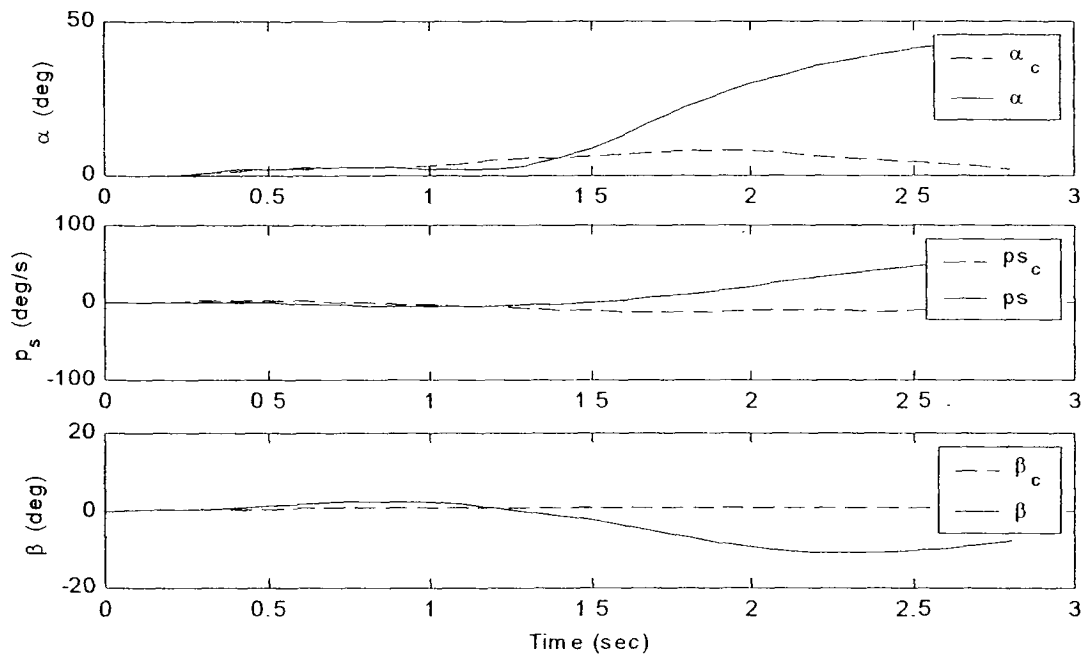


**Figure 4-93: ICE Inner Loop SMC Tracking with Boundary Layer**



**Figure 4-94: ICE SMC Control Outputs with Boundary Layer**

The SMC design is now complete, the resulting tracking performance is remarkably good, and the system is (nearly) invariant to system parameter changes. The next step is the inclusion of the actuators. Figure 4-95 shows the inner loop tracking results with the actuators now included. As expected, the nominal system goes unstable.



**Figure 4-95: Inner Loop Tracking, Nominal ICE, SMC with Actuators**

The next steps are to design the observers and hedge models. As introduced in Section 3.3, the individual Bode plots of the equivalent plant/observer transfer functions with unity feedback ( $\frac{\hat{\alpha}}{u_{c\alpha}}$ ,  $\frac{\hat{p}}{u_{cp}}$  and  $\frac{\hat{\beta}}{u_{c\beta}}$ ) are examined for varying observer speeds (with no hedging). Observer speeds of 100, 50, 20, 10, 5, and 1 rad/s are tried. The Bode plots for  $\alpha$ ,  $p_s$  and  $\beta$  are shown in Figure 4-96, Figure 4-97, and Figure 4-98 respectively

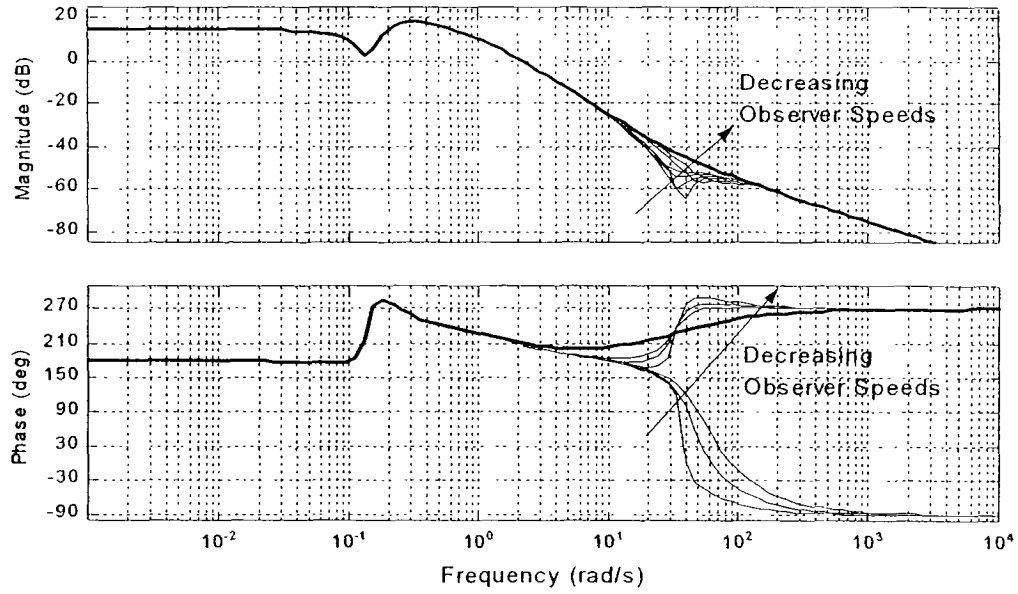


Figure 4-96: Bode Plots,  $\frac{\hat{\alpha}}{u_{ca}}$ , ICE, Various Observer Speeds

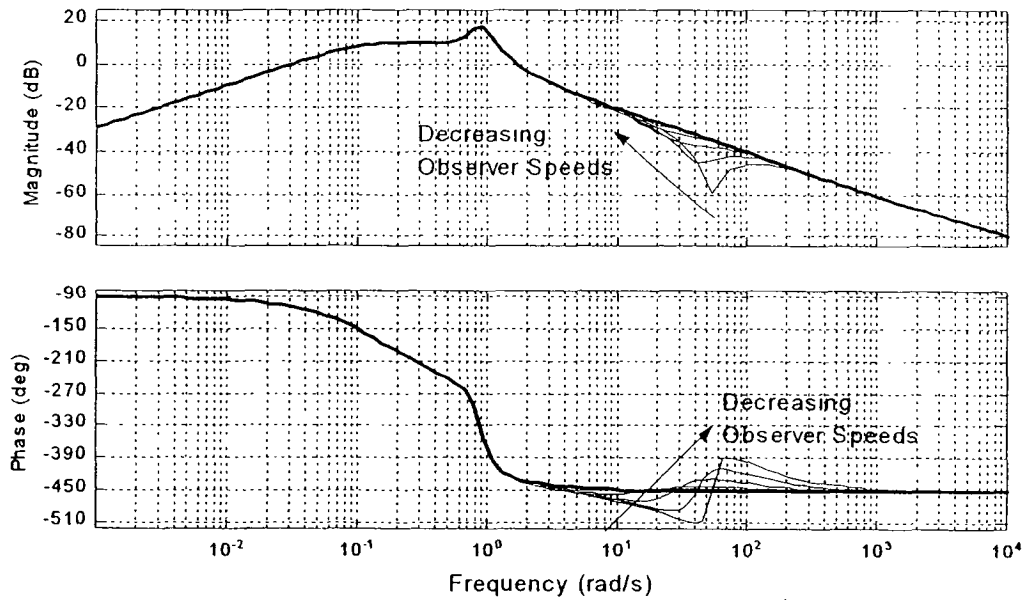


Figure 4-97: Bode Plots,  $\frac{\hat{p}}{u_{cp}}$ , ICE, Various Observer Speeds

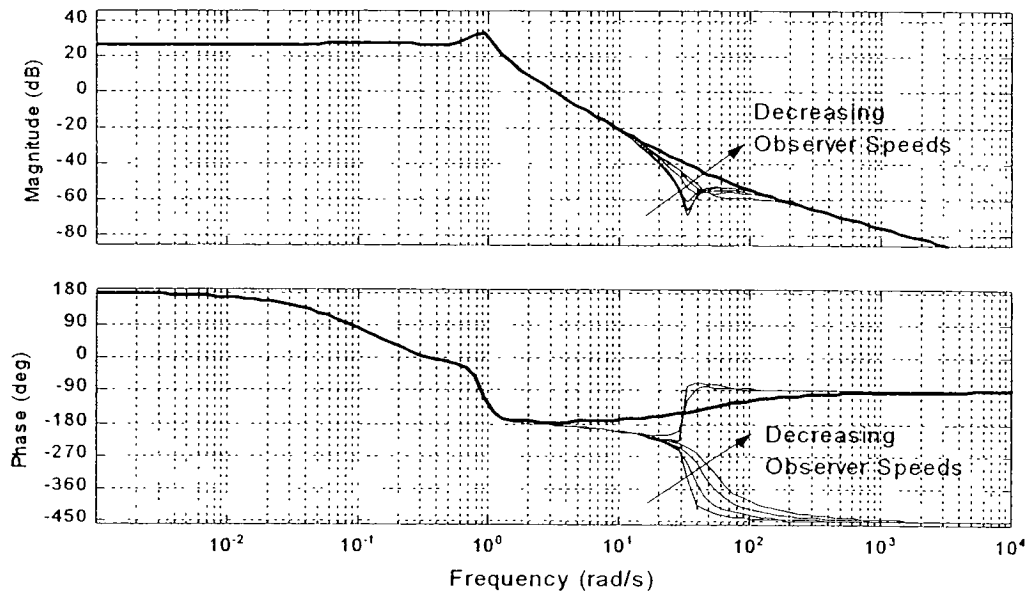
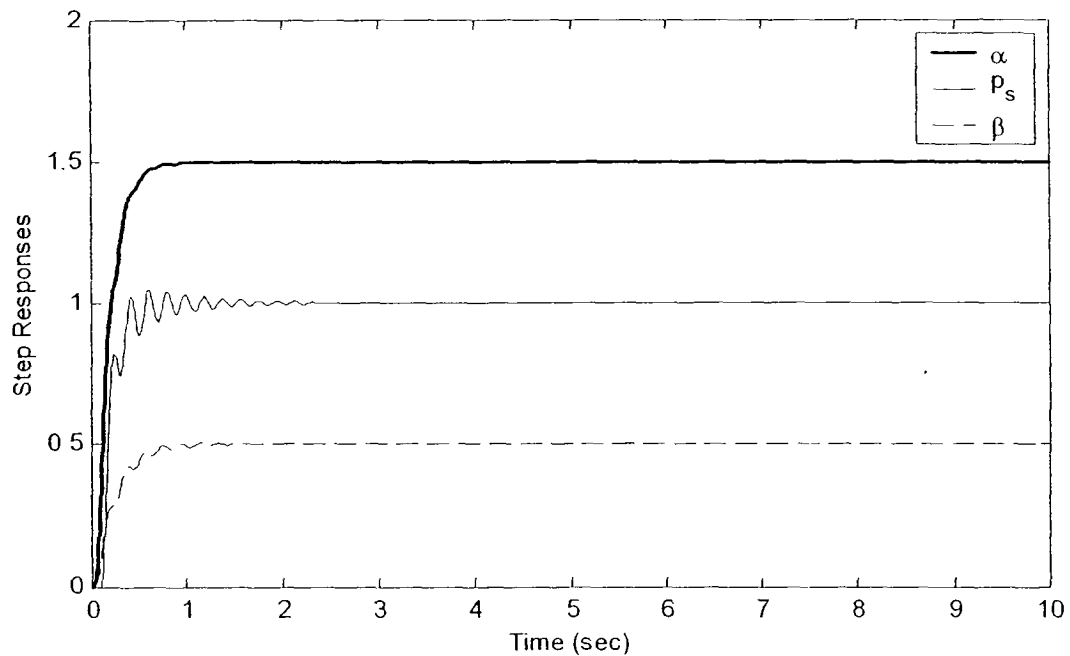


Figure 4-98: Bode Plots,  $\frac{\hat{\beta}}{u_{cp}}$ , ICE, Various Observer Speeds

These plots show that the  $\alpha$ -channel observer must run at 10 rad/s or less; the p-channel observer can run as fast as 100 rad/s, and the  $\beta$ -channel must run at 5 rad/s or less. It appears that hedging will help some in the  $\alpha$ -channel, is not necessary in the p-channel, and is probably required in the  $\beta$ -channel. Select 5 rad/s, 10 rad/s, and 1 rad/s for the  $\alpha$ , p, and  $\beta$  observers respectively and check the step responses without hedging. Step inputs of  $u_\alpha = 1.5$ ,  $u_p = 1.0$ , and  $u_\beta = 0.5$  are used. The results are shown in Figure 4-99. It is clear that hedging is required in the  $\beta$ -channel, and there appears to be undesirable cross-coupling between  $p_s$  and  $\beta$ .



**Figure 4-99: Inner Loop Step Responses, ICE, SMC with Observers**

Before designing the hedge models, the transfer functions of the cross-coupled variables are examined. The Bode plots of the open loop transfer functions for the nominal plant are given below. Figure 4-100 shows the angle of attack transfer functions ( $\alpha$  to  $\alpha$ -command,  $\alpha$  to  $p$ -command, and  $\alpha$  to  $\beta$ -command). Figure 4-101 shows the stability axis roll rate transfer functions ( $p$  to  $\alpha$ -command,  $p$  to  $p$ -command, and  $p$  to  $\beta$ -command). Figure 4-102 shows the sideslip angle transfer functions ( $\beta$  to  $\alpha$ -command,  $\beta$  to  $p$ -command, and  $\beta$  to  $\beta$ -command).

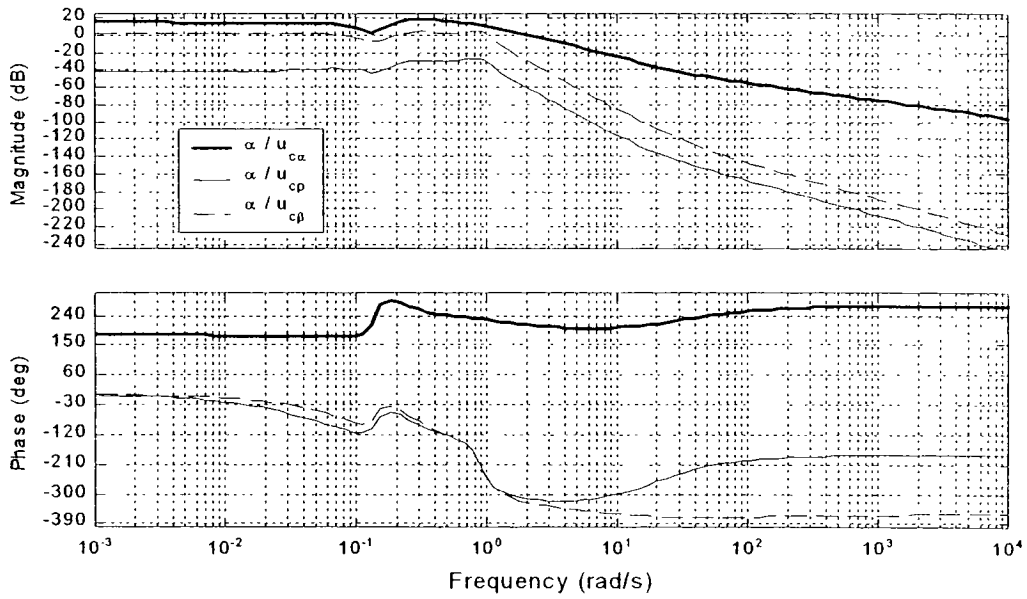


Figure 4-100: Bode Plots,  $\frac{\alpha}{u_{c\alpha}}$ ,  $\frac{\alpha}{u_{cp}}$  and  $\frac{\alpha}{u_{c\beta}}$ , ICE Nominal Vehicle

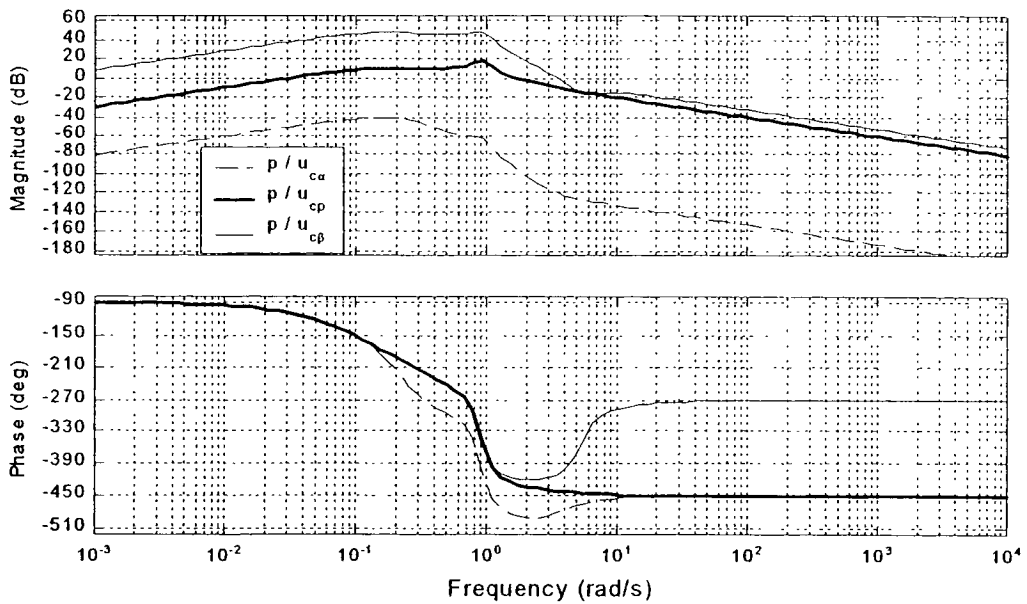
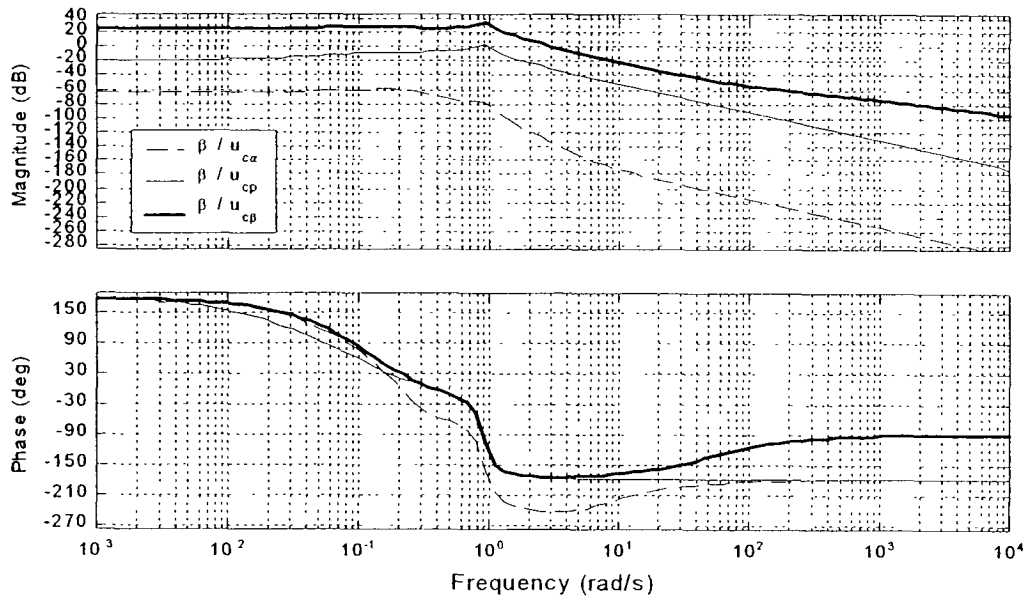


Figure 4-101: Bode Plots,  $\frac{p}{u_{c\alpha}}$ ,  $\frac{p}{u_{cp}}$  and  $\frac{p}{u_{c\beta}}$ , ICE Nominal Vehicle



**Figure 4-102: Bode Plots,  $\frac{\beta}{u_{c\alpha}}$ ,  $\frac{\beta}{u_{c\beta}}$  and  $\frac{\beta}{u_{c\gamma}}$ , ICE Nominal Vehicle**

Figure 4-100 shows some coupling between  $\beta$ -command and  $\alpha$ . Therefore, a  $\frac{\alpha_h}{u_{c\beta}}$  term

will be included in the hedge model. The influence of roll rate command on angle of attack is a couple orders of magnitude less than angle of attack command, so that cross-coupling term will be neglected. Figure 4-101 shows very strong coupling between  $\beta$ -command and  $p_s$ . In fact the cross-coupled term is an order of magnitude greater than

the primary transfer function. The  $\frac{p_h}{u_{c\beta}}$  term must be included in the hedge model

Although Figure 4-102 shows only a weak coupling between  $\beta$  and roll rate command, a

$\frac{\beta_h}{u_{c\beta}}$  term will be included in the hedge model. All other cross-coupling terms are

negligible and will be ignored. Following the design procedures outlined in Section 3.4, the following parameters are chosen for the observer and hedging models.

Channel	Observer Poles
$\alpha$	$\lambda = -10.0, -10.1, -10.2, -10.3, -10.4, -10.5, -10.6, -10.7$
$p_s$	$\lambda = -40.0, -40.1, -40.2, -40.3, -40.4, -40.5, -40.6, -40.7$
$\beta$	$\lambda = -1.0, -1.1, -1.2, -1.3, -1.4, -1.5, -1.6, -1.7$
Hedge Model	
$\frac{\alpha_h}{u_{c\alpha}}$	$\left(\frac{s}{s+10}\right)\left(\frac{4}{s^2+4s+4}\right)$
$\frac{p_h}{u_{cp}}$	$\left(\frac{s}{s+50}\right)\left(\frac{4}{s^2+4s+4}\right)$
$\frac{\beta_h}{u_{c\beta}}$	$\left(\frac{s}{s+5}\right)\left(\frac{2}{s^2+3s+2}\right)$
$\frac{\alpha_h}{u_{c\beta}}$	$0.0001 \left(\frac{s}{s+10}\right)\left(\frac{4}{s^2+4s+4}\right)$ $\alpha$ cross term
$\frac{p_h}{u_{c\beta}}$	$-0.2 \left(\frac{s}{s+50}\right)\left(\frac{64}{s^2+16s+64}\right)$ $p_s$ cross term
$\frac{\beta_h}{u_{cp}}$	$0.02 \left(\frac{s}{s+5}\right)\left(\frac{1}{s^2+2s+1}\right)$ $\beta$ cross term
Hedge Gain	
$\alpha$	1.0
$p_s$	2.0
$\beta$	10.0

**Table 4-6: Observer and Hedge Models for ICE**

The design Bode plots for each channel are given below.

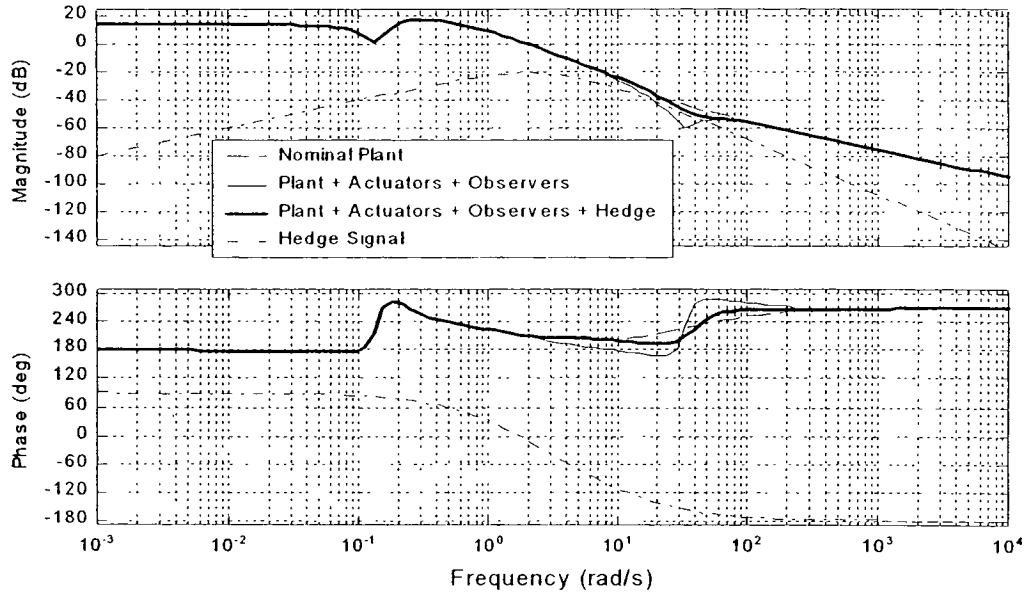


Figure 4-103: Bode Plots,  $\frac{\hat{\alpha}_h}{u_{c\alpha}}$ , ICE Hedge Design

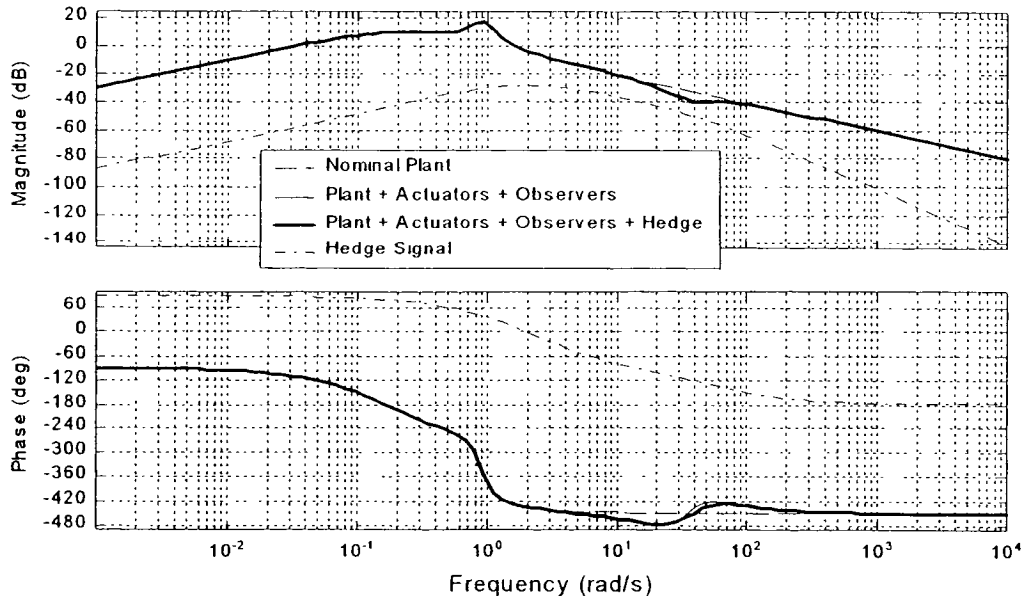


Figure 4-104: Bode Plots,  $\frac{\hat{p}_h}{u_{cp}}$ , ICE Hedge Design

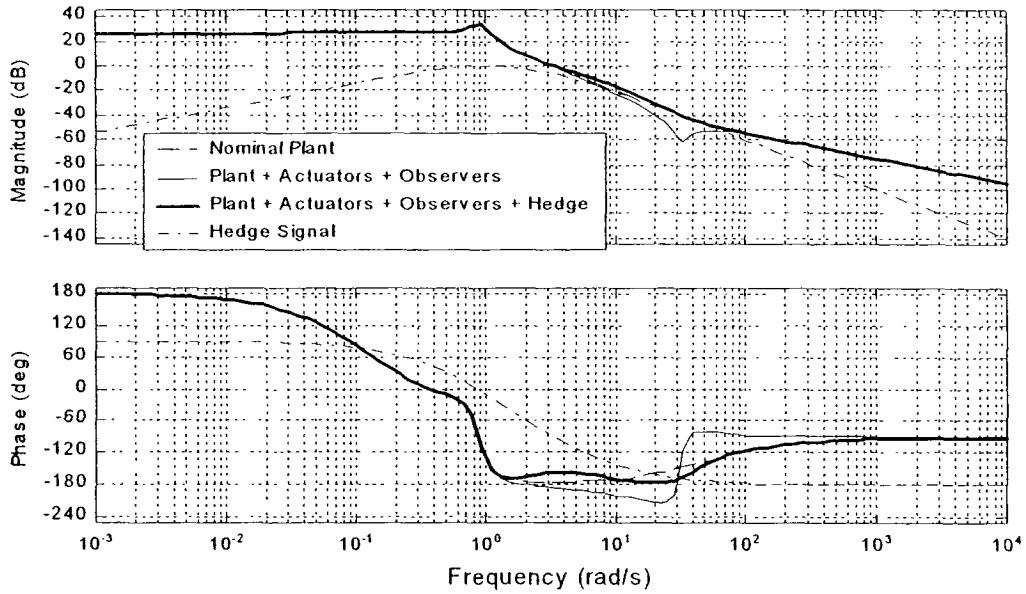


Figure 4-105: Bode Plots,  $\frac{\hat{\beta}_h}{u_{c\beta}}$ , ICE Hedge Design

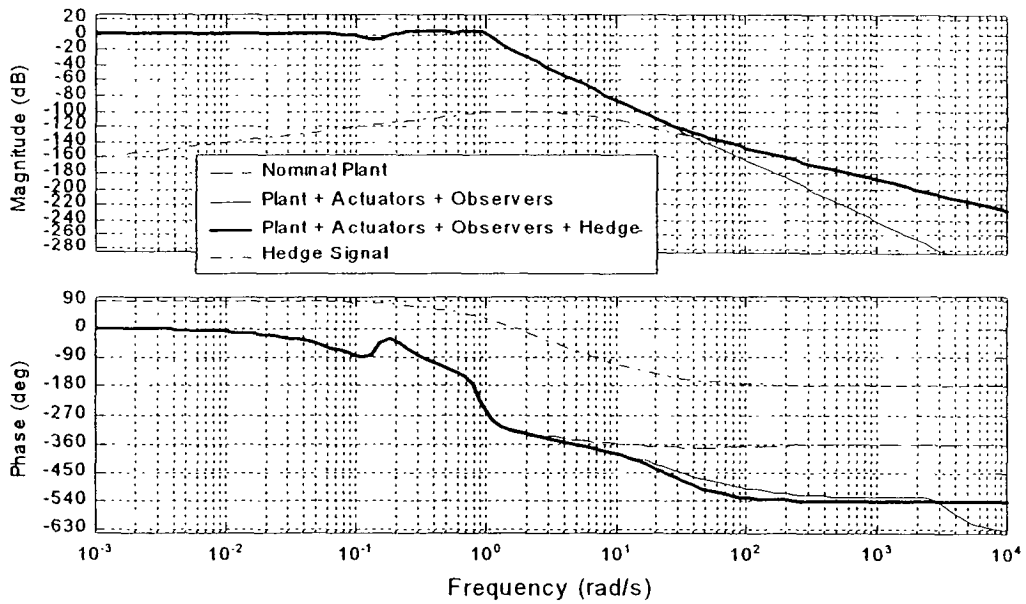


Figure 4-106: Bode Plots,  $\frac{\hat{\alpha}_h}{u_{c\beta}}$  (cross term), ICE Hedge Design

Figure 4-107: Bode Plots,  $\frac{P_h}{u_{cp}}$  (cross term), ICE Hedge Design

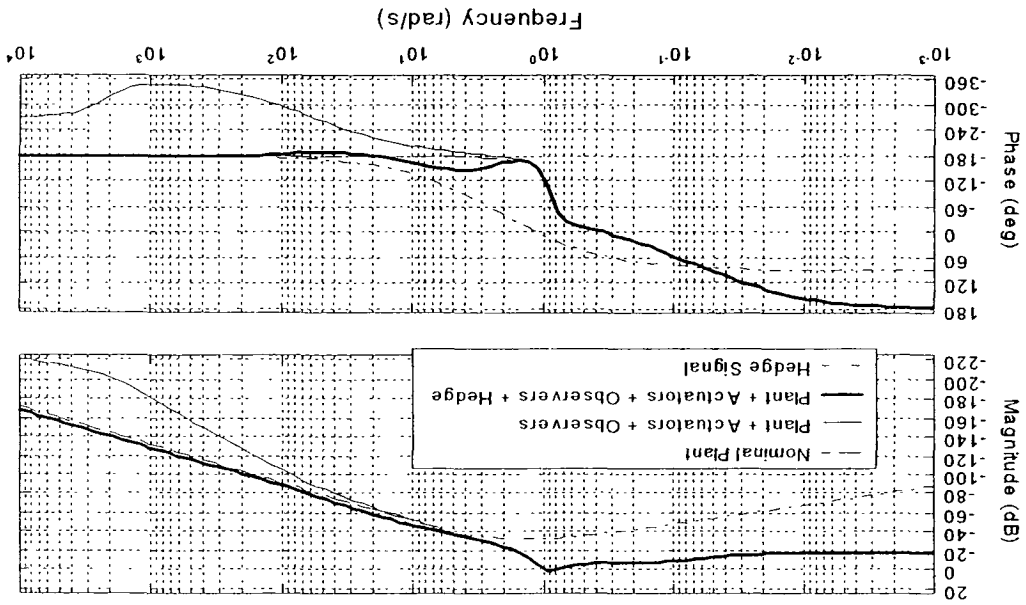
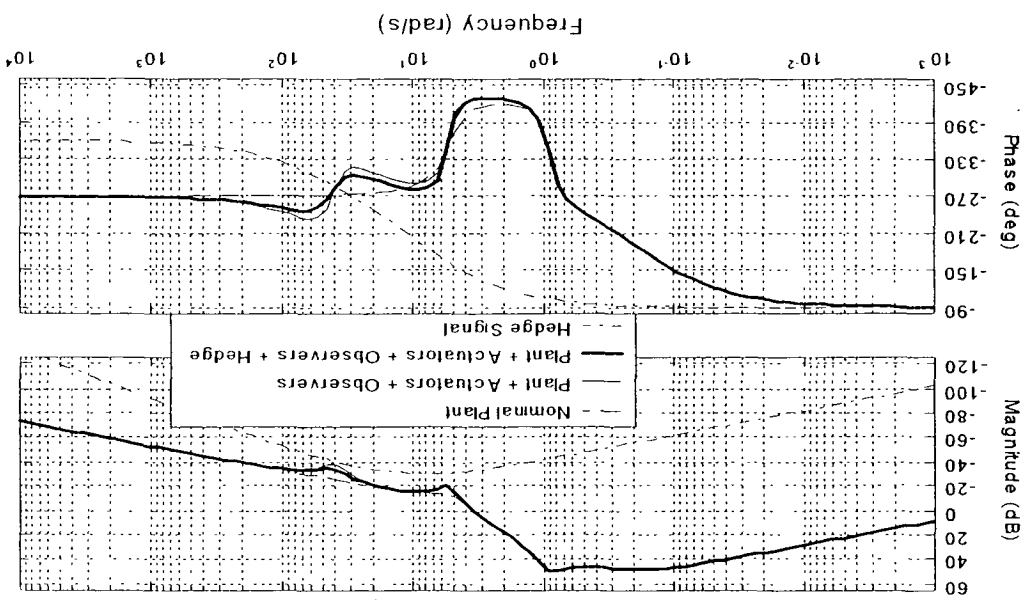
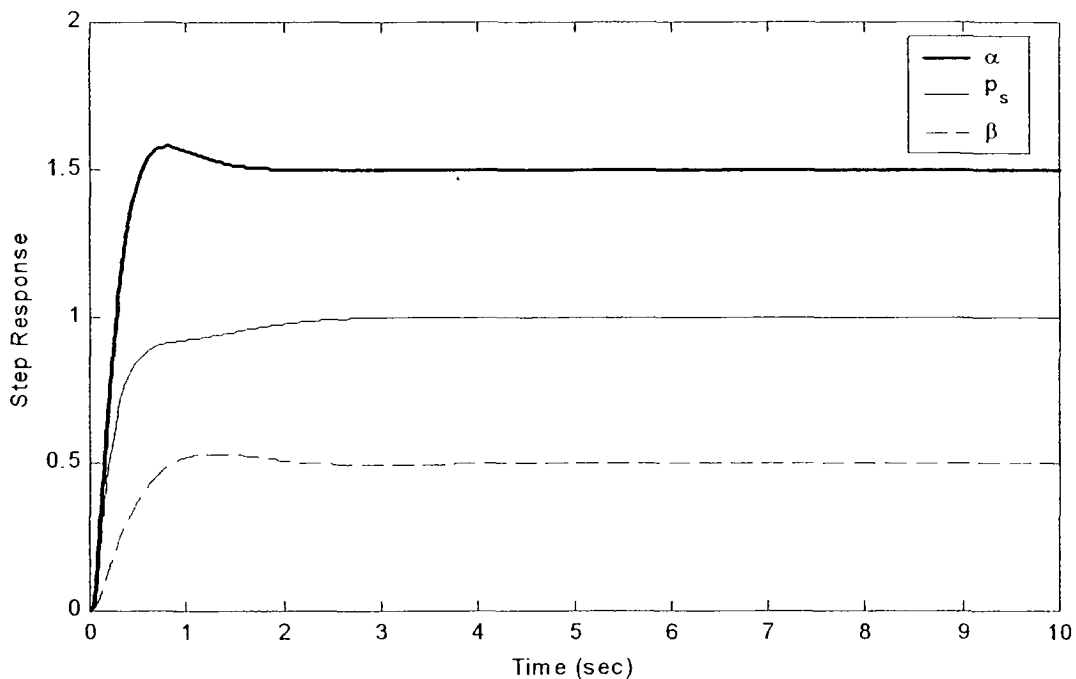


Figure 4-108: Bode Plots,  $\frac{P_h}{u_{cp}}$  (cross term), ICE Hedge Design



With the observer and hedge models designed, the system is now tested. First the step responses for the inner loop are checked. The results with the given observer and hedge models are shown below. Again, step inputs of  $u_\alpha = 1.5$ ,  $u_p = 1.0$ , and  $u_\beta = 0.5$  are used. The three steps are commanded simultaneously in order to test the effects of cross-coupling



**Figure 4-109: Inner Loop Step Responses, ICE, SMC with Observers and Hedging**

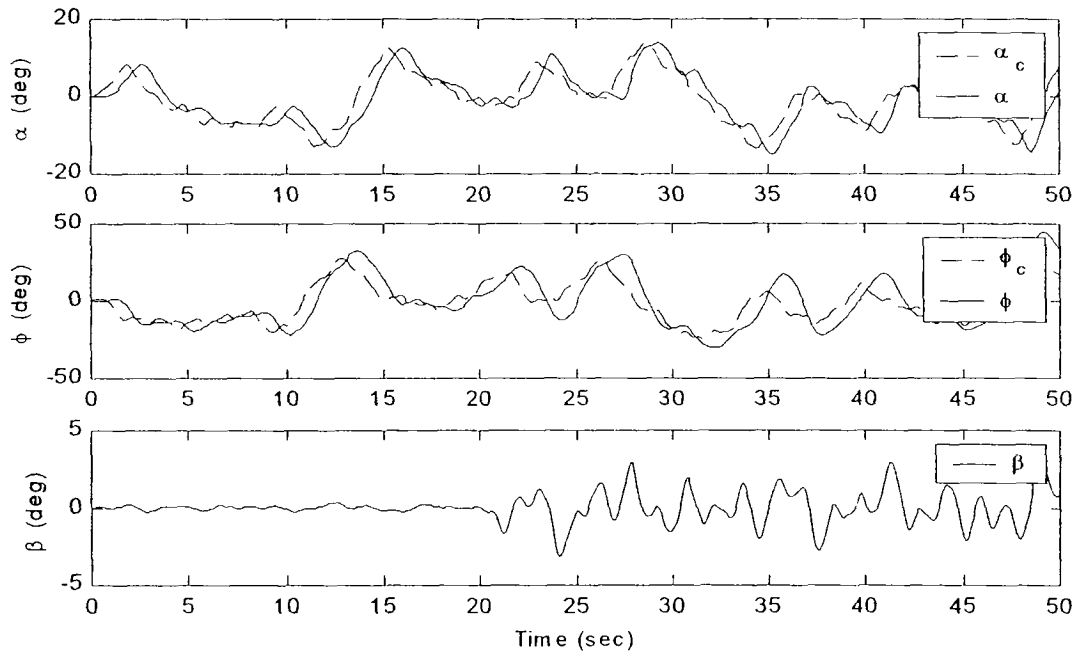
It is possible to achieve much better inner loop tracking by shaping the hedge models and adjusting the hedge gains; however, some design trade-offs are made to enhance robustness to actuator damage. The hedge signals are designed with a fairly broad range of  $-20$  dB slope and hedge gains that are a little higher than needed for the nominal case. This results in slightly slower tracking response and some overshoot in the unfaulted

vehicle. Again, all the design decisions are made using the Bode plots in Figure 4-103 through Figure 4-108 and the step responses in Figure 4-109.

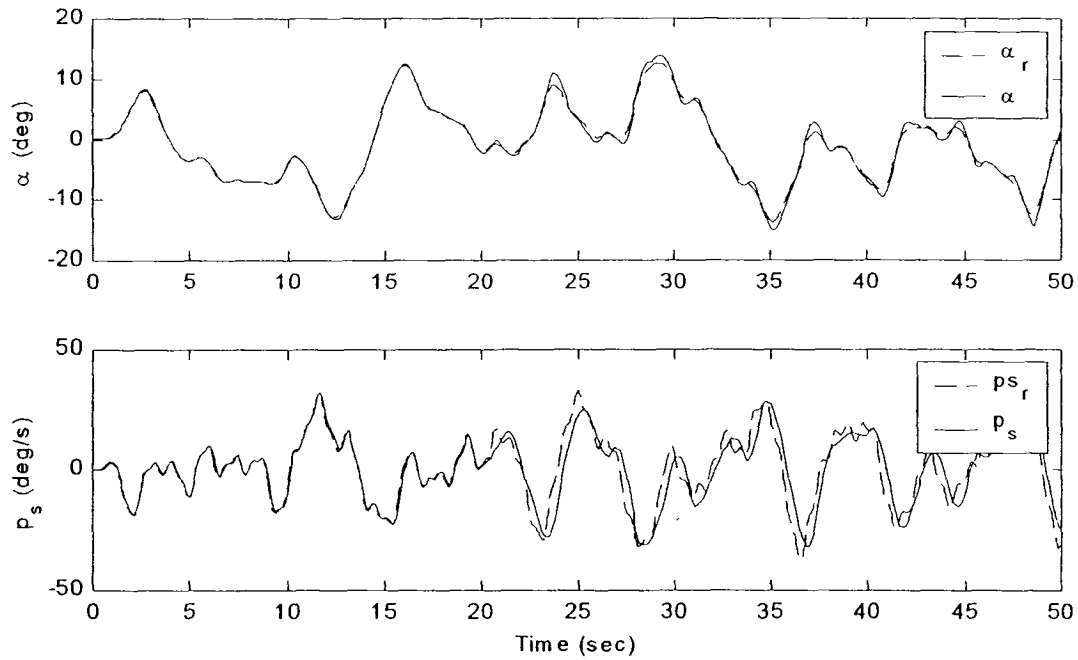
Finally, exercise the full system with measurement noise, system failure, and the pilot in the loop. The Simulink<sup>®</sup> simulation is run with an ODE2 solver using a fixed time step of  $\Delta t = 0.0005$  sec. Vehicle failure occurs at  $t = 20$  sec. Vehicle failure is defined as:

- Plant failure (**A**-matrix is multiplied by 2—with the exception of the elements describing kinematic relationships; **B**-matrix is multiplied by 0.75)
- All actuators experience a 50 ms time delay
- Left elevon rate limits are reduced from 150 deg/s to 10 deg/s, position limits are reduced from  $\pm 30$  deg to  $\pm 15$  deg
- Symmetric pitch flap undamped natural frequency is reduced from 63 rad/s to 10 rad/s
- Left leading edge flap is jammed at +5 deg
- Pitch nozzle actuator undamped natural frequency is reduced from 39 rad/s to 10 rad/s
- Yaw nozzle actuator undamped natural frequency is reduced from 39 rad/s to 10 rad/s

The resulting outer loop tracking is shown in Figure 4-110. Figure 4-111 shows the inner loop SMC tracking



**Figure 4-110: Outer Loop Tracking ( $\alpha$ ,  $\phi$ , and  $\beta$ ), ICE, with SMC, Actuators, Observers, Hedging, and Noise, Failure at  $t = 20$  sec**



**Figure 4-111: Inner Loop Tracking ( $\alpha$ , and  $p_s$ ), ICE, with SMC, Actuators, Observers, Hedging, and Noise, Failure at  $t = 20$  sec**

Before the failure, the controller does a very good job. Desirable, decoupled tracking of the controlled variables is seen. Roll rate tracking could be better, but as explained earlier, this is a design tradeoff that is made to enhance robustness. As shown in Figure 4-112 and Figure 4-113, Level I handling qualities are predicted and PIO tendencies are mild for the nominal vehicle.

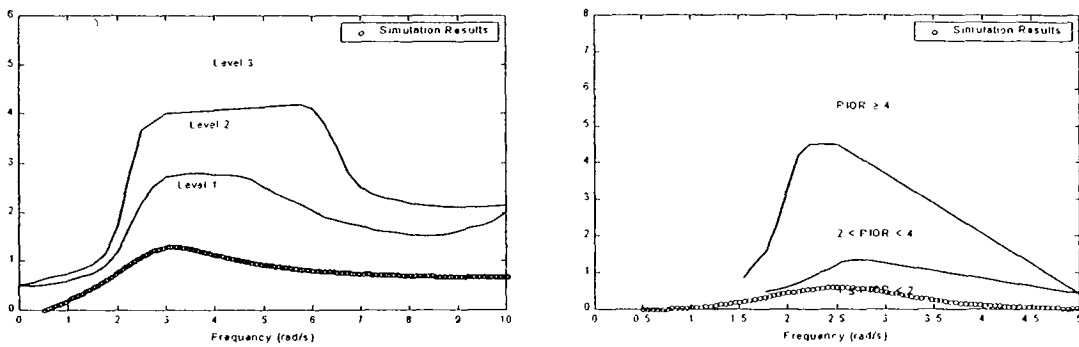


Figure 4-112:  $\alpha$ -Tracking Task HQ and PIO Predictions, ICE Nominal System

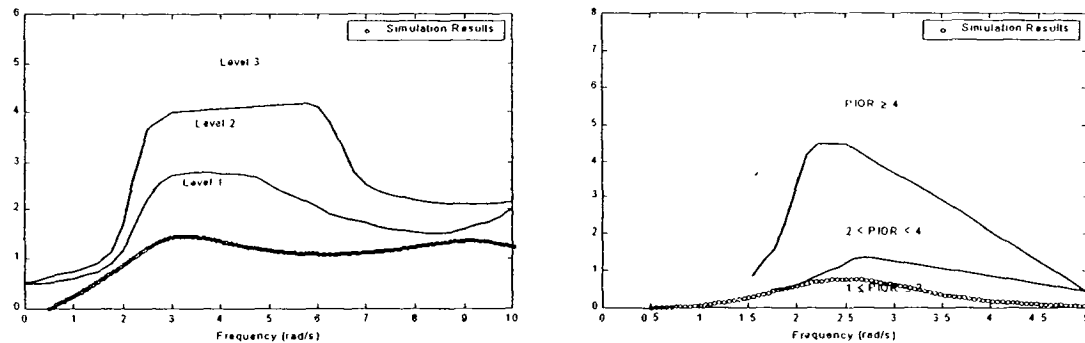
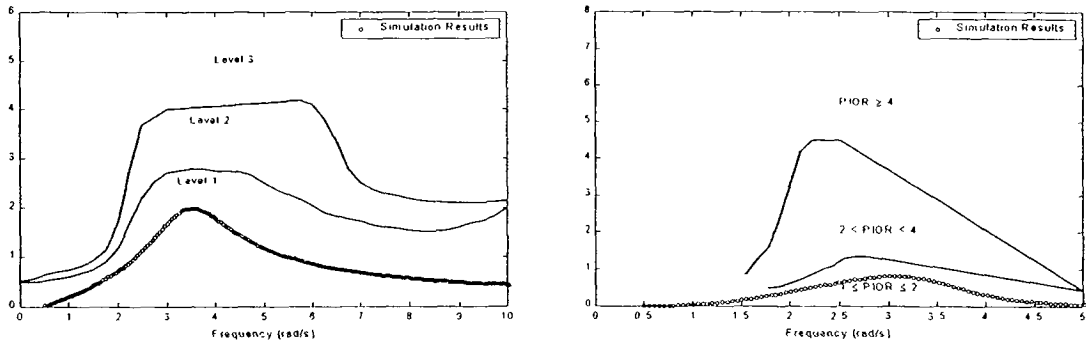


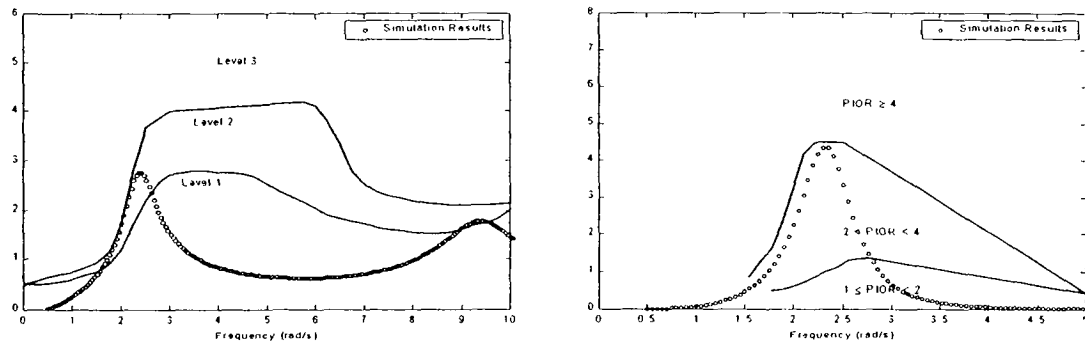
Figure 4-113:  $\phi$ -Tracking Task HQ and PIO Predictions, ICE Nominal System

After system failure, tracking is noticeably degraded, but the vehicle remains stable. The actuator deflections are not shown since there are eleven. Upon examination, however, it is seen that nearly all the actuators are in almost constant rate saturation after

the failure. As seen in Figure 4-114 and Figure 4-115, Level I handling qualities are still predicted for the  $\alpha$ -tracking task, although PIO susceptibility is increased. Level II handling qualities are predicted for the  $\phi$ -tracking task, and PIO tendencies are moderately strong.



**Figure 4-114:  $\alpha$ -Tracking Task HQ and PIO Predictions, ICE Failed System**



**Figure 4-115:  $\phi$ -Tracking Task HQ and PIO Predictions, ICE Failed System**

In viewing these results, take into account a several factors. First of all, this is a significant system failure, and it is remarkable that the controller is even able to maintain stability. Second, the input maneuvers are very aggressive. After a failure of this magnitude, a pilot would not be commanding such a demanding profile. Third, the HQ and PIO level predictions assume a static pilot model. In actuality, a real pilot would

compensate for the perceived change in vehicle dynamics. Therefore, the results shown above are conservative.

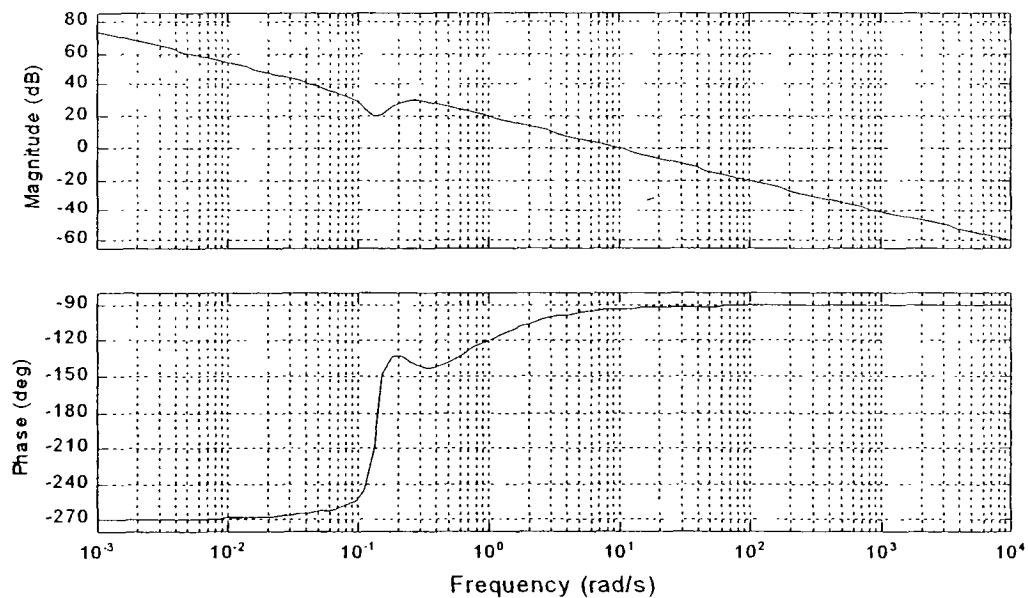
In order to compare these results with a baseline controller, a classic loop-shaped controller is designed. Using a sequential loop-shaping technique, the following controller is selected

$$G_{\alpha}(s) = 56 \left( \frac{s^2 + 1.7s + 0.52}{s^2 + 32s} \right)$$

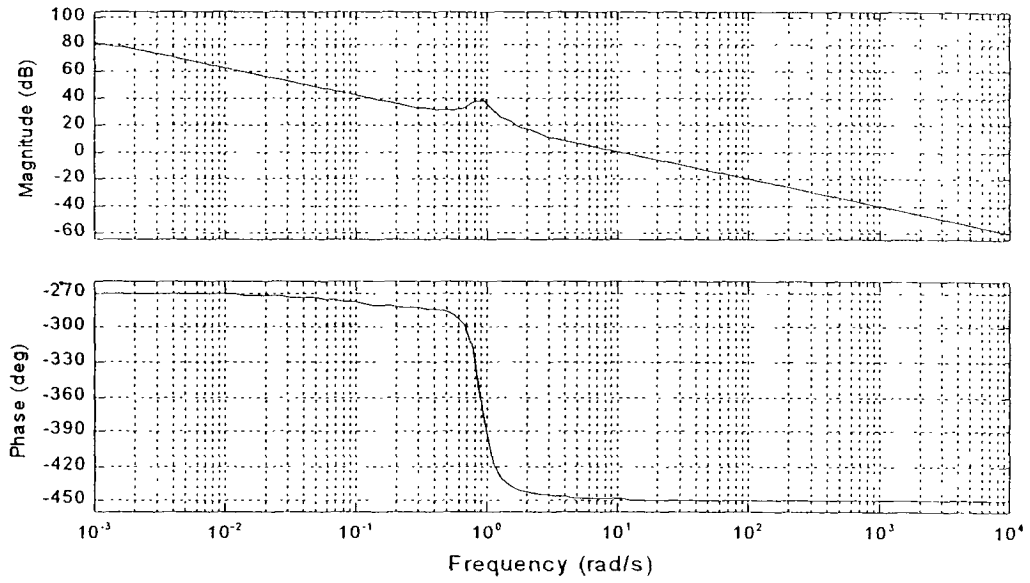
$$G_p(s) = 10 \left( \frac{s^2 + 0.4s + 0.04}{s^2} \right) \quad (4.28)$$

$$G_{\beta}(s) = 50 \left( \frac{s^2 + 2s + 1}{s^2 + 50s} \right)$$

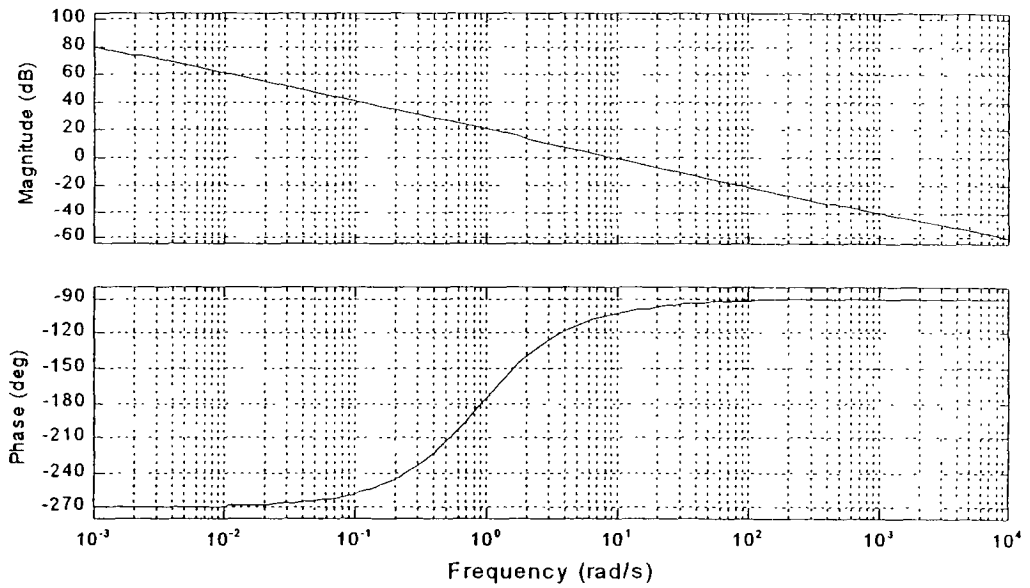
The design Bode plots are given below for reference.



**Figure 4-116: ICE Loop Shaped Controller,  $\alpha$ -Loop Transmission of Compensator\*Plant,  $p$ -Loop Open,  $\beta$ -Loop Open**

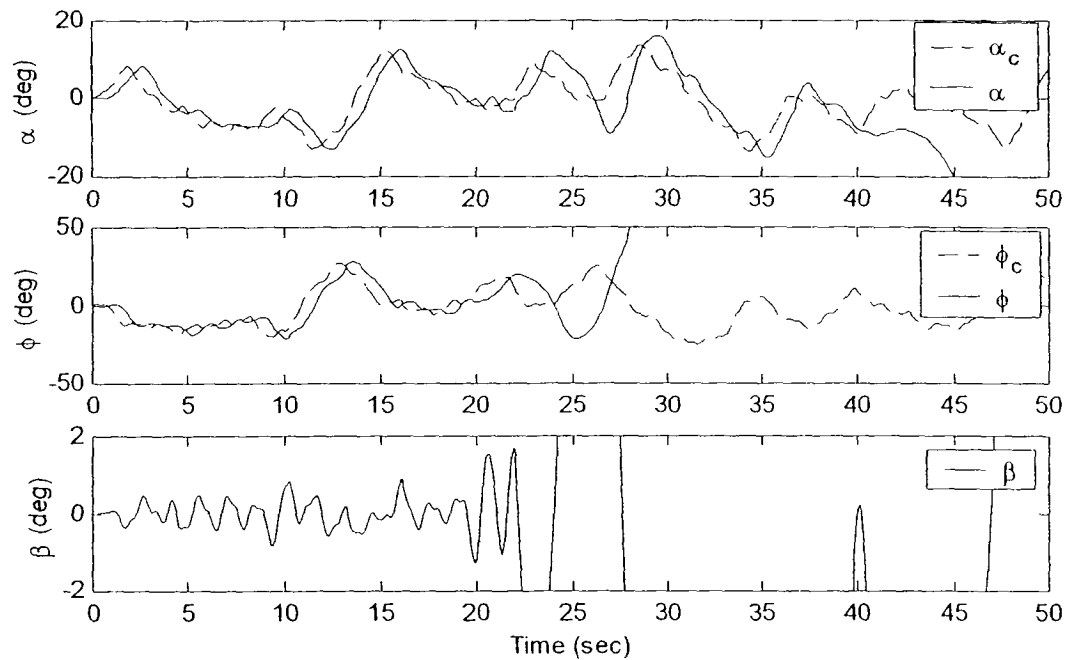


**Figure 4-117: ICE Loop Shaped Controller, p-Loop Transmission of Compensator\*Effective Plant,  $\alpha$ -Loop Closed,  $\beta$ -Loop Open**



**Figure 4-118: ICE Loop Shaped Controller,  $\beta$ -Loop Transmission of Compensator\*Effective Plant,  $\alpha$ -Loop Closed, p-Loop Closed**

This design results in very good tracking of the nominal system. Level I handling qualities are predicted for both the  $\alpha$  and  $\phi$  tracking tasks. Figure 4-119 shows the outer loop tracking using this controller. The same failure as given above occurs at  $t = 20$  sec. As seen, the system goes unstable almost immediately after failure.



**Figure 4-119: Outer Loop Tracking (  $\alpha$ ,  $\phi$ , and  $\beta$  ), ICE, with Loop-Shaped Controller, Actuators, and Noise, Failure at  $t = 20$  sec**

In conclusion, a MIMO observer-based SMC with hedging is demonstrated for a challenging, highly coupled, six degree-of-freedom system. While providing excellent decoupled tracking of the controlled variables, it is shown to be extremely robust to both system plant variations and actuator failures and is seen to be superior to a traditional design.

# Chapter 5

---

## Conclusions and Recommendations

### 5.1 Summary

Sliding mode controllers are extremely attractive for use in a reconfigurable flight control system. Their invariance to matched uncertainty enable them to adapt to huge unmodeled plant failures without any changes to the control law. In fact, if they could handle parasitic dynamics, the job would be done. Unfortunately, all real mechanical systems with limited bandwidth actuators make the application of SMC more difficult. Using asymptotic observers with SMC has been shown to help mitigate the adverse effects of parasitic dynamics, and a design method for choosing observer gains has been presented. A form of model reference hedging has been shown to be equivalent to an SMC pre-filter which helps shape the feedback loop--thus partially removing the effects of actuator dynamics. A complete design procedure has been presented which incorporates a frequency domain approach to select 1) the sliding manifold, 2) the observer eigenvalues, and 3) the hedging dynamics. Finally, three aircraft applications have been demonstrated, each showing exceptional robustness to both system parameter changes and actuator variations. As with most research, however, this work has introduced as many questions as answers. There are many directions that future research can take. Below are several key areas

## 5.2 Potential Future Research

### 5.2.1 Robustness Proofs

The control schemes used are not fail-proof, and a quantitative measure of their robustness has not been found. Robustness proofs for true sliding mode controllers can be obtained using Lyapunov analyses; however, even these are problematic for practical problems. It is not clear which parameters are “matched” and which are “unmatched”. It appears that most of the parameters are partially matched, and it also appears that matching conditions change depending on frequency. It is clear that the observer-based SMC retains considerable robustness, and it is clear that the observer-based SMC is performing some kind of internal adaptation, however, no formal proofs of stability and robustness are known. This is a major research area which requires serious consideration.

### 5.2.2 Full Flight Envelope Issues

The examples given are for single point flight conditions, and no effort is made to extend the analysis to the full flight envelope. One advantage to using a sliding mode controller is that the control law does not need to change for a class of system plants. As long as the SMC gain,  $\rho$ , is chosen large enough, the SMC can easily handle varying flight conditions. There are certainly conditions for which the sliding manifold itself would require adjustment, but most conditions would probably require no changes to the SMC. Unfortunately, a pure SMC can not be directly implemented due to the actuators, and the methods developed here require a nominal model of the plant in the observer. It is shown that the observer-based SMC is robust to changes in the plant parameters; therefore, changes in flight condition can be handled to a certain extent. However, if the

aircraft then experiences damage in an off-design flight condition, stability is doubtful. If, however, the nominal model in the observer changed with the flight condition, the observer-SMC system should perform very well. This could be accomplished by using a scheduled observer with various pre-determined nominal plant models as a function of flight condition (similar to controller gain scheduling). It could also be accomplished in a more sophisticated manner using some type of adaptive observer. This would probably require some form of parameter identification and would bring with it all the complexities of that problem. However, since flight condition parameters change relatively slowly and the observer-SMC is robust to modeling inaccuracies, some of the difficulties with parameter identification would be less critical here. These are questions which deserve further investigation.

### **5.2.3 Adaptive Hedging**

It is observed that varying the hedge gain in the hedging scheme introduced here can dramatically affect system stability and performance. In general, increasing the hedge gain reduces the control activity and introduces a perceived phase lag to the pilot. Reducing the hedge gain increases performance to a point, but further reduction can lead to instability due to the parasitic dynamics. It would be desirable to find an adaptive scheme by which the performance, robustness, and control effort tradeoffs could be made on-line. Several attempts were made to implement an adaptive scheme, but none of them were entirely successful. This is because there are at least two fundamental problems with the implementation. First, the system is very sensitive to dynamic changes in hedge gain. Even if an optimum hedge gain could be calculated on-line, it does not appear to be possible to change the hedge gain quickly enough to counter a

system failure because a dynamic hedge gain drives the system unstable. Second, as seen in the application examples, varying hedge gain alone is not sufficient. Changes in actuator dynamics may require changes to the hedge plant and filter—not just the hedge gain. The issue of an adaptive hedge gain is an open topic which may deserve further study.

#### 5.2.4 Dynamic Hedged Observer

Recognizing that the purpose of hedging is to remove the effects of actuator dynamics, a completely different scheme which tries to capture the original spirit of hedging was tried. Here, a method (which still makes use of an observer) attempts to completely hide the effects of the actuators from the SMC. This scheme requires knowledge of the actuator positions. Although not specifically mentioned before, a soft constraint on all the work done here is that no knowledge of actuator positions should be assumed. If this constraint is relaxed, the following architecture for an observer can be realized.

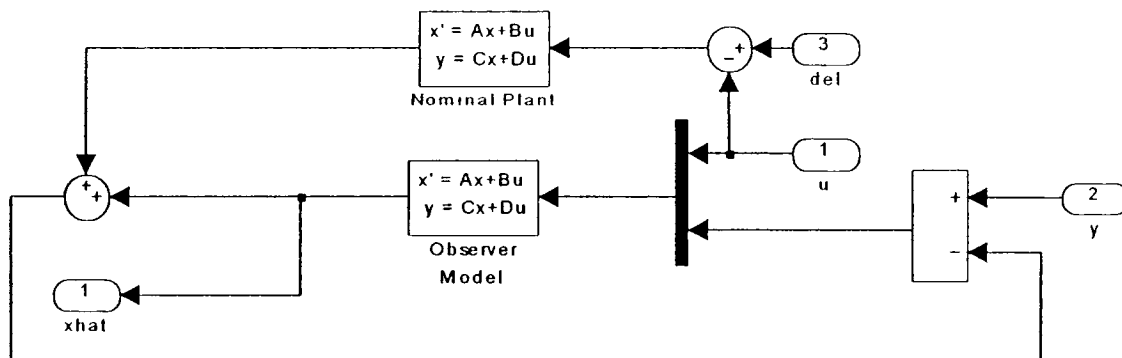
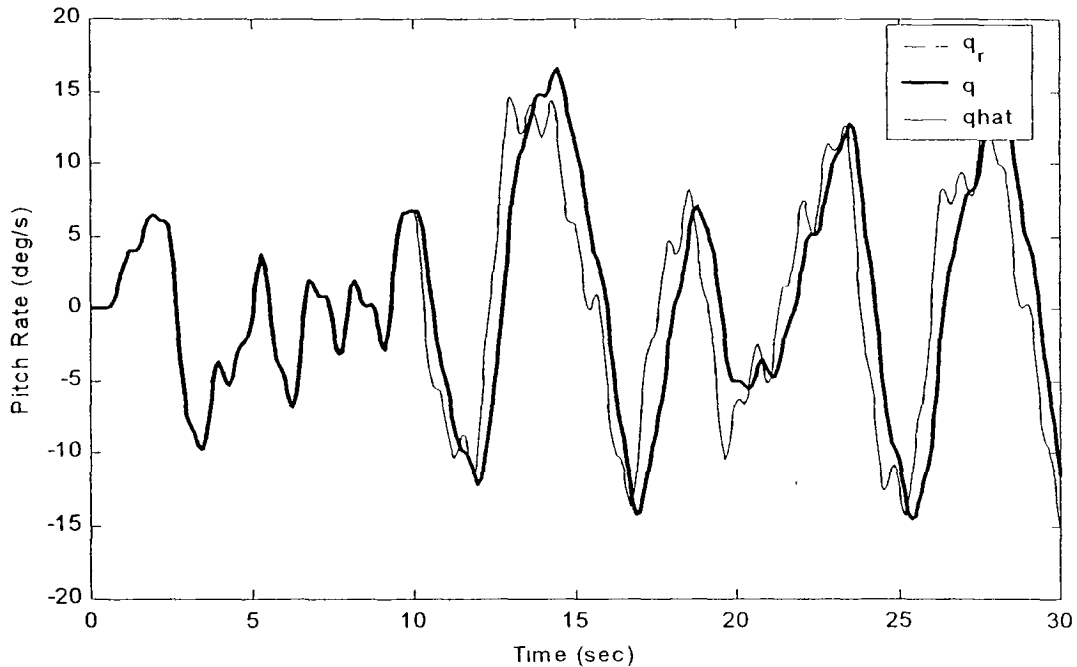


Figure 5-1: Hedged Observer

In this model,  $u$  is the vector output of the SMC controller (which is fed to the actuators),  $del$  is the vector of actual actuator positions;  $y$  is the vector of measured states; and  $x_{hat}$  is the vector of observed states which are fed back to the controller. The input to the block labeled *Nominal Plant* is the difference between the commanded control and the achieved control. Its output, then, represents the deficit in the system state due to the unachieved control input. Usually, in an observer, the measured states are compared with the observed states in a feedback loop. In this model, the observer feedback loop also contains the effects of the actuator dynamics. This means the output of the observer block represents the state vector of the system if there were no actuators. This signal is the one that is passed to the controller, and the effects of the actuator dynamics are completely hidden from the SMC. Since the SMC does not “see” the actuators, the observer can be run very fast to ensure excellent convergence of the observer error. This scheme works very well—the actuators are hidden from the SMC and the SMC gives its expected near-perfect tracking and invariance to changes in system parameters. For example, the F-18/HARV longitudinal model from Chapter 4 is run with this new scheme. Failure #2 occurs at time  $t = 10$  sec. Results are shown in Figure 5-2. Although not detectable on this plot,  $q_r$  and  $q_{hat}$  are coincident, i.e., the observed state perfectly tracks the reference signal before and after failure. However, the actual state does not track the reference signal after the failure. Although unexpected at first, this result makes sense. The SMC is tracking the system it sees. Nowhere do the actual states get fed back to the controller. Even though this approach does not solve the ultimate problem, it does appear to be a very promising first step. A hedged observer has been used to reconstruct the states of the system as it would exist if there were no



**Figure 5-2: Inner Loop Pitch Rate Tracking, F-18/HARV, Dynamic Observer Hedging, Failure #2 at  $t = 10$  sec**

actuators. The near-invariance of the SMC is recaptured. A potential solution to complete this scheme is to wrap an outer loop around this inner loop, feeding back actual measured states through an additional controller. The form that this controller should take is not clear. Introduction of another sliding mode controller is tempting; however, the apparent system that this controller must control has a relative order of plant plus the actuators. This presents the same problem as including the actuators in the model in the first place. For a system with second order actuators, two derivatives of the state variable would be required in the calculation of the sliding manifold. This is completely impractical. Traditional linear controllers could be used. Even these, however, present problems because some derivative action is going to be required due to the loop shape of the apparent inner loop system. Therefore, noise is a primary concern. Initial tests using

an inner loop SMC with a dynamic hedged observer combined with an outer loop controller show some promise. However, there are implementation issues which require further work.

### 5.2.5 Dynamic Control Allocation

All the control allocation done in this work has been static. It seems clear that additional performance could be realized if dynamic control allocation is employed. This, however, requires knowledge of several system elements that are not easily obtained. The system  $\mathbf{B}$  matrix must be known. This would require some form of parameter identification. Also, the actuator positions must be known. Additionally, actuator rate and position limits must be known. For these reasons, dynamic control allocation has been avoided. However, other research efforts utilize dynamic control allocation, and incorporation of it in this work may warrant further investigation.

### 5.2.6 Actuator Position Limiting Issues

The issue of actuator position limiting has not been satisfactorily addressed. All the systems used in this work have redundant control effectors. Therefore, if one effector saturated in position, the system did not go unstable because the redundant effector was able to compensate for the loss of control effort. If there were no redundant effectors, or if all the effectors reached position limits, the SMC would fail. It still seems that the initial concept of hedging the reference model may be a solution to this problem. This limits the amount of the commanded signal by the amount that is unattainable due to the saturated actuators. No successful implementation of this method was obtained. Whether by model reference hedging or some other scheme, the issue of control position saturation requires much work.

## Bibliography

<sup>1</sup>Eslinger, R. A., and Chandler, P. R., "Self-Repairing Flight Control System Program Overview," *Proceedings of National Aerospace and Electronics Conference*, IEEE, 1988, pp. 504-511.

<sup>2</sup>Burken, J. J., and Burcham, F. W. J., "Flight-Test Results of Propulsion-Only Emergency Control System on MD-11 Airplane," *Journal of Guidance, Control, and Dynamics*, Vol. 20, No. 5, 1997, pp. 980-987.

<sup>3</sup>Ward, D. G., and Barron, R., "A Self-Designing Receding Horizon Optimal Flight Controller," *Proceedings of American Control Conference*, Vol. 5, IEEE, Seattle, WA, 21-23 Jun 1995, pp. 3490-3494.

<sup>4</sup>Page, A. B., and Steinberg, M. L., "A Closed-Loop Comparison on Control Allocation Methods," *Proceedings of Guidance, Navigation, and Control Conference*, AIAA-2000-4538, AIAA, Denver, CO, 14-17 Aug 2000.

<sup>5</sup>Page, A. B., and Steinberg, M. L., "Effects of Control Allocation Algorithms on a Nonlinear Adaptive Design," *Proceedings of Guidance, Navigation, and Control Conference*, AIAA-99-4282, AIAA, Portland, OR, 9-11 Aug 1999.

<sup>6</sup>Chandler, P. R., Pachter, M., and Mears, M., "System Identification for Adaptive and Reconfigurable Control," *Journal of Guidance, Control, and Dynamics*, Vol. 18, No. 3, 1995, pp. 516-524.

<sup>7</sup>Urnes, J., Yeager, R. B., and Stewart, J., "Flight Demonstration of the Self-Repairing Flight Control System in a NASA F-15 Aircraft," *Proceedings of National Aerospace and Electronics Conference*, Dayton, OH, 1990

<sup>8</sup>Caglayan, A. K., et al., "Detection, Identification, and Estimation of Surface Damage/Actuator Failure for High Performance Aircraft," *Proceedings of American Control Conference*, Atlanta, GA, Jun 1988, pp. 2206-2212.

<sup>9</sup>Eide, P. K., and Maybeck, P. S., "An MMAE Failure Detection System for the F-16," *IEEE Transactions on Aerospace and Electronic Systems*, Vol. 32, No. 3, 1996, pp. 1125-1136.

<sup>10</sup>Maybeck, P. S., and Stevens, R. D., "Reconfigurable Flight Control via Multiple Model Adaptive Control Methods," *IEEE Transactions on Aerospace and Electronic Systems*, Vol. 27, No. 3, 1991, pp. 470-480.

- <sup>11</sup>Stepaniak, M. J., and Maybeck, P. S., "MMAE-Based Control Redistribution Applied to the VISTA F-16," *IEEE Transactions on Aerospace and Electronic Systems*, Vol. 43, No. 4, 1998, pp. 1249-1260.
- <sup>12</sup>Maybeck, P. S., "Multiple Model Adaptive Algorithms for Detecting and Compensating Sensor and Actuator/Surface Failures in Aircraft Flight Control Systems," *International Journal of Robust and Nonlinear Control*, Vol. 9, 1999, pp. 1051-1070.
- <sup>13</sup>Koshkouei, A. J., and Zinober, A. S. I., "Sliding Mode State Observers for Linear Multivariable Systems," *Proceedings of 34th Conference on Decision & Control*, IEEE, New Orleans, LA, Dec 1995, pp. 2115-2120.
- <sup>14</sup>Yang, H., and Saif, M., "Fault Detection in a Class of Nonlinear Systems via Adaptive Sliding Observer," *Proceedings of IEEE International Conference on Systems, Man and Cybernetics*, Vol. 3, IEEE, Vancouver, B.C., 22-25 Oct 1995, pp. 2199-2204.
- <sup>15</sup>Sreedhar, R., Fernández, B. R., and Masada, G. Y., "Robust Fault Detection in Nonlinear Systems Using Sliding Mode Observers," *Proceedings of 2nd Conference on Control and Applications*, Vol. 2, IEEE, Vancouver, B.C., 13-16 Sep 1993, pp. 715-721.
- <sup>16</sup>Ioannou, P. A., and Sun, J., *Robust Adaptive Control*, PTR Prentice-Hall, Upper Saddle River, NJ, 1996.
- <sup>17</sup>Morelli, E. A., "Real-Time Parameter Estimation in the Frequency Domain," *Proceedings of Guidance, Navigation, and Control Conference*, AIAA-99-4043, AIAA, Portland, OR, 9-11 Aug 1999.
- <sup>18</sup>Buffington, J. M., Chandler, P. R., and Pachter, M., "On-Line System Identification for Aircraft with Distributed Control Effectors," *International Journal of Robust and Nonlinear Control*, Vol. 9, 1999, pp. 1033-1049.
- <sup>19</sup>Eberhardt, R. L., and Ward, D. G., "Indirect Adaptive Flight Control Interactions," *International Journal of Robust and Nonlinear Control*, Vol. 9, 1999, pp. 1013-1031.
- <sup>20</sup>Peterson, J. A. M., and Bodson, M., "Control Allocation for Systems with Coplanar Controls," *Proceedings of Guidance, Navigation, and Control Conference*, AIAA-2000-4540, AIAA, Denver, CO, 14-17 Aug 2000.
- <sup>21</sup>Buffington, J. M., Chandler, P. R., and Pachter, M., "Integration of On-Line System Identification and Optimization-Based Control Allocation," *Proceedings of Guidance, Navigation, and Control Conference*, AIAA-98-4487, AIAA, Boston, MA, Aug 1998, pp. 1746-1756.

- <sup>22</sup>Bodson, M., and Groszkiewicz, J., "Multivariable Adaptive Algorithms for Reconfigurable Flight Control," *Transactions on Control Systems Technology*, Vol. 5, No. 2, 1997, pp. 217-229.
- <sup>23</sup>Bodson, M., and Pohlchuck, W. A., "Command Limiting in Reconfigurable Flight Control," *Journal of Guidance, Control, and Dynamics*, Vol. 21, No. 4, 1998, pp. 639-646.
- <sup>24</sup>Brinker, J. S., and Wise, K. A., "Nonlinear Simulation Analysis of a Tailless Advanced Fighter Aircraft Reconfigurable Flight Control Law," *Proceedings of Guidance, Navigation, and Control Conference*, AIAA-99-4040, AIAA, Portland, OR, 9-11 Aug 1999.
- <sup>25</sup>Eberhardt, R. L., and Ward, D. G., "Indirect Adaptive Flight Control of a Tailless Fighter Aircraft," *Proceedings of Guidance, Navigation, and Control Conference*, AIAA-99-4042, AIAA, Portland, OR, 9-11 Aug 1999.
- <sup>26</sup>Ochi, Y., "Application of Feedback Linearization Method in a Digital Restructurable Flight Control System," *Journal of Guidance, Control, and Dynamics*, Vol. 16, No. 1, 1993, pp. 112-117.
- <sup>27</sup>Ochi, Y., and Kanai, K., "Design of Restructurable Flight Control Systems Using Feedback Linearization," *Journal of Guidance, Control, and Dynamics*, Vol. 14, No. 5, 1991, pp. 903-911.
- <sup>28</sup>Ochi, Y., and Kanai, K., "Application of Restructurable Flight Control System to Large Transport Aircraft," *Journal of Guidance, Control, and Dynamics*, Vol. 18, No. 2, 1995, pp. 365-370.
- <sup>29</sup>Pachter, M., Chandler, P. R., and Mears, M., "Reconfigurable Tracking Control with Saturation," *Journal of Guidance, Control, and Dynamics*, Vol. 18, No. 5, 1995, pp. 1016-1022.
- <sup>30</sup>Pachter, M., Chandler, P. R., Nelson, E., and Rasmussen, S., "Parameter Estimation for Over-Actuated Aircraft with Nonlinear Aerodynamics," *Proceedings of Guidance, Navigation, and Control Conference*, AIAA-99-4046, AIAA, Portland, OR, 9-11 Aug 1999.
- <sup>31</sup>Steinberg, M. L., "A Comparison of Intelligent, Adaptive, and Nonlinear Flight Control Laws," *Proceedings of Guidance, Navigation, and Control Conference*, AIAA-99-4044, AIAA, Portland, OR, 9-11 Aug 1999.
- <sup>32</sup>Ward, D. G., Monaco, J. F., and Bodson, M., "Development and Flight Testing of a Parameter Identification Algorithm for Reconfigurable Control," *Journal of Guidance, Control, and Dynamics*, Vol. 21, No. 6, 1998, pp. 948-956.

<sup>33</sup>Ward, D. G., Monaco, J. F., and Schierman, J. D., "Reconfigurable Control for VTOL UAV Shipboard Landing," *Proceedings of Guidance, Navigation, and Control Conference*, AIAA-99-4045, AIAA, Portland, OR, 9-11 Aug 1999.

<sup>34</sup>Wise, K. A., Brinker, J. S., Calise, A. J., Enns, D. F., Elgersma, M. R., and Voulgaris, P. G., "Direct Adaptive Reconfigurable Flight Control for a Tailless Advanced Fighter Aircraft," *International Journal of Robust and Nonlinear Control*, Vol. 9, 1999, pp. 999-1012.

<sup>35</sup>Brinker, J. S., and Wise, K. A., "Flight Testing of a Reconfigurable Flight Control Law on the X-36 Tailless Fighter Aircraft," *Proceedings of Guidance, Navigation, and Control Conference*, AIAA-2000-3941, AIAA, Denver, CO, 14-17 Aug 2000.

<sup>36</sup>Chandler, P. R., Pachter, M., Mears, M., and Sheldon, S., "Regression Techniques for Aircraft Parameter Identification from Noisy Measurements in Maneuvering Flight," *Proceedings of 31st Conference on Decision and Control*, Vol. 2, IEEE, Tucson, AZ, 16-18 Dec 1992, pp. 2311-2316.

<sup>37</sup>Bodson, M., "An Adaptive Algorithm with Information-Dependent Data Forgetting," *Proceedings of American Control Conference*, Vol. 5, IEEE, Seattle, WA, 21-23 Jun 1995, pp. 3485-3489

<sup>38</sup>Ch'en, H.-f., and Guo, L., *Identification and Stochastic Adaptive Control*, Birkhauser, Boston, MA, 1991.

<sup>39</sup>Morelli, E. A., "In-Flight System Identification," *Proceedings of Atmospheric Flight Mechanics Conference*, AIAA-98-4261, AIAA, Boston, MA, Aug 1998, pp. 238-247.

<sup>40</sup>Hess, R. A., Siwakosit, W., and Chung, J., "Accommodating Actuator Failures in Flight Control Systems," *Proceedings of 37th Aerospace Sciences Meeting*, AIAA-99-0634, AIAA, Reno, NV, 1999.

<sup>41</sup>Hess, R. A., and McLean, C., "Development of a Design Methodology for Reconfigurable Flight Control Systems," *Proceedings of 38th Aerospace Sciences Meeting & Exhibit*, AIAA-2000-0890, AIAA, Reno, NV, 10-13 Jan 2000.

<sup>42</sup>Hess, R. A., Siwakosit, W., and Chung, J., "Accommodating a Class of Actuator Failures in Flight Control Systems," *Journal of Guidance, Control, and Dynamics*, Vol. 23, No. 3, 2000, pp. 412-419.

<sup>43</sup>Siwakosit, W., Snell, S. A., and Hess, R. A., "Robust Flight Control Design with Handling Qualities Constraints Using Scheduled Linear Dynamic Inversion and Loop-Shaping," *IEEE Transactions on Control Systems Technology*, Vol. 8, No. 3, 2000, pp. 483-494.

<sup>44</sup>Wang, H., Liu, G. P., Harris, C. J., and Brown, M., *Advanced Adaptive Control*, 1 ed., Pergamon, Oxford, U.K., 1995.

<sup>45</sup>Cox, C., Stepniewski, S., Jorgensen, C., Saeks, R., and Lewis, C., "On the Design of a Neural Network Autolander," *International Journal of Robust and Nonlinear Control*, Vol. 9, 1999, pp. 1071-1096.

<sup>46</sup>Cox, C., and Saeks, R., "Adaptive Critic Control and Functional Link Networks," *Proceedings of Conference on Systems, Man, and Cybernetics*, Vol. 2, IEEE, San Diego, CA, 11-14 Oct 1998, pp. 1652-1657.

<sup>47</sup>Calise, A. J., Lee, S., and Sharma, M., "Development of a Reconfigurable Flight Control Law for the X-36 Tailless Fighter Aircraft," *Proceedings of Guidance, Navigation, and Control Conference*, AIAA-2000-3940, AIAA, Denver, CO, 14-17 Aug 2000.

<sup>48</sup>Schumacher, C., "Adaptive Flight Control Using Dynamic Inversion and Neural Networks," *Proceedings of Guidance, Navigation, and Control Conference*, AIAA-99-4086, AIAA, Portland, OR, 9-11 Aug 1999.

<sup>49</sup>Smith, L., Chandler, P. R., and Pachter, M., "Regularization Techniques for Real-Time Identification of Aircraft Parameters," *Proceedings of Guidance, Navigation, and Control Conference*, AIAA-97-3740, AIAA, New Orleans, LA, Aug 1997, pp. 1466-1480.

<sup>50</sup>Bodson, M., and Groszkiewicz, J., "Multivariable Adaptive Algorithms for Reconfigurable Flight Control," *Proceedings of 33rd Conference on Decision and Control*, Vol. 4, IEEE, Buena Vista, FL, 14-16 Dec 1994, pp. 3330-3335.

<sup>51</sup>Napolitano, M. R., and Swain, R. L., "New Technique for Aircraft Flight Control Reconfiguration," *Journal of Guidance, Control, and Dynamics*, Vol. 14, No. 1, 1989, pp. 184-190.

<sup>52</sup>Boškovic, J. D., and Mehra, R. K., "Intelligent Adaptive Control of a Tailless Advanced Fighter Aircraft (TAFE) in the Presence of Wing Damage," *Proceedings of Guidance, Navigation, and Control Conference*, AIAA-99-4041, AIAA, Portland, OR, 9-11 Aug 1999.

- <sup>53</sup>Dhayagude, N., and Gao, Z., "Novel Approach to Reconfigurable Control System Design," *Journal of Guidance, Control, and Dynamics*, Vol. 19, No. 4, Engineering Notes, 1996, pp. 963-967.
- <sup>54</sup>Groszkiewicz, J. E., and Bodson, M., "Flight Control Reconfiguration Using Adaptive Methods," *Proceedings of 34th Conference on Decision & Control*, Vol. 2, IEEE, New Orleans, LA, 13-15 Dec 1995, pp. 1159-1164
- <sup>55</sup>Rusnak, I., Guez, A., Bar-Kana, I., and Steinberg, M. L., "On-Line Identification and Control of Linearized Aircraft Dynamics," *IEEE Aerospace and Electronics Systems Magazine*, Vol. 7, No. 7, 1992, pp. 56-60.
- <sup>56</sup>Bacon, B. J., and Ostroff, A. J., "Reconfigurable Flight Control Using Nonlinear Dynamic Inversion with a Special Accelerometer Implementation," *Proceedings of Guidance, Navigation, and Control Conference*, AIAA-2000-4565, AIAA, Denver, CO, 14-17 Aug 2000.
- <sup>57</sup>Singh, S. N., Steinberg, M. L., and Page, A. B., "Adaptive Control of High-Performance Aircraft with Multiple Control Effectors," *Proceedings of Guidance, Navigation, and Control Conference*, AIAA-99-4280, AIAA, Portland, OR, 9-11 Aug 1999.
- <sup>58</sup>Steinberg, M. L., and Page, A. B., "Nonlinear Adaptive Control with Genetic Algorithm Design Optimization," *International Journal of Robust and Nonlinear Control*, Vol. 9, 1999, pp. 1097-1115.
- <sup>59</sup>Ferrara, A., and Giacomini, L., "Control of a Class of Mechanical Systems With Uncertainties Via a Constructive Adaptive/Second Order VSC Approach," *Journal of Dynamic Systems, Measurement, and Control*, Vol. 122, No. 1, 2000, pp. 33-39.
- <sup>60</sup>Willis, P. A., "Decentralized Adaptive Neuro-Fuzzy Longitudinal Control of High Performance Aircraft," *Proceedings of Guidance, Navigation, and Control Conference*, AIAA-99-4083, AIAA, Portland, OR, 9-11 Aug 1999.
- <sup>61</sup>Morse, W. D., and Ossman, K. A., "Model Following Reconfigurable Flight Control System for the AFTI/F-16," *Journal of Guidance, Control, and Dynamics*, Vol. 13, No. 6, 1990, pp. 969-976.
- <sup>62</sup>Akella, M. R., Subbarao, K., and Junkins, J. L., "Non-Linear Adaptive Autopilot for Uninhabited Aerial Combat Vehicles," *Proceedings of Guidance, Navigation, and Control Conference*, AIAA-99-4218, AIAA, Portland, OR, 9-11 Aug 1999.

- <sup>63</sup>Shtessel, Y. B., Buffington, J. M., and Banda, S. S., "Multiple Timescale Flight Control Using Reconfigurable Sliding Modes," *Journal of Guidance, Control, and Dynamics*, Vol. 22, No. 6, 1999, pp. 873-883.
- <sup>64</sup>Shtessel, Y. B., Buffington, J. M., Pachter, M., Chandler, P. R., and Banda, S. S., "Reconfigurable Flight Control on Sliding Modes Addressing Actuator Deflection and Deflection Rate Saturation," *Proceedings of Guidance, Navigation, and Control Conference*, AIAA-98-4112, AIAA, Boston, MA, Aug 1998, pp. 127-137.
- <sup>65</sup>Shtessel, Y. B., Buffington, J. M., and Banda, S. S., "Multiple Time Scale Flight Control Using Re-configurable Sliding Modes," *Proceedings of 37th Conference on Decision and Control*, Vol. 4, IEEE, Tampa, FL, 16-18 Dec 1998, pp. 4196-4201.
- <sup>66</sup>Shtessel, Y. B., Buffington, J. M., and Banda, S. S., "Tailless Aircraft Flight Control Using Multiple Time Scale Re-Configurable Sliding Modes," *Proceedings of Guidance, Navigation, and Control Conference*, AIAA-99-4136, AIAA, Portland, OR, 9-11 Aug 1999, pp. 966-976.
- <sup>67</sup>Burken, J. J., Lu, P., and Wu, Z., "Reconfigurable Flight Control Designs with Application to the X-33 Vehicle," *Proceedings of Guidance, Navigation, and Control Conference*, AIAA-99-4134, AIAA, Portland, OR, 9-11 Aug 1999.
- <sup>68</sup>Lyshevski, S. E., "Flight System Design: Robust Control and Accommodation of Failures," *Proceedings of International Conference on Control Applications*, IEEE, Oct 1997, pp. 463-468.
- <sup>69</sup>Durham, W. C., "Constrained Control Allocation," *Journal of Guidance, Control, and Dynamics*, Vol. 16, No. 4, 1993, pp. 717-725.
- <sup>70</sup>Ikeda, Y., and Hood, M., "An Application of L1 Optimization to Control Allocation," *Proceedings of Guidance, Navigation, and Control Conference*, AIAA-2000-4566, AIAA, Denver, CO, 14-17 Aug 2000.
- <sup>71</sup>Hess, R. A., and Snell, S. A., "Flight Control System Design with Rate Saturating Actuators," *Journal of Guidance, Control, and Dynamics*, Vol. 20, No. 1, 1997, pp. 90-96.
- <sup>72</sup>Pan, Z., and Basar, T., "Parameter Identification for Uncertain Linear Systems with Partial State Measurements Under an  $H_\infty$  Criterion," *Proceedings of 34th Conference on Decision & Control*, Vol. 1, IEEE, New Orleans, LA, 13-15 Dec 1995, pp. 709-714.
- <sup>73</sup>Durham, W. C., "Constrained Control Allocation: Three-Moment Problem," *Journal of Guidance, Control, and Dynamics*, Vol. 17, No. 2, 1994, pp. 330-336.

<sup>74</sup>Peterson, J. A. M., and Bodson, M., "Fast Control Allocation Using Spherical Coordinates," *Proceedings of Guidance, Navigation, and Control Conference*, AIAA-99-4215, AIAA, Portland, OR, 9-11 Aug 1999.

<sup>75</sup>Durham, W. C., "Attainable Moments for the Constrained Control Allocation Problem," *Journal of Guidance, Control, and Dynamics*, Vol 17, No. 6, 1994, pp. 1371-1373.

<sup>76</sup>Durham, W. C., and Bordingnon, K. A., "Computationally Efficient Control Allocation," *Proceedings of Guidance, Navigation, and Control Conference*, AIAA-99-4214, AIAA, Portland, OR, 9-11 Aug 1999.

<sup>77</sup>Buffington, J. M., "Modular Control Law Design for the Innovative Control Effectors (ICE) Tailless Fighter Aircraft Configuration 101-3," USAF, AFRL-VA-WP-TR-1999-3057, June, 1999.

<sup>78</sup>Enns, D. F., "Control Allocation Approaches," *Proceedings of Guidance, Navigation, and Control Conference*, AIAA-98-4108, AIAA, Boston, MA, Aug 1998, pp. 98-108.

<sup>79</sup>Buffington, J. M., "Tailless Aircraft Control Allocation," *Proceedings of Guidance, Navigation, and Control Conference*, AIAA-97-3605, AIAA, New Orleans, LA, Aug 1997, pp. 737-747

<sup>80</sup>Barker, J. M., and Balas, G. J., "Flight Control of a Tailless Aircraft Via Linear Parameter-Varying Techniques," *Proceedings of Guidance, Navigation, and Control Conference*, AIAA-99-4133, AIAA, Portland, OR, 9-11 Aug 1999.

<sup>81</sup>Bordingnon, K. A., and Durham, W. C., "Null-Space Augmented Pseudo-Inverse Solutions to Constrained Control Allocation Problems," *Proceedings of Guidance, Navigation, and Control Conference*, AIAA-95-3209, AIAA, Baltimore, MD, Aug 1995, pp. 328-333.

<sup>82</sup>Gao, Z., and Antsaklis, P. J., "Stability of the Pseudo-Inverse Method for Reconfigurable Control Systems," *International Journal of Control*, Vol. 53, No. 3, 1991, pp. 717-729.

<sup>83</sup>Glaze, M., and Durham, W. C., "Design and Implementation of a Control Allocation Toolbox for MATLAB v. 5.0," *Proceedings of Guidance, Navigation, and Control Conference*, AIAA-98-4436, AIAA, Boston, MA, Aug 1998, pp. 1544-1553.

<sup>84</sup>Bordingnon, K. A., "Constrained Control Allocation for Systems with Redundant Control Effectors," Ph.D. Thesis, Virginia Polytechnic Institute and State University, 1996.

<sup>85</sup>Bugajski, D., Enns, D. F., and Hendrick, R., "Nonlinear Control Law Design for High Angle-of-Attack," *Proceedings of High-Angle-of-Attack Projects and Technology Conference*, NASA Dryden Flight Research Facility, Edwards AFB, CA, 21-23 Apr 1992.

<sup>86</sup>Davidson, J. B., et. al., "Development of a Control Law Design Process Utilizing Advanced Synthesis Methods with Application to the NASA F-18 HARV," *Proceedings of High-Angle-of-Attack Projects and Technology Conference*, NASA Dryden Flight Research Facility, Edwards AFB, CA, 21-23 Apr 1992.

<sup>87</sup>Bordingnon, K. A., and Durham, W. C., "Closed-Form Solutions to Constrained Control Allocation Problem," *Journal of Guidance, Control, and Dynamics*, Vol. 18, No. 5, 1995, pp. 1000-1007.

<sup>88</sup>Utkin, V. I., Guldner, J., and Shih, C-h., *Sliding Mode Control in Electromechanical Systems*, Taylor & Francis, Philadelphia, PA, 1999.

<sup>89</sup>Itkis, Y., *Control Systems of Variable Structure*, Wiley, New York, NY, 1976.

<sup>90</sup>Utkin, V. I., "Variable Structure Systems with Sliding Mode," *IEEE Transactions on Automatic Control*, Vol. AC-22, No. 2, 1977, pp. 212-222.

<sup>91</sup>Edwards, C., and Spurgeon, S. K., *Sliding Mode Control*, Taylor & Francis Ltd, Bristol, PA, 1998.

<sup>92</sup>DeCarlo, R., A., Zak, S. H., and Drakunov, S. V., "Section 57.5: Variable Structure, Sliding Mode Design," *The Control Handbook*, Levine, W. S. eds., CRC Press, Inc., Boca Raton, FL, 1996, pp. 941-951.

<sup>93</sup>DeCarlo, R., A., Zak, S. H., and Mathews, G. P., "Variable Structure Control of Nonlinear Multivariable Systems: A Tutorial," *Proceedings of the IEEE*, Vol. 76, No. 3, 1988, pp. 212-232.

<sup>94</sup>Fernández, B. R., and Hedrick, J. K., "Control of Multivariable Non-Linear Systems by the Sliding Mode Method," *International Journal of Control*, Vol. 46, No. 3, 1987, pp. 1019-1040.

<sup>95</sup>Hung, J. Y., Weibing, G., and Hung, J. C., "Variable Structure Control: A Survey," *IEEE Transactions on Industrial Electronics*, Vol. 40, No. 1, 1993, pp. 2-23.

<sup>96</sup>Utkin, V. I., "Sliding Mode Control Design Principles and Applications to Electric Drives," *IEEE Transactions on Industrial Electronics*, Vol. 40, No. 1, 1993, pp. 23-36.

<sup>97</sup>Young, K. D., Utkin, V. I., and Özgüner, Ü., "A Control Engineer's Guide to Sliding Mode Control," *IEEE Transactions on Control Systems Technology*, Vol. 7, No. 3, 1999, pp. 328-342.

<sup>98</sup>Utkin, V. I., *Sliding Modes in Control and Optimization*, Springer-Verlag, Berlin, Ger., 1992.

<sup>99</sup>Slotine, J.-J. E., and Li, W., *Applied Nonlinear Control*, Prentice Hall, Englewood Cliffs, NJ, 1991.

<sup>100</sup>Poznyak, A. S., Yu, W., and Sanchez, E. N., "Identification and Control of Unknown Chaotic Systems via Dynamic Neural Networks," *IEEE Transactions on Circuits and Systems-I: Fundamental Theory and Applications*, Vol. 46, No. 12, 1999, pp. 1491-1495.

<sup>101</sup>Levant, A., "Robust Exact Differentiation via Sliding Mode Technique," *Automatica*, Vol. 34, No. 3, 1998, pp. 379-384.

<sup>102</sup>Hsu, K.-C., "Decentralized Sliding Mode Control for Large-Scale Time-Delayed Systems With Series Nonlinearities," *Journal of Dynamic Systems, Measurement, and Control*, Vol. 121, No. 4, 1999, pp. 708-713.

<sup>103</sup>Salamci, M. U., Özgören, M. K., and Banks, S. P., "Sliding Mode Control with Optimal Sliding Surfaces for Missile Autopilot Design," *Journal of Guidance, Control, and Dynamics*, Vol. 23, No. 4, 2000, pp. 719-727.

<sup>104</sup>Schumacher, C., and Singh, S. N., "Nonlinear Control of Multiple UAVs in Close-Coupled Formation Flight," *Proceedings of Guidance, Navigation, and Control Conference*, AIAA-2000-4373, AIAA, Denver, CO, 14-17 Aug 2000, pp. 1-7.

<sup>105</sup>Singh, S. N., Pachter, M., Chandler, P. R., Banda, S. S., Rasmussen, S., and Schumacher, C., "Input-Output Invertibility and Sliding Mode Control for Close Formation Flying," *Proceedings of Guidance, Navigation, and Control Conference*, AIAA-2000-4374, AIAA, Denver, CO, 14-17 Aug 2000.

<sup>106</sup>Shtessel, Y. B., and Tournes, C. H., "Flight Control Reconfiguration on Sliding Modes," *Proceedings of Guidance, Navigation, and Control Conference*, AIAA-97-3632, AIAA, New Orleans, LA, Aug 1997, pp. 1288-1298.

<sup>107</sup>Filippov, A. F., "Differential Equations with Discontinuous Right Hand Sides," *Am. Math Soc. Transl.*, Vol. 42, 1964, pp. 193-231.

<sup>108</sup>Choi, J.-H., Misawa, E. A., and Young, G. E., "A Study on Sliding Mode State Estimation," *Journal of Dynamic Systems, Measurement, and Control*, Vol. 121, No. 2, 1999, pp. 255-260.

<sup>109</sup>Brown, M. D. J., Shtessel, Y. B., and Buffington, J. M., "Finite Reaching Time Continuous Sliding Mode Control with Enhanced Robustness," *Proceedings of Guidance, Navigation, and Control Conference*, AIAA-2000-3964, AIAA, Denver, CO, 14-17 Aug 2000.

<sup>110</sup>Buffington, J. M., and Shtessel, Y. B., "Saturation Protection for Feedback Linearizable Systems using Sliding Mode Theory," *Proceedings of American Control Conference*, Vol. 2, IEEE, Philadelphia, PA, 24-26 Jun 1998, pp. 1028-1032.

<sup>111</sup>Doskocz, E., Shtessel, Y. B., and Katsinis, C., "MIMO Sliding Mode Control of a Robotic 'Pick and Place' System Modeled as an Inverted Pendulum on a Moving Cart," *Proceedings of 30th Southeastern Symposium on System Theory*, IEEE, Morgantown, WV, 8-10 Mar 1998, pp. 379-383.

<sup>112</sup>Krupp, D. R., and Shtessel, Y. B., "Chattering-Free Sliding Mode Control with Unmodeled Dynamics," *Proceedings of American Control Conference*, Vol. 1, IEEE, San Diego, CA, 2-4 Jun 1999, pp. 530-534.

<sup>113</sup>Krupp, D. R., Shklonikov, I. A., and Shtessel, Y. B., "2-Sliding Mode Control for Nonlinear Plants with Parametric and Dynamic Uncertainties," *Proceedings of Guidance, Navigation, and Control Conference*, AIAA-2000-3965, AIAA, Denver, CO, 14-17 Aug 2000.

<sup>114</sup>Shklonikov, I. A., and Shtessel, Y. B., "Tracking MIMO Nonlinear Nonminimum Phase Systems Using Dynamic Sliding Manifolds," *Proceedings of Guidance, Navigation, and Control Conference*, AIAA-99-4088, AIAA, Portland, OR, 9-11 Aug 1999, pp. 826-836.

<sup>115</sup>Shklonikov, I. A., and Shtessel, Y. B., "Nonminimum Phase Tracking in MIMO Systems with Square Input-Output Dynamics via Dynamic Sliding Manifolds," Vol. 337, No. 1, 2000.

<sup>116</sup>Shtessel, Y. B., and Lee, Y.-J., "New Approach to Chattering Analysis in Systems with Sliding Modes," *Proceedings of 35th Conference on Decision and Control*, Vol. 4, IEEE, Kobe, Japan, 11-13 Dec 1996, pp. 4014-4019.

<sup>117</sup>Shtessel, Y. B., and Tournes, C. H., "Nonminimum Phase Output Tracking in Dynamic Sliding Manifolds with Application to Aircraft Control," *Proceedings of 35th Conference on Decision and Control*, Vol. 2, IEEE, Kobe, Japan, 11-13 Dec 1996, pp. 2071-2076.

<sup>118</sup>Shtessel, Y. B., "Nonlinear Output Tracking in Conventional and Dynamic Sliding Manifolds," *IEEE Transactions on Automatic Control*, Vol. 42, No. 9, 1997, pp. 1282-1286.

<sup>119</sup>Shtessel, Y. B., and Buffington, J. M., "Continuous Sliding Mode Control," *Proceedings of American Control Conference*, Vol. 1, IEEE, Philadelphia, PA, 24-26 Jun 1998, pp. 562-563.

<sup>120</sup>Shtessel, Y. B., and Buffington, J. M., "Finite-Reaching-Time Continuous Sliding Mode Controller for MIMO Linear Systems," *Proceedings of 37th Conference on Decision and Control*, Vol. 2, IEEE, Tampa, FL, 16-18 Dec 1998, pp. 1934-1935.

<sup>121</sup>Kachroo, P., "Existence of Solutions to a Class of Nonlinear Convergent Chattering-Free Mode of Control Systems," *IEEE Transactions on Automatic Control*, Vol. 44, No. 8, 1999, pp. 1620-1625.

<sup>122</sup>Bartolini, G., Ferrara, A., and Usai, E., "Chattering Avoidance by Second-Order Sliding Mode Control," *IEEE Transactions on Automatic Control*, Vol. 43, No. 2, 1998, pp. 241-267.

<sup>123</sup>Bartolini, G., and Pydynowski, P., "An Improved Chattering Free V S.C. Scheme for Uncertain Dynamical Systems," *IEEE Transactions on Automatic Control*, Vol. 41, No. 8, 1996, pp. 1120-1226.

<sup>124</sup>Zhou, F., and Fisher, D. G., "Continuous Sliding Mode Control," *International Journal of Control*, Vol. 55, No. 2, 1992, pp. 313-327.

<sup>125</sup>Fridman, L. M., and Acosta, P., "Chattering in Sliding Mode Control Systems with Fast Actuators," *Proceedings of 2nd International Conference on Control of Oscillations and Chaos*, Vol. 2, IEEE, St. Petersburg, Russia, 5-7 Jul 2000, pp. 311-314.

<sup>126</sup>Fridman, L. M., "Chattering in High Gain Control Systems with Fast Actuators," *Proceedings of 36th Conference on Decision and Control*, Vol. 4, IEEE, San Diego, CA, 10-12 Dec 1997, pp. 3232-3233.

<sup>127</sup>Levant, A., Pridor, A., Gitizadeh, R., Yaesh, I., and Ben-Asher, J. Z., "Aircraft Pitch Control via Second-Order Sliding Technique," *Journal of Guidance, Control, and Dynamics*, Vol. 23, No. 4, 2000, pp. 586-594.

<sup>128</sup>Levant, A., "Sliding Order and Sliding Accuracy in Sliding Mode Control," *International Journal of Control*, Vol. 58, No. 6, 1993, pp. 1247-1263.

<sup>129</sup>Choi, J. Y., and Farrell, J. A., "Nonlinear Adaptive Control Using Networks of Piecewise Linear Approximators," *IEEE Transactions on Neural Networks*, Vol. 11, No. 2, 2000, pp. 390-401.

<sup>130</sup>Hedrick, J. K., and Gopalswamy, S., "Nonlinear Flight Control Design via Sliding Modes," *Journal of Guidance*, Vol. 13, No. 5, 1990, pp. 850-858.

- <sup>131</sup>Utkin, V. I., Chen, D.-S., and Chang, H.-C., "Block Control Principle for Mechanical Systems," *Journal of Dynamic Systems, Measurement, and Control*, Vol. 122, No. 1, 2000, pp. 1-10.
- <sup>132</sup>Madani-Esfahani, S. M., Hached, M., and Zak, S. H., "Estimation of Sliding Mode Domains of Uncertain Variable Structure Systems with Bounded Controllers," *IEEE Transactions on Automatic Control*, Vol. 35, No. 4, 1990, pp. 446-449.
- <sup>133</sup>McRuer, D., Ashkenas, I., and Graham, D., *Aircraft Dynamics and Automatic Control*, Princeton University Press, Princeton, NJ, 1973.
- <sup>134</sup>Johnson, E. N., Calise, A. J., El-Shirbiny, H. A., and Rysdyk, R. T., "Feedback Linearization with Neural Network Augmentation Applied to X-33 Attitude Control," *Proceedings of Guidance, Navigation, and Control Conference*, AIAA-2000-4157, AIAA, Denver, CO, 14-17 Aug 2000, pp. 1-11.
- <sup>135</sup>Maciejowski, J. M., "Chapt. 5," *Multivariable Feedback Design*, Addison-Wesley, Wokingham, UK, 1989,
- <sup>136</sup>Chan, M.-L., Tao, C. W., and Lee, T.-T., "Sliding Mode Controller for Linear Systems with Mismatched Time-Varying Uncertainties," *Journal of The Franklin Institute*, Vol. 337, 2000, pp. 105-115.
- <sup>137</sup>Choi, H. H., "On the Existence of Linear Sliding Surfaces for a Class of Uncertain Dynamic Systems with Mismatched Uncertainties," *Automatica*, Vol. 35, 1999, pp. 1707-1715.
- <sup>138</sup>Hess, R. A., "Unified Theory for Aircraft Handling Qualities and Adverse Aircraft-Pilot Coupling," *Journal of Guidance, Control, and Dynamics*, Vol. 20, No. 6, 1997, pp. 1141-1148.
- <sup>139</sup>Maciejowski, J. M., "Chapt. 1," *Multivariable Feedback Design*, Addison-Wesley, Wokingham, UK, 1989,
- <sup>140</sup>Hess, R. A., Zeyada, Y., and Heffley, R. K., "Modeling and Simulation for Helicopter Task Analysis," *Proceedings of American Helicopter Society 57th Annual Forum*, Washington, D.C., 9-11 May 2002.
- <sup>141</sup>"NASA Facts: F-18 High Angle-of-Attack (Alpha) Research Vehicle," Internet Website, [www.dfrc.nasa.gov/PAO/PAIS/HTML/FS-002-DFRC.html](http://www.dfrc.nasa.gov/PAO/PAIS/HTML/FS-002-DFRC.html), 5 May 1999, NASA Dryden Flight Research Facility, FS-1999-04-002 DFRC, Accessed 7 Jan 02.

<sup>142</sup>Adams, R. J., Buffington, J. M., Sparks, A. G., and Banda, S. S., "An Introduction to Multivariable Flight Control Design," USAF Wright Laboratory, WL-TR-92-3110, Wright-Patterson AFB, OH, Oct, 1992.

<sup>143</sup>Kish, B. A., Mosle, W. B., III, Remaly, A., Seo, J., Cabiati, R., and Kromberg, J., "A Limited Flight Test Investigation of Pilot-Induced Oscillation Due to Elevator Rate Limiting (HAVE LIMITS)," USAF TPS/EDB, AFFTC-TR-97-12, Edwards AFB, CA, June, 1997.

<sup>144</sup>Hess, R. A., "Model for Human Use of Motion Cues in Vehicular Control," *Journal of Guidance, Control, and Dynamics*, Vol. 13, No. 3, 1990, pp. 476-482.

<sup>145</sup>Hess, R. A., "A Unified Theory for Aircraft Handling Qualities and Adverse Aircraft-Pilot Coupling," *Proceedings of 35th Aerospace Sciences Meeting and Exhibit*, AIAA-97-0454, AIAA, Reno, NV, 6-10 Jan 1997, pp. 1-12.

<sup>146</sup>Siwakosit, W., and Hess, R. A., "A Reconfigurable Scheme for Accomodating Actuator Failures in Multi-Input, Multi-Output Flight Control Systems," *Journal of Guidance, Control, and Dynamics*, to appear.

<sup>147</sup>"Innovative Control Effectors," USAF, WL-TR-96-3043, Jan, 1996.

## Subject Index

### A

AFTI/F-16 · 23

### C

Control allocation · 25, 26  
 attainable moment subset (AMS) · 27  
 cascaded · 34  
 daisy chaining · 35  
 direct allocation · 27  
   edge bisecting · 30  
   sequential facet search · 28  
   spherical coord · 30  
 ganging · 27  
 linear programming · 31  
 pseudo-inverse · 33  
 quadratic programming · 33

### D

DC-8 · 104  
   actuators · 105  
   airframe, lat/dir · 104  
 Design procedure · 165  
 Direct adaptive · 20, 22  
 Dynamic hedged observer · 273  
 Dynamic inversion · 23

### F

F-16 · 91, 160  
   airframe, longitudinal · 92  
 F-18/HARV · *See* HARV  
 Failure detection · 5

### H

Handling qualities assessment · 169  
 HARV  
   lat/dir  
     actuators · 201  
     airframe · 200  
     control distribution · 202  
     description · *See* HARV longitudinal  
     failure #1 · 224  
     failure #2 · 235  
     hedge design · 214  
     loop-shaped design · 229

observer design · 211  
 SMC design · 204  
 longitudinal  
   actuators · 172  
   airframe · 171  
   description · 171  
   failure #1 · 186  
   failure #2 · 194  
   hedge design · 190, 193  
   loop-shaped design · 198  
   observer design · 182  
   SMC design · 175

Hedging · *See* Model Reference Hedging  
 HQSF · 170

### I

#### ICE

actuators · 242  
 airframe · 239  
 control distribution · 243  
 description · 238  
 failure · 263  
 hedge design · 258  
 loop-shaped design · 267  
 observer design · 252  
 SMC design · 246  
 Indirect adaptive · 20, 21  
 Inverted pendulum on cart · 64, 83

### M

MD-11 · 24  
 Model reference hedging  
   creating the model · 135  
   cross-coupling · 139  
   definition · 124  
   hedge filter · 127  
   hedge gain · 131, 137  
   hedge loop shape · 135  
   hedge plant · 127  
   hedged reference model · 125  
   simplified model · 133  
   with failed plants · 141  
 MRAC system · 23  
 Multiple model adaptive estimation · 21

**N**


---

 Neural net · 23
**O**


---

 Observer

- dynamic hedged · 273
- equivalent unity feedback · 112, 120
- with failed plants · 121, 141

Observer/hedge equivalent unity feedback · 128

**P**


---

 Parameter estimation · 7

- correlated effectors · 10, 18
- dithering · 11
- frequency domain · 11
- least squares, time domain · 10
- neural nets · 17
- persistent excitation · 9
- reduced order · 16

Parasitic dynamics · 83

PID

- linear controller · 158
- parameter ID · *See* Parameter estimation

PIOR · 170

**R**


---

 Receding horizon optimal control · 21

Reconfigurable control · 2, 5

 RESTORE · *See* TAFA

Robustness issues · 148

- boundary layers · 150
- hybrid structure · 157
- Lyapunov proofs · 150
- matching conditions · 151

**S**


---

 Sliding mode control · *See* SMC

SMC · 44, 47

- actuator position limits · 62
  - actuator rate limits · 62
  - boundary layer · 60, 89, 158
  - chatter · 59
  - design procedure · 165
  - dynamic boundary layer · 91, 99
  - equivalent control · 48, 70
  - equivalent linear control · 158
  - history · 41
  - ideal sliding mode · 44, 61
  - instantaneous adaptation · 160
  - invariance · 52, 57
  - Lyapunov · 54, 148
  - matched uncertainty · 51, 56, 57
  - observer-based · 89, 111
    - MIMO · 118
    - SISO · 113
  - parasitic dynamics · 83
  - prefilter · 90
  - properties · 47, 50
  - pseudo-sliding · 61
  - reaching condition · 53
  - reaching phase · 44
  - regular form · 55, 66
  - second order (2-SMC) · 62
  - square feedback linearization · 57, 77
  - switching surface · 44
- Sum-of-sines input profile · 173

**T**


---

 TAFA · 23, 25
**V**


---

 Variable structure controls · 42
**X**


---

 X-33 · 24